

**INTEGRATED WATER RESOURCE MODELLING  
FOR IMPROVED AGRICULTURAL  
PRODUCTIVITY IN OMO-GIBE BASIN ETHIOPIA**

Thesis

Submitted in partial fulfilment of the requirement for the degree of

**DOCTOR OF PHILOSOPHY**

by

**MUDESIR NESRU KEBEDE**

Reg.No. 165086AM16F03



**DEPARTMENT OF WATER RESOURCES AND OCEAN  
ENGINEERING  
NATIONAL INSTITUTE OF TECHNOLOGY KARNATAKA,  
SURATHKAL, MANGALORE – 575025**

May 2021



**INTEGRATED WATER RESOURCE MODELLING  
FOR IMPROVED AGRICULTURAL  
PRODUCTIVITY IN OMO-GIBE BASIN ETHIOPIA**

Thesis

Submitted in partial fulfilment of the requirement for the degree of

**DOCTOR OF PHILOSOPHY**

by

**MUDESIR NESRU KEBEDE**

Reg.No. 165086AM16F03

Under the Guidance of

Prof. Amba Shetty

Prof. M.K. Nagaraj



**DEPARTMENT OF WATER RESOURCES AND OCEAN  
ENGINEERING**

**NATIONAL INSTITUTE OF TECHNOLOGY KARNATAKA,  
SURATHKAL, MANGALORE – 575025**

**May 2021**



## DECLARATION

I hereby declare that the research Thesis entitled “**Integrated Water Resource Modelling for Improved Agricultural Productivity in the upper Omo-Gibe basin, Ethiopia,**” which is being submitted to the **National Institute of Technology Karnataka, Surathkal,** in partial fulfillment of the requirements for the award of the Degree of **Doctor of Philosophy in Department of Water Resources and Ocean Engineering** is a bonafide report of the research work carried out by me. The material contained in this research synopsis has not been submitted to any University or Institution for the award of any degree.



**Mudesir Nesru**

(Register Number: 165086AM16F03)

Department of Water Resources and Ocean Engineering

NITK, Surathkal, India

Place: Surathkal

Date: 5/05/2021



## CERTIFICATE

This is to certify that the research synopsis entitled “**Integrated Water Resource Modelling for Improved Agricultural Productivity in the upper Omo-Gibe basin, Ethiopia**” submitted by **Mr. Mudesir Nesru** (Register Number: 165086AM16F03), as the record of the research work carried out by him, is accepted as the research synopsis submission in partial fulfillment of the requirements for the award of the degree of **Doctor of Philosophy**.

Research Guide(s)



(Prof. Amba Shetty)

for



(Prof. MK. Nagaraj)

Department of Water Resources and Ocean Engineering NITK, Surathkal, India



Chairman - DRPC

Department of Water Resources and Ocean Engineering NITK, Surathkal, India



## **ACKNOWLEDGMENTS**

First and foremost, Praise is to the Almighty Allah, the most compassionate the most merciful, for giving me persistence and potency to accomplish this research work successfully.

I would like to extend my sincere thanks and appreciation to my research supervisors Prof. Amba Shetty and Prof. M.K. Nagaraj. Without their scientific advice and encouragement, helpful recommendations, exceptional patience, and support from the beginning until the end of my Ph.D. research, it would have been difficult to complete this Ph.D. study. I will always remember their positive approach, compassion, and academic excellence to support in all situations.

I express my sincere gratitude to the Research Progress Appraisal Committee members, Prof. Harsha Vardhan, Department of Mining, and Dr. Subrahmanya Kundapura, Department of Water Resource and Ocean Engineering, for their continued support, motivation, and logical feedback during my work. I also extend my gratitude to the Department of Water Resources and Ocean Engineering professors for their professional advice, assistance, and motivation during the study. I am thankful and acknowledged the National Meteorological Agency, Ethiopia (NMAE), Ministry of Water Resources, and Energy department of hydrology to supply valuable data for this research work.

Most importantly, my heartfelt appreciation and thanks go to my kind and decent wife, Merry Kedir, for her love, understanding, encouragement, care, patience, and all the inconvenience she has faced in my absence throughout my study period. And to my lovely sons Fawzan and Humaid, you always bring inspiration and make sense of my life. I would like to extend my gratitude and thank my father Nesru Kebede, my mother Aysha Kemal, my mother in law Workinesh Seid, my father in law Kedir Shifa, my brothers and sisters for being there to keep on very close, loving, and helping me, knowing that they always held me in their thoughts and prayers gave me the capacity to continue.

I would like to acknowledge the help and support of all the faculties, staff, friends of the Department of Water Resources and Ocean Engineering, and all other well-wishers for

their direct and/or indirect support at various stages of this research work and, in particular, to thank Mr. Sinan Nizar for his continuous encouragement and selfless support.

  
(Mudesir Nesru)

## **DEDICATION**

This thesis is dedicated to

My Respected Mother W/ro Aysha Kemal, and my father, Ato Nesru Kebede

My kind and decent wife Merry Kedir, lovely sons Fawzan Mudesir and Humaid  
Mudesir

## ABSTRACT

The lack of data in many river basins hinders the effective management of water resources. This is true in many river basins of Ethiopia. In this study, remote sensing images and the hydrological model were used jointly to bridge the gap in understanding of the hydrological processes of a watershed with sparse measured data. Understanding of water balance components is imperative for proper policy and decision-making. Such assessments are not available in many river basin across the globe, specifically in the upper part of the Omo-Gibe basin (UOGB) Ethiopia. The objective of this study was; (i) to explore the possibility of assessing consumption and availability of water using freely available satellite data and secondary data, (ii) to test the efficiency of satellite-based actual evapotranspiration in the HBV hydrological model to render the catchment water balance using multi-variable calibration and (iii) to come up with a strategy to increase cereals production by 2030 using available water resources in the upper Omo-Gibe basin. The Surface Energy Balance System (SEBS) is used to estimate spatiotemporal variability of actual evapotranspiration of the basin, while the Hydrologiska Byran's Vattenbalansavdelning (HBV) rainfall-runoff hydrological model is used to simulate streamflow as well as actual evapotranspiration.

A spatial average of rainfall was computed using the Thiessen polygon approach. Actual evapotranspiration (ET<sub>a</sub>) was estimated through the Surface Energy Balance System (SEBS). Temporal MODIS images were used to estimate the spatial distribution of actual evapotranspiration covering the crop cycle during the study year. Additionally, Priestly and Taylor's approach was used to estimate reference evapotranspiration (ET<sub>0</sub>). The result of estimated precipitation and ET<sub>a</sub> showed that the UOGB received 41,080Mm<sup>3</sup> of precipitation for the given study period, while 24,135Mm<sup>3</sup> become evapotranspired. The assessed outflow from the basin is 17.6% of the precipitation and demonstrated that water is a scarce resource in the UOGB.

Conventional practice of calibration of any hydrological model in any river basin is performed using a single hydrological variable, namely streamflow. Spatially distributed hydrological modelling provides an opportunity to enhance the use of multi-variable

calibration models. Five years (2000-2004), meteorological data, streamflow, and actual evapotranspiration (ETa) based on remote sensing were used for calibration and validation purposes. The performance of the HBV model and the efficiency of SEBS-ETa were evaluated using certain calibration criteria (objective function). The model is first calibrated using only streamflow data to test HBV model performance and then calibrated using a multi-variable (streamflow and ETa) dataset to evaluate the efficiency of SEBS-ETa. Both model setups were validated in a multi-variable evaluation using streamflow and ETa data. In the first case, the model performed well enough for streamflow and poor for ETa, while in the latter case, the performance efficiency of SEBS-ETa and streamflow data shows satisfactory to good. This implies that the performance of hydrological models is enhanced by employing multi-variable calibration.

Maize crops production yield in the water-scarce UOGB, can be increased by increasing crop water productivity and improving agricultural management. Based on the CWP and ETa/ETp analysis, the seasonal average Abelti maize CWP is 0.3 Kg/m<sup>3</sup>. In addition, the ETa of rainfed maize over the main maize growth period is 520 mm per season. Crop production function analysis and its planting can be studied as a function of the amount of seeds, fertilizers, and water utilized to evaluate the crop yield in the study area for the rainfed maize area. A total of 30,287.17 ha of suitable pastoral land has been converted/expanded to a rainfed maize area in the three slope classes (namely fairly, suitable land sloping classes, the moderately suitable land sloping classes, and the average suitable sloping class)of the basin. The two strategies identified to meet the expected 2030 UOGB rainfed maize production target are assessed based on a one-fourth, two-fourth, and three-fourth increase in yield gaps. In the first strategy, the increase in yield gaps by one-fourth, two-fourth, and three-fourth contributes 23.12%, 46.23 %, and 69.35% of the total targeted production in the current rainfed maize area of the basin in the same order. Whereas, in the second strategy, the increase in production for additional suitable land contributed 0.80, 0.39 and 0.68, 1.61, 0.79 and 1.36, and 2.41, 1.18, and 2.04% of the planned target production in the same order.

## **TABLE OF CONTENTS**

<b>ABSTRACT</b> .....	<b>ii</b>
<b>LIST OF FIGURES</b> .....	<b>vii</b>
<b>LIST OF TABLES</b> .....	<b>ix</b>
<b>LIST OF ABBREVIATION</b> .....	<b>xi</b>
<b>CHAPTER 1: INTRODUCTION</b> .....	<b>1</b>
1.1.    Water Resource in General and its Management.....	1
1.2    Statement of the Problem.....	7
1.3    Objectives of the Study.....	8
1.4    Layout of the Thesis.....	9
<b>CHAPTER 2: LITERATURE REVIEW</b> .....	<b>10</b>
2.1.    Introduction.....	10
2.2.    Water Resource and Crop Production.....	10
2.2.1    Water resources in Ethiopia .....	13
2.3.    Water Resource Management .....	14
2.3.1.    Water Resource Management in Ethiopia .....	16
2.4. Role of remote sensing and hydrological modelling in water resources management.....	17
2.4.1. Remote sensing.....	17
2.4.2. Hydrological Modelling and classification.....	30
2.5. Literature Summary.....	46
2.6. Literature Gap.....	47
<b>CHAPTER 3: STUDY AREA AND RESEARCH METHODOLOGY</b> .....	<b>49</b>
3.1.    Introduction.....	49
3.2.    Location of the Study Area .....	50
3.3.    Topography .....	51
3.4.    Climate.....	51
3.4.1.    Rainfall.....	52
3.4.2.    Temperature .....	53

3.5.	Geology, Soil and Land Use .....	54
3.6.	Data used.....	61
3.7.	Research Methodology .....	62
<b>CHAPTER 4: ASSESSMENT OF CONSUMPTION AND AVAILABILITY OF WATER .....</b>		<b>64</b>
4.1.	Introduction.....	64
4.2.	Methodology .....	67
4.2.1	Precipitation .....	67
4.2.2.	Data Quality and Homogeneity Testing .....	67
4.2.3.	Actual Evapotranspiration .....	70
4.3	Results and Discussion .....	72
4.3.1	Spatial and Temporal Variability of Precipitation .....	72
4.3.2	Actual Evapotranspiration .....	80
4.3.3	Comparison of SEBS ETa to Other Methods .....	85
4.3.4	Water Balance .....	86
4.4	Summary and Conclusions .....	88
<b>CHAPTER 5: MULTI-VARIABLE CALIBRATION OF HYDROLOGICAL MODEL IN THE UPPER OMO-GIBE BASIN, ETHIOPIA.....</b>		<b>90</b>
5.1.	Introduction.....	90
5.2.	Sub catchments and Data .....	94
5.3.	Methods.....	95
5.3.1.	Time-series trends of actual evapotranspiration .....	95
5.3.2.	Hydrological model .....	98
5.3.3.	Model performance assessment and parameter estimation.....	99
5.4.	Results and Discussion .....	102
5.4.1.	Time series patterns of actual evapotranspiration.....	102
5.4.2.	Case 1-Model Calibration and Validation on Streamflow.....	105
5.4.3.	Case 2- Evaluating the performance of SEBS-ETa using multi-variable.	108
5.4.4.	Parameter estimation and Uncertainty of Model Parameters .....	<b>Error!</b>
<b>Bookmark not defined.</b>		
5.5.	Conclusions and Recommendations .....	127

<b>CHAPTER 6: STRATEGIES TO INCREASE RAINFED MAIZE PRODUCTION IN THE UPPER OMO-GIBE BASIN, ETHIOPIA.....</b>	<b>129</b>
6.1. Introduction.....	129
6.2. Land use, soil and water consumptions of the UOGB.....	134
6.2.1. Land use and soil .....	134
6.2.2. Water consumption .....	135
6.3. Crop water productivity and Relative evapotranspiration .....	136
6.4. Methodology .....	137
6.4.1. Assessment of rainfed maize production .....	138
6.4.2. Land suitability .....	138
6.5. Result and Discussion .....	139
6.5.1. Rainfed maize production .....	139
6.5.2. Crop production function.....	141
6.5.3. Land suitability for rainfed maize.....	142
6.5.4. Rainfed maize production strategies.....	144
6.6. Conclusions.....	149
<b>CHAPTER 7: SUMMARY AND CONCLUSIONS .....</b>	<b>151</b>
7.1. Summary .....	151
7.2. Conclusions.....	151
7.2.1. Actual evapotranspiration estimation and water balance analysis.....	151
7.2.2. Calibration, validation, and performance evaluation of HBV hydrological model	153
7.2.3. Increasing maize production .....	154
7.3. Contribution from this research .....	155
7.4. Recommendations and Perspectives for Future Studies .....	155
<b>References.....</b>	<b>158</b>
PUBLICATIONS .....	195

## LIST OF FIGURES

Figure 1-1 The 12 River basin and streams of Ethiopia .....	5
Figure 2-1 HBV model parameters relations (a) Runoff response to the increment of rainfall, (b) Relationship between actual and potential evapotranspiration .....	44
Figure 3-1 Location of upper Omo-Gibe basin.....	50
Figure 3-2 DEM of the upper Omo-Gibe basin.....	52
Figure 3-3 Average monthly rainfall for the upper Omo-Gibe basin (National Meteorological Agency of Ethiopia, 1980-2013).....	53
Figure 3-4. Average monthly maximum and minimum temperature for UOGB (National Meteorological Agency of Ethiopia, 1980-2013).....	54
Figure 3-5 Major Soil types of the UOGB (FAO, 1998).....	57
Figure 3-6 Land use types of the UOGB (MoWIE). .....	60
Figure 3-7 Research Methodological Framework of the Study.....	63
Figure 4-1 location of selected rain gauges station for upper Omo-gibe basin .....	70
Figure 4-2 Mean Annual rainfall and annual coefficient of Variation for the selected meteorological station in the Basin .....	73
Figure 4-3 Coefficient of Variation for the selected meteorological station in the basin.	74
Figure 4-4 Seasonal rainfall distribution of upper Omo-gibe basin. ....	75
Figure 4-5 Rainfall volume for the study area from Nov1980- Oct 2013 .....	76
Figure 4-6 Spatial distribution of annual precipitation in the upper Omo-Gibe basin from November 2003 to October 2004 .....	77
Figure 4-7 Variation of monthly precipitation volumes (mm) in the upper Omo-Gibe sub- catchments for the period of November 2003 to October 2004 .....	78
Figure 4-8 Spatial Distribution of annual ETa in the upper Omo-Gibe basin for the study period.....	81
Figure 4-9 Variation of monthly evapotranspiration volumes (mm/d) in the upper Omo- Gibe sub-catchments for the period November 2003 to October 2004.....	83

Figure 4-10 Comparison of the SEBS-ETa with the Penman-Monteith ETa calculated from the meteorological data collected at Assendabo station (37.23 <sup>0</sup> N Latitude, 7.77 <sup>0</sup> E Longitude) in the upper Omo-gibe basin.....	85
Figure 4-11 the major Sub-basin of the upper Omo-Gibe basin.....	87
Figure 5-1 Time series of SEBS-ETa for Abelti, Gibe, Gojeb, and Wabe sub-catchments. ....	104
Figure 5-2 Time series of observed and simulated daily streamflow for calibration and validation period for 1 <sup>st</sup> Jan 2000-31 <sup>st</sup> Dec 2004 for (a) Abelti, (b) Gibe, (c) Gojeb, and (d) Wabe Sub-catchments for case 1. ....	114
Figure 5-3 Time series of observed and simulated daily ETa for calibration and validation period for 1 <sup>st</sup> Jan 2000-31 <sup>st</sup> Dec 2004 for (a) Abelti, (b) Gibe, (c) Gojeb, and (d) Wabe Sub-catchments for case 1.....	118
Figure 5-4 Time series of observed and simulated daily streamflow for calibration and validation period for 1st Jan 2000-31st Dec 2004 for (a) Abelti, (b) Gibe, (c) Gojeb, and (d) Wabe Sub-catchments for case 2. ....	122
Figure 5-5 Time series of observed and simulated daily ETa for calibration and validation period for 1st Jan 2000-31st Dec 2004 for (a) Abelti, (b) Gibe, (c) Gojeb, and (d) Wabe Sub-catchments for case 2.....	126

## LIST OF TABLES

Table 1-1 Area and surface water resource by major river basin .....	6
Table 2-1 Merits, Demerits and input parameters of different remote sensing evapotranspiration estimation methods .....	25
Table 2-2 Summary of different hydrological models.....	39
Table 2-3 Summary of different hydrological models (Cont.) .....	40
Table 2-4 Summary of different hydrological models (Cont.) .....	41
Table 3-1 Area coverage of the major soil types in the UOGB.....	56
Table 3-2 Area coverage of the dominant land-use types in the UOGB .....	60
Table 4-1 Variation of monthly precipitation volumes (Mm <sup>3</sup> ) in the upper Omo-Gibe sub- catchments for the study period.....	79
Table 4-2 Acquisition dates of TERRA-MODIS images from November 2003 to October 2004 for upper Omo-Gibe basin (source: <a href="http://ladsweb.modaps.eosdis.nasa.gov/">http://ladsweb.modaps.eosdis.nasa.gov/</a> )	80
Table 4-3 Variation of monthly evapotranspiration volumes (Mm <sup>3</sup> ) in the upper Omo- Gibe sub-catchments for the study period .....	84
Table 4-4 Water balance for the whole basin and major sub-basins (Mm <sup>3</sup> ) from November 2003 to October 2004 .....	86
Table 5-1 Details of the four sub-catchments in UOGB.....	95
Table 5-2 Acquisition dates of TERRA-MODIS images in the upper Omo-Gibe basin for the study period (source: <a href="http://ladsweb.modaps.eosdis.nasa.gov/">http://ladsweb.modaps.eosdis.nasa.gov/</a> ).....	97
Table 5-3 Model parameters and their prior ranges used in the MCS procedure .....	102
Table 5-4 Average parameter values for the four major sub-catchments for the given two cases.....	103
Table 5-5 HBV Model performance evaluation for daily streamflow prediction for the four major sub-basins. ....	106
Table 5-6 HBV Model performance evaluation for daily ETa prediction for the four major sub-basins. ....	108

Table 5-7 Model performance evaluation for daily streamflow and ETa prediction for the four major sub-catchments. ....	110
Table 6-1 the three major categories of land use type with their corresponding area in the UOGB .....	134
Table 6-2 Average and highest rainfed maize crop yield, ETa, seed rate, and fertilizer in the Abelti sub-catchment. ....	140
Table 6-3 Correlation coefficients between crop yield (maize), ETa, seed rate, and fertilizer in the Abelti sub-catchment. ....	142
Table 6-4 Suitable pastoral land area for the three slope classes for the expansion of rainfed maize .....	143
Table 6-5 increase yield production in existing yield of a maize field .....	145
Table 6-6 Maize production for the three slope classes.....	147
Table 6-7 Overview of the two strategies for producing rainfed maize in the UOGB for 2030. ....	148

## LIST OF ABBREVIATION

Abbreviations	Description
ALFA	measure for non-linearity of the flow in the upper store zone of HBV model
amsl	above mean sea level
ASL	Atmospheric Surface Layer
ATSR	Along Track Scanning Radiometer
ASTER	Advanced Space borne Thermal Emission and Reflection Radiometer
AVHRR	Advanced very high-resolution radiometer
BCM	billion cubic meter
BETA	parameter accounting for the non-linearity of indirect runoff from the soil layer in HBV model
cf	capillary flow
CFLUX	maximum value for capillary flow
CFR	refreezing factor
CSA	Central Statistical Agency of Ethiopia
$C_p$	specific heat of air
CV	Coefficient of Variation
CWP	Crop Water Productivity
DEM	Digital Elevation Model
EBBR	Energy Balance Bowen Ratio
$EF_r$	relative evaporation
ET	Evapotranspiration
ETa	Actual Evapotranspiration
ETp	potential evapotranspiration
ET <sub>0</sub>	reference evapotranspiration

ETMA	Enhanced Thematic Mapping Algorithm
FAO	Food and Agricultural Organization
FC	maximum water holding capacity of the soil
FCV	fractional vegetation cover
GDP	Gross Domestic Product
GIS	Geographic Information System
GTP	Growth and Transformation Plan
$G_0$	soil heat flux
H	turbulent sensible heat flux
HBV	Hydrologiska Byran's Vettenbalansavdeling
ITCZ	Inter-tropical Convergence Zone
IWRM	Integrated Water Resources Management
Kc	crop coefficient
kf	recession coefficient for quick runoff
ks	recession coefficient for base flow
LAI	Leaf Area Index
LAS	Large Aperture Scintillometers
LIDAR	Light Detection and Ranging
LP	potential evapotranspiration limit
LST	Land Surface Temperature
LZ	actual storage in the lower zone store in HBV model
METRIC	Mapping evapotranspiration at high Resolution with Internalized Calibration
MODIS	Moderate Resolution Imaging Spectroradiometer
MoWE	Ministry of Water and Energy
MoWIE	Ministry Water, Irrigation and Energy
MoWR	Ministry of Water Resources

NDVI	Normalized Difference Vegetation Index
NMAE	National Meteorology Agency, Ethiopia
NSE	Nash and Sutcliffe simulation efficiency
NPC	National Planning Commission
P	precipitation
PBL	Planetary Boundary Layer
$Q_0$	quick runoff
$Q_d$	direct runoff
$Q_{in}$	indirect runoff
$R^2$	Coefficient of determination
$r_a$	aerodynamic resistances
$r_s$	surface resistances
$R_n$	net radiation
RS	Remote sensing
RVE	Relative Volume Error
SEBS	Surface Energy Balance System
SM	soil moisture
SNNPR	Southern Nations Nationalities and People Regional State
SRTM	Shuttle Radar Topography Mission
$T_0$	air temperature
$T_s$	bulk land surface temperature
UN	united nations
UNESCO	United Nations Educational, Scientific and Cultural Organization.
UOGB	upper Omo-Gibe basin
USDA	United States Department of Agriculture
UZ	actual storage in the upper zone of HBV model
VIC	Variable Infiltration Capacity

WFP	World Food Program
WHO	world health organization
WMO	world meteorological organization
$Z_{oh}$	reference height
$Z_{om}$	momentum roughness length
$\lambda E$	turbulent latent heat flux
$\epsilon_a$	air emissivity
$\epsilon_0$	surface emissivity
$\sigma$	Stefan-Boltzmann constant
$\rho_{air}$	air density
$\rho_w$	density of water
$\Delta S$	changing in storage during the time interval
$\Delta$	slope of the saturated vapor pressure curve

## **CHAPTER 1: INTRODUCTION**

### **1.1. Water Resource in General and its Management**

Water is vital for all living organisms on earth. Human beings use water for transportation, irrigation, domestic use, recreation, power development, and industrial purposes. For centuries, people have been investigating the sources of water and its sinks, why part of it is salty, and part is fresh, why sometimes there is scarcity, and sometimes there is abundance. Water is also a major factor in food security. The world's freshwater is less than 3% (35 million cubic kilometers) of the total water resource (1386 million cubic kilometers), and its withdrawals from groundwater and surface water for agriculture are around 70% of the total amount. Owing to increasing water demand for agriculture, industries, urbanization, recreation, and environmental flow, more pressure is enforced on available freshwater in the world (Biradar et al. 2008). Irrigated agriculture is estimated to increase from 100 million ha in the year 1950 to 260 million ha. It accounts for about 17% of the world's arable land, supplying 40% of food and fiber. It also provides hunting areas and a source of food for wildlife in addition to local and migratory birds (Evans and Sadler 2008).

Agricultural development is one of the key elements for the survival and intensification/growth of civilization. At the beginning of the industrial revolution or in the year 1970s, the world population was 800 million (SDSN 2013); in the mid of 2015, the population reached 7.3 billion. Today the global population is growing more slowly than in the last decade. For example, in the past ten years, the world population has grown by 1.24% per year and recently reduced to 1.18% per year (addition of 83million per year) and is projected to be 9.7 billion in the year 2050 (Melorose et al. 2015). These show that an additional 2.4 billion population are expected between the year 2015 and 2050; more than half of the projected population is contributed from Africa (1.3 billion), Asia (0.9 billion), Latin America, Northern America, Oceania, and the Caribbean (0.2 billion). The majority of these population increase are in developing countries (Wallace 2000). Such an

increase in population will need more and more irrigation water to meet increasing demands for food.

Since the 1960s, national and global food supplies have become more extensive through the contribution of irrigated agriculture; thus, irrigated agriculture plays a significant role in feeding the increasing number of population in the world. However, in the global and developing countries, water withdrawal for irrigation is considered 72% and 90%, respectively; due to the increase in water use for the non-agricultural sector, water availability for irrigation is reduced (Cai and Rosegrant 2003).

Shiklomanov (2000), Gleick (2003), and FAO (2003) estimated that the world freshwater ranges from 42700 to 44540 billion cubic meters. Out of which, 3784 billion cubic meters of water are withdrawn for agriculture, domestic, and industry in 2000. This indicates that the three sectors are the major water withdrawal sectors. The estimated water withdrawn for agriculture is 2675 billion cubic meters. From this, around 50% is consumed as evaporation and transpiration. Based on the available agricultural land area between 2010 and 2050, the irrigated agriculture water consumption would increase from 1563 to 1662 billion cubic meters, which shows that irrigation water consumption in the year 2050 would be 6% higher than in 2010 (Chartres and Sood 2013). Also, in the industrial and municipal sectors, water consumption increases from 434 to 1807 billion cubic meters and 212 to 1497 billion cubic meters, respectively.

Ethiopia is an entirely landlocked country in the world, occupying a significant portion of the Horn of Africa, located between  $3^{\circ}$ - $15^{\circ}$ N latitude and  $33^{\circ}$ - $48^{\circ}$ E longitude. It shares the North and South boundary with Eritrea and Kenya, in the East and West with Djibouti and South Sudan, in the North West with Sudan, and the South East with Somalia. The country covers about 1.1 million  $\text{km}^2$  of area (around 1 million  $\text{km}^2$  land area and 0.1 million  $\text{km}^2$  water area). Ethiopia is the second-most populous country in Africa, followed by Nigeria, with a total population of 91 million (estimated for 2016 based on the 2007 census of CSA) and an annual growth rate of 2.6%. An increasing number of the population is a severe problem in the highland areas of crop farming. Only 17% of this population is estimated to

live in urban areas of the country (Ethiopia Central Statistical Agency (ECSA) & World Food Program (WFP) 2014).

Ethiopia is a country with different land diversity due to separating tectonic plates; these include the highlands of mountains, the Great Rift Valley, and plateaus. There are also deserts along with tropical forests in the south and the eastern border though Ethiopia faces deforestation problems. The altitude ranges from 126m below sea level in Denakil depression in the Northern border to the highest mountain Rasdashen 4620m above mean sea level in Gonder North of Lake Tana.

As National Planning Commission [NPC] (2016) indicates, agriculture contributes to an average of 38.5% of the Gross Domestic Product (GDP), and the service sector and industry contribute to the remaining 46.3% and 15.1%, respectively in the year 2014/15. As the report indicates, agriculture is the major sector in terms of contribution to the overall economic growth and development by supplying food for domestic consumption and raw materials for the domestic producing industries and first export commodities that earning as high as 86% of the total foreign exchange. The country's economic system, therefore, is much related to agricultural sector performance. Moreover, the sector accounts presently for 85% of employment and provides 70% of the raw material needs of native industries.

Ethiopia has ample annual rainfall and other significant water sources that could be developed for irrigation and other development needs. In the country, rainfall is available in multiple forms that can be used for agriculture and irrigation. These forms include surface water (perennial and seasonal rivers), renewable groundwater, wetlands, soil moisture, and rainwater (Awulachew et al. 2010). The rainfall is highly variable both spatially and temporally, affecting livelihoods and land use. The unimodal rainfall is observed in the western parts of the country, beginning in February/March and ending in October/November. The Bimodal rainfall seasons are also found in the eastern parts, with one major and one minor season, whereas the bimodal season in the southern parts is more evenly distributed (Asana Dawa et al. 2007).

There are twelve river basins in the four major drainage systems of Ethiopia (Figure 1.1, Table 1.1). Most of the rivers in these basins cross the national boundary (MoWR 2001). No additional water resources are entering the country, and therefore, Ethiopia is known to be the 'Water Tower of East Africa,' a water tower providing water to neighboring countries with an estimated 96,500 million cubic meters of water each year (FAO 2016, Sundin 2017). The total annual surface runoff excluding groundwater is estimated to be 122 billion cubic meters in the twelve river basins. The three largest river basins (Abbay, Baro-Akobo, and Omo-Gibe) contribute 76 percent of the total surface runoff from a catchment area comprising only 32 percent of the total area of the country. As indicated in Table 1.1, those three river basins have much larger specific discharges than the other seven river basins (MoWR 2002). The country has 11 fresh, four crater and nine saline lakes and more than 12 major wetlands. The majority of the lakes are found in the country's Rift Valley basin and are rich in fish. The total area of the lakes is 7,500 sq. km. The country has a lesser amount of groundwater compared to surface water resources and is estimated to be 2.6 billion cubic meters (Awulachew et al. 2007). Especially for the agricultural area, Ethiopia has merely used its groundwater resource due to hydrogeological complexity and cost (Awulachew et al. 2010), which makes an average of 1575 m<sup>3</sup> physically available water per person per year. Though, due to large spatial and temporal rainfall variation and lack of infrastructure for water storage, there is not sufficient water for farmers to crop more than a crop annually.

Sustainable growth of food production can be achieved through the efficient use of water resources, land, and human resources development. The agricultural sector can influence Ethiopian economic performance. The government of Ethiopia has paid attention since the 1950s to the reduction of famine and drought through increasing agriculture production. These include traditional irrigation and construction of small-scale, medium-scale, and large-scale irrigation schemes (Awulachew et al. 2007). Ethiopia has large agricultural potential development of about 51.3 million hectares of arable land, whereas currently, the cultivated area being only 11.7 million hectares (Chanyalew et al. 2010).

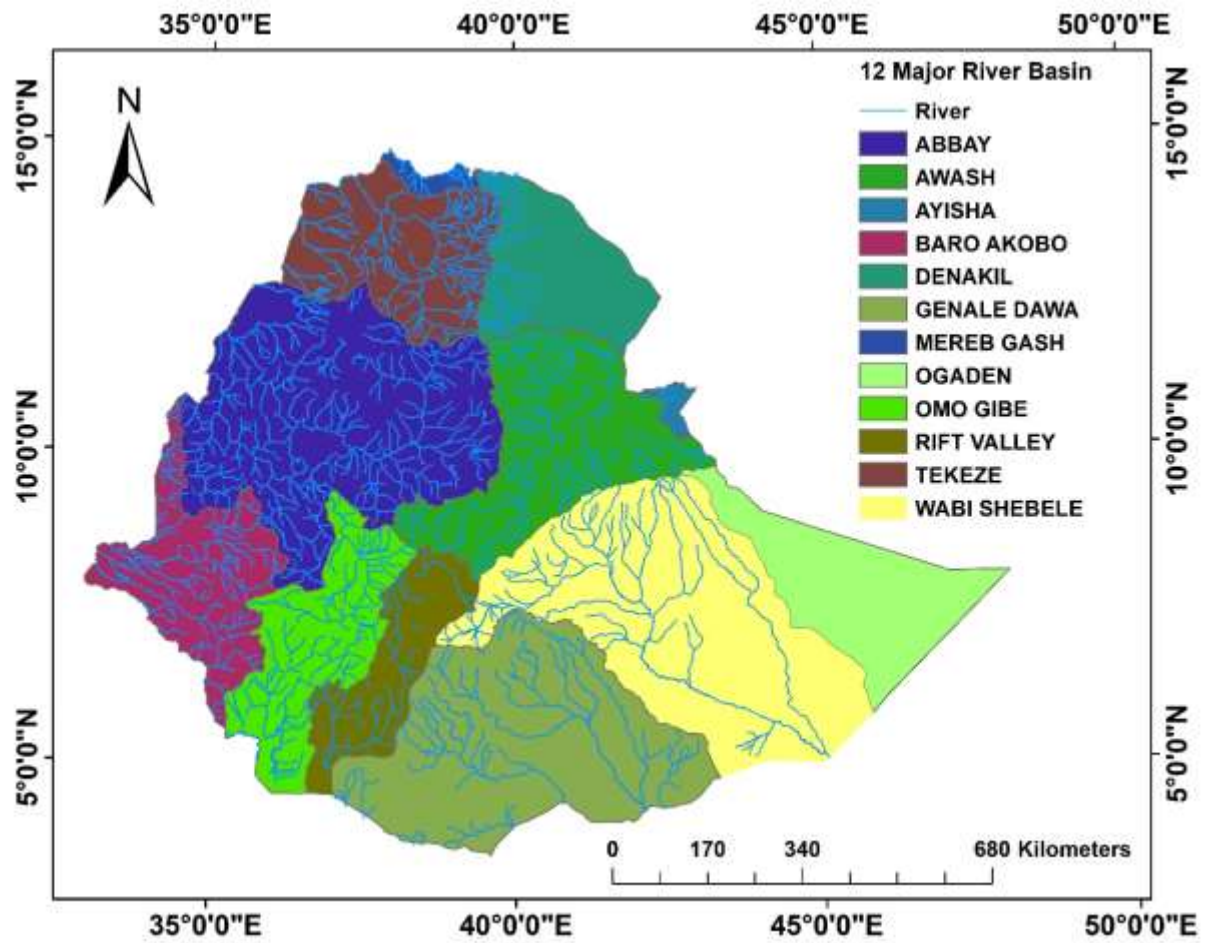


Figure 1-1 The 12 River basin and streams of Ethiopia

Table 1-1 Area and surface water resource by major river basin

S. No	Major Drainage System	River Basins	Catchment area (km <sup>2</sup> )	As % of the total area	Annual surface runoff (BM <sup>3</sup> )	As % of surface runoff
1	<b>Nile Basin</b>		<b>368612</b>	<b>32.4</b>	<b>84.09</b>	<b>69</b>
		Abbay	199 812	17.6	52.6	42.9
		Baro-Akobo	74 100	3.5	23.6	19.3
		Tekeze	89 000	7.8	7.63	6.2
		Mereb	5 700	0.5	0.26	0.6
2	<b>Rift Valley</b>		<b>317640</b>	<b>27.6</b>	<b>28.96</b>	<b>23.7</b>
		Awash	112 700	9.9	4.6	3.7
		Afar-Danakil	74 000	6.5	0.86	0.7
		Omo-Gibe	78 200	6.9	17.90	14.7
		Rift Valley	52 740	4.6	5.60	4.6
3	<b>Shebelli-Juba</b>		<b>371264</b>	<b>32.7</b>	<b>8.95</b>	<b>7.3</b>
		Wabe Shebele	200 214	17.6	3.15	2.6
		Genale – Dawa	171 050	15.1	5.80	4.7
4	<b>North- East coast</b>		<b>79300</b>	<b>7.0</b>	<b>0.0</b>	<b>0</b>
		Ogaden	77 100	6.8	0	0
		Aysha	2 200	0.2	0	0
		Total	1 136 816	100.0	122.0	100

Source: MoWR 2002 Water Sector Development Program Volume II, FAO 2016

Water resource management is the movement and control of water resources to reduce damage to life, property and to maximize efficient, beneficial use. Sometimes water management involves changing practices, such as groundwater withdrawal rates or allocation of water for different purposes (USDA 2017). Rockström et al. (2005) stated that irrigated and rain-fed agriculture water consumption based on 92 developing countries' data is estimated to be 4500 billion cubic meters per year in 2002. An additional 2200 billion cubic meters per year of fresh water used is needed in 2015 to feed 50% of under-feeding people in the world. Furthermore, an additional 3000 billion cubic meters per year of freshwater is required for irrigation to eradicate hunger in the year 2030. If water is managed efficiently in agriculture, there will be enough water and land to fulfill the world's food needs for the next 50 years (DeFraiture and Wichelns 2010). Therefore to increase the required agricultural production, it is clear that effective management for water is a must.

## **1.2 Statement of the Problem**

Ethiopia has surface runoff amounts to 122 billion cubic meters of water from 12 major river basins and 2.6 to 6.5 Bm<sup>3</sup> of groundwater sources. Still, the distribution of water resources in terms of population settlements, seasons, or geographic location does not give adequate opportunity for sustainable crop production and water supply. The distribution and availability of water are erratic both in space and time. Although the country has an abundance of water resources in some parts, the country is highly water-scarce due to a lack of water storage structures. Water is not only for domestic use but also plays a crucial role in producing food crops. In addition to domestic consumption, water is just an instrument for crop production for human beings and animals. In spite of all these importance, there is limited analysis on the quantification of water balance components at the river basin level.

Omo-Gibe-basin is one of the areas existing in combination with big rivers called Omo and Gibe and has located in the part of the Southern Nations Nationalities and People Regional State (SNNPR) and Oromia region. In the area, there are different water uses, i.e., domestic, livestock, and irrigation. There is a high shortage of access to domestic water, in which

there is a lacking water supply system to the rural areas where the population is highly concentrated. There may be several natural reserves of both surface and ground waters that demand protection, environmental management, and proper structures for domestic supply and irrigation projects. The Omo-Gibe River is flowing to the Lake Turkana.

The development of the small-scale, medium-scale, and large-scale irrigation scheme in the basin for domestic and livestock water supply and population growth requires the improvement of the accessibility to water. On top of this, the erratic rainfall and the effect of climate change may decrease the available water resources to satisfy these increasing demands.

The government and development agencies have tried to encourage farmers to adopt water harvesting techniques and irrigation; however, those technologies did not perform up to the expectations. Much effort had taken to increase food production and sustainable resource use. However, population growth had put pressure on limited resources (water, soil, etc.). The study area has a high population density, and food production is limited to a small plot of land and produce once a year. Due to climate change, the amount, frequency, and timing of rainfall are seriously unpredictable. Most of the time, a dry spell is frequent and fails in crop production. As a result, agricultural crop production decreases from time to time, the population of the area faces a shortage of food, inadequate domestic water supply, and even the animals getting highly affected/ starved due to forage's inadequacy.

### **1.3 Objectives of the Study**

This study's main objective is to quantify the spatial and temporal distribution of water availability for agriculture in the upper Omo-Gibe basin in Ethiopia by an integrated approach. This analysis will be further used to determine the potential increase of cereal production in the basin within existing water resource constraints. The specific objectives of this study are:

1. To explore the possibility of assessing consumption and availability of water using freely available satellite data and secondary data,

2. To test the efficiency of satellite-based actual evapotranspiration in the HBV hydrological model to render the catchment water balance using multi-variable calibration and
3. To come up with a strategy to increase cereals production by 2030 using available water resources in the upper Omo-Gibe basin.

#### **1.4 Layout of the Thesis**

**Chapter 2** Reviews literature relating to water resources and crop production, and its management in the Ethiopian context, satellite remote sensing, and hydrological models applied in water resource management. This chapter also includes a description of the SEBS and HBV hydrological models.

**Chapter 3** presents the salient features of the study area, a description of the different data sets used, and the overall research methodology adopted in this study.

**Chapter 4** discusses the assessment of consumption and availability of water in the upper Omo-gibe basin. The spatiotemporal distribution of precipitation and actual evapotranspiration is estimated through the satellite-based and Thiessen polygon methods.

**Chapter 5** discusses the effectiveness of satellite-based actual evapotranspiration and streamflow in a semi-distributed hydrological model in the upper part of the Omo-Gibe basin. Results are based on streamflow and actual evapotranspiration in the basin.

**Chapter 6** focuses on the strategies to increase maize crop production in the water-scarce of the upper Omo-Gibe basin, Ethiopia

**Chapter 7** is devoted to the presentation of the summary and conclusions of the present research. Recommendations based on results are also included. In addition, the scope and limitations of the research for possible studies are presented.

The next chapter reviews the literature relevant to the objectives of this research work.

## **CHAPTER 2: LITERATURE REVIEW**

### **2.1. Introduction**

This chapter provides a comprehensive set of relevant literature to provide background information on remote sensing and hydrological modelling in order to achieve the research objectives. The surface energy balance system is used to estimate actual evapotranspiration in the basin, while the hydrological model is used to simulate streamflow as well as actual evapotranspiration. This chapter is organized into four themes, namely:

- ✚ Water Resource and crop production in general and the Ethiopian scenario in particular
- ✚ Water Resource management
- ✚ Remote Sensing and hydrological modelling
- ✚ Hydrological modelling classification and integration with remote sensing and GIS

### **2.2. Water Resource and Crop Production**

Though water is more yet a scarcer resource compared to land, it is difficult to understand how it can be used in a more productive, efficient, and fair manner. Conventionally, farm productivity is a significant measure of the production of irrigated agricultural land, expressed as the ratio of grain yield to a harvested unit area (kg/ha) (Bastiaanssen et al. 1999). In areas of water-scarce overall production is improved by rising crop water productivity (CWP). Higher CWP, as reported by Zwart & Bastiaanssen (2004), is either a result of the use of fewer water resources for the same production or the use of the same water resource for higher production. The amount of crop ET has a direct relation to crop yield. To achieve more crop yield to its physical limit, it is possible only if more water is provided for crop evapotranspiration. Sometimes increasing crop water productivity (i.e., increasing the productivity of water consumed by ET) also suggested one way of alternatives to enrich crop yield.

The productivity of water is expressed as the ratio between the mass of production/economic value and crop evapotranspiration or the ratio between the mass of

production/economic value and supply/depletion of water, i.e., the productivity of water is defined as the tangible value (kg) or economic value (\$). On the other side, the amount of water quantities can either be consumed or supplied ( $m^3$ ). Proportionally low and high in sub-Saharan Africa and developed countries, respectively (Cai & Rosegrant 2003). Several studies have shown that there is an improvement in CWP to save water (Cai & Rosegrant 2003; Zwart & Bastiaanssen 2004). Such improvements can be accomplished by increasing the mass of production per hectare of land (grain yield) by enhancing crop varieties and practicing greater agronomy (Erkossa 2011; Sadras et al. 2012), as well as by improving water management and the development of related materials. For instance, the use of fertilizer at the farm level and allocating available world water resources between and within irrigated & rain-feed agriculture to make the land use more efficient (Nangia et al. 2008). Moreover, Sadras et al. (2012) address the behavior between agronomy and breeding, usually apart from over-edged.

Furthermore, the majority of grain crop water productivity is increased by enhancing long-term yield potential without any significant change in the absorption of crop water (Sadras et al. 2012), raise the fertility of the soil by increasing photosynthesis through increasing canopy size, nutrient, and water absorption through the development of root growth (Erkossa 2011). Various factors affect the productivity of the water resource compared to the land resource. These include water management and availability in the well, canal management, soil salinity, farm water management, agronomic practice, water table depth, and crop varieties (Bastiaanssen et al. 1999). They argued that CWP is more homogenous than land production (kg/ha). Water productivity can also be influenced by other factors, such as size, amount, timing, and season of rainfall events, and nitrogen deficit (Sadras et al., 2012).

Both agricultural water and the agricultural land use area will increase rapidly from 301 million ha in 2009 to 318 million ha in 2050. Depending on the availability of data, the agricultural withdrawal will further increase from 2900  $km^3/yr$  to 3000  $km^3/yr$  by 2050. It means that by 2050, the water withdrawal from agriculture will be 10% higher than it is now (FAO 2011). Zwart and Bastiaanssen (2004) depict that, on the global scale, crop

water productivity for irrigated maize (*Zea mays* L.) varies between 1.1 and 2.7 kg m<sup>-3</sup>. They concluded that the achievement of the maximum yield of maize using a wise irrigation system in the water-scarce region contributes to the achievement of CWP under favorable conditions. This is attributable to the sowing of maize on the bottom (tape) of the irrigation of the furrow (Ibrahim and Atta 2014).

In the worldwide, only 13-18% of the water is used by irrigated crops in the form of transpiration, which is correlated with yield and production. Limited quality and quantity of water supply for growing crops, increased social, economic, and environmental costs for developing large-scale irrigation schemes would lead to small-scale irrigation development. Such development affects the use of rain-fed water for irrigation efficiency (Wallace and Gregory 2002). Whereas rain-fed agriculture in the semi-arid regions of developing countries produces more irrigation products, accounting for around 90% in some countries. The primary option would be to increase crop production in these regions by increasing rain-fed agriculture, which ensures that the freshwater supply will not be under strain in irrigated agriculture (Wallace 2000). In the initial analysis for water stress, Falkenmark (1997) supposed that the annual per capita of freshwater demand from irrigated agriculture in the semi-arid area is around 785m<sup>3</sup>. Of which 50% from the estimated total annual per capita of water requirement and the remaining 50% of food is found from rain-fed agriculture. In both rain-fed and irrigated agriculture areas, water from the given area has been losing through surface runoff; these are due to high rainfall amount, less soil infiltration rate, and steeper slope of the land. Fallis (2013) and Shiklomanov (1998) estimated global water withdrawal by their demand in the three major sectors agriculture, industries, and municipal (domestic). Irrigated agriculture uses the most considerable portion of the world's annual freshwater resource (Shiklomanov 1998; FAO 2011; SDSN 2013; Fallis 2013). This accounts for 69% of annual water withdrawals worldwide (The United Nations 2016). This affects the daily life of human beings in different ways, both indirectly and directly.

Falkenmark (1997) has obtained annually per capita availability of freshwater in 21 different regions of the world for the current and the year 2050. Using Falkenmark data

Wallace (2000) reveals that currently, around 7% of the world's population lives in areas where there is some degree of water stress. When the same annual renewable freshwater resources are shared among the world population estimated for 2050, it is expected that about one in six of the world's population will have insufficient water to meet their basic requirements ( $> 2,000 \text{ m}^3$ ). Presently, the availability of per capita water in North Africa is less than 1,000 cubic meters, which appears to be the countries with the most extreme water scarcity in the region; there is also some water scarcity in southern Africa and the Middle East. This condition would spread to large regions of Africa and the Middle East. The annual availability of water in Ethiopia is also approximately  $1,220 \text{ m}^3$  per capita, showing water-stress circumstances. It has also been distinguished that two of the twelve river basins in the country are water surpluses (Abbay and Baro-Akobo), of which eight are water deficits at various levels (Tekeze, Mereb, Awash, Afar-Denakil, Omo Gibe, Rift Valley, Wabi Shebele and Genale Dawa) and the remaining two are dry (Ogaden and Aysha). There are always issues related to water in dry and deficit basins that have an impact on the community's growth and livelihoods activities (Adeba et al. 2016). Most regions of the world, with already enough water, would face some degree of water scarcity, such as India, the Far East, and parts of China. In order to estimate water stress globally and regionally, it is imperative to combine the estimates of the UN population and the estimated amount of annual renewable freshwater resources with the amount of water needed to grow basic per capita food requirements (Wallace 2000).

### **2.2.1 Water resources in Ethiopia**

Ethiopia has a significant amount of available water resources (Berhanu et al. 2014; FAO 2016). Even though the potential for water resources in the country is remarkable, river basin developments are rarely carried out. The water resource is essential to the country's development. In addition, water-based production is the key to the country's growth and transformation. The country's Growth and Transformation Plan (GTP) also recognizes and aims to improve the use of the country's water resources (Berhanu et al. 2014). The country is estimated to have a total volume of 112 BCM of surface water and some 2.6 BCM of groundwater. The western half of the country receives a

sufficient amount of precipitation and has many seasonal rivers and streams, while the precipitation is negligible in the eastern half of the country. As a result of the rapid land loss that is taking place at present, the amount of water entering the land taken away from it must have risen more than ever before. The amount of water available on the spot was therefore reduced, especially in the eastern half of the country. The country's river's primary source is the highlands of Ethiopia, which flow towards the West and the Southwest. Such rivers are Abbay, Baro-Akobo, Tekeze, Mereb, Awash, and Omo (Paulos 2002).

### **2.3. Water Resource Management**

Water balance is the basis for policy-making and management on several critical issues related to water resource management, such as flood forecasting, water supply systems design, management of water ecosystem, use and allocation of water, virtual water management, wastewater and stormwater management in urban areas and water trading (Ghandhari and Alavi Moghaddam 2011). In all of these fields, the basin's policymakers and managers require excerpt information on demand for water, change in storage, and water resource volume in the basin. The definition of water balance has acquired significant popularity among hydrologists, geologists, meteorologists, geographers, climatologists, and other disciplines primarily concerned with water problems. Therefore, it is beneficial to research the water balance and apply this principle in the study of an agricultural area to achieve better and efficient planning, management, and rational conservation of water resources in the cropland. Water balance may be defined as the income of water from precipitation and other sources and the loss or outflow of water by means of evapotranspiration. Moreover, water balance is important in arid and semi-arid regions as it can be used to assess the hydrology of the area. It also allows an evaluation of the quality of the data and the identification of inconsistencies. The measurement of the water balance can be carried out for both small and large areas of the basin. The water balance analysis in the catchment can be as short as one second and as long as many years.

The state of water resource for quantitative understanding is used for safe water management. Properly managing water resources is an essential component of growth, equity and poverty reduction, social and economic development, and sustainable environmental services (UNESCO 2009). The availability of sufficient and reliable data is required for monitoring, sound policy, participation, and research (Awad et al. 2009). Compromised validity of information due to an insufficiency of reliable and sufficient data is used for subsequent decision making and assessment purposes (UNESCO 2009). Economically secure and equitable water resources with integrated water resource management (IWRM) in the river basin are considered viable options to safeguard environmentally sustainable growth. IWRM is a mechanism that promotes integrated land, water, and associated resource management and development. It starts with a comprehensive collection of basin data, such as physical and socio-economic data, and the development of physical systems models such as hydrology, hydrogeology, and hydraulics (Ako et al. 2010).

Water is considered as a free commodity in the past, i.e., unregulated in quality and available as needed. However, a resulting increase in population and urbanization, diversification, and a rapid increase in resource demands are becoming limited and lower quality water resources. Diversification comprises irrigation water, industrial process, municipality, conservation of aquatic ecosystems, generation of hydropower, and fisheries (Mensah 2010). For example, various information is required to allocate freshwater for agricultural irrigation and other purposes and gain the best possible outcomes. These include consumption of water by vegetation and crops, availability of water and streamflow, and related crop production (Albek et al. 2004; Young 2006; Awad et al. 2009). Having said that, locating this information in any area is difficult. Globally, for instance, due to unreliable and incomplete data on water quality and quantity, adequate management of water resources is given by the water observation network; however, these networks are in danger of potential declines (UNESCO 2009). In addition, recorded streamflow data are not available globally in different river basins due to the degeneration of the gauging station. FAO (2003) reported that, out of a total of 7782 streamflow gauging

stations in the Mediterranean region, only 1868 have more than 30 years of time-series records.

### **2.3.1. Water Resource Management in Ethiopia**

Ethiopia has a generous endowment of water, but this water is distributed unevenly in space and time. Unmitigated hydrological variability, compounded by climate change, has been estimated to cost the country roughly one-third of its growth potential (World Bank 2006). Today, the production of water resources to promote 'green growth' and poverty reduction is a key plank of government policy as the country aims to achieve middle-income status by 2025. Ethiopia's Growth and Transformation Plan (GTP) sets ambitious goals for a six-fold increase in irrigated land and a quadrupling hydropower generation capacity between 2015 and 2020 (NPC 2016).

Water has played a major role in Ethiopian society; it is almost a source of input for all forms of output and a force for destruction. There has been a struggle across society to increase productivity and reduce the negative effects of productivity in the country. This challenge has increased over the last century as the population has grown rapidly. The increase in population requires effective management of the country's land and water resources. Today, Ethiopia's development is critically constrained by a complicated legacy of water resources and a lack of access to and management of these water resources (World Bank 2006).

Ethiopia's rich natural water resource endowment, its rapidly growing economy, and its ambitious government agenda offer significant opportunities. It is essential to understand what these opportunities are and capitalize on them. For example, the formulation of the second GTP (GTP-2) can provide an entry point to reinforce the links between WRM and land resource management and set aside funding to establish stakeholder collaboration and data sharing mechanisms' at all levels. WRM in Ethiopia is hampered by a lack of knowledge of resource conditions, patterns of use and drivers of change, and a lack of capacity and capacity within organizations to manage the distribution of water, determine impacts and trade-offs, and ensure 'climate-smart' planning.

## **2.4. Role of remote sensing and hydrological modelling in water resources management**

### **2.4.1. Remote sensing**

When precipitation reaches the surface of the earth in the form of rainfall, some parts percolate and fill the aquifer; some parts evaporate into the atmosphere, and the remaining parts will flow as surface runoff. Depending on this, drought can occur in some areas of the basin, while the other region faces challenges related to local floods. Such issues can be solved by valuable information on hydrological data; hydrological data is important for the planning and management of water resources. The presence of crops in arid and semi-arid regions means that there is almost a cultivated land in the field that absorbs water, from which there is a loss of water due to evaporation, transpiration, and infiltration. Conservation of unusable water intake by evaporation from soils and open water sources and by transpiration from crops and plants improves agricultural production without additional water (Farnsworth et al. 1984).

Evapotranspiration (ET) is the major part of the water cycle to represent the irrigation water demand. It is defined as a combined loss of liquid water vapor from the open water surface, bare soil, irrigated land, and vegetative surface called evaporation and from within the leaves/canopy of plants called transpiration, which co-occurs (Jia et al. 2017; Peng et al. 2019; Trajkovic et al. 2019). Evaporation is the major component of the hydrological cycle over both regional and global scale (Zhang et al. 2016a; b; Chen et al. 2019; Dinpashoh et al. 2019; Parajuli et al. 2019; Zheng et al. 2019). It is also affected by climate change (Dinpashoh et al. 2019; Gomis-Cebolla et al. 2019). Therefore, it is essential for water resource management to be particularly important in water-scarce regions (Jamshidi et al. 2019; Trajkovic et al. 2019). It is also a key process of water balance and an important energy balance element, especially in arid and semi-arid regions (Zhao et al. 2013; Walker et al. 2019). In addition to that, it is the most challenging flux to measure directly on a regional as well as global scale and shows spatial heterogeneousness with the availability of water resource, vegetation type, the variability of vapor pressure, and temperature (Rungee et al. 2019). Globally it is estimated to be 60% of precipitation (Li et al. 2009).

The evaporation from a crop growing area was decided by solar radiation division that reaches the surface of the earth, especially the crop area. This division decreases the growing term of the crop as the stage of crop development; evaporation was the dominant factor. When the crop is well established, the soil is covered by the crop canopy (i.e., the leaves of the crop are increased and the soil surface is shaded), transpiration was dominant (Elhaddad and Garcia 2008).

Evapotranspiration is a governing factor in the hydrological budget, and measurements are needed in the fields of hydrology, ecology, forestry, meteorology, and agriculture (Loheide and Gorelick 2005; Trajkovic et al. 2019). Spatially and temporally distributed point measurements of ET may not be representative and may be difficult to upscale. Remote sensing has been used to measure the spatial and temporal distribution of ET, as it is the easiest method by which local and global changes can be accomplished economically (Loheide and Gorelick 2005).

Measurement of water consumption and loss in irrigable areas, especially in water scarcity areas, is important for planning, regulating, and managing water resources. Satellite remote sensing techniques may have the capability to measure spatial and temporal surface characteristics in order to determine the precise distribution of evapotranspiration, crop yield and estimate the productivity of water and land in areas where the availability of hydrological data is limited (Bastiaanssen et al. 1999).

Remote sensing is the process of understanding measurements of the upwelling electromagnetic radiation (which are reflected and emitted by the land) of surface parameters from the earth's terrestrial and aquatic ecosystems and atmosphere (Schmugge et al. 2002). The important contribution of satellite remote sensing research in hydrology has been the development of approaches for estimating hydro-meteorological fluxes (e.g., evapotranspiration) as a residual of surface energy balance and hydro-meteorological state variables (e.g., near-surface soil moisture, land surface temperature, snow cover/water equivalent, landscape roughness, water quality, land use, and vegetation cover) (Schmugge et al. 2002). The remote sensing of hydro-meteorological state variables are determined

through different wavelengths of electromagnetic radiation. These are (i) surface soil moisture from passive microwave length, (ii) land surface temperature from a thermal infrared length, (iii) snow cover using both visible and microwave length, (iv) landscape surface roughness using LIDAR, (v) water quality using visible and near-infrared length and (vi) vegetation cover from visible, infrared and microwave length (Schmugge et al. 1988; Schmugge et al. 2002).

Quantifying water for agriculture is the key to irrigation water management, water regulation, and water resource planning. Water management is an integral part of a water budget. Some components of the water budget, such as inflows into irrigation canals and outflows from irrigation canals, can be easily measured. Other components, such as deep percolation and seasonal evaporation, are difficult to measure (Elhaddad and Garcia 2014). Obtaining accurate measurements of actual crop evapotranspiration is the main input for quantifying water management, water allocation, and water resource planning in local and regional water balance studies (Bashir et al. 2008; Salama et al. 2015; Al Zayed et al. 2016; Ayyad et al. 2019). In so doing, it tells decision-makers about the amount of crops used to consume water and allows them to relate better the available water resource to different land uses (Bastiaanssen et al. 2005). Lysimeter is one of the conventional ways to measure unerring ET. However, conventional techniques for evaluating the daily and seasonal ET in an agricultural area are carried out by performing a crop classification in the area covered by the different crop types and crop development stages. For each crop, a weather-based crop coefficient  $K_c$  and reference crop ET are used, finally multiplying them by each's crop area and integrating them as crop water use.

The remote sensing approach to estimating seasonal ET has more benefits than conventional techniques. Many conventional techniques use point measurements by limiting their competency to obtain ET in spatial and temporal variation. This cannot be applied to a large area based on hydrological intricacy and natural heterogeneity, which is only used in a few places. Such techniques include Energy Balance Bowen Ratio (EBBR) (Verma 1990), Pan Measurement (Snyder 1992), Weighing Lysimeter (Edwards 1986),

eddy covariance (Swinbank 1951), Scintillometer (De Bruin et al. 1995), Sap Flow (Cermak and Nadezhkina 1998; Meiresonne et al. 1999), etc. A regional estimate of the seasonal ET is given by the satellite remote sensing method. The model of the remote sensing surface energy balance estimates the actual ET that is occurring in the plant region (Allen et al. 2007; Elhaddad and Garcia 2008; 2011). Remote sensing (RS) can provide survey data from a few  $\text{cm}^2$  to several  $\text{km}^2$ , including all field data over a short period of time (Hatfield 1983). It can also provide spatial distribution and temporal evolution of NDVI (Normalized Difference Vegetation Index), LAI (Leaf Area Index), surface emissivity, and radiometric surface temperature from mid and thermal infrared bands. Additionally, surface albedo from visible and near-infrared bands, most of which are indispensable for models that divide the available energy (Mauser and Schädlich 1998; Li et al. 2009; Liou and Kar 2014). Moreover, RS recaptures near-surface variables (Liou and Kar 2014). The satellite remote sensing approach extends the limited application of energy balance equations to homogeneous areas with uniform vegetation, topography, and soil moisture (Kustas et al. 1994; Li et al. 2009; Liou and Kar 2014).

Furthermore, when combining satellite-based remote sensing with critical value (Vegetation Indices (VI) and albedo), developed land surface ET based on remote sensing varies greatly in degree of model structure complexity and mechanism, model inputs and outputs, and their advantage and disadvantage. Consequently, taking into account the characteristics and significance of the various ET methods developed over the last decades, the measurement of ET over a regional scale based on remote sensing technology has become an ultimate question in various ET-related applications and studies. Summaries and comparisons of different remote sensing-based ET are necessary to understand better the mechanism that occurs amid the earth's atmosphere, biosphere, and hydrosphere.

A variety of physical, empirical, and semi-empirical models have been developed for the estimation of reference evapotranspiration using meteorological data in different land cover and environmental conditions (Doorenbos and Pruitt 1977; Allen et al. 1998). Most of these are on the basis of point data to evaluate evapotranspiration, which makes them

appropriate only on a local scale and does not extend to large areas. At present, various remote sensing algorithms using the Surface Energy Balance model in the agricultural area of the water budget are used to estimate actual evapotranspiration in large areas. Most of these surface energy balance models have been formulated in the last two decades (Bastiaanssen et al. 1998a; b; Timmermans et al. 2004; Nagler et al. 2005; Allen et al. 2005b; Kustas and Norman 2009). The surface energy balance model uses digital image data collected from satellite imagery to estimate evapotranspiration (Nishida et al. 2003). Such instruments are the Advanced Spaceborne Thermal Emission and Reflection Radiometer (ASTER), advanced very high-resolution radiometer (AVHRR), moderate resolution imaging spectra radiometer (MODIS), and Landsat.

### **Surface Energy balance model**

High resolution spatiotemporal remote sensing instrument is helpful for providing evapotranspiration information for irrigation management, water allocation, and water resource planning and management. Generally, the remote sensing approach to ET estimation is recognized to improve this irrigation management, water allocation, and water resource planning and management systems (Bastiaanssen et al. 2005; Anderson et al. 2012). Based on RS data, there are several methods for estimating ETa spatially and temporally (Bastiaanssen et al. 1998a; b; Roerink et al. 2000; Su 2002; Loheide and Gorelick 2005; Senay et al. 2007). The surface energy balance (SEB) algorithm is the most commonly used RS method for estimating ETa in irrigated areas (Liou and Kar 2014). The SEB method is a wide-ranging and has a high degree of accuracy for ETa estimation (Immerzeel et al. 2006). However, at the field scale, several SEB's approaches were widely verified (Bastiaanssen et al. 2005; Chirouze et al. 2014; Bhattarai et al. 2019), have been applied in rare case to map ET in the local scale in data scarce region (Bhattarai et al. 2019). Additionally, it captures the condition of the actual crop.

The earth system operates an equal amount of energy that enters and emerges from the earth system. Yet there has been a continuation of the earth system in space and time. Depending on this change, the surface energy balance system, i.e., the amount of energy

transmitted and stored within the earth system, will be affected (Liou and Kar 2014). The majority of residual surface energy balance models are used for mapping ET for different spatial time scales. The energy balance equation can be written as follows:

$$\lambda E = R_n - G_0 - H \quad 2.1$$

Where,  $R_n$  is the net radiation (sum of all incoming and outgoing shortwave and longwave radiation at the surface) ( $\text{W}/\text{m}^2$ ),  $G_0$  is the soil heat flux ( $\text{W}/\text{m}^2$ ),  $H$  is the turbulent sensible heat flux ( $\text{W}/\text{m}^2$ ), and  $\lambda E$  is the turbulent latent heat flux ( $\lambda$  is the latent heat of vaporization and  $E$  is the actual evapotranspiration) ( $\text{W}/\text{m}^2$ ). The latent heat flux is the latent heat loss rate from the surface due to evapotranspiration and is calculated as a residual term in the surface energy budget equation. The sign convention of the Eq. (2.1) is that  $R_n$  is considered positive when radiation is directed towards the surface and is considered negative (or  $G_0$ ,  $H$ , and  $\lambda E$ , are considered positive) when directed away from the surface of the soil. Components  $R_n$ ,  $G_0$ , and  $H$  can be calculated using a combination of remote sensing-based parameters and short wave albedo with a number of ground-based meteorological variables and other auxiliary surface measurements.

Net radiation reflects the total radiant energy concentration at the surface, separated into  $G_0$ ,  $H$ , and  $\lambda E$ . The formula to determine net radiation is given by equation (2.2).

$$R_n = R_s^\downarrow + R_s^\uparrow + R_L^\downarrow - R_L^\uparrow \quad 2.2$$

Where,  $R_s^\downarrow$  is the incoming short wave radiation ( $\text{W}/\text{m}^2$ ),  $R_s^\uparrow$  is the outgoing short wave radiation ( $\text{W}/\text{m}^2$ ),  $R_L^\downarrow$  is the incoming longwave radiation ( $\text{W}/\text{m}^2$ ), and  $R_L^\uparrow$  is the outgoing longwave radiation ( $\text{W}/\text{m}^2$ ). Equation (2.2) is often referred to as a land surface radiation balance equation (Zhou et al. 2018). The net shortwave radiation can be written as:

$$\sum R_s = (1 - \alpha)R_s^\downarrow \quad 2.3$$

Where,  $\alpha$  is the surface albedo

The incoming longwave radiation is the downward thermal radiation flux from the atmosphere and written as:

$$R_L^\downarrow = \varepsilon_a \cdot \sigma \cdot T_0^4 \quad 2.4$$

Where,  $\varepsilon_a$  is the air emissivity,  $\sigma$  is the Stefan-Boltzmann constant ( $\text{W}/\text{m}^2\text{K}^4$ ), and  $T_0$  is the air temperature (K).

The outgoing longwave radiation is written as:

$$R_L^\uparrow = \varepsilon_0 \cdot \sigma \cdot T_s^4 \quad 2.5$$

Where,  $\varepsilon_0$  is the surface emissivity, and  $T_s$  is the bulk land surface temperature (K).

Soil heat flux ( $G_0$ ) is described as the rate of heat storage by conduction in soil and vegetation. The soil heat flux is empirically calculated as  $G_0/R_n$  fraction of which is read as:

$$G_0 = R_n[\Gamma_c + (1 - f_c)(\Gamma_s - \Gamma_c)] \quad (2.6)$$

Where,  $\Gamma_c$  is the ratio of soil heat flux to net radiation, which is assumed that 0.315 for bare soil (Kustas and Daughtry, 1990) and 0.05 for full vegetation canopy (Monteith 1973),  $f_c$  is the fractional vegetation cover, which can be determined from RS data (Choudhury et al. 1994). Using this  $f_c$  value, interpolation is then performed between the case of full vegetation and bare soil.

The value of  $f_c$  can be computed as:

$$f_c = 1 - \left[ \frac{NDVI - NDVI_{min}}{NDVI_{max} - NDVI_{min}} \right]^p \quad (2.7)$$

Where,  $p$  is the ratio of leaf angle distribution and constant, which is 0.625, NDVI is the normalized difference vegetation index.  $NDVI_{min}$  and  $NDVI_{max}$  are the NDVI of bare soil and full vegetation cover, respectively.

Turbulent sensible heat flux (H) is expressed as the rate of heat loss to air due to a temperature gradient. H is mathematically stated as a function of surface roughness and temperature gradient. The surface roughness is the function of wind velocity (u). The value of H is determined using the aerodynamic function and is read as:

$$H = \rho_{air} \cdot C_p \frac{dT}{r_{ah}} \quad (2.8)$$

Where,  $\rho_{air}$  is the air density ( $\text{kg m}^{-3}$ ),  $C_p$  is the specific heat of the air (1004 Joules [J] per kilogram [ $\text{kg}^{-1}$ ] per degree Kelvin [ $\text{K}^{-1}$ ]),  $dT$  is the near-surface and air-temperature difference (K) ( $dT=T_a-T_s$ ), and  $r_{ah}$  is the aerodynamic resistance to heat transfer ( $\text{s m}^{-1}$ ) over the vertical distance. The aerodynamic resistance to heat transfer is affected by the combined factors of surface roughness (vegetation height, vegetation structure), wind speed and atmospheric stability, etc.

In general, multiple satellite remote sensing techniques have been developed for estimating regional surface flux (e.g., ET). Such methods have shown reliable results over uniform hydro-climatic areas. These are the surface energy balance Index (SEBI) (Menenti and Choudhury 1993), two source model (TSM) (Norman et al. 1995), the surface energy balance algorithm for Land (SEBAL) (Bastiaanssen et al. 1998a, b) the Simplified surface energy balance Index (SSEBI) (Roerink et al. 2000), the surface energy balance system (SEBS) (Su 2002), ET Mapping algorithm(ETMA) (Loheide and Gorelick 2005), Mapping evapotranspiration at high Resolution with Internalized Calibration (METRIC) which is a variation of SEBAL (Allen et al. 2007a), and the simplified surface energy balance (SSEB) (Senay et al. 2007). Their comparisons are summarized and indicated in Table 2.1.

Table 2-1 Merits, Demerits and input parameters of different remote sensing evapotranspiration estimation methods

Methods	Input parameter	Merits	Demerit
SEBI	$T_{pbl}$ , $h_{pbl}$ , $v$ , $T_s$ , $R_n$ , $G$	The effects of surface temperature ( $T_s$ ) and aerodynamic resistance ( $r_a$ ) are directly related to $\lambda E$	It requires ground-based measurements
TSM	$T_{air}$ , $h_a$ , $v$ , $T_s$ , $R_n$ , $G$ , $T_c$ , $Fr$ or LAI	(1) View geometry is included (2) For the need of excess resistance, empirical corrections are eliminated	A lot of ground measurements and components are needed.
SEBAL	$h_a$ , $v$ , $VI$ , $T_s$ , $R_n$ , $G$	(1) Requires minimum ground-based auxiliary data; (2) There is no need for a strict correction of the atmospheric effect on surface temperature; and (3) Internal calibration has been performed within each of the analyzed images.	(1) Applied over flat terrain; (2) in the determination of anchor blocks, it possesses uncertainty
S-SEBI	$T_s$ , $\alpha_s$ , $R_n$ , $G$	Ground-based measurements are not needed.	Its extreme temperatures are specific for the location
SEBS	$T_{air}$ , $h_a$ , $v$ , $T_s$ , $R_n$ , $G$	(1) Limited uncertainties in meteorological variables or surface temperature due to limiting case energy balance consideration; (2) Instead of using constant values new formulation of roughness height is developed for heat transfer; (3) No need for prior knowledge of actual turbulent heat flux; (4) Every pixel is independent of each other.	When data is not readily available, too many parameters are required, and the solution of the turbulent heat flux is relatively complex.
METRIC	$h_a$ , $v$ , $VI$ , $T_s$ , $R_n$ , $G$	It is similar to SEBAL but considers aspects and the slope of the surface	In the determination of anchor blocks, it possesses uncertainty.

Abbreviations:  $T_{pbl}$  =Average planetary boundary layer temperature,  $h_{pbl}$  =height of PBL,  $v$  =wind speed,  $T_s$  =surface temperature,  $R_n$  =net radiation,  $G$  =soil heat flux,  $\alpha_s$  =surface shortwave albedo,  $T_{air}$  =Air temperature measured at a reference height,  $h_a$  =measurement height of wind speed and air temperature and VI= vegetation index.

All of the methods mentioned in Table 2.1, except the SEBS method, utilized physical models and empirical relationships from meteorological and satellite remotely sensed data (Gibson et al. 2011). The later solves the energy balance equation by integrating in-situ measured meteorological and satellite-based remote sensing data (McCabe and Wood 2006). One of the most appropriate algorithms these days used for remote sensing primarily based on estimation of daily evapotranspiration is the surface energy balance system (SEBS) developed by (Su 2002). The SEBS model has been selected on the basis of: (1) Limited uncertainties in meteorological variables or surface temperature due to limiting case energy balance consideration; (2) instead of using constant values new formulation of roughness height is developed for heat transfer; (3) no need of prior knowledge of actual turbulent heat flux; and; (4) each pixel is independent of each other. Such input parameters within the SEBS model for accurate estimation of actual evapotranspiration are more suitable than other related models (Su et al. 2001; Allen et al. 2007), and globally, it has a wide application. This model has shown strong rationality in numerous studies in diverse climatic and geographic circumstances (Gokmen et al. 2012; Ma et al. 2013; Ershad et al. 2013). Additionally, multiple studies have already validated this model, and they showed that the evapotranspiration and energy flux estimates by SEBS are comparable with the field measurements (Su 2002; Jia et al. 2003; Van Der Kwast 2009).

### ***Surface Energy Balance System (SEBS)***

Another modification of the SEBI energy balance model, which uses satellite-based remote sensing data to estimate land surface energy balance called the Surface Energy Balance System (SEBS) proposed by (Su 2002; Su et al. 2003). SEBS uses a combination of proper meteorological and remote sensing data to measure both the evaporative fraction and the ambient turbulent flux. Su (2002) has shown that SEBS consists of a group of tools that

measure surface temperature, surface albedo, vegetation cover and emissivity; measurement of the heat transfer of roughness length; and an estimate of the evaporative fraction at limiting case founded on energy balance. In SEBS, determining  $T_a$  and  $T_s$  in equation (2.6) in a remote sensing image entails the position of a wet (cold) pixel with a low  $T_s$  value (in irrigated agricultural settings) and a dry (hot) pixel with a high  $T_s$  value (in a fallow agricultural field). Once these pixels have been set, the value of wet and dry sensible heat flux can be determined from equation (2.1). Under the dry-limit condition, evaporation cannot take place due to the limitation of soil moisture; the latent heat becomes zero, and the sensible heat flux attains maximum value. Then  $H_{dry}$  can be written as:

$$\lambda E_{dry} = R_n - G_0 - H_{dry} = 0 \text{ Or}$$

$$H_{dry} = R_n - G_0 \quad (2.9)$$

Under the wet-limit condition, where the evaporation is limited only by the energy available for a specific surface and atmospheric conditions (i.e., the evaporation takes place at the potential rate), which can be computed by considering zero internal resistance from the Penman-Monteith combination equation, the sensible heat flux ( $H_{wet}$ ) takes its minimum value. Then  $H_{wet}$  can be written as:

$$\lambda E_{wet} = R_n - G_0 - H_{wet} = 0 \text{ Or}$$

$$H_{wet} = R_n - G_0 - \lambda E_{wet} \quad (2.10)$$

The relative evaporation  $EF_r$  is an expression for the ratio of actual evapotranspiration of latent heat flux ( $\lambda E$ ) to a latent heat flux of wet limit ( $\lambda E_{wet}$ ). Then  $EF_r$  is computed as:

$$EF_r = \frac{\lambda E}{\lambda E_{wet}} = 1 - \left[ \frac{\lambda E_{wet} - \lambda E}{\lambda E_{wet}} \right] \quad (2.11)$$

Substitute Equation (2.1), (2.9) and (2.10) in equation (2.11) and after rearranging it gives:

$$EF_r = 1 - \left[ \frac{H - H_{wet}}{H_{dry} - H_{wet}} \right] \quad (2.12)$$

The net energy available may have different time scales from the time of the satellite overpasses to the daily combined values, or for intervals between two consecutive satellite imageries. For a time scale of a day, a month, year, or season the equation developed by Bastiaanssen et al. (2002) has been used to estimate ET<sub>a</sub> over the region. In this case, G<sub>0</sub> can be overlooked and net available energy reduced to net radiation. The daily time scale actual evapotranspiration is constructed by assuming a constant evaporative fraction over the day:

$$ET_{a24} = \frac{8.64 \cdot 10^7}{\lambda \rho_w} * EF * R_{n24} \quad (2.13)$$

Where ET<sub>a24</sub> (mm/day) and R<sub>n24</sub> (W/m<sup>2</sup>) are the actual evapotranspiration and values of mean net radiation for the given time interval, respectively; EF is the evaporative fraction; λ is the latent heat of vaporization (J/Kg), and ρ<sub>w</sub> is the density of water (Kg/m<sup>3</sup>).

In the SEBS approach to set the Planetary Boundary Layer (PBL) as a reference height of potential air temperature, separation is made between PBL and Atmospheric Surface Layer (ASL) to analyze the heat flux. SEBS used ground-based meteorological measurement and remote sensing land parameters as input. Jia et al. (2003) used ground-based data from numerical weather prediction and satellite remote sensing data from Along Track Scanning Radiometer (ATSR) for the SEBS algorithm to estimate the sensible heat flux. They validated the result with Large Aperture Scintillometers (LAS) located in Spain. In the Southern Great Plains (SGP) area of the USA, Wood et al. (2003) applied SEBS to estimate latent heat flux and compared the result with the measured latent heat flux from Energy Balance Bown Ratio (EBBR) sites. They found that SEBS has a high potential to integrate data by estimating surface heat flux from space. Under the regime of all atmospheric stability, Su (2002) point out that SEBS can be used for both local and regional scaling to estimate daily, monthly, and annual evapotranspiration. Su et al. (2005) used the SEBS model to estimate land surface fluxes using available meteorological and remotely sensed data. They found that the accuracy of the estimated evaporation gets close to 10 to 15% of the in-situ measurement.

SEBS has various applications in the river basins in different parts of the world. For instance, it is used to estimate ETa over the Helmand and Kabul basins of Afghanistan to monitor and assess the performance of irrigated agriculture (Senay et al. 2007); the Heith River basin in China for improving water budget predictions (Qin et al. 2008); the Yellow River Delta wetland (Jia et al. 2009); the Karkheh River basin in Iran to assess the available water balance (Muthuwatta et al. 2010); the Upper Awash basin of Ethiopia to assess the available water balance (Kurkura 2011); the Upper Manyama catchment of Zimbabwe (Rwasoka et al. 2011); Mbire District of Zimbabwe to assess the available water balance (Samboko 2016); the Medjerda river basin in Northern Tunisia (Abid et al. 2019); the Nagqu river basin of the Northern Tibetan Plateau (Zhong et al. 2019). In addition to that, Jin et al. (2005), Matinfar and Soorghali (2014), and Ncube et al. (2016) applied SEBS for estimation of evapotranspiration in the Taiyuan basin of China, Silakhor plain, Lorestan province of Iran, and Nyazvidzi Sub-Catchment of Zimbabwe, respectively. It is also applied for drought monitoring in North China (Su et al. 2003); 3-hourly and daily energy and water fluxes estimation in the Haihe River basin in China (Zhao et al. 2019); and sensible heat flux estimation in the Tomelloso area of Spain (Jia et al. 2003) and Arou area (Wang and Li 2011), respectively. Furthermore, Wu et al. (2015) used SEBS to estimate irrigation water efficiency in the Heihe River in northwestern China.

The surface energy balance model is in need of a number of remote sensing data as input, such as Fractional Vegetation Cover (FVC), Normalized Difference Vegetation Index (NDVI), Leaf Area Index (LAI), Land Surface Temperature (LST), and Surface albedo. Because the model uses, such mentioned remote sensing data estimation of ETa has exposed to several uncertainties (Gibson et al. 2011). Such uncertainties are the selected formula of fractional vegetation cover, land surface and air temperature gradient, the spatial variability representation of various properties of the study area, and the height at which wind speed is measured and the selected displacement height. A number of satellite sensors were utilized to validate the SEBS applications. The SEBS method set out in Su (2002) provide reliable estimates of sensible heat flux. The variables utilized for sensible heat flux estimation are in the range of 50% of their actual values. To evaluate the pixel size effect

for the Walnut Creek watershed in Iowa, McCabe and Wood (2006) utilized MODIS and ASTER satellite sensor and Landsat-ETM data. The tower-based eddy covariance measurements were utilized to compare estimated SEBS-ETa, and the result showed that the average deviation of 2, 0.6, and 0.2 mm per day for MODIS, ASTER, and Landsat at the pixel scale, respectively was well accepted.

On the other hand, as compared to ASTER and Landsat, the deviation of ETa based on the MODIS sensor are 2.9% and -3.6%, respectively. In the Tibetan Plateau, Ma et al. (2009) utilized in-situ measurements of ETa to compare with estimated SEBS-ETa. They found that the deviated value of SEBS-ETa was high and 10% relative to the in situ measurements. For wet vegetated areas, Jia et al. (2009) compared daily ET estimation from meteorological data using the FAO Penman-Monteith equation and SEBS-ETa estimation of MODIS imagery. They revealed that the performance of the SEBS model in the daily ET simulation was acceptable. Moreover, Jin et al. (2019) compared SEBS-ETa with ET based on the water budget in Yinchuan and Weining (YW) Plains, China. They found that the yearly ET based on the water budget relatively compared well with the SEBS result. Additionally, Losgedaragh and Rahimzadegan (2018) implemented SEBS, METRIC, and SEBAL to estimate the amount of evapotranspiration for every pixel of the satellite images in Amirkabir dam, Iran. They computed the result with the ground truth data on the reservoir bank, which is pan evaporate measurements. Regarding the result, the SEBS model shows a relatively good performance.

#### **2.4.2. Hydrological Modelling and classification**

Generally, Hydrological modelling is an important tool for knowledge grasping on the hydrological responses of the catchment area (Kim et al. 2018). These models comprise portions of the hydrologic cycle characterized by the set of mathematical equations (Singh and Woolhiser 2002) and are primarily founded on a set of mathematical equations that govern extraordinarily complicated natural phenomena. This equation abstract mathematical forms and attempt to convert the physical laws. The better model provides results close to real value using optimal parameters and least model complexity (Devi et

al. 2015). Every model has its own unique features. Nowadays, for applications in hydrological modelling and water resources lessons, various types of computer-based hydrological models have been developed across the globe (Dhami and Pandey 2013). These models are ranging from those that deal with a simple empirical relationship that contains various kinds of models that have a certain degree of physicality to stochastic and to more recent numerically complex physically-based distributed models (Borah et al. 2003; Dhami and Pandey 2013).

With the increase in demand for usage, potential applications, and the models' extensive characteristics, it is becoming a challenging task for the probable model users to pick out a best-acceptable model for the given problem (Dhami and Pandey 2013). The continuous modifications of the current models and new versions of models are also accessible each year. Therefore, updated, reliable, and comprehensive evaluations of hydrological models are an ongoing need for the practitioners. A model can be evaluated by comparing the model outputs to another model or other anticipated/specific responses. In the past, many attempts have been initiated to evaluate the inter-comparison of hydrological models (World Meteorological Organization 1975; 1992; Borah et al. 2003; Migliaccio and Srivastava 2007; Golmohammadi et al. 2014).

#### **2.4.2.1. Classification of hydrological models**

Moreover, hydrologic models could be very complicated and depend on a physically-based flow equation using a distributed model called distributed (Abbott et al. 1986) or semi-distributed (Reggiani and Rientjes 2005) approach. The two main sets of well-known hydrological models are deterministic/ process-based and stochastic models.

##### ***i. The hydrological model can be distinguished as Process-Based/ deterministic models.***

These models represent the observed physical processes. They use physical variables, which are functions of both space and time, and are quantifiable (Devi et al. 2015). Moreover, for their calibration, they do not require wide-ranging meteorological and hydrologic data, but the assessment of the huge quantity of variables depicting the state

features of the area is needed (Abbott et al. 1986). If all parameters are considered free from random-variation, the model is non-probabilistic distribution; then, the model is called a deterministic model. Mostly, these models contain representations of evapotranspiration, groundwater flow, and surface run-off, but they can be much more complicated. For a single set of input values, these models will give the same result. These models characterize a reasonable thought of simple conceptual basics that simulate processes happening in the catchment.

#### *ii. The hydrological model can also contain Stochastic models*

These models rely on data and using statistical and numerical ideas to interrelate a certain input value with the model output. Unlike deterministic models, these models generate different output values for a single set of inputs (Devi et al. 2015). The aim of this model is to symbolize one or more time-series significant properties of statistical data instead of probabilistic to emphasize the time dependence of the hydrologic parameters associated with the model. Some of the common techniques used are regressions, transfer-functions, neural-networks, and system evaluation (Devi et al. 2015).

#### *Descriptions of some hydrological models*

##### **Soil and Water Assessment Tool (SWAT) model**

It is a complex, physically-based, time-series, conceptual, distributed watershed-scale, long-term hydrologic model envisioned to envisage land-use impact trends on sediment, hydrology pollutants conveyance in large, complex in ungauged basins (Arnold et al. 1998; Dhimi and Pandey 2013). It effectively performs long-term simulations to large ungauged water-basin in which the water-basin is split into several sub-basins that are further broken down into specific land use or soil classes known as the Hydrologic Response Unit (HRU) (Islam 2011). The model is a derivative of numerous predecessors (Davie 2004). These are:

- SWRRB (Simulator for Water Resources in Rural Basins):-which gives the principal watershed hydrology of the area of interest.
- CREAMS (Chemicals, Run-off, and Erosion from Agricultural Management Systems):- used in minerals and solute conveyance.
- GLEAMS (Ground-water Loading Effects on Agricultural Management Systems): used to understand subsurface water quality components.
- EPIC (Erosion Productivity Impact Calculator):- used in understanding the relationship between erosion, sediment transportation, and nutrient losses or gains.

The physical processes taken into account in the SWAT model are evapotranspiration, infiltration, interception, percolation, rainfall, subsurface-runoff, and surface-runoff (Islam 2011). Numerous process descriptions exist for all the basic hydrologic processes that could be studied. The SWAT model is known for its complexity and requires vast data; however, only limited data could be effectively met (Islam 2011).

### **System Hydrologique European (MIKE-SHE) model**

This is a deterministic, spatially-distributed process-based model that has the ability to simulate all basic processes in the land levels of the hydrological cycle (DHI 2007; Dhami and Pandey 2013; Golmohammadi et al. 2014). These processes can be expressed at a multitude of points of spatial dissemination and difficulty based on the accessibility of site data, the goal of the modelling, and selections outlined by the modeler (Butts et al. 2004; Dhami and Pandey 2013). This system has no limits on the extent of the water-basin; rather, it requires sub-dividing the water-basin into adjacent polygons using site information that includes land-use, type of soil, and rainfall. The MIKE-SHE system models hydrologic elements such as the surface water flow, saturated and unsaturated groundwater flow, evapotranspiration, open channel flow, and flows between surface and subsurface water. This system simulates sediment, mineral, and chemical transport as variables to water quality in the study area. It can also model water uses and handling encompassing irrigation systems, pump-wells, and several water-barrier structures (Golmohammadi et al. 2014). However, the required quantity of input data that simulates the model is too much, and it

is, therefore, hardly to find out a water-basin with full needed data to run the model as a well measured and accessible (Dhami and Pandey 2013).

### **Hydrologiska Byråns Vattenbalansavdelning (HBV) model**

It is part of a semi-distributed model which requires less input data and produces better simulation results, which means that in addition to a number of sub-basins, the entire basin is able to split into different vegetation zones and elevations (Bergstroem 1976; Devi et al. 2015; Xu et al. 2016). It requires daily and monthly data on air temperature, precipitation, and evapotranspiration. Currently, several versions of models are available in different countries of the world, and these are used for different climatic situations. To simulate snowmelt and snow accumulation, a degree day technique is used. Actual evaporation, runoff, and groundwater recharge are modeled as functions of definite storage of water. The latest type of HBV model is called HBV-light, which uses a period of comfortable temperature, wherein physical variables get suitable values per parameter and meteorological data (Devi et al. 2015; Xu et al. 2016).

### **Topography based hydrological model (TOPMODEL)**

It is part of the semi-distributed model that utilizes topographic data associated with runoff generation (Devi et al. 2015). Utilizing gridded elevation data for the entire basin, it can also be used in different sub-basins. Additionally, it helps in the estimation of the hydrological behavior of the water-basin. The important factors taken into consideration in this system are the basin's physical and soil water transmissivity factor (Islam 2011). This model is based on the concept of a topographic index (Beven and Kirkby 1979; Islam 2011). This model's major goal is to calculate the depth of the groundwater table or local storage deficit at any point for every time step. The value of groundwater table depth is a function of  $\ln(a/\tan\beta)$  (called topographic index), where  $a$ , and  $\tan\beta$  respectively are drained area per unit-contour length at a point and surface gradient at that point. The index is used as a measure of hydrologic resemblance in the points by assuming all locations with identical topographic index values respond in a similar way to the hydrologic processes.

The output of the model is only for representative indices values when the index is depending on the topography of the basin (Islam 2011). TOPMODEL is based on three sets of assumptions that include downward transmissivity, the dynamics, and the hydraulic gradient of the saturated zone (Islam 2011). Depending on the infiltration excess technique for calculating runoff value, it uses the Beven (1984) method known as the exponential Green-Ampt method and is recommended to minimize the number of parameters for the input data. The result of the model is in the form of simulated hydrographs or area maps (Devi et al. 2015).

#### **Agricultural Policy Environmental Extender (APEX) model**

It is a flexible, dynamic system that has the ability to model impacts of land-use and management for entire ranches and small water basins (Gassman and Williams 2009; Golmohammadi et al. 2014). It is a multi-field version but can also be implemented for single sites and whole ranch or water-basin that is further split down based on site's soil type, land-scape locations, or sub-watersheds. It can be used for modelling the effects of numerous mineral/nutrient management approaches, cultivation processes, soil-water conservation skills, alternative farming habits, and other similar action on run-off, sediment losses, nutrient, and other contaminant indicators based on short-term to long-term continuous simulation (Gassman and Williams 2009). APEX is also a good choice in innovative land administration approaches such as buffer-strip effects on pollutant leakages from up-slope farms, rigorous grazing situations, vegetated grassed channels, and dung application or surface impoundments. Additionally, it is one of the rare current models that have the ability to modelling flow and contaminant conveyance routing at the field-scale, as stated by (Gassman and Williams 2009).

#### **Annualized Agricultural Non-point Source (AnnAGNPS) model**

It is a basin-scale, a batch-process model developed to support the assessment of prolonged hydrological and water quality data to agronomic activities (Bingner & Theurer 2005; Parajuli et al. 2010; Dhimi and Pandey 2013; Luo et al. 2015). This model combines the

up-to-date developments of data management in Geographic Information Systems (GIS) with a physical description of water-basins, creating simulation prospects for un-gauged sites with inadequate data, which hinders the role of a model that depends on the input parameters calibration (Dhami and Pandey 2013; Luo et al. 2015). In this model, the analyzed water-basin is split into several similar (based on soil types, land-uses, and land-management scenarios) cells or sub-basins to numerically evaluate run-off and sediments well as nutrients and pesticides loadings (Hua et al. 2012; Luo et al. 2015).

### **Gridded Surface Subsurface Hydrologic Analysis (GSSHA) model**

It is part of distributed physical-based, water-basin simulation used for modelling of hydrological components, hydraulic parameters, sediments/mineral carriage in arid and wet regions (Downer and Ogden 2004). It splits the water-basin into cells, and these cells are used to routing flows and solutes in a cascading fashion (Dhami and Pandey 2013). GSSHA computes mass-balancing results of partial differential equations (PDEs) and carefully links hydrological elements to guarantee an over-all mass-balance and accurate response. Spatial heterogeneity is considered by dividing the water-basin into cells embracing an even finite-difference grid. The processes are computed for every grid-cell, secondly the results from the specific grid-cells are combined to give water-basin response.

### **Distributed Hydrology Vegetation Soil (DHVSM) model**

It is part of a physical-based distributed parameter model that offers a joint re-presentation of water-shed processes at the spatial-scale marked by DEM data (Wigmosta et al. 2002). It models most elements of the hydrologic cycle, at grid points through the entire water-basin (Davie 2004).

### **Patuxent landscape model (PLM)**

It is an explicit multi-scale, process-based model intended to work as a tool in an organized study of interactions between the water basin's biological and physical dynamics, conditioned on socio-economic characteristics in the site (Costanza et al. 2002; Davie

2004). This model works on a grid-cell network (known as general ecosystem model-GEM) functioning at each grid-cell. The GEM is analyzing flux-balances in each grid-cell and transferring-mass between cells. The GEM is made of three modules: Hydrology (rainfall, evapotranspiration, infiltration, and percolation) ; Nutrients (Nitrogen and Phosphorus input and output with cycling) and Plants (biomass-accumulation). Within each grid-cell, the hydrologic components, nutrients, and plant conditions are modeled within a daily time-step and then a distinct routine analyses the fluxes between cells.

### **Hydrological Predictions for the Environment (HYPE) model**

It is a semi-distributed physical-process-based and conceptual hydrologic model developed to simulate different multi-basin regions (small-scale and large-scale), encompassing wide variations in geomorphology, soil types, land uses and topography (Lindström et al. 2010; Dhimi and Pandey 2013). HYPE links land-landscape components and hydrologic sections sideways the flow path with mineral turn-over and conveyance. The parameters of this model are associated with soil type, land use (Dhimi and Pandey 2013).

### **Hydrologic Modelling System (HEC-HMS)**

It is developed for both continuous and event-based hydrological modelling. It provides several different options to the users for modelling various components of the hydrologic cycle. Initially, it was designed to model the run-off process of dendritic-catchments patterns but lately was modified to address wide ranges of problems comprising huge river-basins and water supply systems flood-hydrographs, and small catchment run-off (USACE-HEC 2010; Dhimi and Pandey 2013).

### **Precipitation Runoff Modelling System (PRMS) model**

It is part of a physical-based, distributed water-basin simulation designed to assess the effects of rainfall, several combinations of land-use and climate on basin-hydrology, stream-flow, and sediment yield (Markstrom et al. 2008; Dhimi and Pandey 2013). Each element of the hydrological cycle is described in terms of recognized empirical

relationships or physical-laws, which have some physical explanation based on quantifiable water-basin features (Dhami and Pandey 2013).

### **Water and Energy Transfer between Soil, Plants, and Atmosphere (Wet Spa) model**

It is part of a distributed hydrologic, grid-based model for envisaging the transfer of water and energy among plants, atmosphere, and soil in the water basin (Wang et al., 1997; De Smedt et al. 2000; Dhami and Pandey 2013). The water-basin is discretized into several grid-cells, and each of this grid-cell is further split into different land cover (e.g., vegetation cover and bare-soil), for which the equations of energy and water balance are maintained (Liu and Smedt 2009; Dhami and Pandey 2013). This model combines daily meteorological time series data, land-use and soil maps, and topography to forecast spatial dissemination of hydrologic variables and discharge hydrographs in the water-basin (Rwetabula et al. 2007; Dhami and Pandey 2013).

### **Variable Infiltration Capacity (VIC) model**

It is part of the grid-based semi-distributed hydrologic model, and it utilizes the equations, both water balance, and energy. The main input data are rainfall, wind velocity, and daily temperature (minimum and maximum values). Within each model grid, it allows lots of land cover types. Dunne-flow generates the surface run-off called excess runoff infiltration, and Hortonian-flow is called excess runoff saturation (Devi et al. 2015). By considering precipitation and heterogeneity of soil, the model simulates excess runoff saturation.

The above section briefly discusses various models available for the simulation of specific processes in the hydrological cycle. The models presented above are classified based on distributed, semi-distributed, stochastic, and process-based deterministic approaches. These models are employed for research applications in sedimentation analysis, sub-surface modelling, hydraulic routing, and hydrological prediction. The criteria used for the assessment of hydrological models are based on the simulation, governing equation, and data availability. The spatial and temporal scale of the models is selected for different components of the hydrological processes. These are the basic requirements that must

always be addressed before selecting any model for future use. Table 2.2 summarizes the comparison of the said hydrological models.

Table 2-2 Summary of different hydrological models.

Sl No	Types of model	Description
1	SWAT	<ul style="list-style-type: none"> <li>✚ Physically-based, distributed watershed-scale, envisioned to envisage land-use impact trends on sediment, hydrology, and pollutant conveyance in large, involved in ungauged basins.</li> <li>✚ It is useful in performing long-term simulations to large ungauged water-basin in which the water-basin is sud divided into HRU.</li> </ul>
2	MIKE-SHE	<ul style="list-style-type: none"> <li>✚ This model is a deterministic, spatially-distributed process-based model which have the ability to simulating all basic processes in the land levels of the hydrological cycle.</li> <li>✚ This system has no limits on the extent of the water-basin; instead, it requires sub-dividing the water-basin into adjacent polygons using site information that includes land-use, type of soil, and rainfall.</li> <li>✚ It is also capable of modelling water uses and handling encompassing irrigation systems, pump-wells, and several water-barrier structures.</li> <li>✚ It requires too much data.</li> </ul>
3	HBV	<ul style="list-style-type: none"> <li>✚ The semi-distributed model requires fewer input data and produces better simulation results.</li> <li>✚ The latest type of HBV model is called HBV-light, which uses a period of a comfortable temperature, wherein physical variables get suitable values per parameter and meteorological data.</li> </ul>
4	TOPMODEL	<ul style="list-style-type: none"> <li>✚ Part of the semi-distributed model which utilizes benefits of topographic data associated with run-off generation.</li> <li>✚ Utilizing gridded elevation data for the entire basin, and can also be used in different sub-basins.</li> <li>✚ The primary goal of this model is to calculate the depth of the groundwater table or local storage deficit at any point for every time step.</li> </ul>

Table 2-3 Summary of different hydrological models (Cont.)

Sl No	Types of model	Description
5	APEX	<ul style="list-style-type: none"> <li>✚ a flexible, dynamic system has the ability to modelling the impacts of land-use and management for entire ranches and small water basins.</li> <li>✚ It can also be used for modelling the effects of numerous mineral/nutrient managing approaches, cultivation processes, soil-water conservation skills, alternative farming habits, and other similar action on run-off, sediment losses, nutrient, and other contaminant indicators based on short-term to long-term continuous simulation.</li> <li>✚ Have the ability to modelling flow and contaminant conveyance routing at the field-scale.</li> </ul>
6	AnnAGNPS	<ul style="list-style-type: none"> <li>✚ A basin-scale, batch-process model developed to support the assessment of prolonged hydrological and water quality data to agronomic activities.</li> <li>✚ Combine GIS with a physical description of water-basins, creating simulation prospects for un-gauged sites.</li> </ul>
7	GSSHA	<ul style="list-style-type: none"> <li>✚ Distributed physical-based, water-basin simulation used for of modelling of hydrological components, hydraulic parameters, sediments/mineral carriage in arid and wet regions.</li> <li>✚ Spatial heterogeneity is considered by dividing the water-basin into cells embracing an even finite-difference grids.</li> </ul>
8	DHVSM	<ul style="list-style-type: none"> <li>✚ Physical-based distributed parameter model which offers a jointed representation of water-shed processes at the spatial-scale marked by DEM data.</li> <li>✚ It models most elements of the hydrologic cycle, at grid points through the entire water-basin.</li> </ul>
9	PLM	<ul style="list-style-type: none"> <li>✚ Process-based model intended to work as a tool in an organized study of interactions between biological and physical dynamics of the water-basin, conditioned on socio-economic characteristics in the sit.</li> <li>✚ This model operates on a grid-cell network.</li> </ul>

Table 2-4 Summary of different hydrological models (Cont.)

Sl No	Types of model	Description
10	HYPE	<ul style="list-style-type: none"> <li>✚ Semi-distributed physical-process based, conceptual hydrologic model, developed to simulate different multi-basin regions (small-scale and large-scale), encompassing wide variations in geomorphology, soil types, land uses, and topography.</li> <li>✚ Links landscape components and hydrologic sections sideways the flow path with mineral turn-over and conveyance.</li> </ul>
11	HEC-HMS	<ul style="list-style-type: none"> <li>✚ Developed for both continuous and event-based hydrological modelling.</li> <li>✚ Provides several different options for modelling various components of the hydrologic cycle.</li> </ul>
12	PRMS	<ul style="list-style-type: none"> <li>✚ Physical-based, distributed water-basin simulation designed to assess the effects of rainfall, several combinations of land-use and climate on basin-hydrology, stream-flow, and sediment yield.</li> </ul>
13	Wet Spa	<ul style="list-style-type: none"> <li>✚ Distributed hydrologic, grid-based model for envisaging the transfer of water and energy among plants, atmosphere, and soil in the water basin.</li> <li>✚ This model combines daily meteorological time series data, land-use and soil maps, and topography to forecast spatial dissemination of hydrologic variables and discharge hydrographs in the water-basin.</li> </ul>
14	VIC	<ul style="list-style-type: none"> <li>✚ Grid-based semi-distributed hydrologic model and is utilizes the equations both water balance and energy.</li> <li>✚ Dunne-flow generates the surface run-off called excess runoff infiltration, and Hortonian-flow called excess runoff saturation.</li> </ul>

For this research work, Hydrologiska Byråns Vattenbalansavdelning (HBV) model is selected due to relatively low complexity with low demand for input data and produce better simulation result (Bergström and Forsman 1973; Seibert and Vis 2012).

#### 2.4.2.2. Application of Hydrological Model

Hydrological modelling techniques are used in a wide range of applications, such as real-time flood forecasting, researching the impact of land use and climate change design, estimating ungauged catchment flows, and operation of hydraulic systems (Kayastha 2014). Additionally, hydrological models try to describe the relationship between rainfall and runoff, and these relationships are very complex due to catchment characteristics and spatiotemporal variability, and non-linearity of the rainfall process. Furthermore, the simulation of hydrological models allows us to understand the basin hydrological behavior, making it possible to use them to assess the management strategies of the water resource and estimate extreme events (Uliana et al. 2019).

The HBV model is a water balance-based conceptual model of catchment hydrology that has applications in simulating discharge using estimates of potential evaporation, temperature, and rainfall (Seibert 1997). Its application is also used for the computation of climate change studies. Applications of these approaches are known for a lumped conceptual model (Seibert 1997), which includes the catchment scale hydrological process and semi-distributed model domains. The HBV model was first developed at the Swedish Meteorological and Hydrological Institute (Bergstroem 1976). Also, it is applied all over the world (Lindström et al. 1997). The new version of the HBV model called HBV light (Seibert 1996) was used for these studies. The model consists of subroutines for snow, the soil and evaporation routine, routines for runoff generation, and groundwater and response routine. The data required for model input is easy to collect in the HBV hydrological model. For model calibration and simulation, observation flow and precipitation data are needed in areas of unavailable snow routine. Potential evapotranspiration is calculated on the basis of climatological data. In the case of available measurements of actual evapotranspiration, it is not necessary to calculate the potential evapotranspiration.

The snowmelt routine is based on a degree-day relation, with an altitude correction for temperature and precipitation:

$$\text{Snowmelt} = \text{CFMAX} (T - T_T) \quad (2.14)$$

Where, CFMAX is the melting factor, T is the altitude-corrected temperature, and TT is the threshold temperature. Usually, the threshold temperature is close to 0°C and is used to describe the temperature above which snowmelt occurs. The threshold temperature is also utilized to determine whether precipitation falls like rain or snow. If the mean air temperature is lower than the threshold temperature, precipitation is considered to be in the form of snow. It is presumed that the snowpack retains the melted water as long as it does not surpass a fraction (given by the WHC parameter) of the snow. When the temperature drops below the threshold temperature, this water is refreezing the formula is written as:

$$\text{Refreezing meltwater} = \text{CFR} * \text{CFMAX} (TT - T) \quad (2.15)$$

Where, CFR is the refreezing factor.

Direct and indirect runoff formation is controlled under the soil moisture routine. Under this routine, when the simulated amount of soil moisture (SM) exceeds the maximum storage capacity, direct runoff (Qd) occurs. The remaining rainfall infiltrates in the reservoir of soil moisture and is added to the upper zone store of the flow of water, and it is called indirect runoff (Qin) or leaves the reservoir of soil moisture by evapotranspiration.

The equation of direct and indirect runoff are given by:

$$Q_d = \max (P + SM - FC, 0) \quad (2.16)$$

$$Q_{in} = \left[ \frac{SM}{FC} \right]^{BETA} \cdot (P - Q_d) \quad (2.17)$$

Where, Qd=direct runoff (mm/day), Qin=indirect runoff (mm/day), P= precipitation (mm), SM=soil moisture depth (mm), FC=maximum water holding capacity of the soil (mm), and BETA=a parameter accounting for the non-linearity of indirect runoff from the soil layer

Equation (2.17) indicates that indirect runoff increases with increasing soil moisture storage but reduces to zero when infiltration is completed. Figure 2.1 (a) illustrates that when soil moisture is increased, the precipitation contribution to runoff is greater and vice versa, and when soil moisture reaches field capacity, all precipitation contributes to runoff.

The soil moisture reserve is also used to measure losses in evapotranspiration. Figure 2.1(b) shows that when SM exceeds a certain ratio of FC (called potential evapotranspiration limit (LP)), the actual evapotranspiration is higher, i.e., the ratio of actual evapotranspiration (ET<sub>a</sub>) to potential evapotranspiration (ET<sub>0</sub>) is equal to one and remains constant until the storage amount of SM reaches the FC. The ET<sub>a</sub> is estimated by equation 2.18:

$$ET_a = \begin{cases} \frac{SM}{LP \cdot FC} \cdot ET_0 & \text{If } SM < (LP \cdot FC) \\ ET_0 & \text{If } SM \geq (LP \cdot FC) \end{cases} \quad (2.18)$$

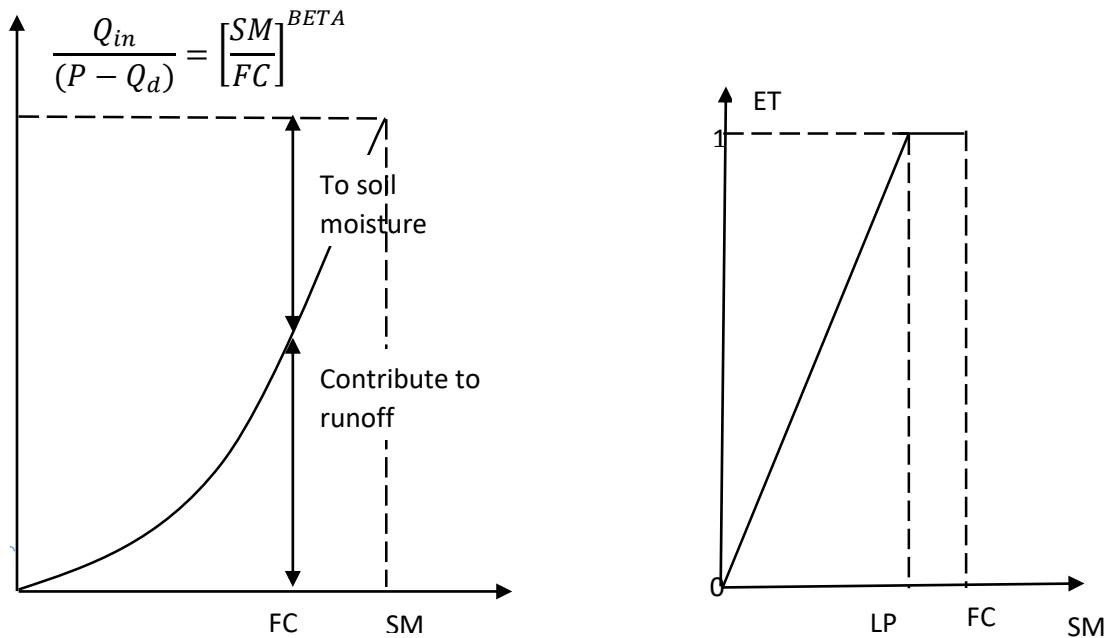


Figure 2-1 HBV model parameters relations (a) Runoff response to the increment of rainfall, (b) Relationship between actual and potential evapotranspiration

When water is available in the upper zone store, percolation occurs in the lower zone store and is treated as a constant value throughout the period of simulation. The capillary transport, Quick runoff, and baseflow are estimated by equation 2.19, 2.20, and 2.21, respectively.

$$Cf = CFLUX \cdot \left( \frac{FC - SM}{FC} \right) \quad (2.19)$$

$$Q_0 = kf \cdot UZ^{(1+ALFA)} \quad (2.20)$$

$$Q_1 = k_s \cdot LZ \quad (2.21)$$

Where,  $cf$  is capillary flow (mm/day),  $CFLUX$  is the maximum value for capillary flow (mm/day),  $Q_0$  is quick runoff (mm/day),  $k_f$  is the recession coefficient for quick runoff (1/d),  $UZ$  is the actual storage in the upper zone (mm),  $ALFA$  is a measure for non-linearity of the flow in the upper store zone,  $k_s$  is recession coefficient for base flow (1/d), and  $LZ$  is the actual storage in the lower zone store.

#### **2.4.2.3. Application of Hydrologic Modelling Integrating with Remote Sensing and GIS**

Hydrological models are integrated with GIS for preprocessing and post processing (Kherde and Sawant 2013). Hydrological processes vary in time and space. Data on meteorological, soil type, land use, and topography are sources for such processes. The development of a hydraulic model with the ability to use GIS data effectively is widely investigated. Advances in computer technology, geographic information systems (GIS), and remote sensing applications have provided a more efficient and cost-effective way to study hydrological systems. Different classifications of satellite data resulting from the GIS framework provide input to hydrological models for various applications (Baumgartner and Apfl 1997). In the case of remote sensing, variations in time over large areas are estimated to offer input data to different hydrological models. The benefit of remote sensing is bringing long-term spatial, temporal, and spectral data sets over relatively large areas that can be used to monitor hydrological conditions and changes of objects on the surface of the earth.

Moreover, GIS has made a significant contribution to monitoring and estimating projects to applied hydrology. Application of spatial knowledge is becoming a developing approach that is capable of collecting, handling, and evaluating the complex problems of river basins. GIS has proved to be a good alternative in recent years to serve as a better decision-making tool for managing, planning, and implementing water resources and soil. GIS technology is a useful computer-based tool that provides input, data storage, retrieval (data management), manipulation and analysis, and output to handle georeferenced data (Raju

2006). One of the most familiar applications of GIS is the use of a digital elevation model (DEM) obtained by ASTER GDEM tiles. This data set is then used for the extraction of hydrological catchment properties by performing a series of operations such as watershed delineation, elevation, slope, fill, sink, flow accumulation and direction, catchment polygon processing (Kherde and Sawant 2013). Interaction between GIS and remote sensing has the capability to efficiently model spatial and temporal variations in hydrological processes, particularly for semi-distributed and distributed hydrological models.

## **2.5. Literature Summary**

Conventionally, farm productivity is a significant measure of the production of irrigated agricultural land. In areas of water-scarce overall production is improved by rising crop water productivity (CWP). Furthermore, the amount of crop evapotranspiration has a direct relation to crop yield. To achieve more crop yield to its physical limit, it is possible only if more water is provided for crop evapotranspiration.

From the previous studies conducted around the world for hydrological processes and water resource management, river basin studies have been described as the most relevant studies for the production and sustainable water resources management for crop production. The method of water balance is commonly used to measure the hydrological components of a river basin. Due to the availability of measured streamflow data at the specified gauging station, the model can be calibrated and validated in terms of space and time.

Measurement of water consumption and loss in irrigable areas, especially in water scarcity areas, is important for planning, regulating, and managing water resources. Satellite remote sensing techniques may have the capability to measure spatial and temporal surface characteristics in order to determine the precise distribution of evapotranspiration, crop yield, and estimate the productivity of water and land in areas where the availability of hydrological data is limited.

The HBV hydrological model has been shown to be familiar in the hydrology simulation of catchments of varying sizes in various hydro-climatic regions of the world. However, there appears to be further room for a detailed evaluation of the model's performance in a watershed of Kolla, Weynadega, Dega, and Wurch climatic zone in the southwest part of Ethiopia.

Since the southwest part of Ethiopia, especially the Omo-Gibe River Basin, is facing water scarcity, land degradation problems, and deforestation due to human activities, it is very important to assess the consumption and availability of water for proper management. Moreover, there needs to be a study for establishing planning and sustainable water resources management linkage in a quantitative manner.

## **2.6. Literature Gap**

Though the study area has a high population density, yet food production is limited to a small land plot, and they produce once a year. Most of the time, a dry spell is frequent and fails in crop production. As a result, agricultural crop production decreases from time to time, the population of the area faces a shortage of food, inadequate domestic water supply, and even the animals getting highly affected/ starved due to forage's inadequacy. Moreover, there is lack of strategic studies on the increase in crop production across the Omo-Gibe basin of Ethiopia to fulfill the annual household food requirements.

The need for water for various uses is increasing, and this necessitates water resource planning and management. The demand for domestic and agricultural water supply is increasing. Besides, the absence of proper management strategies will make the demand likely to exceed the available supply. Also, assessing the watershed's water potential/ source is required to plan, manage, and satisfy its future water demands and make wise decisions. Due to the deterioration of stream gauging stations, poor policy designs, redundancy of information, time-consuming and cost expensiveness of traditional methods, information about water resources has become scarce. In many of the river basin across the globe, most of water balance components for water resource management are not known. It's very true in the case of semi-arid region in Ethiopia, especially in the

UOGB due to data scarcity. When sufficient observed data are lacking to generate information for decision making, modeling tools, along with the use of scenario analysis of the water source can be used to indicate the water resource management or development strategies to be carried out. In this condition, hydrological modeling tools are used to simulate streamflow. A few of these models quantify the spatial and temporal availability of the resource and predict the impacts of natural and human-made changes on water resources. However, in complex situations, streamflow requires simulation, such as changing land use in areas with no adequate streamflow data. In such an instance, standard hydrological approaches can often be adopted. There is a constraint in field measured data for model calibration, uncertainty, and fundamental error in hydrological modeling in many areas. Therefore, to get a particular hydrological estimated variable, we should pay attention to a better calibration procedure to make the best decision by understanding water resource management. Besides, there is lack of studies on the performance of HBV hydrological model to simulate major hydrological process in the semiarid region of Ethiopia. It's not been tested on the UOGB also.

Many researchers have used satellite remote sensing approaches in the field of water resource planning and management in areas of insufficient available data or restriction of required data. Complementing water management at different scales supplied spatial and temporal distributed parameters such as hydrological and biophysical parameters. For example, to allocate water for different crop consumption, it requires valuable information/data. Measuring actual evapotranspiration is needed for estimating water consumption by different crops. Though the estimation of actual evapotranspiration using conventional techniques is necessary for water balance studies, direct measurement is difficult for extending over large areas because it is a point measurement. So based on the difficulties, hydrological complexity, and natural heterogeneity, satellite remote sensing is used to estimate water consumption over a large area.

The next chapter explains the study area, data used, and overall methodology of the research work.

## **CHAPTER 3: STUDY AREA AND RESEARCH METHODOLOGY**

### **3.1. Introduction**

Looking at the Ethiopia's rainfall variability by river basins, the eastern river basins (Genale-Dawa and Wabishebele) receive low to medium rainfall, while the mean annual rainfall range is medium to high for those flowing west (Abay, Baro-Akobo, Omo-Gibe, and Tekeze) (Berhanu et al. 2014). Omo-Gibe river basin is among those who receive a medium to high annual rainfall and one of the third largest river basins in Ethiopia, with such a combination of large rivers called Omo and Gibe. It is located in the Southern Nationalities and People's Regional State (SNNPR) and the Oromia Region. Various uses of water resources are increasing in the area, i.e., domestic, livestock, and irrigation are present in the basin. In spite of the potential, availability of land resources, and demand for water resources and products, the development of the water sector is still in its early stage, where the population is quite concentrated (Berhanu et al. 2014).

In addition to rainfall variation, half of the country's total area is covered by arable land, approximately  $55 \times 10^6$  ha of land. Arable land potential includes both rain-fed and irrigable land that is agro-ecologically suited to producing various grain crops, vegetables, oilseeds, pulses, and tree crops. An estimated  $10 \times 10^6$  ha land is suitable for irrigation without taking into account the availability of water. Although such large arable land resources are available, only 30% of the arable land potential is being cultivated, while the remaining 70% of the potential land is being used in other ways, such as grazing (MoWR 2002b). In the upper Omo-Gibe basin, in addition to arable land, pastoral land covers an area of 667,039ha.

In Ethiopia, the agricultural sector contributes 38.5% of the country's GDP and accounting for an estimated 85% of employment, and provides 70% of the raw material needs of native industries (NPC 2016). The Omo-Gibe basin is selected for this study owing to the suitability of the basin for agricultural production to fulfill the annual household food requirements, animal feeds, industrial purposes, as cooking fuel, fencing material, and fodder and the basin exhibit average to maximum rainfall variability.

### 3.2. Location of the Study Area

The Abbay and Awash River basin bound the upper part of the Omo-Gibe basin in the North, the Riftvally River basin in the East, and the Baro-Akobo River basin in the west. It is located in the South-Western part of Ethiopia, covering a part of the Oromia area and some part of Southern Nations Nationalities and People Regional State (SNNPR). It is situated between  $6^{\circ}51'55.81''$ - $9^{\circ}22'26.05''$  N latitude and  $35^{\circ}31'49.63''$ - $38^{\circ}23'43.85''$  E longitude. It covers an area of 33,276sq km (Figure 3.1). Also, the Omo-Gibe River is the major tributary for Lake Turkana (in Kenya), which is located on the border of the country.

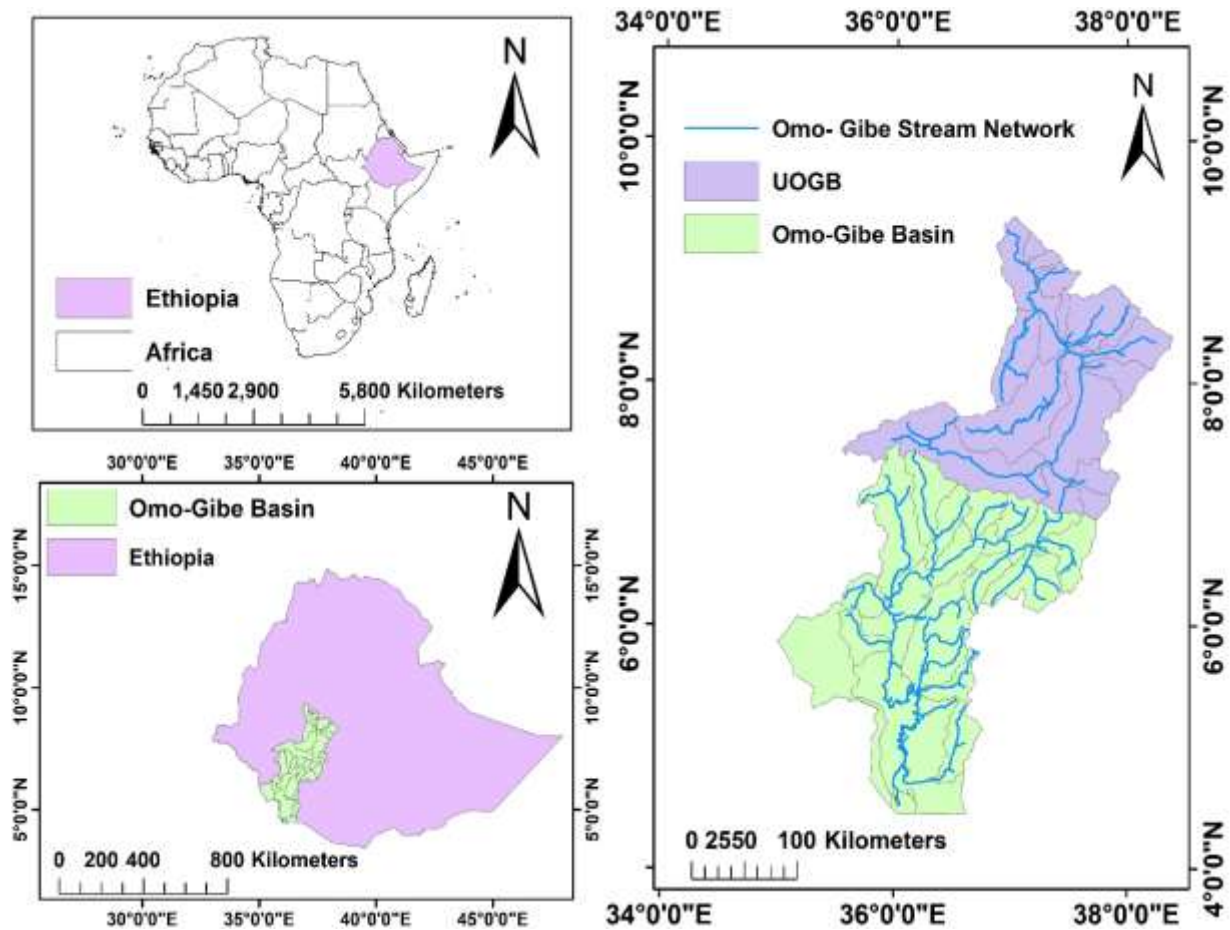


Figure 3-1 Location of upper Omo-Gibe basin

### **3.3. Topography**

The basin topography, all in all, is characterized by physical variation. 66% of the basin in the North has mountainous to hilly terrain cut by deeply incised gorges of the Gojeb, Omo, and Gilgel-Gibe rivers. While 33% of the basin in the southern part is a flat alluvial plain punctuated by hilly areas. The northern and central half of the basin is located at an altitude of more than 1500 masl with a maximum elevation of 3360 m above mean sea level (located between the tributaries of Gilgel-Gibe and Gojeb). The northern part of the basin has a number of tributaries. Many of the rivers from the upper part of the catchment drain are mostly agricultural land. The headwaters of the Great Gibe River are at an altitude of around 2200 m above mean sea level. The mean elevation of the basin is 1923 m. DEM of the basin is shown in Figure 3.2.

### **3.4. Climate**

The climatic conditions of Ethiopia are monitored by both global variability and atmospheric circulation as a result of local topography. Whereas its climate trends are controlled mainly throughout the year by the Asian Monsoon influence and interchange and latitudinal migration of the Inter-tropical Convergence Zone (ITCZ) across the equator (Camberlin and Philippon 2002). Because of climatic variabilities from dry to highly humid with further differentiation at the local scale, the transition between highlands and lowlands are often very sharp. In addition, precipitation varies with altitude, increasing from North to the south of the basin. Simultaneously, the weather conditions are often profoundly influenced by physiography and elevation, especially regarding the characteristics of the anemometric flow meter and distribution of temperature in the country (Fazzini et al. 2015).

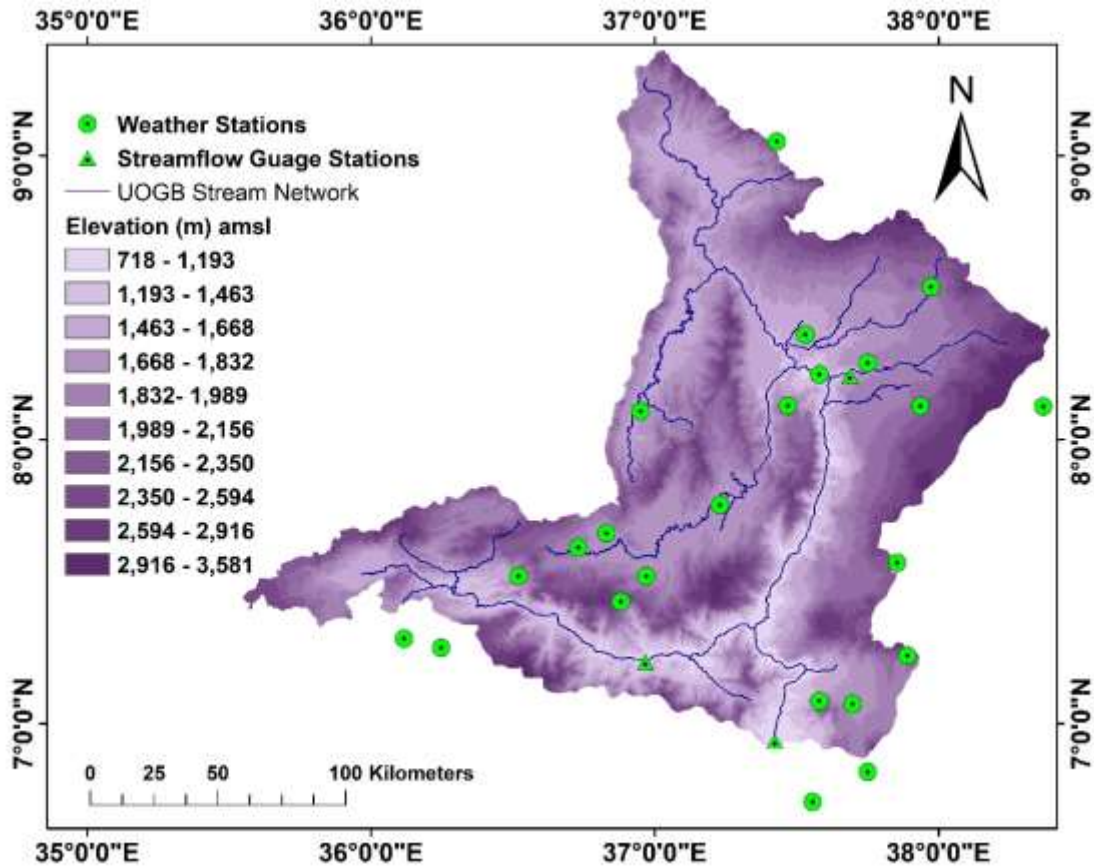


Figure 3-2 DEM of the upper Omo-Gibe basin.

The climatic condition of the study area is moderately diverse, which has been classified as from hot and dry climate to cold climate because of considerable relief and altitude variations. The country’s annual precipitation patterns are primarily bimodal. They are well-known as dry periods (the Bega in the local language) from October to February, minor rainy season (Belg in the local language) from March to May (Legesse et al. 2003). The main rainy season (Kiremt in the local language) from June to September accounts for 50-80 percent of the country’s annual precipitation (Korecha and Barnston 2007).

### 3.4.1. Rainfall

Rainfall in the basin occurs in three different seasons, namely (1) Bega called dry season: from the month of October to January (2) Belge called short rainy season: from the month

of February to May and kiremt called monsoon or rainy season: from the month of June to September. In the basin, around 58% of annual average rainfall occurs in the rainy season, and 16% is its peak value and occurred in the month of July (Figure 3.3). The average annual precipitation within and nearby the basin recorded from 23 rain gauge stations based on 34 years of precipitation data is 1335 mm. Rainfall in the basin varies from about 2050 mm per year in Bonga and Wushwush stations to less than about 400 mm in Indibir. Therefore based on its high variability and unpredictability, there is no relation with elevation.

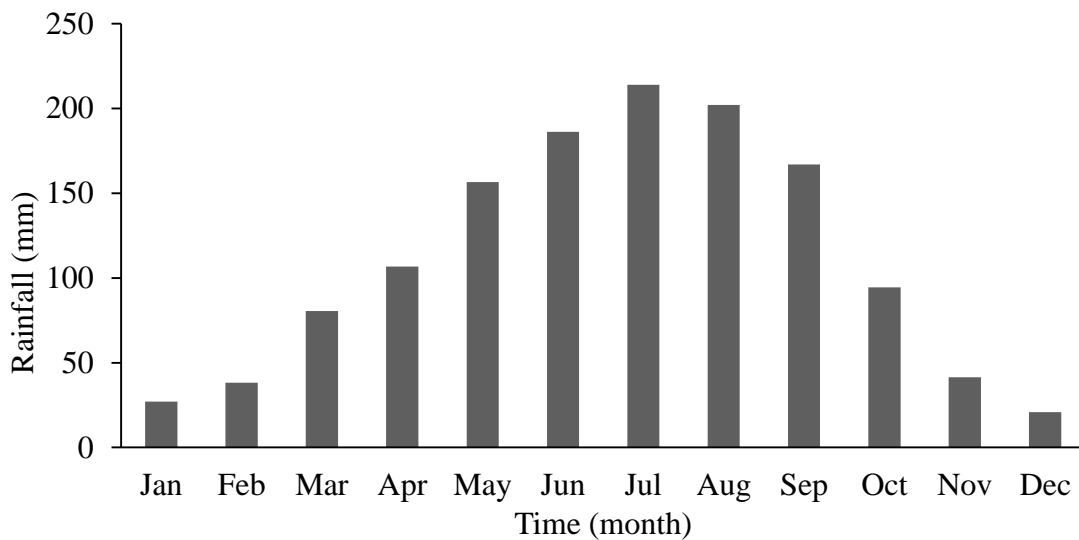


Figure 3-3 Average monthly rainfall for the upper Omo-Gibe basin (National Meteorological Agency of Ethiopia, 1980-2013)

### 3.4.2. Temperature

Depending on temperature and altitude, classification of climate in Ethiopia falls in three different zones, namely: Dega (cool climate with its temperature varies near freezing to 16<sup>0</sup>C, and at an altitude more than 2400m above mean sea level), Woina Dega (warm zone temperatures varies from 16<sup>0</sup>C to 30<sup>0</sup>C and altitude between 1500 to 2400m above mean sea level) and Kola (hot and dry form, temperatures varies between 30<sup>0</sup>C to 50<sup>0</sup>C and altitude less than 1500m above mean sea level (MoWR 2001). In addition, the mean annual temperature in the basin varies from around 16<sup>0</sup>C in the highlands of the North near the

Gedo rain gauge station to 21°C near the Areka station. Whereas the mean monthly temperature is also higher during the short rainy season (March through May) and lowers during the rainy season (June to mid-September) (Figure 3.4).

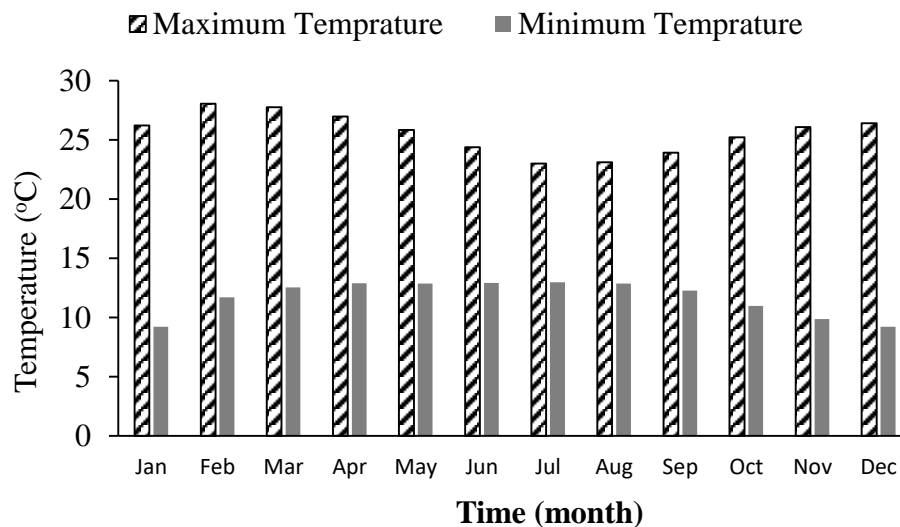


Figure 3-4. Average monthly maximum and minimum temperature for UOGB (National Meteorological Agency of Ethiopia, 1980-2013).

### 3.5. Geology, Soil and Land Use

In general, the geology of the Omo-Gibe basin is characterized by tertiary and quaternary-age rhyolite, basalt volcanic with quaternary alluviae above the pre-Cambrian basement gneisses and granites in the Omo, Gilgel-Gibe, Gibe, and Gojeb gorges (Woodrooffe and Associates 1996). The northern mountains around Sako are Pleistocene-Holocene in age form part of the basalt plateau. In the East, volcanic tertiary ages occur around Weliso and Welkite. Such rocks are trachytes, rhyolites, and basalts, commonly coated with volcanic ash. The eastern border of the basin, from the Welkite region to south of Sodo, consists of tuffs, rhyolite, unconsolidated ash, and consolidated ash flow (Tertiary Ignimbrites). The most recent volcanic regions of similar geology but also containing pumice, pitchstone, and obsidian are interspersed among these acidic igneous rocks. Most of the middle of the basin consists of the Tertiary (Eocene-Oligocene) volcanic of Jima. Such Jima volcanic are divided into upper rhyolites with minor basalts and lower basalts. Rhyolite originates in

the North and center of the volcanic region of Jima, occurring primarily to the west of the Gibe Gorge and forming a highland north of the line between Sodo and Bonga. They often grow abutting the lower Omo alluviae and are often bounded by fault.

Additionally, the lower basalts are exposed in the gorges of Gojeb and Gibe and also originate in the upper Gojeb and are prevalent in the highlands. The basin's southern portion is characterized by a central alluvial plain flanked primarily by pre-Cambrian basement rocks in the East and by tertiary volcanic in the west. The central Nyalabong Hills, which lie in the middle of the alluvial plain, is made up of Plio-Pleistocene basalts of small tufts, clay, silt, and sand. In the East, the hills adjoining the lower Omo alluvial plain are composed of siliceous gneisses and pre-Cambrian mafic basement with occasional granite outcrops. Such basement rocks are trending NW-SE and have undergone a high degree of metamorphism. In the west, the Maji Hills are made up of Jima basalts with irregular boulders of basement gneisses and ignimbrites, rhyolites, and Miocene age Surma basalts. The lower Omo alluvial plain primarily consists of Pleistocene-Holocene age and lacustrine alluviae of Holocene and undistinguishable fluvial tiles. These sediments are formed in the East and North of the Omo River. The sediments to the west of the Omo are primarily the deposition of clays, silts, and sands with some interstratified volcanic ash.

In an inclusive term, most of the northern catchments of the upper Omo-Gibe basin is under extensive cultivation with increased land pressure, meaning the expansion of cultivated areas into increasingly marginal lands. Deforested areas are now confined to areas too steep and inaccessible to farm. The flatter, poorer drained bottomlands of the northern catchments are usually not cultivated but are used for dry season grazing and eucalyptus tree plantations.

The eastern part of the basin has some of the most densely populated and intensively farmed areas in the country, let alone the basin. The main gorges of the basin are relatively unpopulated and support a cover of silvopastoral and silviculture. The south of the basin is

more sparsely populated with a greater population of natural vegetation, though even here, the forest is decimated at an alarming rate.

More detailed soil analyzes in the basin have concentrated on the potential of the Lower Omo Valley water system with some research on disintegration and conservation measures. During the study of the Omo-Gibe Integrated Development Master Plan, a thorough examination of the soil survey was carried out, especially in the upper part of the basin. Thus, in the analysis, based on the revised FAO-UNESCO-ISRIC legend, the four major soil groups were found in the basin, which are Alisols, Leptosols, Luvisols, and Vertisols (Figure 3.5). The dominant soil group in the UOGB is the Nitosols (33.4%), followed by Vertisols (22.17%) and Alisols (21.19%) (Table 3.1).

Table 3-1 Area coverage of the major soil types in the UOGB

Sl. No	Soil Types	Area (Km <sup>2</sup> )	%age cover
1	Alisols	7050.359	21.19
2	Leptosols	4808.751	14.45
3	Luvisols	2920.934	8.74
4	Nitosols	11115.319	33.40
5	Vertisols	7377.319	22.17
6	Water Body	3.640	0.01
Total		33,276.10	100%

According to the study of soil surveys in the basin, 25 soil units were determined in terms of current erosion and erosivity (depending on the structure, texture, slope, land cover, and available water capacity), land use, position in the landscape, morphology, fertility (general indication taking into account N%, OC%, pH, and Ppm).

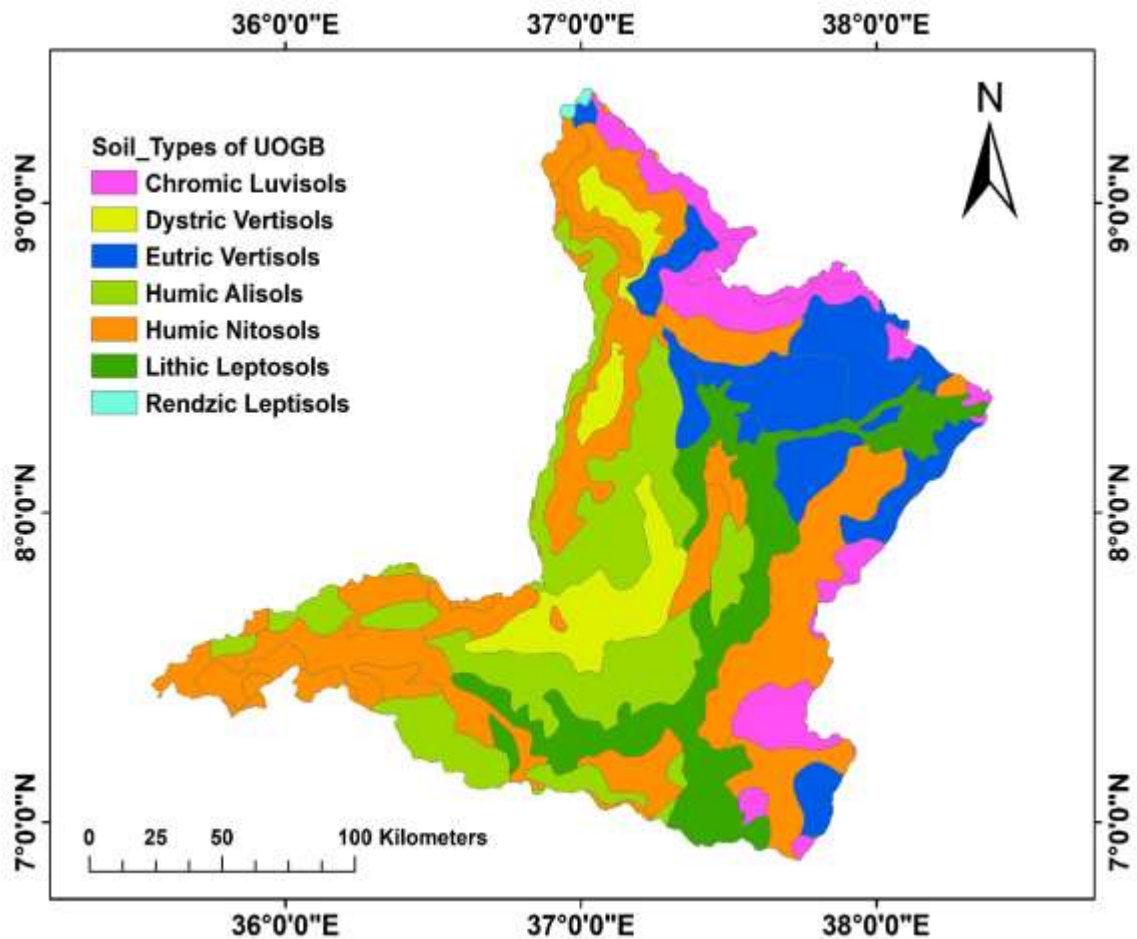


Figure 3-5 Major Soil types of the UOGB (FAO, 1998).

The majority of soils in the basin are reddish-brown, red, and medium to very low clay loams over clay (Soil Units 1, 5). The structure is somewhat weakly formed, indicating its young age, and the consistency is crumbly. These soils are non-calcareous and well-drained. They are common in the entire northern basin, which is gently undulating to the hilly topography from Sako in the North to Jinka in the south. These occur in conjunction with similar weakly developed soils vulnerable to erosion as in the Gurage region (Soil Unit 2), with shallower soils (Soil Units 10, 11) in hilly to mountainous areas and with less well-drained soils (Soil Units 7, 13, 14, and 16) in low-lying areas.

Soils formed from volcanic parent products, often with ash or pumice deposits, tend to occur on high ground within the basin. These are moderately deep to very deep, well-

drained, dark brown to dark reddish-brown sandy loams of clay, although most of them are typically clay loams. Structures again are low, leading to massive, with very friable topsoils over friable subsoil. They're non-calcareous. They occur on the northern boundary, from Gedo via Shenen to Wenchi Caldera, and are so prevalent on the western boundary south to Sodo. They also occur in the south of Jima around Chida and Ameya (Soil Units 4, 4a, 4b). They are well-drained, coarse-grained sandy loams to sandy clays of a large structure, yellowish-brown, moderately deep to very deep and crumbly consistency (Soil Units 17, 18). They are sandy loams over the clay, brownish and greyish in color, fairly deep to very deep and mottling. The soil structure is formed weakly too firmly, but often massively in subsoil with a crumbly to firm consistency (Soil Units 7, 12). They are generally correlated with better-drained upland soils (Soil Units 1, 6) while in the upper Basin, Soil Unit 12 is dominant in river levees.

Shallow soils (Soil Units 10, 11) exist across the basin, but they are most common in areas with low rainfall and steep slopes. They can be ranging from massive to highly organized and any color and texture. They are typically predominate in the southern mountains and basin gorges and well-to-excessively drained but often occur in combination with almost every other soil unit.

The presence of gilgai characterizes vertisols (Soil Units 8 and 9), a surface micro-relief feature, caused by the swelling and shrinking and slick sides of the soil profile, indicating the movement of peed faces against each other. They also occur in association with dominant shallow soils throughout the basin and other clay soils (Soil Unit 20) along the Omo River near Hana. They are also popular in the lower Omo plains where they occur in combination with poorly drained sodic clays (Soil Unit 25) and as minor inclusions in many other mapping units where low lying areas are poorly drained.

Alluvial and Colluvial soils of the lower Omo can be divided into those soils which are distinguished by their extremely heterogeneous existence in terms of texture, both vertically and laterally (Soil Units 19,21,22,23) and those who are more homogeneous (Soil Units 20, 24, 25).

The majority of the northern catchments of the basin is under extensive cultivation with expanded land pressure. The main gorges of the basin are comparatively unpopulated and support a Silvopastoral and Silviculture coverage; the eastern part of the basin has the most closely populated and intensively agricultural areas. The southern part of the basin is more lightly populated with a larger population of natural vegetation. A large portion of the basin is dominated by agricultural and Silvopastoral (Fig. 3.6).

The land uses of UOGB are agricultural, Silvicultural, Pastoral, water bodies, and urban areas where agricultural land is the dominant one, accounting for about 66.71% of the total area (Table 3.2). The dominant cereal crops grown in the basin are mainly Maize (*Zea mays* L.), wheat (*Triticum aestivum*), Teff (*Eragrostis tef*), barley (*Hordeum vulgare*), and Sorghum (*Sorghum bicolor*).

The Omo-Gibe River Basin has a number of tributaries from the NE, the main of which is the Wabi River and the Walga River. These rivers drain mostly from cultivated land with relatively impaired drainage. In the SW direction of the basin, the rivers Tunjo and Gilgel-Gibe are another important tributaries, which also drain mainly in agricultural land. Gilgel-Gibe and Tunjo sub-catchments have a higher proportion of permeable soil compared to Wabi and Walga sub-catchments.

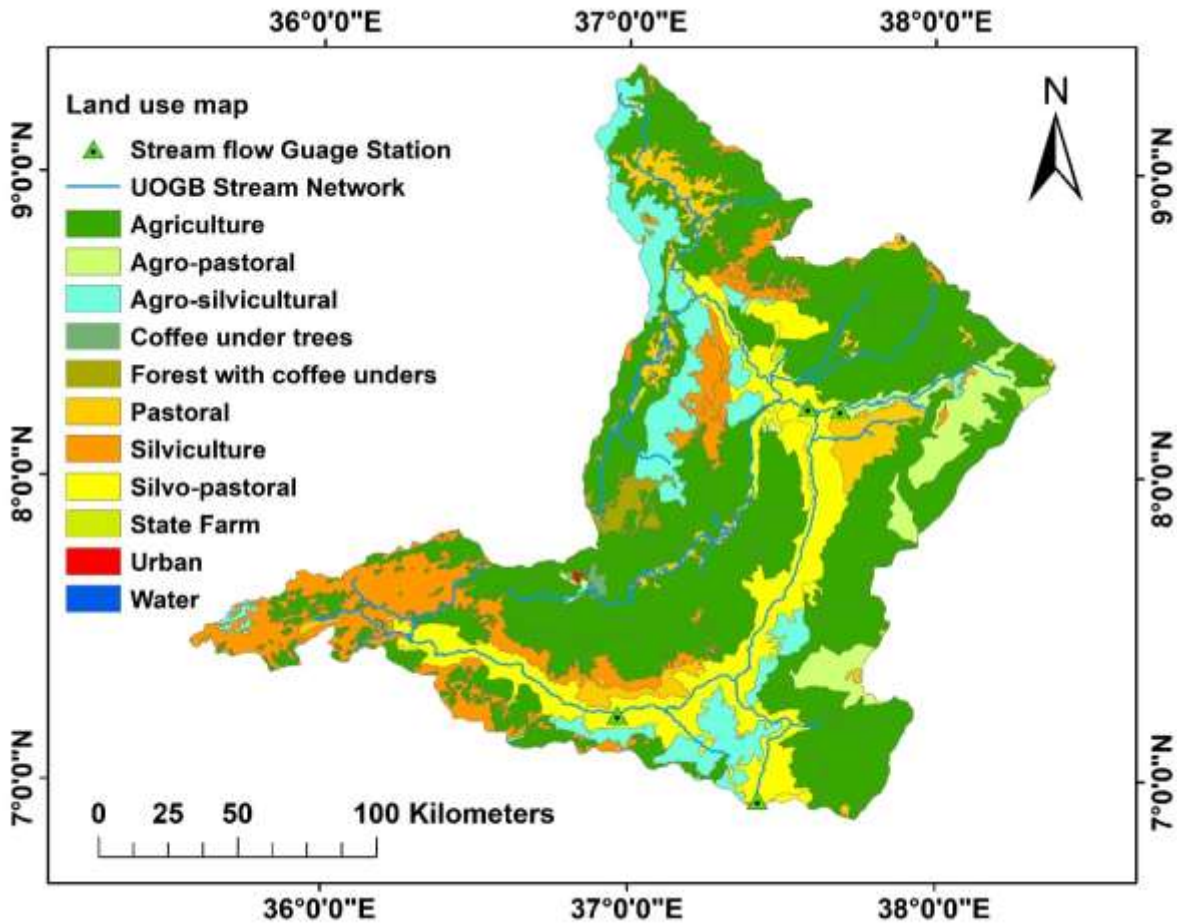


Figure 3-6 Land use types of the UOGB (MoWIE).

Table 3-2 Area coverage of the dominant land-use types in the UOGB

Sl. No	Land Use Types	Area (Km <sup>2</sup> )	%age cover
1	Agriculture	22197.32	66.71
2	Silviculture	8446.27	25.38
3	Pastoral	1908.92	5.74
4	Urban Areas	136.68	0.41
5	Forest	457.36	1.37
6	Water Body	129.25	0.39
Total		33,276.10	100%

### 3.6. Data used

In hydrological modelling, the key application of GIS is to define the direction of flow, the length of flow, the catchment area, the slope, and the aspect of a catchment and the delineation of streams and watersheds (Shrestha et al. 2014). For this research work, GIS application is used to investigate the patterns of the stream network and to delineate the landscape catchment area from 30 m by 30 m resolution DEM which is obtained from the USGS website. DEM defines the topography, which elucidates the altitude of any position in a given area at a particular spatial resolution. Additionally, the application is used to extract stream network features, the gradient of the slope, and the terrain slope length from DEM. The HBV hydrological model requires necessary spatial input datasets, which are hydrological data, meteorological data, and potential evaporation data. Whereas, the input data required for SEBS include the following: (1) remote sensing data (which all are estimated from daily or composite MODIS land products, such as leaf area index, surface temperature, surface albedo, land surface emissivity, and fractional vegetation cover); (2) measured meteorological data at reference height ( $Z_{oh}$ ) such as wind speed, air pressure, humidity, and air temperature; and (3) downward solar radiation, which can also be determined using empirical calculations, measured meteorological data, or remote sensing model outputs. The MODIS Level 1B data, which comprised visible and near-infrared bands 1–7, Near-Infrared bands 17–19, and thermal bands 31 and 32, were used to retrieve the necessary input parameters for the SEBS model. For the 23 meteorological stations for the period of 1980 to 2013, the required meteorological data were obtained from the National Meteorology Agency, Ethiopia (NMAE). Which encompassed daily records of rainfall, temperature (maximum and minimum), wind speed, relative humidity, solar radiation, and directions located in and around the Omo-Gibe basin. During this time the monthly, and daily discharge for the stream gauging stations for the Omo-Gibe basin have been obtained from the Ministry of Water, Irrigation, and Electricity (MoWIE, Ethiopia) department of hydrology. Also, 145 cloud-free MODIS imageries covering UOGB were acquired from <https://ladsweb.modaps.eosdis.nasa.gov/search/>.

Complete details of the various data used in the present study are provided in relevant chapters of this thesis.

### **3.7. Research Methodology**

A specific research methodology has been designed to achieve the objectives of this research work. This included water consumption and availability and the examination of multi-variable calibration in the upper Omo-Gibe basin, the implementation of the SEBS model through the incorporation of various input data into the GIS framework, and, finally, the simulation of the hydrological study in the basin. Figure 3.7 indicates the flow chart of the undertakings carried out in this study.

The following chapters of this study include a detailed explanation for these undertakings and a discussion of the results.

Next chapter discusses the quantification of consumption and availability of water in the basin under investigation.

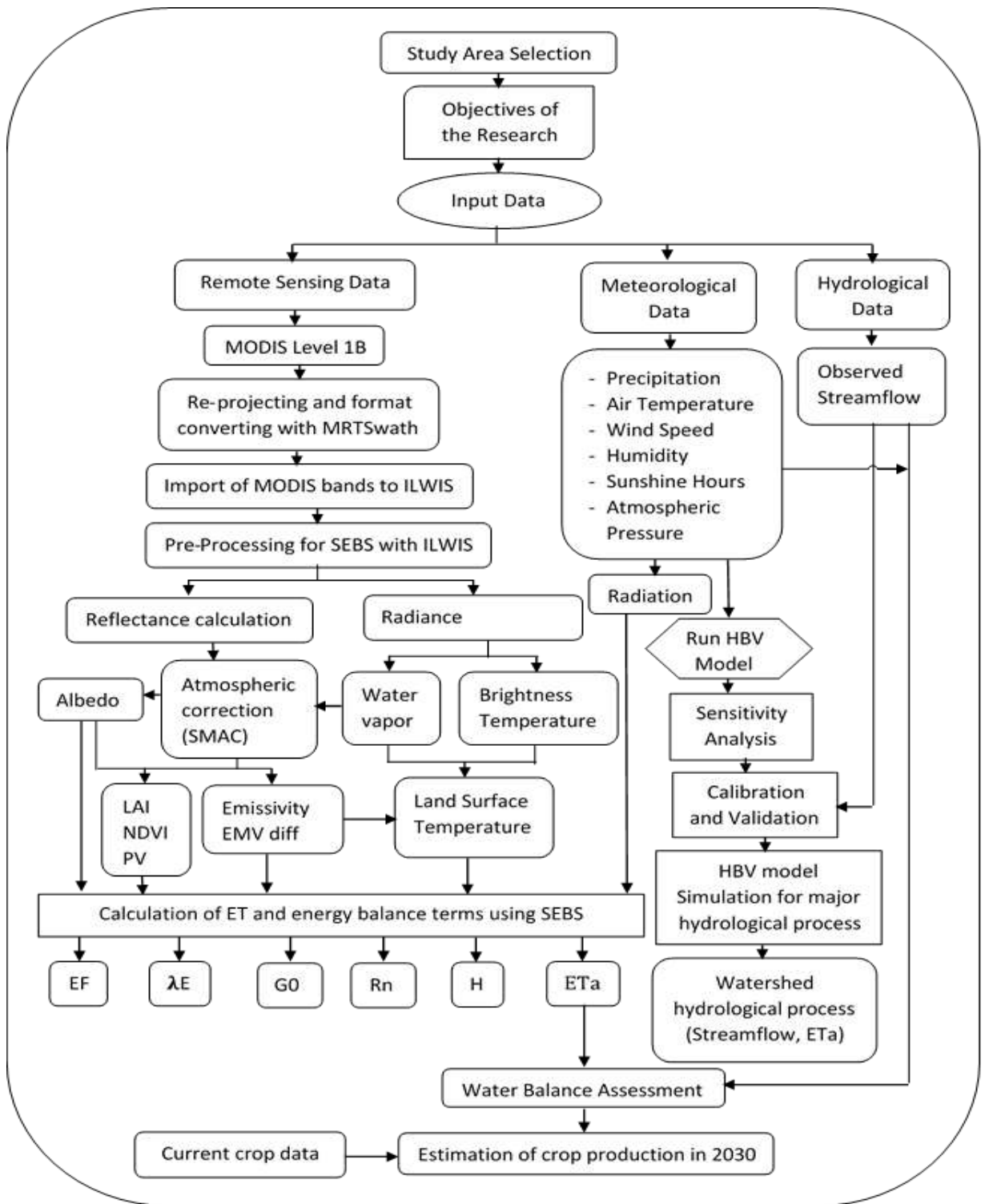


Figure 3-7 Research Methodological Framework of the Study.

## **CHAPTER 4: ASSESSMENT OF CONSUMPTION AND AVAILABILITY OF WATER**

### **4.1.Introduction**

Water resource scarcity is a hindrance to agricultural activities and sustainable development in various parts of the world. As discussed by Fraiture et al. (2003) and Rijsberman (2006), inadequate water resource causes a severe constraint on agricultural production, and this is especially important in arid and semi-arid regions of the earth. The scarcity of water is demonstrated by drainage ratio (it is defined as the ratio between the volume of water drained from an area to volume of water enter into the area) (Bos 2005). If the drainage ratio's value is between 0.0 and 0.1, it is called a very scarce area/region, whereas the value between 0.1 and 0.2 indicates water-scarce areas (Bos 2005). In such circumstances to gratify the demands for different water uses, effective water management is needed, and it requires certain spatiotemporal information on the availability and consumption of water. However, careful and sensible water resource management and planning are difficult due to lack of field information on the actual availability and water resource consumption. Furthermore, knowledge of all terms of water balance components is essential for effective water resource management to realize the hydrological system behavior.

The hydrological system is represented by a river basin, commonly described by natural and artificial units. These units are natural vegetation, rivers, municipalities, industrial parks, agricultural areas, etc. To realize the hydrological behavior of a river basin, it is essential to know the information about the water balance components. However, water balance estimation activities for given rivers, streams, agricultural areas, natural vegetation, and municipalities are complex tasks due to their physical appearances. The availability of water resources is affected by the process of evapotranspiration. Such processes are evaporation from open water bodies and bare soils and transpiration from crops, forests, native vegetation, weeds, and herbs. Apart from the nature of evaporating material, the process of evaporation is affected by spatiotemporal variation due to the

complication of physical characteristics and climatic conditions of evaporating material and soil water differences (Droogers and Bastiaanssen 2002). The limits set out in the above are relevant to the estimation procedures of the water balance components, which, in theory, should capture spatiotemporal variations in order to allow measurements of the water balance.

Numerous studies of water resource showed that actual evapotranspiration (ET<sub>a</sub>) is estimated as a residual in most practical water balance computations. The term 'residual' indicates that the surface parameter is not actually measured, but is derived remainder of energy balance (EB). This technique results in the EB toward the surface of land where ET<sub>a</sub> is determined as a residual of the EB approach (Roerink et al. 2000a). The ET<sub>a</sub> estimation is accurate if any shortcomings and weaknesses of the modelling process are hidden and are balanced by the estimated ET<sub>a</sub>. In watershed-scale streamflow model is calibrated by modifying the ET<sub>a</sub> (Domingo et al. 2001; Loukas et al. 2005). To correct the water stress, weather-based crop coefficient (K<sub>c</sub>) and reference evapotranspiration (ET<sub>0</sub>) are alternative approaches to estimate field specific ET<sub>a</sub>. The ET<sub>a</sub> estimation on an agricultural area is done by executing a crop classification on the area, which is covered by different crop types and crop development stages. Likewise, ET<sub>0</sub> is estimated for reference grass using measurement data taken from meteorological stations. Then, for each crop type, the K<sub>c</sub>, water stress coefficient (K<sub>s</sub>), and ET<sub>0</sub> values are multiplied by corresponding crop areas to provide the crop water use of the area.

More advanced field procedures for ET<sub>a</sub> estimations are the scintillation method and eddy correlation equipment (Hemakumara et al. 2003). However, there is a limitation on those two approaches due to point estimates, and the data is acquired only for few spatial variations, so ET<sub>a</sub> estimation is not determined for over large areas such as river basin. In such circumstances considering spatiotemporal variation effects of surface characteristics cannot be satisfied with the estimation of ET<sub>a</sub> over large areas (Ahmad et al. 2006). Furthermore, Bastiaanssen and Chandrapala (2003), Bandara (2003), Bos (2004), and Ahmad et al. (2009) demonstrated a more convenient ET<sub>a</sub> estimation over large spatial

domains by introducing a remote sensing approach which affords more advantages than conventional techniques. However, observation through satellite-based (SB) remote sensing methodology gives information over large areas. This approach permits a combination of hydrological indices in wide spatial coverage for the study period. These points of interest required the improvement of methodologies and calculations to estimate the spatially distributed ETa.

For water balance computations, it is significant to evaluate forms of spatiotemporal variability of rainfall. Precise evaluations of spatiotemporal variations in rainfall spreading require a dense network of rain gauge stations with a minimum period of one-day recording precipitation. Since recorded information indicates observations at a point scale, spatial interpolation strategies on land at spatial coverage are desired. The precipitation information is collected over the selected period, and a typical Thiessen polygon interpolation technique is used to measure rainfall coverage in the study area.

Many researchers applied Surface Energy Balance System (SEBS) for ETa estimation (Kurkura 2011; Rwasoka et al. 2011; Matinfar and Soorghali 2014; Samboko 2016; Ncube et al. 2016) in different parts of the world. It is also applied for drought monitoring (Su et al. 2003) and sensible heat flux estimation (Jia et al. 2003). To our knowledge of proper management of agricultural activities in Ethiopia, there is very little knowledge of water availability and consumption. It is not practically feasible to use other conventional methods of ETa projection because of the larger area of the basin.

In the present study, the Thiessen polygon interpolation approach is used to examine the spatial rainfall coverage in the upper Omo-Gibe basin at the sub-basin scale. In addition, the ETa is estimated using the Surface Energy Balance System (SEBS) adopted from (Su 2002) to assess the water consumption in the study area. To examine the monthly time steps of availability and utilization of water, the spatiotemporal variation of precipitation and ETa estimation were employed.

## **4.2. Methodology**

### **4.2.1 Precipitation**

Daily records of meteorological data were obtained from the National Meteorological Agency of Ethiopia (NMAE) for the 23 selected rain gauge stations from 1980-2013 within or near the upper Omo-Gibe basin. In this study, daily rainfall, daily temperature, and average daily wind speed for the selected station and monthly discharge for the stream gauging station were collected. These data were used to estimate the spatial and temporal variations of actual evapotranspiration and precipitation. Summaries of the meteorological station along with its coordinates, elevations, and measured mean annual basin rainfall for 34 years are shown in Appendix 1. Fig. 4.1 indicates the location of the selected rain gauge station. Most of the northern portion of the study area is in the mountains, and the terrain is difficult, so it is impossible to track orographic precipitation. Similarly, the meteorological stations are sparse and lie at comparatively flat locations.

### **4.2.2. Data Quality and Homogeneity Testing**

Precipitation quality assessment is a crucial preliminary step in the use of weather data for further hydrological analysis. In this analysis, a particular focus was placed on quality control and data set collection. In view of that, a first selection was made across all available stations prior to further regulation of data quality and homogeneity in order to ensure continuity across the station networks. The daily recorded weather data from the twenty-three meteorological stations for the period of 1980 to 2013, is obtained by the National Meteorological Agency of Ethiopia, were checked for homogeneity.

The data were selected from the twenty-three weather stations based on the significant combination of standards related to homogeneity, consistency, and length of data and the spatial distribution of the series over the upper Omo-Gibe basin. Some weather record stations have incomplete records; thus, only stations with less than 3% of missing values have been used. Any given month and year was considered to be full if no more than three days, and no more than 15 days, respectively, were missing. Basic quality controls have

been applied to all weather stations with the goal of detecting data errors; daily data has been checked for outliers (anomaly values).

The daily precipitation data were organized and sorted in the Excel sheet and tested for homogeneity using the standard normal homogeneity test called RAINBOW (which is a software package for analyzing hydrologic data) (Raes et al. 2006). The application is designed to perform a frequency analysis of rainfall and evaporation data and to check the homogeneity of hydrological records. For frequency analysis, data need to be homogeneous and independent. The constraint of homogeneity guarantees that the measured data are from the same population. RAINBOW provides a homogeneity test that is based on average deviations from the mean and also conducts statistical tests to assess if the results match a certain distribution. The homogeneity of time series data is checked by appraising the average and the distribution of cumulative mean deviations (Raes et al. 2006). RAINBOW also enables the study of time series of zero or near zero events (the so-called null values) by separating the null values temporarily from the non-null values. In this analysis, the data series from the twenty-three weather stations in the upper Omo-Gibe basin were found to be homogeneous. A detailed analysis of the data showed that the total missing data for all stations was approximately 0.13% for the period 1980 to 2013. In order to fill out the missing precipitation data during this analysis, a well-known technique known as the inverse distance weighting method has been used, based on data from a variety of neighboring stations. The locations of these neighboring stations are so close to and approximately evenly spaced around the site with the missing data.

Within and around a particular precipitation gage, there can often be major physical adjustments at a station. Such adjustment of stations in a given year would start affecting rain gauge data being recorded from that particular station. After a number of years, it may be felt that the station's data do not provide consistent rainfall values. In order to test any such inconsistency, a procedure called a double mass curve approach is widely used to correct and adjust the observed precipitation values (Garg 2005; Wang et al. 2013). In this method, to construct a double mass curve, a doubtful station with 5 to 10 neighboring stations are selected in and around the basin. The annual rainfall values recorded by the

doubtful station are serial for each year against these values. Such annual rainfall values of the doubtful stations are serially ordered in reverse chronological order. Moreover, the average annual rainfall values for the surrounding stations are determined on the basis of the annual rainfall values recorded from the serial of this group of stations for each consecutive year. The cumulative values for both columns are then worked out. According to the result, the three stations, namely Durame, Hosana, and Indibir, showed inconsistency. Due to the occurrence of inconsistency, corrections have been made on the recorded rainfall data at these three stations. Therefore, all the stations have been used for hydrological and simulation purposes.

***Thiessen polygon (TP) approach***

For spatial distribution of precipitation (P) estimation in the basin, the Thiessen polygon (TP) approach was used for interpolating the values between points. TP is chosen because it is straightforward and simple. The TP approach assumes that the estimated values of precipitation at any point on the basin are the same as those of the observed values at the closest station. This approach requires the construction of a TP network. The perpendicular bisectors make these polygons of the lines connecting nearby rain gauges stations. Hence, every polygon contains only one rain gauge, and areas of their corresponding regions are the weights of the corresponding rain gauges. The total rainfall (RT) for each sub-basin is calculated by Equation 4.1.

$$R_T = \frac{R_1A_1 + R_2A_2 + \dots + R_nA_n}{A_T} = \frac{1}{A_T} \sum_{i=1}^n R_iA_i \quad 4.1$$

where  $R_T$  is the total precipitation in the sub-catchment;  $R_i$  and  $A_i$  have measured precipitation and associated area of Thiessen polygon for the station  $i$ , respectively; and  $A_T$  is the total area of the sub-basin. Details of the selected meteorological station for upper Omo-Gibe basin are shown in Appendix 1.

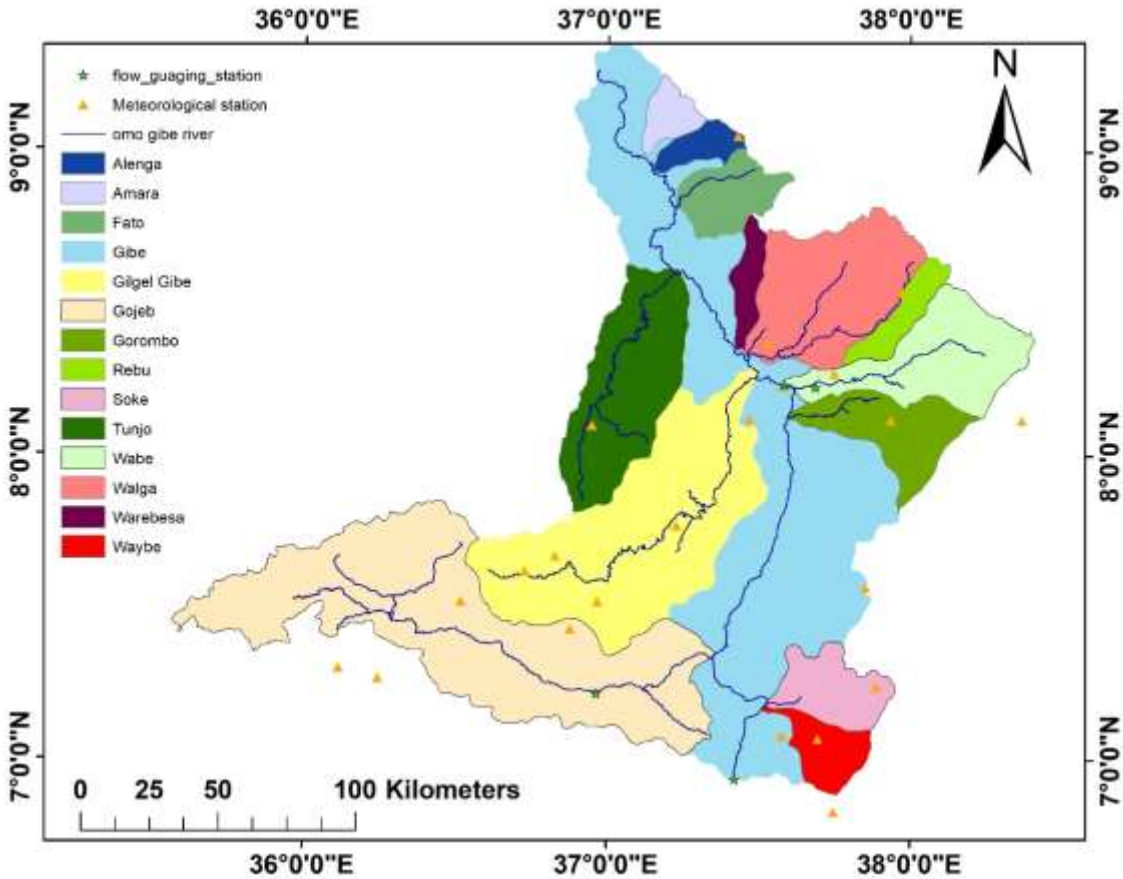


Figure 4-1 location of selected rain gauges station for upper Omo-gibe basin

#### 4.2.3. Actual Evapotranspiration

In this study, the Surface Energy Balance System (SEBS) proposed by (Su 2002) was used to estimate ETa. SEBS was established to resolve the energy balance by combining remote sensing data in the near, visible, and thermal infrared bands and meteorological data from ground measurements (Chapter 2, section 2.4). The input data required for the surface energy balance system includes (1) remote sensing data (which all are estimated, such as leaf area index, surface temperature, surface albedo, land surface emissivity and fractional vegetation cover, (2) measured meteorological data at reference height ( $Z_{oh}$ ) such as wind speed, air pressure, humidity, and air temperature and (3) downward solar radiation. In the agricultural area, momentum roughness length ( $Z_{om}$ ) is used to determine  $Z_{oh}$  as adapted from Allen et al. (2007). Likewise, the downward solar radiation can also be determined

using empirical calculations, measured meteorological data, or remote sensing model outputs. Figure 3.2 shows the flow chart of the SEBS model. SEBS comprises numerous distinct modules to estimate the net radiation, soil heat flux, and the partitioning of available energy into sensible and latent heat fluxes. The equation of surface energy balance is stated in chapter 2 (Equation 2.1)

The daily net radiation computation primarily depends on the daily incoming extraterrestrial solar radiation, atmospheric transmittance, and surface albedo in the given equation. Furthermore, the SEBS model has the benefit of using each of the bulk Atmospheric Similarity (BAS) (Brutsaert 1999) and the Monin–Obukhov Atmospheric surface Layer (MASL). Both can be utilized for regional and conventional scale estimates of the turbulent fluxes. As discussed by Su (2002), SEBS was applied in determining the evaporative fraction (EF) at a wet and dry limits conditions using the energy balance (EB) equation. Accordingly, EF is defined as the proportion between latent energy and the available energy of the region. At the wet limit condition, the ET occurs at the potential rate and to compute the sensible heat flux, a parameterization based on Penman-Monteith (Monteith 1981) is primarily utilized. At the wet limit, the internal resistance in the Penman-Monteith is considered zero (0). Likewise, at the dry limit condition, the latent heat flux is set to be zero, and the maximum sensible heat flux value equals the available energy because of limitation of soil moisture.

Daily net radiation is determined mainly on the basis of surface albedo, daily atmospheric transmission, and daily incoming extraterrestrial solar radiation. Daily evapotranspiration is estimated from the total daily available energy by assuming that the evaporative fraction (EF) is constant during the day. Shuttleworth et al. (1989) revealed the constancy of the evaporative fraction during the daylight hours. They analyzed records from four clear days of the sky over relatively homogeneous grasslands. They also found that the evaporative fraction of the noon is almost equal to the regular sunlight hour's evaporative fraction. Nichols and Cuenca (1993) used seventy-two days of records and reported that the noon evaporative fraction was significantly associated with the average evaporative fraction of

daylight. The assumption of a constant evaporative fraction over a day is also used to estimate actual evapotranspiration (Farah et al. 2004; Akbari et al. 2007).

The equation developed by Bastiaanssen et al. (2002) for over a month, year, or season time integration is adopted (Equation 4.2) for ETa estimation in the upper Omo-Gibe basin.

$$ET_{aint} = \frac{8.64 \times 10^7 * dt}{\lambda \rho_w} * EF * R_{n24t} \quad (4.2)$$

where,  $ET_{aint}$  (mm/day) and  $R_{n24t}$  ( $W/m^2$ ) are the actual evapotranspiration and values of mean net radiation, respectively for the time interval  $dt$ ;  $EF$  is the evaporative fraction;  $\lambda$  is the latent heat of vaporization ( $J/Kg$ ) and  $\rho_w$  is the density of water ( $Kg/m^3$ ).

### 4.3 Results and Discussion

#### 4.3.1 Spatial and Temporal Variability of Precipitation

##### Temporal Variability of Precipitation

To examine the temporal change of hydro-meteorological variables, evaluation has been done at decadal intervals for monthly average values. Spatiotemporal variability analyzes of hydro-meteorological factors are critical for further understanding of hydrological methods and hydro-meteorological modelling. Historically, temporal variability has been quantitatively characterized using a coefficient of variation, which is mainly based on statistics. The calculated annual coefficient of variation (CV) values of rainfall range from 0.12 to 0.23. Figure 4.2, shows that the yearly mean variety of rainfall using selected meteorological stations within and near the basin. Generally, the CV value is low in the upper Omo-Gibe basin. The result indicates that there is an insignificant temporal variation in the basin. Based on the calculated CV value of annual rainfall for the given meteorological station, an interpolated CV map was formed for the upper Omo-Gibe basin (Fig. 4.3).

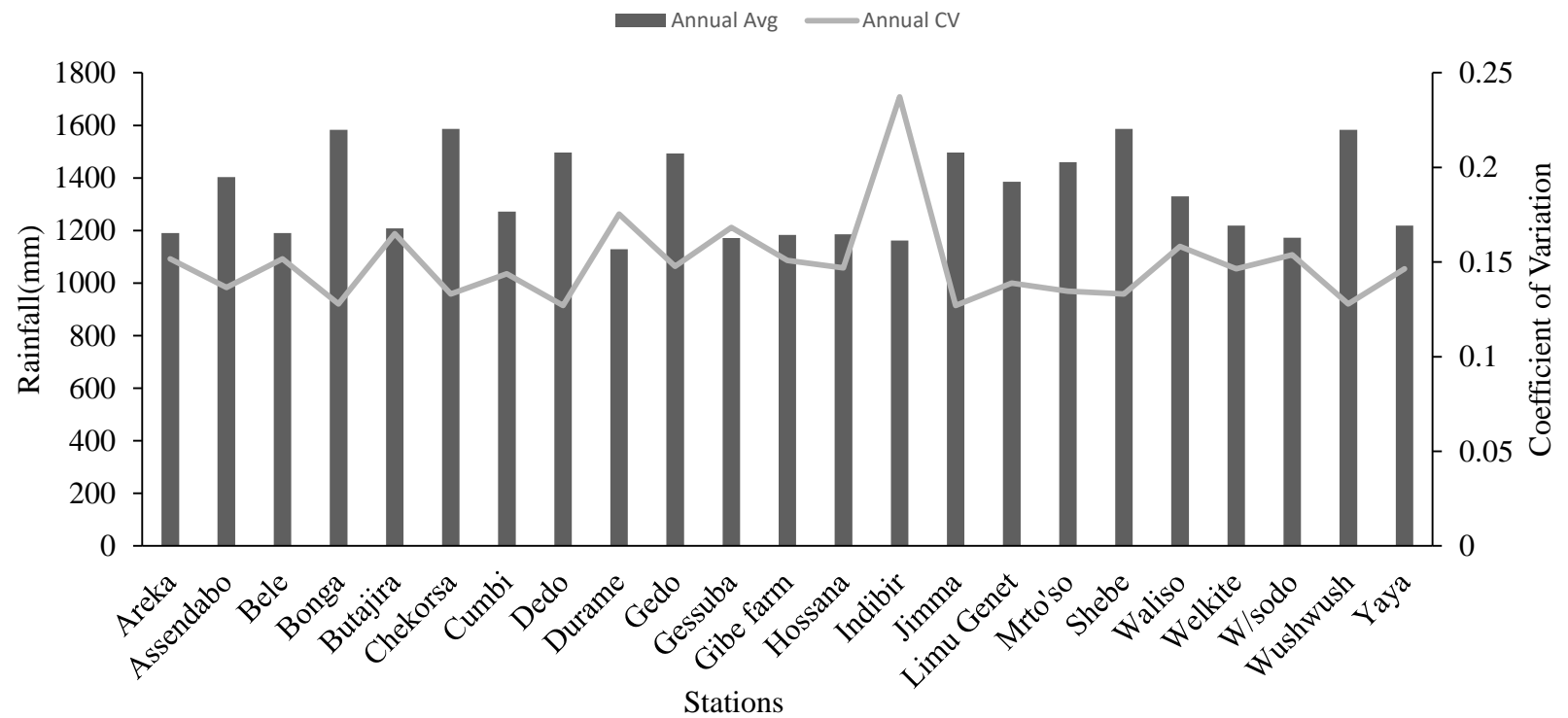


Figure 4-2 Mean Annual rainfall and annual coefficient of Variation for the selected meteorological station in the Basin

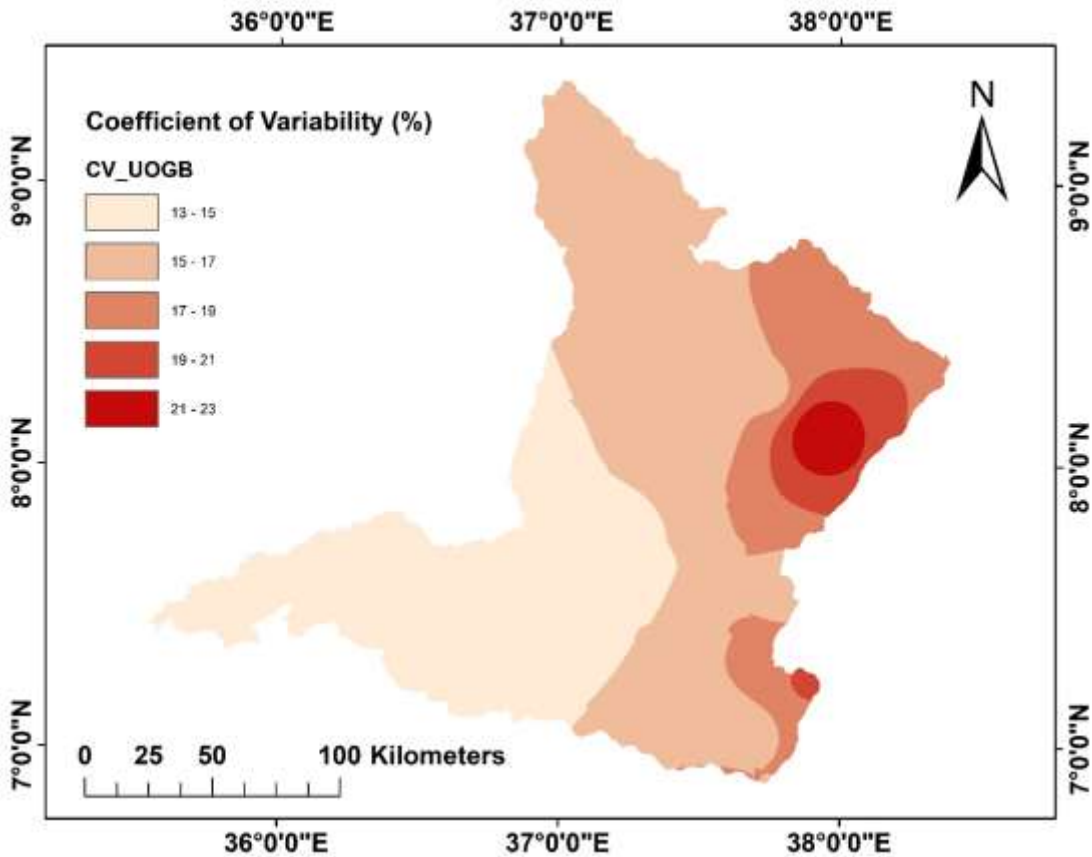


Figure 4-3 Coefficient of Variation for the selected meteorological station in the basin

From the Fig. 4-3, it can be seen that rainfall is highly variable in the Eastern portion of the basin. In contrast, the inter-annual variability of rainfall is less variable in the Western portion of the basin, which has the highest values of precipitation in comparison with other parts of the basin. Also, moderate variability is noticed in the remaining regions. In general, the inter-annual rainfall variability gradually reduces from East to West.

The seasonal pattern in the basin has somewhere unimodal as well as Bimodal rainfall characteristics. The unimodal rainfall is dominant in the basin, with a major peak rainfall value of 310.7 mm at Gedo station (from July to August months). The bimodal rainfall was also found in the Eastern portion of the basin with one major and one minor season (Fig. 4.4).

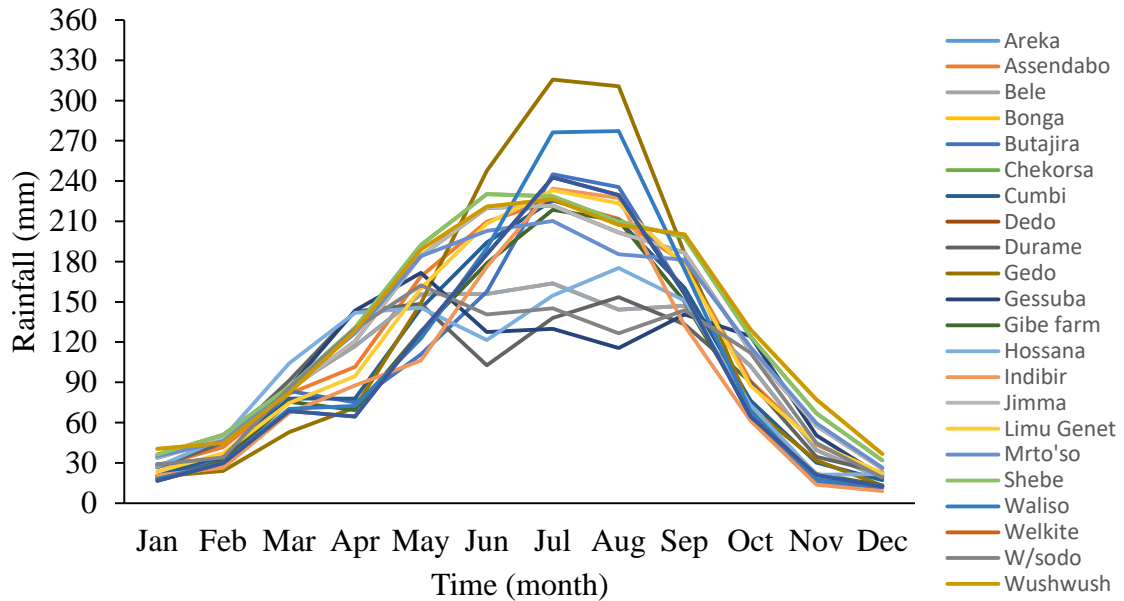


Figure 4-4 Seasonal rainfall distribution of upper Omo-gibe basin.

### Spatial Variability of Precipitation

The spatial yearly rainfall analysis for the period of 1980 to 2013 was conducted using precipitation records collected from 23 rain gauge stations in the UOGB with a maximum and minimum annual rainfall values of 59,952 and 36,494  $Mm^3/year$ , respectively. The duration of November 2003 to October 2004 was considered as a study period because of the lack of readily available streamflow data in the basin. In order to determine the annual rainfall quantity of the study period, four categories were made at an interval of 5000  $Mm^3$  each starting from 35,000  $Mm^3$  onwards from the collected maximum and the minimum rainfall values of the 1980 to 2013 years. Accordingly, nearly a total of 13 years of rainfall data, fall within the range of 40,000 to 45,000  $Mm^3$  (Fig. 4.5). Hence, the UOGB has received an annual rainfall value of 41,080  $Mm^3$  during the selected study period. Moreover, the rain gauge stations have also received a minimum and maximum rainfall values ranging from 1019 to 1,439 mm, respectively, during the study period (Fig.4.6).

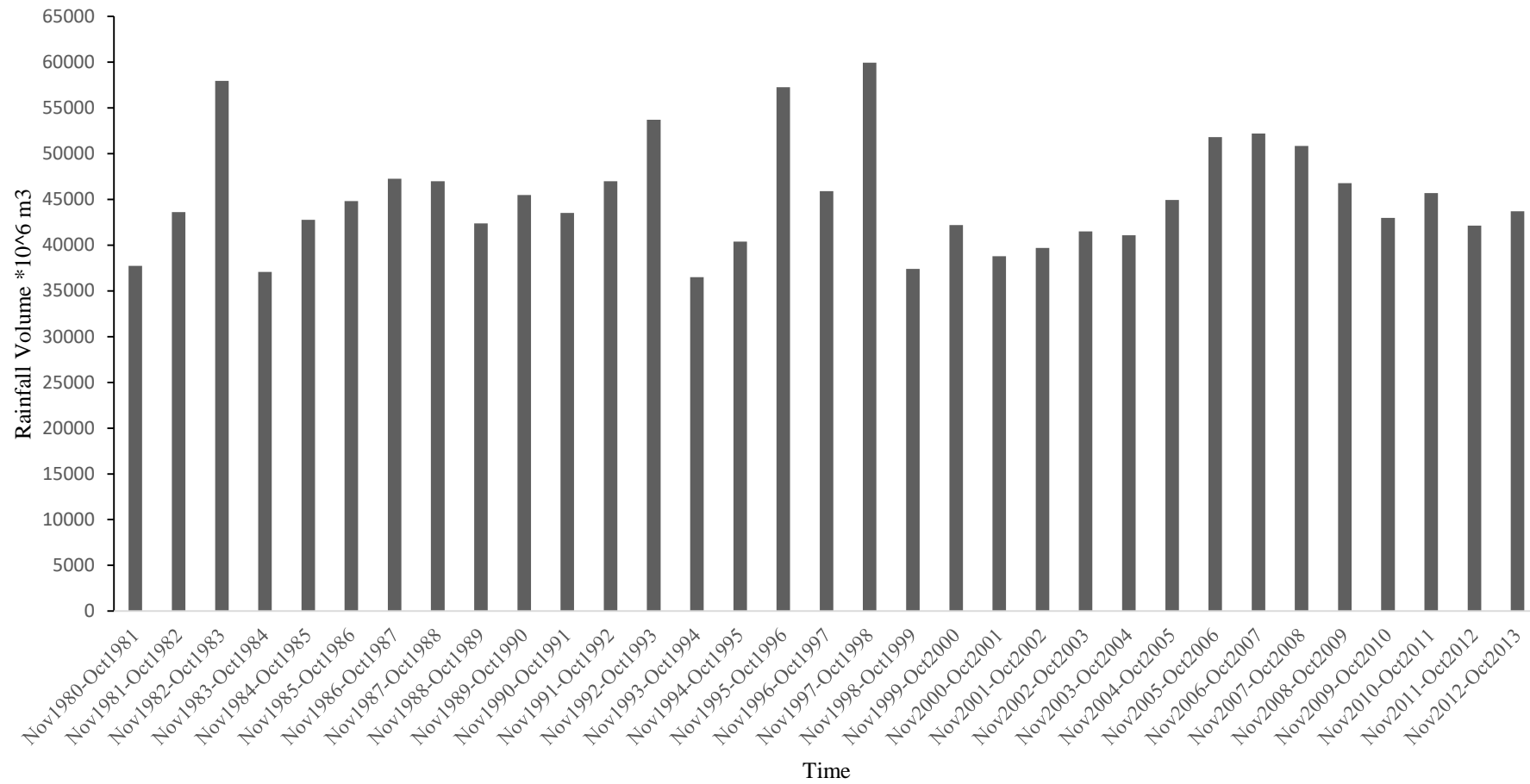


Figure 4-5 Rainfall volume for the study area from Nov1980- Oct 2013

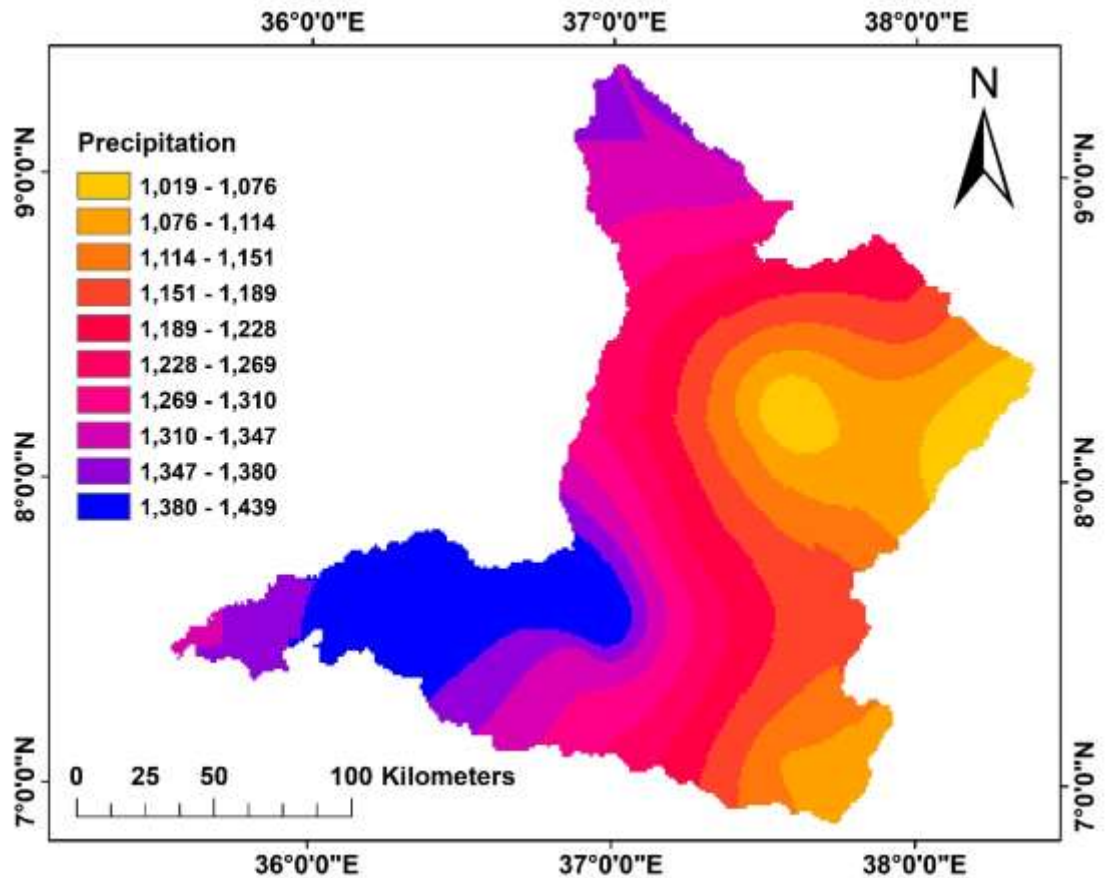


Figure 4-6 Spatial distribution of annual precipitation in the upper Omo-Gibe basin from November 2003 to October 2004

Significant spatial rainfall variation was observed in the upper Omo-Gibe basin for the given study period, as shown in Table 4.1. As such, a result of monthly precipitation volumes at the sub-catchment scale is presented in Fig. 4.7. These rainfall values were converted to volumes to permit for water balance calculation. Due to considerable climatic and topographic changes in the study area, water balance estimations at a monthly time step are considered the most important task in determining spatial rainfall variability in each sub-catchment.

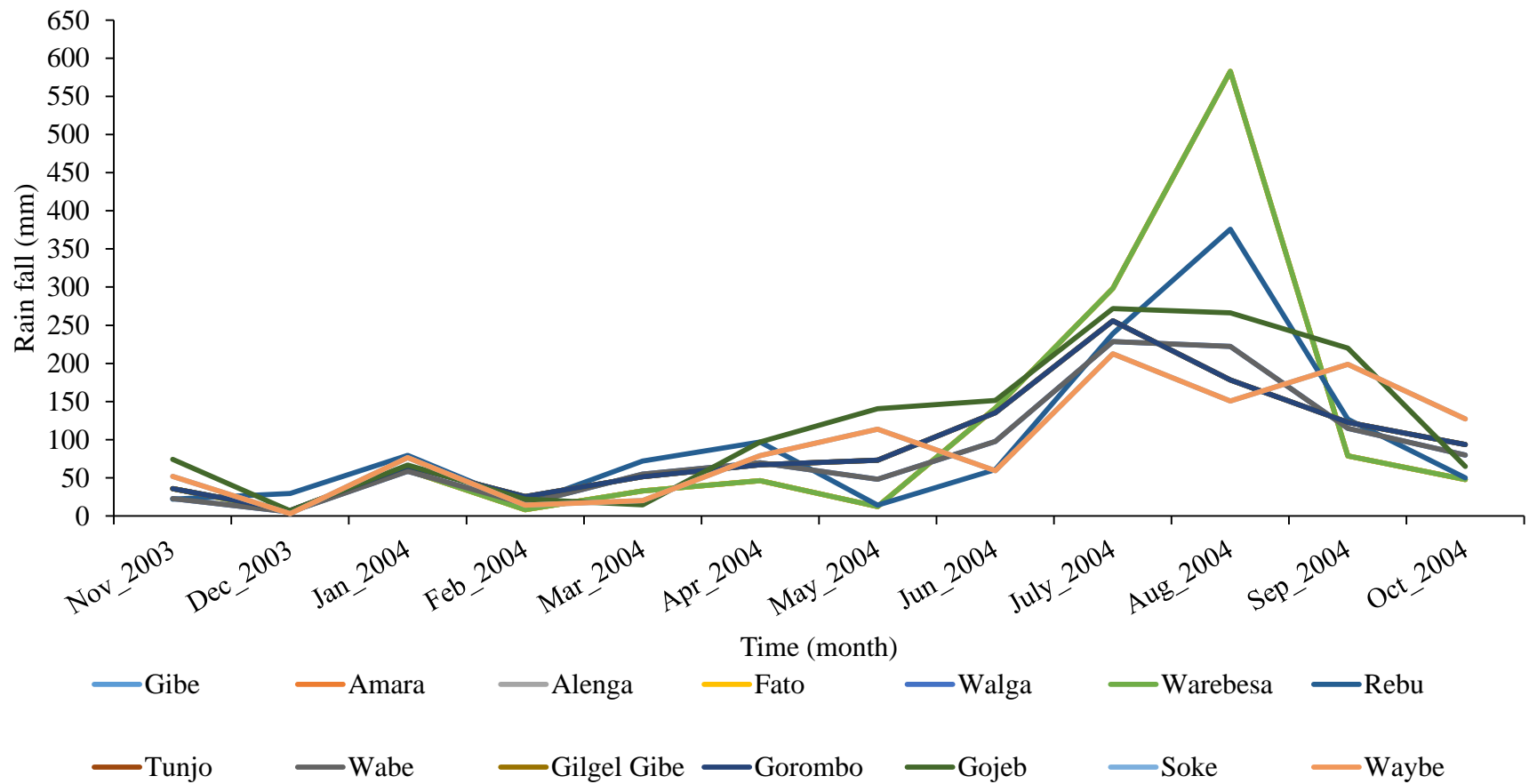


Figure 4-7 Variation of monthly precipitation volumes (mm) in the upper Omo-Gibe sub-catchments for the period of November 2003 to October 2004

Table 4-1 Variation of monthly precipitation volumes (Mm<sup>3</sup>) in the upper Omo-Gibe sub-catchments for the study period

Sub-Catchment	Area (Km <sup>2</sup> )	Nov	Dec	Jan	Feb	Mar	Apr	May	Jun	July	Aug	Sep	Oct	Sum
Gibe	9247	325	49	661	152	435	797	634	1055	2141	2564	1328	801	10942
Amara	353	13	2	21	3	12	16	4	50	105	206	28	17	477
Alenga	342	12	2	21	3	11	16	4	48	102	200	27	16	462
Fato	810	29	5	49	7	27	37	10	115	242	472	64	39	1094
Walga	2461	55	39	172	45	162	191	64	186	617	844	264	146	2784
Warebesa	372	9	2	23	7	22	23	12	35	98	129	34	24	417
Rebu	481	11	11	36	8	33	42	10	33	118	173	56	26	556
Tunjo	2460	109	16	138	54	100	156	239	460	675	551	350	250	3099
Wabe	1943	30	39	116	29	139	160	58	151	430	568	242	146	2107
Gilgel Gibe	5152	376	40	403	115	142	456	485	816	1297	1086	958	532	6707
Gorombo	1221	8	18	49	14	50	76	57	124	294	327	186	118	1321
Gojeb	6932	606	73	628	177	103	724	994	755	1706	1610	1536	538	9451
Soke	901	43	8	78	19	34	115	88	51	169	126	142	124	998
Waybe	600	31	2	46	9	12	47	68	36	128	90	119	76	665
Sum	33,276	1,658	306	2,441	642	1,281	2,858	2,729	3,912	8,122	8,945	5,333	2,853	41,080

### 4.3.2 Actual Evapotranspiration

MODIS Level 1B (MOD021KM) satellite data with their corresponding geo-location files (MOD03) and daily temporal and spatial resolution of 1 km<sup>2</sup> were collected by the Terra (EOS AM) satellite in the MODIS sensor launched in December 1999 (Table 4. 2). These data were used to estimate the daily ETa for the study period starting from November 2003 to October 2004 in UOGB. For the estimation of monthly and annual ETa, the evaporative fractions calculated for days of the satellite overpasses have been taken into account as being representative for defined time periods. Accordingly, a representative evaporative fraction was calculated using the energy balance equation for each day of satellite overpass for a selected consecutive duration of 2 to 35 days with a verified and validated cloud-free images. Those durations were selected based on a set of NOAA-AVHRR images for cumulative time estimates of ETa (Bastiaanssen et al. 2002). Their procedure was validated by a set of ETa values as determined by the Bowen ratio method. In the present study, a similar satellite image duration (i.e., 2 to the 35-day range) was considered in the upper Omo-Gibe basin except for one image (out of range at the 47<sup>th</sup> day) which is taken in the month of August and fall in the rainy season. Following the procedures outlined in the methodology part of this paper, the spatial distribution of the yearly ETa map was developed. Thus, the soil moisture dynamics and indirect precipitation events control long-term seasonal fluctuations of the evaporative fraction (Farah et al. 2004). Therefore, the assumption of a representative evaporative fraction over this period can be reasonably as acceptable due to the fact that major changes in soil moisture are not anticipated at any point in the rainy season. Following the procedures outlined in the methodology part of this thesis (section 3.5), the spatial distribution of the yearly ETa map was developed (Fig. 4.8).

Table 4-2 Acquisition dates of TERRA-MODIS images from November 2003 to October 2004 for upper Omo-Gibe basin (source: <http://ladsweb.modaps.eosdis.nasa.gov/>)

Year	Jan	Feb	Mar	Apr	May	Jun	Jul	Aug	Sep	Oct	Nov	Dec
2003											01	03
2004	04	05	08	09, 25	11, 27	12, 28	14	31	16	02, 18		

Due to complete cloud cover for 28 days in the MODIS Level 1B data, it was impossible to generate a continuous daily ET data set for the period 1<sup>st</sup> November 2003 to 31<sup>st</sup> December 2004 using SEBS estimates of ETa. In this study for time integration over a month, the linear interpolation technique by (Muhammed 2012) is used

$$ET_2 = \left( \frac{ET_3 - ET_1}{X_3 - X_1} \right) (X_2 - X_1) + ET_1 \quad 4.2$$

Where,  $ET_2$  is the unknown daily ET value (mm/d);  $ET_1$  is the first known daily ET value (mm/d);  $ET_3$  is the next known daily ET value (mm/d);  $X_1$  is the Julian day for  $ET_1$ ;  $X_2$  is the Julian day for  $ET_2$  and  $X_3$  is the Julian day for  $ET_3$ .

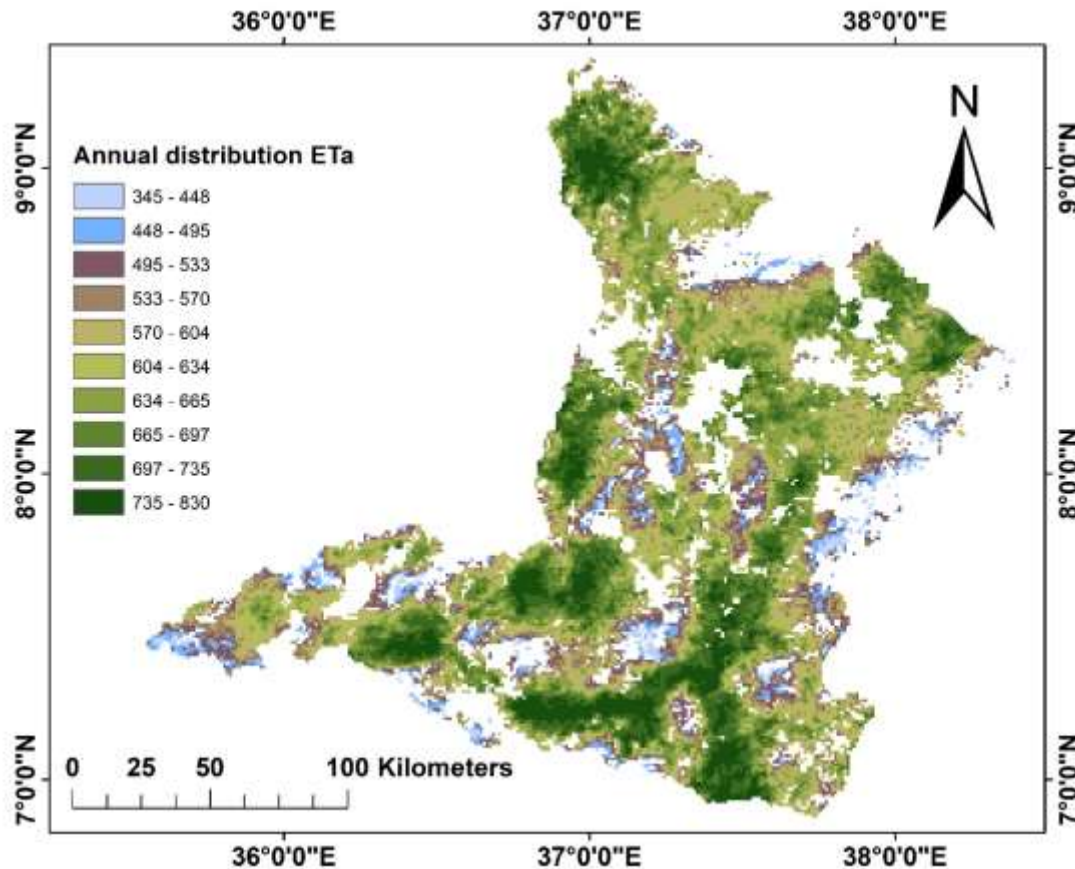


Figure 4-8 Spatial Distribution of annual ETa in the upper Omo-Gibe basin for the study period

Figure 4.8 shows that the spatial distribution of the annual ETa values for the study duration and is varying between 345 and 830 mm. At the sub-catchment scale, spatiotemporal variations of monthly ETa are shown in Fig. 4.9 and Table 4.3.

In general, the highest monthly ETa values are observed during the months April to October, which indicates an overall growing period of rainfed crops like wheat, barley, teff, maize, etc. The period between April to June called the Belge period and is the cropping period for Maize crops only. The analysis also indicated that ETa is high during summer months, called Kiremt, this is mainly due to water supply by a stream, and it is also the main growing period for all crops.

The land use map shown in Figure 3-6 has been used to select various land uses. However, due to the spatial resolution of MODIS data (1km<sup>2</sup>) and the distributed nature of land use in some parts of the basin, due to the phenomenon of mixed pixels it was not possible to avoid. For this reason, ETa was determined for mixed pixels, as it was not possible to extract ETa for each land use present in such pixels (McCabe and Wood 2006). It should be remembered that these considerations constrain the estimation of ETa for particular land use. However, it is possible to distinguish homogeneous pixels due to the presence of agricultural areas and forests.

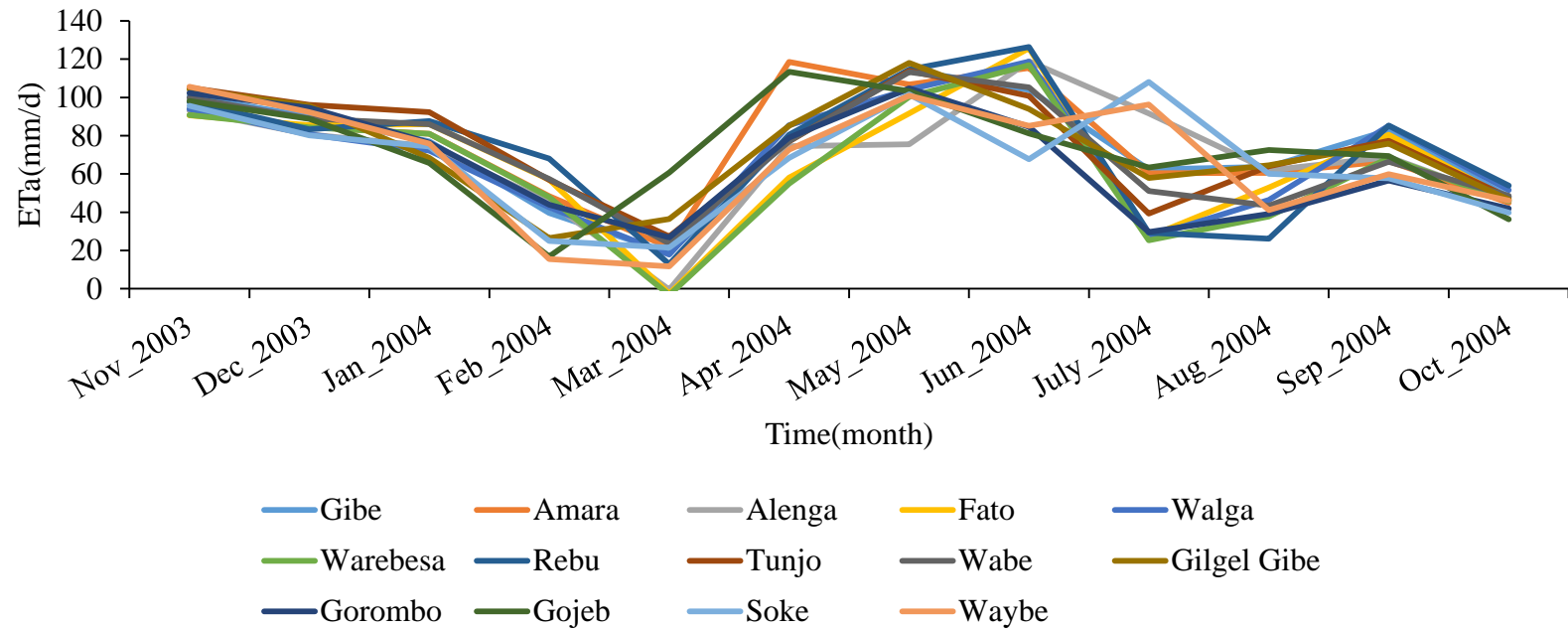


Figure 4-9 Variation of monthly evapotranspiration volumes (mm/d) in the upper Omo-Gibe sub-catchments for the period November 2003 to October 2004

Table 4-3 Variation of monthly evapotranspiration volumes (Mm3) in the upper Omo-Gibe sub-catchments for the study period

Sub-catch	Area (km2)	Nov	Dec	Jan	Feb	Mar	Apr	May	Jun	July	Aug	Sep	Oct	Sum
Gibe	9247	367	127	531	211	268	605	600	862	1010	1124	765	619	7089
Amara	353	13	6	18	10	8	18	21	32	69	21	25	19	260
Alenga	342	13	6	17	9	5	12	14	21	65	22	26	19	229
Fato	810	30	14	43	24	9	23	43	84	104	40	69	47	530
Walga	2461	93	43	114	60	46	96	139	132	402	101	205	143	1574
Warebesa	372	13	6	19	10	4	10	16	19	11	16	28	20	172
Rebu	481	19	8	26	15	8	18	31	28	13	15	44	31	256
Tunjo	2460	101	48	132	68	47	95	180	244	445	147	202	141	1850
Wabe	1943	77	36	101	54	36	100	109	108	210	90	126	98	1145
Gilgel Gibe	5152	209	100	213	94	115	383	364	603	604	426	408	389	3908
Gorombo	1221	49	23	56	28	22	38	59	76	132	60	68	53	664
Gojeb	6932	520	127	253	97	216	568	881	365	898	796	483	317	5521
Soke	901	34	16	39	16	17	57	84	41	94	51	62	47	558
Waybe	600	25	12	26	10	9	18	58	34	69	26	58	34	379
Sum	33276	1563	572	1588	706	810	2041	2599	2649	4126	2935	2569	1977	24135

### 4.3.3 Comparison of SEBS ETa to Other Methods

Due to non-availability of instruments (like Bowen ratio or weighing lysimeters and eddy covariance) to directly measure ETa, the estimated SEBS daily ETa value were compared with a reference evapotranspiration (ET<sub>0</sub>) value determined by the Penman-Monteith method (Allen et al. 1998). The fundamental concept was to confirm the values of the estimated SEBS-ETa with Penman-Monteith in order to evaluate the spatial and temporal distribution of ETa in the study basin. In addition, the ET<sub>0</sub> outcomes were verified by sub-catchment scale water balance analysis. Numerous studies show that satellite-based ETa has been compared to point estimations of ET<sub>0</sub> (Koloskov et al. 2007; Muthuwatta et al. 2010; Esmaeilabadi 2014; Shoko et al. 2015; Samboko 2016). In this study, a pixel ETa values close to Assendabo meteorological station in the Gibe sub-catchment is compared to the values of ET<sub>0</sub> in that station (Fig. 4.10). From the comparison, it has been observed that average of the SEBS-ETa values have the same result as the PM-ETa. Whereas there is some deviation between SEBS-ETa and PM-ETa in the extreme case value.

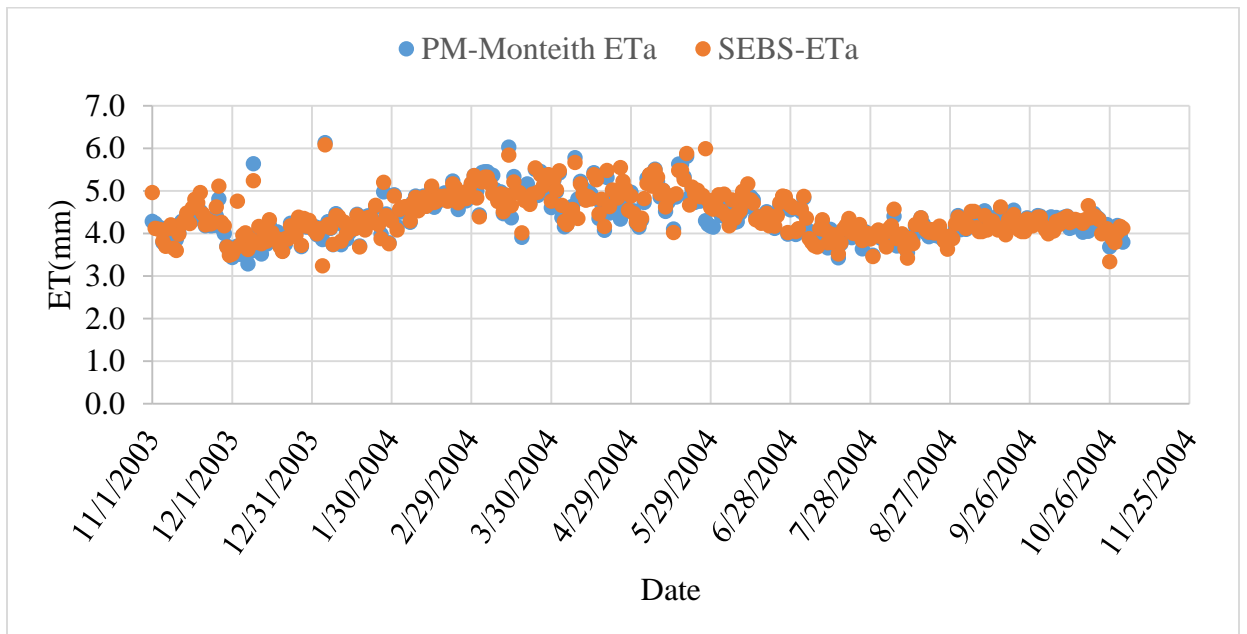


Figure 4-10 Comparison of the SEBS-ETa with the Penman-Monteith ETa calculated from the meteorological data collected at Assendabo station (37.23<sup>0</sup>N Latitude, 7.77<sup>0</sup>E Longitude) in the upper Omo-gibe basin.

#### 4.3.4 Water Balance

The sub-basin water balance was calculated by inserting the estimated spatiotemporal  $ET_a$  and rainfall values and the measured streamflow data in equation 4.3. Then, the computed results from the water balance equation are shown in Table 4.5. For each sub-catchment, the suggested precipitation values are calculated by the Thiessen polygon method, and the  $ET_a$  values are defined by dividing the sum of the pixel values by the number of pixels. These values were changed into volumes by multiplication with the sub-catchment area. For detailed analysis, based on the availability of streamflow gauging stations, the upper Omo-Gibe basin was divided into four sub-basins. The four main sub-basins of the upper Omo-Gibe basin are shown in Figure 4.11.

$$\Delta S = P + Q_{in} + G_{in} - ET_a - Q_{out} - G_{out} \quad (4.3)$$

Where,  $\Delta S$  is changing in storage during the time interval, which includes surface water moisture, groundwater storage, and soil moisture.  $P, Q_{in}$  and  $G_{in}$  are precipitation, surface water inflow, and groundwater inflow, respectively and  $ET_a, Q_{out}$  and  $G_{out}$  are the actual evapotranspiration, surface water outflow, and groundwater outflow, respectively. For a reason that water balance estimations are on the sub-basins scale and calculated for an entire water year, it is assumed that groundwater storage changes are negligible (Table 4.4).

Table 4-4 Water balance for the whole basin and major sub-basins (Mm<sup>3</sup>) from November 2003 to October 2004

Sub-basin	Outflow to the basin		Outflow from the basin		Change in storage, $\Delta S$	Closure %
	P	$Q_{in}$	$ET_a$	$Q_{out}$		
Abelti	19694.6		13120	6574.6		
Gojeb	7039	734	3600	4173		
Wabe	2066		1295	769.6	1.4	0.07
			Total	11517.2	Flow in Gibe sub-basin	
Gibe	12281	11517.2	10653	9729	3416.2	14.35
Entire basin	41080.6		28668	9729	2683	6.54

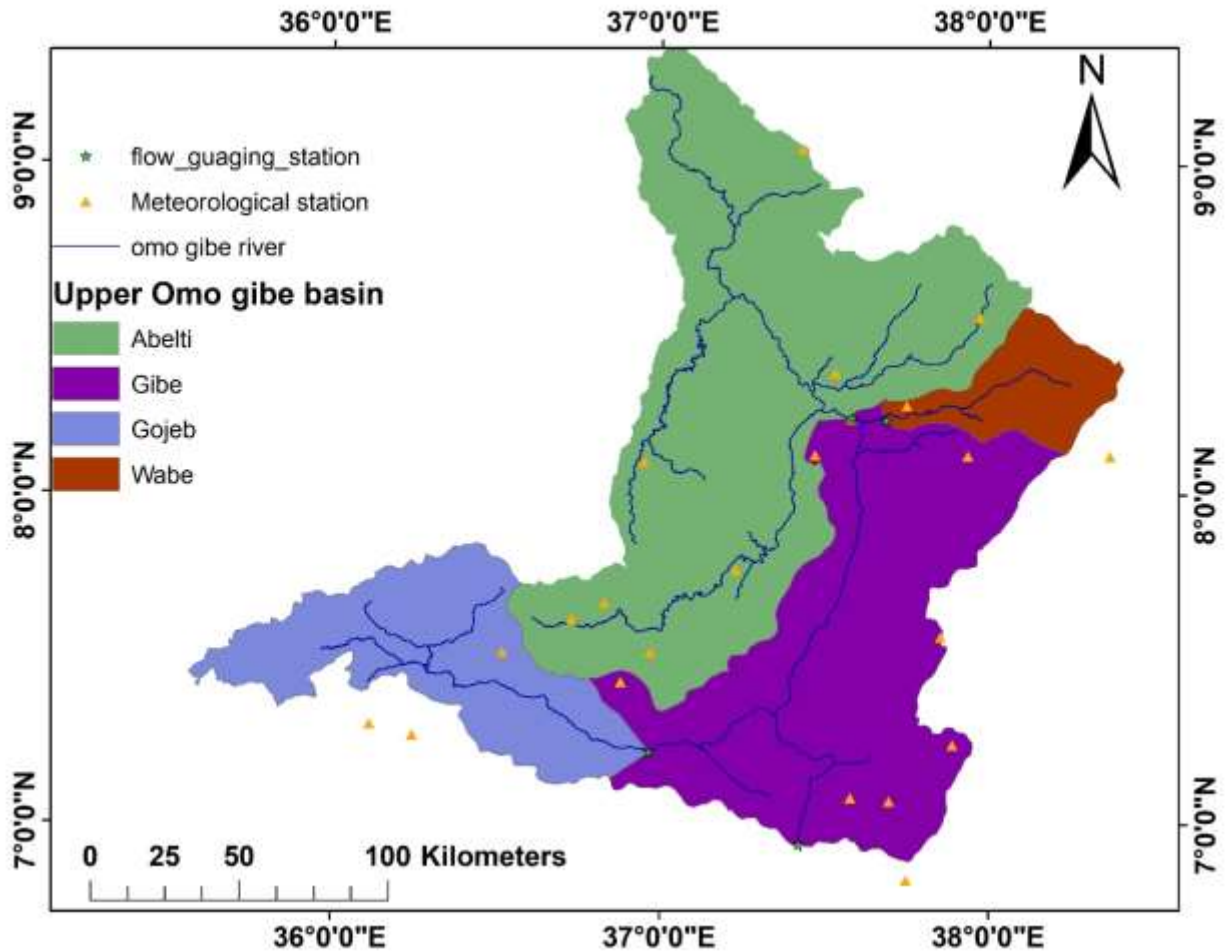


Figure 4-11 the major Sub-basin of the upper Omo-Gibe basin

From November 2003 to October 2004, the upper Omo-Gibe basin received  $41,080 \text{ Mm}^3$  of precipitation and released  $9,729 \text{ Mm}^3$  and  $28,668 \text{ Mm}^3$  in the form of surface runoff and evapotranspiration, respectively. The difference between the basin inflow and outflow is  $7,216 \text{ Mm}^3$ . Therefore, the remained uncountable water volume (also called closure term) for the UOGB is 6.54% of precipitation, which is  $2,683 \text{ Mm}^3$ . The closure term in the basin depends on the occurrence of an error due to the accuracy of the observed precipitation, the observed discharge, the estimated  $\text{ET}_a$ , and the negligible storage change assumption. Also, water storage changes in groundwater, surface water, and soil moisture content. Moreover, 0 to 6.54% of water closure values are also enlisted in Table 4.4 for the major sub-basins in the study area. A similar study was conducted for water closure estimation

by Muthuwatta et al. (2010) for five sub-catchments out of the seven sub-catchments in the Karkheh basin, Iran, and have found water closure values ranging from 0.6% to 7.2%. In addition, water closure estimation was also performed in three sub-catchments of the Mbire District, Zimbabwe, the result varies from 7.4% to 16.5% (Samboko 2016). However, the water closure values of the study area showed relatively acceptable values compared to the study, by earlier researchers. The main reason for such occurrence of closure term value is enlargements of the sub-catchment area in the UOGB. Therefore, the uncountable volume of water is the maximum possible discharge for UOGB. Hence, further portioning of the large sub-catchments into smaller sub-basin is a must in order to introduce effective water management approach in the basin.

Based on the simplistic assumption, the SEBS algorithm uses various relationships to estimate the energy flux (i.e.,  $ET_a$ ). It should be noted that these algorithms use some empirical equation for the estimation of  $ET_a$ , which would lead to some error. During this analysis, the temperature of the planetary boundary layer, the incoming longwave radiation, and the emissivity of the air is calculated as a function of the temperature of the surface. Interpolated meteorological data were used for this period to establish the temperature of the air. Once more, we tend to assume that this might introduce some errors in the quantities described above and in the final estimations of  $ET_a$ .

#### **4.4 Summary and Conclusions**

An attempt has been made in the upper Omo-Gibe basin to quantify the inter-annual and spatial patterns of consumption through evapotranspiration and availability of water using remotely sensed parameters, meteorological data, and streamflow data. In this study, prior to the use of observed precipitation data for hydrological analysis, quality and homogeneity test of precipitation records were performed via double mass curve analysis and the RAINBOW software package. Three of the stations had inconsistency and were set right. As a result, the observed precipitation data are homogeneous and consistent. SEBS algorithm was employed for the period of November 2003 to October 2004 to estimate the  $ET_a$  value in the study area using meteorological data for 23 rain gauge stations collected

from NMEA and 16 cloud-free MODIS-TERRA satellite images collected from <https://ladsweb.modaps.eosdis.nasa.gov/search/>. In the SEBS algorithm, the estimation of spatial variation of evapotranspiration is performed on a daily basis, while the analysis of the water balance is performed on a monthly basis. So, to change the estimated daily ET<sub>a</sub> to a monthly basis in the study area, add them up and fit a scaling function from daily to monthly.

The Thiessen polygon method was applied for computation of average precipitation.

Moreover, the analysis of temporal variation shows that the inter-annual rainfall variability, which gradually reduces from East to West in the basin. In addition, The Penman-Monteith reference evapotranspiration approach was used to compare the ET<sub>a</sub> values estimated by SEBS. From the comparisons, it has been observed that some of the estimated ET<sub>a</sub> values have the same result as the calculated ET<sub>a</sub> ones. Moreover, based on the availability of streamflow gauging stations, the upper Omo-Gibe basin was divided into four sub-basins for detailed analysis. For the given study period, the water balance result showed that the upper Omo-Gibe basin received 41,080 Mm<sup>3</sup> of water in the form of precipitation, while 28,668 Mm<sup>3</sup> was evapotranspired. The uncountable amount of water volume from the basin during the study period is 6.54% of the total precipitation, which is 2,683 Mm<sup>3</sup>, i.e., the difference between precipitation, evapotranspiration, and surface outflow from the basin. This indicates that the uncountable volume of water is the maximum possible discharge for the entire basin. Since these values are lower as groundwater recharge, surface water and soil moisture occur. Therefore, it is recommended to further divide the large sub-catchments into smaller sub-basin and increase the number of streamflow stations for effective water management practices, agricultural development, and water productivity in the UOGB.

The next chapters detail the analysis of the hydrological model and its performance assessment.

## **CHAPTER 5: MULTI-VARIABLE CALIBRATION OF HYDROLOGICAL MODEL IN THE UPPER OMO-GIBE BASIN, ETHIOPIA**

### **5.1.Introduction**

Knowing the reliable information on the components of the water balance equation is crucial for water management in a river basin system. Hydrological modelling is an important tool for knowledge grasping on the hydrological responses of the catchment area (Kim et al. 2018) and is a challenging task (Romanowicz et al. 2013). In a conceptual rainfall-runoff model, it is challenging to measure different parameters directly. It requires the optimization of some hydrological variables through calibration to achieve good correlation and closely match between simulated and observed variables. Calibration with historical data is the most common method for the identification of an optimized model parameter set (Wagener et al. 2003; De Vos et al. 2010).

In hydrological modelling, an integrated response parameter streamflow with runoff from different processes are commonly used for model calibration. However, the use of streamflow compels the assessment of model performance. Since the deviation between simulated and observed, matching parts come from different possible reasons. Some of the causes are errors as a result of lack of complete representations of hydrological data, for instance, evapotranspiration and precipitation, the incorrectness of parameter values, deficiencies in model structure, and error due to observations of calibration variables. Furthermore, sources of error related to the use of boundary fluxes and model initialization to permit water to pass through the boundaries of the model are other causes (Carrera and Neuman 1986; Boulet et al. 2002). Based on mass conservation principles, hydrological model performances are influenced by the occurrence of any model error in the volume of water, which means the amount of water entered into the model or out from the model. To overcome these errors for the solution of a practical problem, all of the hydrological models should be calibrated (Gupta et al. 1998). The process of hydrological model calibration can take place either manually or automatically. The former one is done manually using a trial-and-error parameter correction process for reducing the error of objectives. While in the

latter case, according to a specific search scheme for optimization of objective functions (certain calibration criteria), parameters that measure the simulation model goodness-of-fit are automatically adjusted. Refsgaard (1997) and Wagener et al. (2001) stated that if the automated calibration employed without enough hydrological know-how could result in incorrect parameter values, it could lead to an unrealistic model response system is uncontrolled by measurements. In addition, however, the models are calibrated well in terms of an independent verification data set parameter values that can't yield good performance (Shafii et al. 2014).

In rainfall-runoff models, problems with the amendment of parameters can be attributed to different factors. As stated in Gupta et al. (1998), during the calibration period, the combination of all the remaining parameters into a single objective function does not demonstrate the insufficiency of the model. For instance, in a single objective function, there is difficulty in differentiating between recession and high-flow model behavior. In this regard, understanding the limitation of single objective function encourages to adopt multi-criteria calibration approaches (Franks and Beven 1997; Gupta et al. 1998; Yapo et al. 1998; Legates and McCabe 1999; Madsen 2000; Beven and Freer 2001; Shafii et al. 2014; Poméon et al. 2018). Multi-objective calibration methods are designed to identify certain parameters that better reproduce multiple outputs from the system. Multi-criteria calibration utilizes multi-index to define the features of the error vector resulting from the corresponding set of the multi-objective equivalence optimal parameter values and an objective-function interchange curve. In addition to that, the process of a characteristic multi-criteria calibration model consists of multiple probability functions utilized for several sets of measurements, such as sediment, discharge, evapotranspiration, snow, etc. Though, to simulate a single output flux, the model assessment could be assumed to be inherently many criteria (Gupta et al. 1998).

Multi-objective calibration of the model varies from a one-objective calibration of the model. To reproduce a record of single independent observation based on the abilities of the model, a traditional single form of objective calibration attempts to define the model parameter sets (McCabe et al. 2005). By utilizing both groundwater level and runoff

observation based on a modelling system called MIKE SHE, Madsen (2003) suggested a general multi-objective structure of an integrated and distributed hydrological model for automatic calibration. In which case, to optimize the catchment runoff performance index in a multi-objective optimization framework, individual groundwater well's performance indices were grouped into a single certain calibration criterion. Meixner et al. (2002) employed a multi-criteria algorithm to calibrate the hydro-chemical model. For assessing the performance of this model, a total of 21 chemicals and hydrological criteria were obtainable. Also, various researchers use a second set of the variable for model output. Such variables are soil moisture or groundwater hydraulic heads for assessment of determining rainfall-runoff model data (Gupta et al. 2008; Khu et al. 2008); graphs of groundwater piezometer (Fenicia et al. 2005; Khu et al. 2008); soil wetness index or simple soil moisture storage indicator (Downer and Ogden 2003); and satellite-based soil moisture estimates (Campo et al. 2006). In addition to streamflow data for 320 Austrian catchments, Parajka et al. (2007a) utilized daily snow cover data for the calibration of a conceptual hydrological model. The concept of most hydrological models combination is to combine state variables with streamflow. It has been pointed out that the combination has an indirect impact on closure of water balance term in the rainfall-runoff model. Since the performance evaluation of these procedures is constrained, there is the uncertainty of how best the model reproduces the performance of the water balance of the study area.

Commonly in hydrological modelling, evapotranspiration is assessed through meteorological data, which helps to evaluate reference evapotranspiration ( $ET_0$ ) and direct measurement data. Since those data may have comparatively insufficient spatial coverage for larger areas of the catchment, it is necessary to assess additional or substitute data sources, enhancing the spatial coverage of the large area. The hydrological model requires large numbers of spatiotemporally distributed data sets to characterize the major catchment hydrological processes and its climate. This introduces remote sensing data as a possible source for this model (Chen et al. 2005; Montzka et al. 2008). Remote sensing is utilized to find hydrological parameters; such parameters are rainfall (Wang et al. 2001; Haile et al. 2013; Rientjes et al. 2013a), soil moisture (Hollenbeck et al. 1996; Kim and Barros

2002), and potential evapotranspiration (Stisen et al. 2008). It also distinguishes areal phenomena, such as clouds (Ouillon et al. 1997), inundated areas (Islam and Sado 2002), and snow cover (Tait et al. 2000).

Based on observed values of ground temperature, latent heat, sensible heat, and soil moisture data, the Biosphere-Atmosphere Transfer Scheme was calibrated (Gupta et al. 1999). Their study identified that to simulate accurate multi-variant, single output variable calibration is not sufficient. Crow et al. (2003) reported that, relative to individual variable calibration, multi-variable calibration reduces 20% calibration error in actual evapotranspiration (ET<sub>a</sub>). Also, to calibrate the semi-distributed Variable Infiltration Capacity (VIC) hydrological model, they used streamflow and space-borne radiometric surface temperature data. In the Krishna basin of southern India, Immerzeel & Droogers (2008) incorporated evapotranspiration based on remote sensing into Soil and Water Assessment Tool (SWAT) model calibration. Their analysis compares the monthly sub-basins output of remote sensing derived ET<sub>a</sub> and ET<sub>a</sub> simulated by the physically-based hydrological model. In the upper Bhima catchment of southern India, Immerzeel et al. (2008) combined remote sensing data and output of the SWAT model to assess productivity and water use. They found that in the watershed, evapotranspiration is the significant water loss term. In the Luangwa river basin in Zambia using remote sensing ET<sub>a</sub> in a conceptual semi-distributed hydrological model, Winsemius et al. (2008) measured the values of the land surface-related parameter. To improve the simulation of discharge based on the energy balance approach in a controlled water system, Hartanto et al. (2017) integrated remote-sensing ET<sub>a</sub> data with a spatially distributed hydrological model low-lying reclamation area of the Rijnland area in the Netherlands. They compared integrated modeled and remote-sensing based ET<sub>a</sub> to simulated data without integration between model and remote-sensing based ET<sub>a</sub>. Herman et al. (2018) examined the overall performance improvement of the SWAT model by utilizing integrated satellite-based ET<sub>a</sub> with the spatially distributed dataset of the hydrological model. They calibrated the model using spatially distributed ET<sub>a</sub> in Creek Watershed, in Michigan and a particular record of point streamflow for the Honeyoey Creek-Pine, USA. To calibrate the model, they employed a

multi-variable and genetic algorithm. They found that there is a great improvement in the performance of the hydrological model since the integration of satellite-based and spatially distributed hydrological data combines with the right calibration method.

Since actual evapotranspiration is part of water balance terms in hydrological studies, it has not paid more attention while performing a multi-variable calibration for water balance studies. For this study, the performance evaluation of hydrological studies was performed through a multi-variable calibration technique, which utilizes two water balance terms. These water balance terms are satellite-based ETa and streamflow. Within a multi-variable calibration formulation, the hydrological process is likely to be satisfactory for an initial assessment of more than a single uncertainty based calibration technique. Moreover, this study estimate and test the utilization of a second calibration variable called satellite-based actual evapotranspiration and give possibility as the water balance with its model performance. This study aims to test the efficiency of satellite-based actual evapotranspiration in the semi-distributed HBV hydrological model to render the catchment water balance by utilizing daily Remote-sensed actual evapotranspiration data and daily streamflow. The HBV light hydrological model (Seibert 1996) was applied to the Upper Omo-gibe basin, Ethiopia.

## **5.2.Sub catchments and Data**

The UOGB is divided into four sub-catchments based on streamflow measuring station to set up the HBV light hydrological model (Fig. 4.11). The largest and smallest sub-catchment is Abelti and Wabe, respectively. At the outlets of each of the four sub-catchments, the mean daily streamflow varies from 2.89 m<sup>3</sup>/s to 4.53 m<sup>3</sup>/s for the year 2000-2004. Abelti, Wabe, and Gojeb sub-catchments receive streamflow from the upstream of the basin, while the Gibe sub-catchment receives from those three sub-catchments. Hydrograph separation methods were used to construct the streamflow hydrograph for each of the sub-catchments. Due to relatively short travel time (i.e., <1 day) and unavailability of data on the Omo-Gibe basin's channel properties, the streamflow routing is ignored. Details of these sub-catchments are indicating in Table 5.1.

Table 5-1 Details of the four sub-catchments in UOGB

S No	Sub-catchment	Area (km <sup>2</sup> )	Upstream sub-catchments	Number of meteorological stations	Average Daily Flow (m <sup>3</sup> /s) from 2000 to 2004
1	Abelti	15,730	-	9	4.32
2	Gibe	10,590	Abelti, Gojeb and Wabe	9	3.59
3	Gojeb	5,091	-	3	4.53
4	Wabe	1,861	-	2	2.89

### 5.3.Methods

#### 5.3.1. Time-series trends of actual evapotranspiration

For the present study to estimate daily ET<sub>a</sub> from the period of January 2000 to October 2004, 145 cloud-free calibrated radiance MODIS Level 1B (MOD021KM) with their corresponding Geo-location files (MOD03), with a daily temporal and spatial resolution of 1 km<sup>2</sup> collected by the MODIS sensor in the Terra (EOS AM) satellite was used (Source: <https://ladsweb.modaps.eosdis.nasa.gov/search/>) (Table 5.2). Due to cloud coverage over time, the collected imageries were irregularly distributed. Moreover, for the HBV hydrological light model to estimate reference evapotranspiration (ET<sub>0</sub>), the Penman-Monteith equation was used. Likewise, to estimate bi-weekly ET<sub>a</sub> in the spatial and temporal variability, the SEBS model developed by Su (2002) has been applied. The meteorological data used to estimate ET<sub>a</sub> in this remote sensing model were recorded at 3:00 local time, which is near the time of satellite overpass (i.e., Between 2:10 and 2:55 local time). Due to no cloud-free imageries found during the rainy seasons' evaporation, it cannot be estimated for an entire twelve-month period using the SEBS model. Accordingly, to calculate ET<sub>a</sub> for all day without satellite imagery, meteorological data and the Penman-

Monteith equation were employed (Bastiaanssen and Bandara, 2001; Immerzeel and Droogers, 2008). For this purpose, meteorological data for 23 stations on wind speed, precipitation, relative humidity, and temperature were used. Then, using surface energy balance algorithms and MODIS images, the latent heat flux ( $\lambda E$ ) is calculated. For days when satellite imageries were obtainable, the values of surface resistance ( $r_s$ ) were inversely determined by replacing  $\lambda E$  in the Penman-Monteith equation. For days without satellite imagery  $r_s$  value were determined through the preceding imagery of  $r_s$  value with recorded daily weather data to all day within the consecutive imageries. The Penman–Monteith equation given by:

$$\lambda E = \frac{\Delta(R_n - G_0) + \rho_a C_p \frac{(e_s - e_a)}{r_a}}{\Delta + \gamma(1 + \frac{r_s}{r_a})} \quad (5.1)$$

where  $(e_s - e_a)$  (kPa) is the vapor pressure deficit of the air,  $\Delta$  (kPa /K) is the slope of the saturated vapor pressure curve,  $\rho_a$  ( $\text{kg/m}^3$ ) is the moist air density,  $r_a$ , and  $r_s$  (s/m) are aerodynamic and surface resistances respectively, and  $\gamma$  (kPa/K) is the psychrometric constant, and the remaining parameters are described in equation 2.1 to 2.4 (Chapter 2). To estimate  $R_n$  at a daily time, step  $G_0$  is assumed to be zero, and sunshine hours can be used. The difference between  $ET_a$  and  $ET_0$  is controlled by  $r_s$ , which means the reference evapotranspiration lies above actual evapotranspiration, and  $r_s$  surpasses a particular minimum value (Bastiaanssen and Bandara 2001). Also,  $r_s$  can be explained concerning solar radiation, vapor pressure deficit, soil moisture, and air temperature (Jarvis 1976). For estimating all values in Eq.2.1(Chapter 2) except the aerodynamic and surface resistances, local daily measurements of wind speed, sunshine hours, minimum and maximum temperature, and relative humidity were obtained from the National Meteorological Agency of Ethiopia. Hence, for all days without satellite imagery, calculating daily values of  $r_a$  and  $r_s$  permits for  $ET_a$  estimation.

Table 5-2 Acquisition dates of TERRA-MODIS images in the upper Omo-Gibe basin for the study period (source: <http://ladsweb.modaps.eosdis.nasa.gov/>).

Month	2000	2001	2002	2003	2004
Jan		06, 18, 23	17, 23, 28	01, 04	04
Feb	28	03, 14, 28	02, 11, 27	05, 18, 21	05
Mar	04, 13, 22	07, 09, 16	29, 31	06, 16, 25	08
Apr	05, 14, 30	08, 17, 26	07, 13, 23	01, 14, 23	09, 25
May	09, 14, 25	03, 15, 19, 24	15, 25, 31	02, 09, 18	04, 27
Jun	01, 13, 26	02, 04	03, 05, 23	01, 10, 26	12, 28
Jul	01, 24, 30	11, 13	02, 12, 23	17, 28	14
Aug	02, 27	12, 19, 25	13, 22, 29	04, 18	31
Sep	03, 09, 16	10, 24, 27	5, 14, 30	05, 12, 19, 30	16
Oct	02, 11, 29	03, 10, 19, 26	16	07, 16, 23	02, 18
Nov	03, 19, 26	02, 11, 18, 27	01, 05, 14, 26	01	
Dec	05, 22, 31	04, 18, 27	05, 12, 26	03	

From the evaporating surface to the air, the transfer of water vapor and heat can be determined by  $r_a$  and is written as:

$$r_a = \frac{\ln\left[\frac{(z_m-d)}{z_{om}} - \psi_m\right] \ln\left[\frac{(z_h-d)}{z_{oh}} - \psi_h\right]}{k^2 u_2} \quad (5.2)$$

where  $Z_m$ ,  $d$ , and  $Z_h$  (m), respectively, are the height measurements of the wind speed, the zero displacements, and humidity.  $Z_{oh}$  and  $Z_{om}$  (m), respectively, are the roughness length governing heat and vapor transfer and the momentum transfer,  $u_z$  the wind speed at height  $z$  (m/s),  $k$  is the Von Karman's constant (-), and  $\Psi_h$  and  $\Psi_m$  (-) respectively are the stability correction functions for heat transport and momentum. The roughness for momentum can be calculated through an experimental relation suggested by (Su et al. 2001) and is written as:

$$Z_{om} = 0.005 + 0.5 \left( \frac{NDVI}{NDVI_{max}} \right)^{2.5} \quad (5.3)$$

To determine the value of  $Z_{oh}$ , the dimensionless quantity  $kB^{-1}$  has been developed through the relationship between roughness length for momentum and heat and vapor transfer. Brutsaert (1982) assigns a value of 2.3 for  $kB^{-1}$ . The equation is presented in (5.4)

$$Z_{oh} = \frac{Z_{om}}{\exp(kB^{-1})} \quad (5.4)$$

### 5.3.2. Hydrological model

For the simulation of the streamflow using rainfall, potential evapotranspiration, and temperature as input, a modified version of the conceptual semi-distributed hydrological model was selected for this study, which is an HBV light model (Seibert 1996). This model uses sub-basins as the most fundamental units of hydrology. The distribution of lakes, forests, glaciers, open areas, and area elevation is also considered in the HBV model. The sub-basins are considered in the spatial variation of different properties, such as the physical properties or meteorological properties of the basin. The HBV model consists of six different routines, precipitation accounting routine representing snowmelt, rainfall, and snow accumulation; soil moisture routing where surface and overland flow and actual evapotranspiration are calculated as a function of actual storage of water; a quick runoff routine representing river discharge, the subsurface flow which is represented by the base flow routine; a transformation routine for flow attenuation and delay and a routing routine (Bergström 1992).

The aim of selecting this simplified version of the HBV model is due to comparatively low demand with low complexity for input data and produce simulation results on par with sophisticated models (Bergström and Forsman 1973). Meanwhile, there have been relatively large sub-catchments in the study area; the transformation function that smoothens the streamflow is not utilized. Even if there were well-known methods for estimation of potential evapotranspiration (Lindström et al. 1997; Merz and Bloßschl 2004), the standard Penman-Monteith equation is employed for evaluation of potential evapotranspiration (Allen et al. 1998). The HBV light model was applied in the upper Omo-Gibe Basin for each of the given four sub-catchments. Commonly, many years of data on flow, temperature, and precipitation for model calibration are needed for the application of hydrological modelling, but these data are not sufficiently available for all catchments worldwide (Etter et al. 2018). Nowadays, some studies have shown that calibration and validation analysis is carried out over a few years of data (Madsen, 2000; Wagener et al. 2003; Rientjes et al. 2013b; Ha et al. 2018; Mohaideen and Varija 2018). For this study, depending on a separate sample test for the periods from January 1<sup>st</sup>, 2000 to December 31<sup>st</sup>, 2002, the model has been calibrated and verified for the periods from January 1<sup>st</sup>, 2003 to December 31<sup>st</sup>, 2004.

### **5.3.3. Model performance assessment and parameter estimation**

General calibration criteria (objective function) Y has been used to test the overall model performance for simulating the behavior of observed streamflow (Akhtar et al. 2009), which combines the Relative Volume Error (RVE) and the Nash-Sutcliffe efficiency coefficient (NSE) (Nash and Sutcliffe 1970). Compared to the measured data variance NSE calculates the relative magnitude of residual difference. NSE refers to the degree to which the plot of the simulated against observed data matches the one to one line. One parameter set may show good correlation according to the criterion of NSE but may imply a weak relationship for RVE and vice versa (Seibert 1999). A combination of values of these particular calibration criteria is difficult because various objective functions are not directly comparable. The equations of objective functions are written as:

$$Y = \frac{NSE}{1+|RVE|} \quad (5.5)$$

$$NSE = 1 - \frac{\sum_{i=1}^n (Q_{si} - Q_{oi})^2}{\sum_{i=1}^n (Q_{oi} - \bar{Q}_0)^2} \quad (5.6)$$

$$RVE = \frac{\sum_{i=1}^N (Q_{si} - Q_{oi})}{\sum_{i=1}^N Q_{oi}} \quad (5.7)$$

In equations 5.5-5.7,  $Q_s$  and  $Q_o$  are simulated and observed discharge respectively,  $i$  is the time step,  $N$  is the total number of time steps, and  $\bar{Q}_0$  is the mean of  $Q_o$  over the calibration or verification period. The efficiency value of RVE should be close to zero, and the value of  $Y$  and NSE should be close to 1 for satisfactory model performance. As stated by Bergström (1992), NSE values tend to one, indicating a perfect fit for the simulation and observation value. While a values approach, zero indicates that simulations are poor or good as the constant value prediction. The values less than zero indicate a very poor fit for the simulation and observation value. The value of  $Y$  ranges from 0 (meaning the model performs poorly) to 1 (meaning the model performs well), with typical values up to 0.6 are considered poor to satisfactory and higher values indicating less error variance (Rientjes et al. 2013b).

In this study succeeding (Harlin and Kung 1992; Seibert 1999; Wagener et al. 2003; Choi and Beven 2007; Booij and Krol 2010), the Monte Carlo simulation (MCS) procedure is employed for parameter optimization to four sub-catchments of the UOGB. In MCS, to evaluate the model performance, a multitude of parameter sets is generated and performed randomly. In the MCS approach, along with various simulations of the model, preeminent objective function values are selected by utilizing randomly generated parameters within the predefined space of the model parameter. Essential characteristics of MCS frameworks are the choice of the objective function(s), the determination of the number of simulations to be performed, the determination of prior parameter spaces, the choice of parameters for calibration, and choosing the likelihood distribution for the calibration parameters.

For calibration of the time series of actual daily evapotranspiration and daily streamflow, parameters have been estimated. Meanwhile, both  $ET_a$  and  $Q$  are major water balance

terms to the hydrological model matching each other directly affect one another. Winsemius et al. (2008) stated that estimated HBV-ETa through employing the lumped HBV model are representatives for the sub-catchment scale. To come to the corresponding estimates for comparison SEBS-ETa with HBV-ETa over the sub-catchments, all pixel estimate values are averaged. To support irrigation from channels of river discharge, estimated ETa cover for water abstraction. Hence, for calibration of the streamflow model, time series at the catchment outlets has been used.

Two model calibration case was defined for this study. The first case is the most common scenario where optimization and calibration of the model parameter are on streamflow. Performance measures are merely applied to evaluate SEBS-ETa with HBV-ETa. In the last case, to optimize the parameter values in model calibration, both actual evapotranspiration and streamflow are used simultaneously. Preference-based objective functions are used for evaluating model performance, which simultaneously reduces the deviation between particular variables.

For HBV hydrological models, the selection of sensitivity parameters was based on studies and simple manual sensitivity of Seibert (1997, 1999), Booij (2005), Göttinger and Bárdossy (2005), Wale et al. (2009), Booij and Krol (2010) and Deckers et al. (2010) for the degree day procedure, for threshold temperature, and for melting factor. The parameters of the model and their prior ranges utilized in the MCS procedure are shown in Table 5.3. For all sets of parameters, a uniform distribution has been assumed, and as defined by the values of parameter ranges, the values of parameters are arbitrarily drawn from the space of the variable.

Table 5-3 Model parameters and their prior ranges used in the MCS procedure

Parameter	Description	Prior range	Unit
TT	Threshold Temperature	-1.5-2.5	°C
FC	Maximum soil moisture storage	100-600	mm
Lp	Soil moisture value above which ETa reaches ETp	0.1-1.0	-
BETA	A parameter that determines the relative contribution to runoff from rain or snow	1.0-1.2	-
PERC	Maximal flow from upper to lower box	0.1-1.1	mm/d
ALFA	Nonlinearity coefficient	0.1-0.4	-
K1	Recession coefficient (upper box)	0.01-0.1	1/d
K2	Recession coefficient (lower box)	0.001-0.15	1/d

## 5.4. Results and Discussion

### 5.4.1. Time series patterns of actual evapotranspiration

For the given four major sub-catchments, the daily basis time series of SEBS-ETa are shown in Fig 5.1.

Fig 5.1, shows the lowest values of ETa observed during the wet season, which shows the planting and growing period of crops, while the highest values were observed during the dry season, which is due to the reduction of soil moisture in the upper part of the saturated zone.

For the best performing parameter set, the model output of average parameter values for the four major sub-catchments for the given two cases are given in Table 5.4.

Table 5-4 Average parameter values for the four major sub-catchments for the given two cases.

Parameter	mm	Case 1	Case 2
TT	°C	0	0
FC	mm	400	600
Lp	-	1	1
BETA	-	1	1
PERC	mm/d	1	1
K1	1/d	0.1	0.01
K2	1/d	0.05	0.15

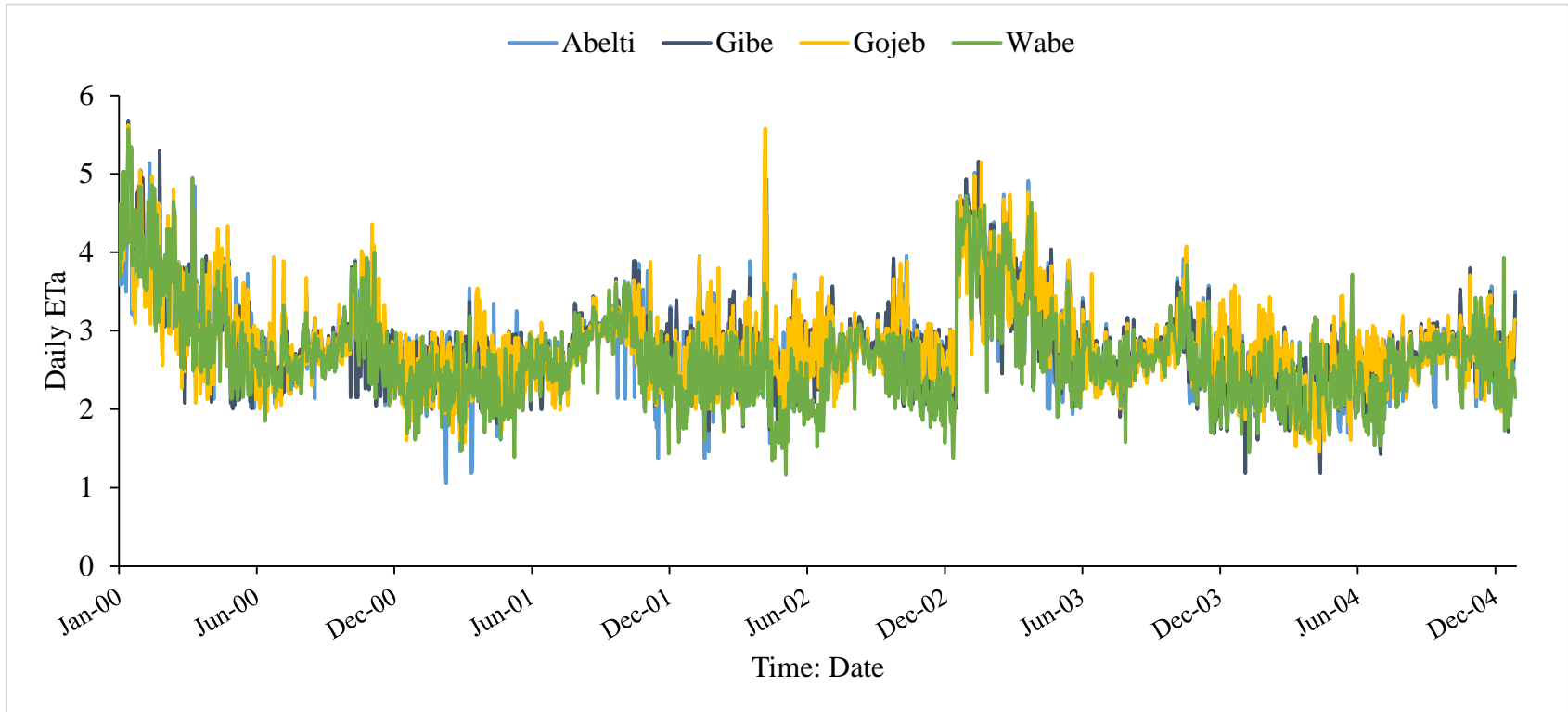


Figure 5-1 Time series of SEBS-ETa for Abelti, Gibe, Gojeb, and Wabe sub-catchments.

#### **5.4.2. Case 1-Model Calibration and Validation on Streamflow**

The simulation was initiated with the default parameter values. The streamflow hydrographs showed comparatively weak matching between the simulated and observed output values. The pairing denotes that, when the HBV model is applied in regions other than it was calibrated, it requires a new calibration. Model calibration is to improve the accuracy of model predictions, which was carried out in the sensitive flow parameters of HBV that are already identified (Table 5.3) and are subjected to minor changes to ensure a good correlation between observed and simulated streamflow. First, the most sensitive parameters are modified, employing a manual calibration process based on the information available in the literature. In this process, the values of the parameters have been iteratively changed within the appropriate ranges to increase the value of NSE (Eq. 5.6). Auto-calibration processes that significantly improved model efficiency were then carried out using sensitive parameters that were defined during sensitivity analysis.

During the calibration step, the first year, i.e., from 01/01/2000 to 31/12/2000, was considered a model warm-up period to establish proper initial conditions and stabilize the model. Calibration was then performed for the next step. Commonly, the trial and error methods were used to calibrate the HBV light hydrological model (Bergström 1992). Therefore, when determining the calibration result, the subjectivity problem must be addressed. Typically during the calibration process to get good results from the model, the user starts from sensitive parameter values that give good results in a similar catchment and maintain them within specific ranges. For example, in southern Sweden (Bergström 1990) found regional differences for the calibrated values of maximum soil moisture storage (FC). The results indicated that such regional differences occurred may be partially due to what the modeler expects. It begins with one value, and since very different FC values can produce good matches, it is possible to keep this value by adjusting certain parameters. With poorly defined parameters, depending on the start values and method of optimization, automated calibration methods will often point out to different sets of parameters, and the user decides to determine what parameter set to use (Kite and Kouwen

1992). The value of model performance indices obtained for daily streamflow predictions during the calibration and verification periods is summarized in Table 5.5.

Measured and simulated flows for daily time steps had a favorable comparison during all the four sub-basins (Table 5.5, Fig. 5.2). This is evident from the values of NSE varied from 0.79 to 0.97, RVE ranging from 0.06 to 0.48, and Y varied from 0.56 to 0.92. Overall, we can say the model performance is very good, consistently across calibration and validation in daily predictions. Figures 5.2 compare the daily simulated flows with observed daily flows for four sub-basins. It is indicated that simulated flows are consistently more than the observed flows. The simulated streamflow values are plotted against the observed streamflow values, and their distribution is approximately 1:1. During the calibration period for both higher and lower values of observed streamflow, the simulated streamflow is distributed uniformly along the 1:1 line. The mathematical comparison between the observed streamflow and the best simulation result showed a good agreement.

Table 5-5 HBV Model performance evaluation for daily streamflow prediction for the four major sub-basins.

Model performance Index	Calibration (01/01/2000-31/12/2002)				Validation (01/01/2003-31/12-2004)			
	Sub Basin							
	Abelti	Gibe	Gojeb	Wabe	Abelti	Gibe	Gojeb	Wabe
NSE	0.97	0.79	0.85	0.83	0.86	0.87	0.88	0.76
RVE	0.06	0.40	0.31	0.48	0.43	0.41	0.41	0.56
Y	0.92	0.57	0.63	0.56	0.60	0.62	0.62	0.49

After the model is calibrated, validation of the model at the Omo-Gibe River basin was performed for an independent dataset, which is different from the calibration periods without further modification of the calibrated parameters. The model has been found to

have a good predictive capability with NSE, RVE, and a Y value ranging from 0.76 to 0.88, 0.41 to 0.56, and 0.49 to 0.62, respectively, for a daily basis. It has been shown that the parameters of the model in the catchment area represent the processes taking place to the best of their ability. The model validation outcomes for daily streamflow showed a good match between the simulated and the measured values. Through statistical model efficiency during the calibration process, the model performed well. Fig. 5.2 shows the time series of simulated and observed daily streamflow calibration and verification for the four sub-catchment. Therefore, HBV hydrological model can be used in basins having similar characteristics.

Similarly, the efficiency values for ETa were performed for the major four sub-catchments of the upper Omo-Gibe basin. Estimated and simulated ETa values for daily time steps had unfavorable comparisons during all of the four sub-basins (Table 5.6). Fig. 5.3 shows the time series of observed and simulated daily ETa calibration and verification for the four sub-catchments. The result indicates that the values of NSE varied from 0.18 to 0.28, RVE ranging from 0.05 to 0.08, and Y varied from 0.17 to 0.27. Likewise, in the verification periods, the model is found to have a poor predictive capability with NSE, RVE, and a Y value ranging from 0.31 to 0.48, 0.04 to 0.09, and 0.28 to 0.51, respectively, for the daily basis. This suggested that the simulated HBV-ETa does not fit SEBS-ETa well.

Comparatively, some variations between SEBS-ETa and HBV-ETa were observed during the dry seasons, while during the rainy season, most of the estimated ETa values have the same result of the simulated ETa ones. During the dry season, this variation indicates that the HBV-ETa shows lower fluxes. The results also showed that as the HBV rainfall-runoff model helps solve the water balance, the only consideration is on suitably balancing the streamflow. Furthermore, with relatively weak model performance values, the simulated ETa has not represented the estimated ETa well. Therefore, the overall model performance did not fulfill the minimum values recommended in the literature during both the wet and dry season.

Table 5-6 HBV Model performance evaluation for daily ETa prediction for the four major sub-basins.

Model performance Index	Calibration (01/01/2000-31/12/2002)				Validation (01/01/2003-31/12-2004)			
	Sub Basin							
	Abelti	Gibe	Gojeb	Wabe	Abelti	Gibe	Gojeb	Wabe
NSE	0.18	0.22	0.28	0.28	0.48	0.48	0.52	0.31
RVE	0.07	0.08	0.05	0.08	0.05	0.06	0.04	0.09
Y	0.17	0.20	0.27	0.26	0.46	0.46	0.51	0.28

#### 5.4.3. Case 2- Evaluating the performance of SEBS-ETa using multi-variable

In this case, multi-variable model calibration and verification were performed for both streamflow and ETa as similar to case 1 to test the effectiveness of SEBS-ETa and within that in mind to test the performance of the HBV hydrological model. For both variables, the objective functions were optimized simultaneously and presented in Table 5.7.

It was found that the model has a well analytical capability for streamflow with NSE, value ranging from 0.66 to 0.69, and 0.62 to 0.68, respectively, for calibration and verification. Additionally, calibration and verification values ranging from 0.04 to 0.45 and 0.38 to 0.54, respectively, for the objective function RVE. Also, for the objective function, Y values ranging from 0.47 to 0.67 and 0.42 to 0.47, respectively, for calibration and verification. Similarly, from the model, efficiency values for ETa for the major sub-catchments show that NSE varied from 0.56 to 0.66, and 0.64 to 0.73, RVE ranging from 0.02 to 0.04, and 0.01 to 0.0, and Y varied from 0.54 to 0.65 and 0.62 to 0.72, for the calibration and verification period respectively.

The comparison was executed similarly with case 1 for both streamflow and ETa. Figures 5.4 and 5.5 shows the time series of both simulated and observed daily streamflow and ETa

calibration and verification for the four sub-catchment of the upper Omo-Gibe basin. Both streamflow and ETa had favorable comparison during all of the four sub-basins. The result indicates that multi-variable model calibration is effective for both streamflow and ETa. From the result, it is shown that as compared to observed data for both streamflow and ETa, the recession and falling limbs were somewhat higher and lower, respectively, in the simulated data. This shows both streamflow and ETa were well represented in a reasonable match for recession and falling limbs. Also, a good fit for ETa during the wet and dry season. Furthermore, as compared to case 1, the results were much better, not only streamflow but also for ETa. This shows the effectiveness of multi-variable model calibration for SEBS-ETa. Overall the result demonstrated that the parameters of the model in the catchment area represent the processes taking place to the best of their ability.

Additionally, in this case, the hydrological catchment behaviors represented as required, and single variable calibration constraints in case 1 was very weak. Moreover, the model verification outcomes, both for streamflow and ETa, showed a good match between the simulated and measured values. The model performed well, though the statistical model efficiency measures are good during the calibration process. Furthermore, the simulations were below the observed value; this showed an underestimation of the simulated flow over the observed ones. The possibility of underestimating the streamflow may be due to the fact that, in such a complex terrain, rainfall is captured through 23 gauges, and the rainfall varies across the catchment from a minimum of 1019 mm to a maximum of greater than 1439 mm. Finally, the result suggested that the use of more than one water balance term in a hydrological model calibration was beneficial.

#### **5.4.4. Parameter estimation and Uncertainty of Model Parameters**

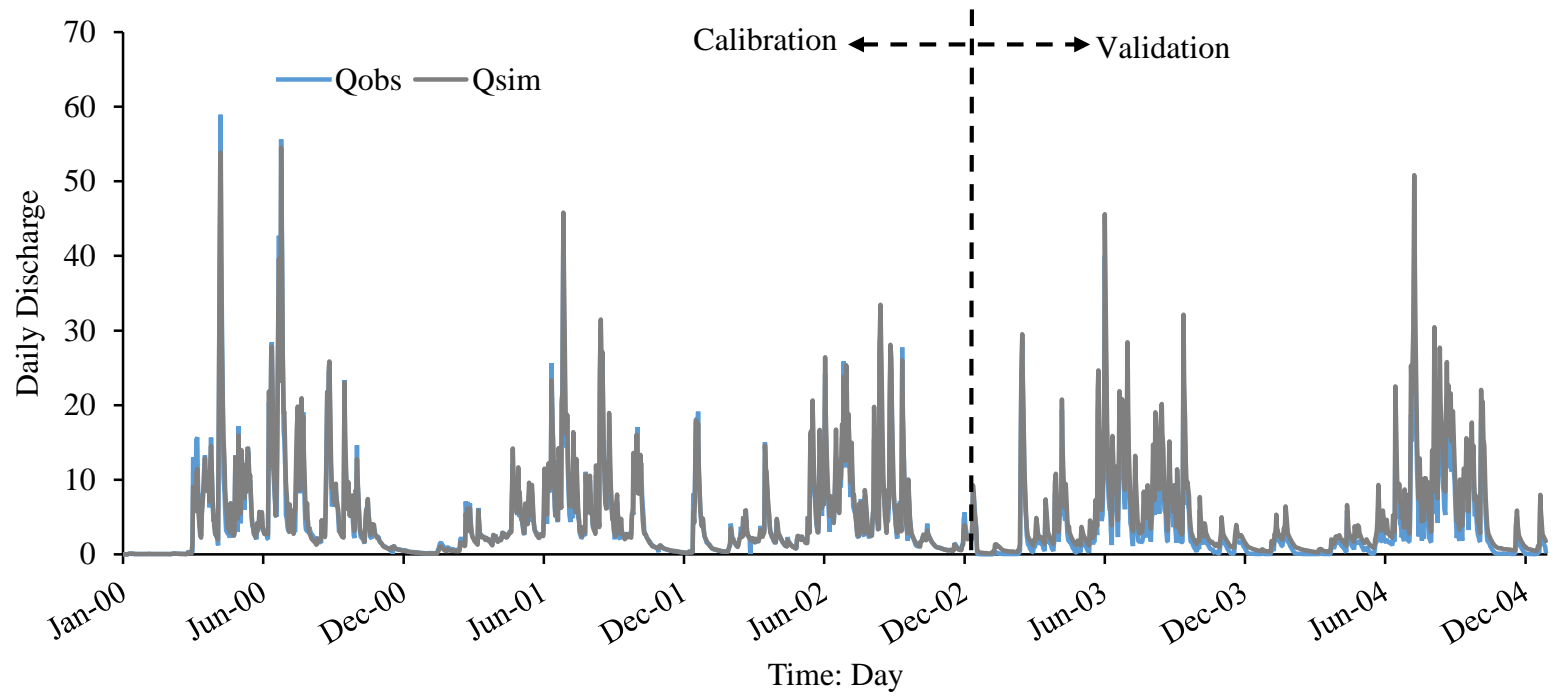
In the HBV rainfall-runoff, model streamflow simulations are directly affected by PERC, K1, K2, and ALFA. Also, ETa simulation is directly affected by LP. While the other parameters like BETA and FC indirectly affect streamflow and ETa simulation. Generally, the spatial variability of the parameters is an indicator of the uncertainty of measurement data. For some parameters of the model, if the number of iteration increases as the spatial

parameter increases, which means increased from the first iteration to second iteration etc. (Parajka et al. 2007b). In the UOGB, the error caused by time series of measured precipitation and streamflow and estimated ETa affects the uncertainty of parameters of the model. In addition, as compared to rain gauge stations, the availability of streamflow gauging stations was small (i.e. Four streamflow gauging stations). This shows that as well as streamflow gauging station, the rain gauge station is not spatially distributed well in the basin. The study area topography, elevation, and influences of cloud affect the accuracy and location of streamflow and rain gauge stations.

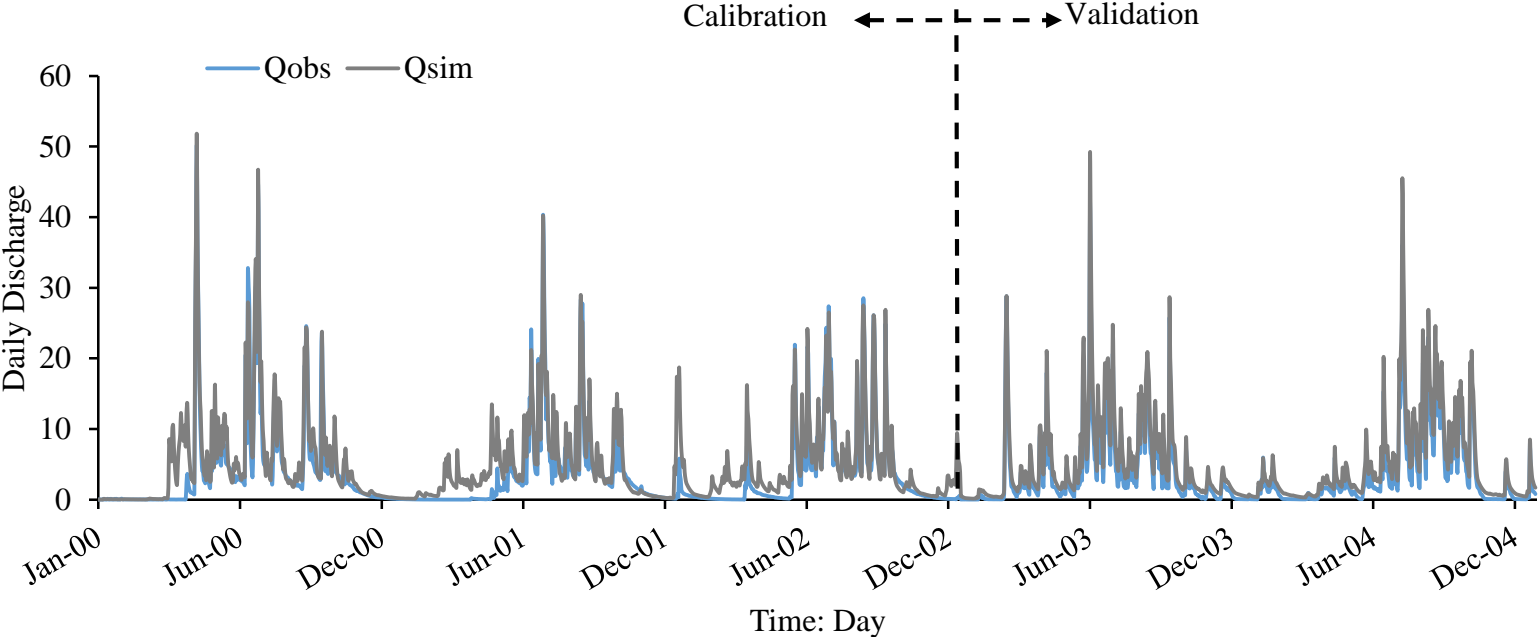
Table 5-7 Model performance evaluation for daily streamflow and ETa prediction for the four major sub-catchments.

variable	Sub-catchment	Model performance Index					
		Calibration period (01/01/2000-31/12/2002)			Validation period (01/01/2003 - 31/12-2004)		
		NSE	RVE	Y	NSE	RVE	Y
Streamflow (Q)	Abelti	0.69	0.04	0.67	0.68	0.40	0.46
	Gibe	0.68	0.37	0.49	0.66	0.38	0.47
	Gojeb	0.66	0.28	0.52	0.62	0.38	0.45
	Wabe	0.68	0.45	0.47	0.65	0.54	0.42
Actual evapotranspiration	Abelti	0.56	0.03	0.54	0.70	0.01	0.69
	Gibe	0.60	0.04	0.58	0.72	0.03	0.70
	Gojeb	0.66	0.02	0.65	0.73	0.01	0.72
	Wabe	0.66	0.04	0.64	0.64	0.04	0.62

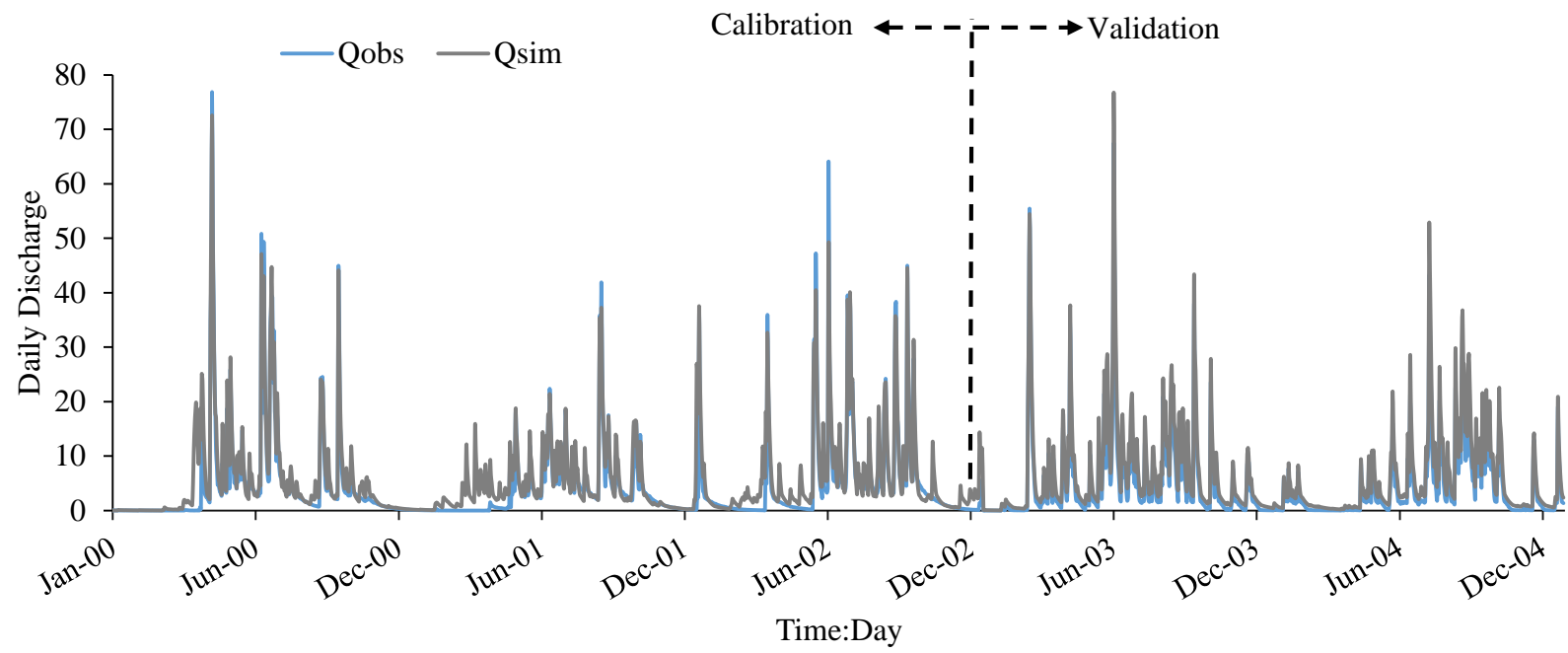
(a) Abelti sub-catchment



(b) Gibe sub-catchment



(c) Gojeb sub-catchment



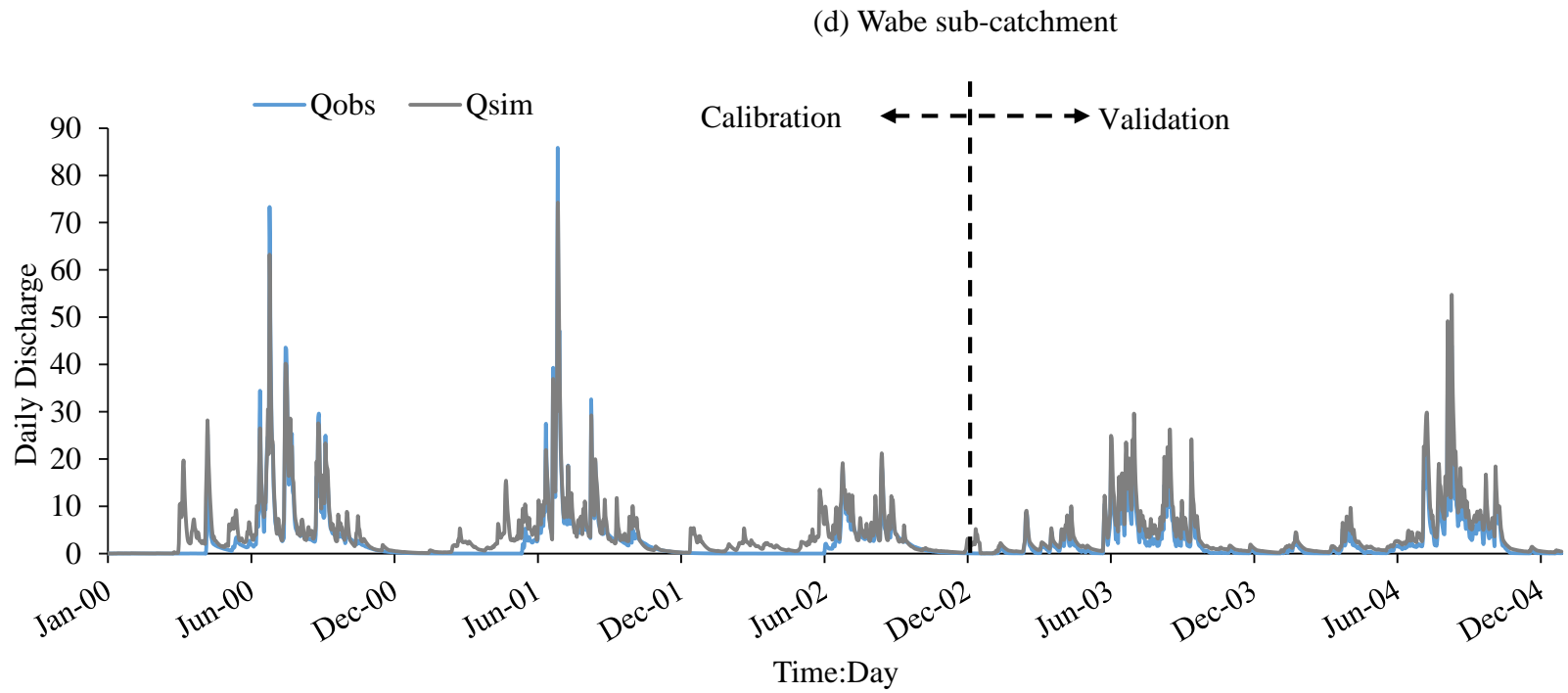
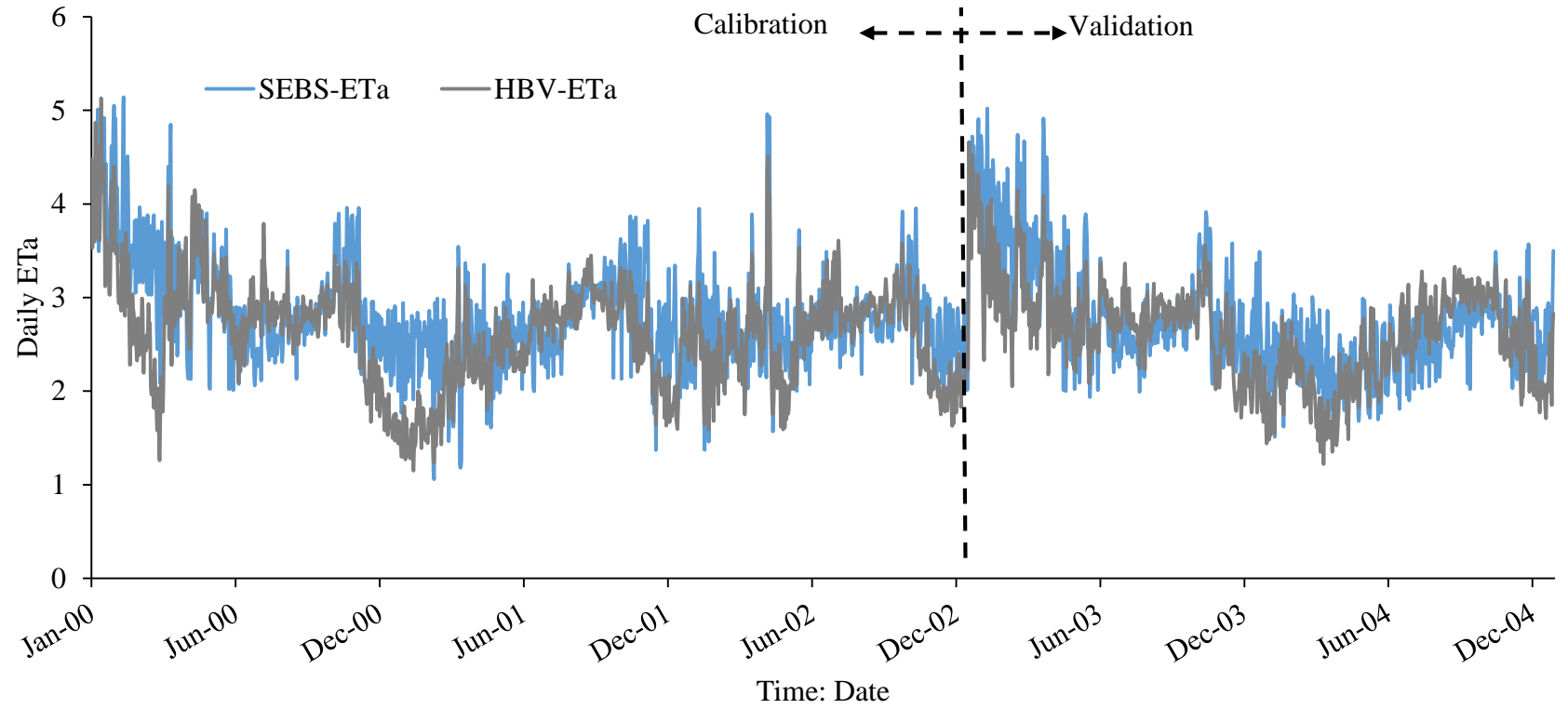
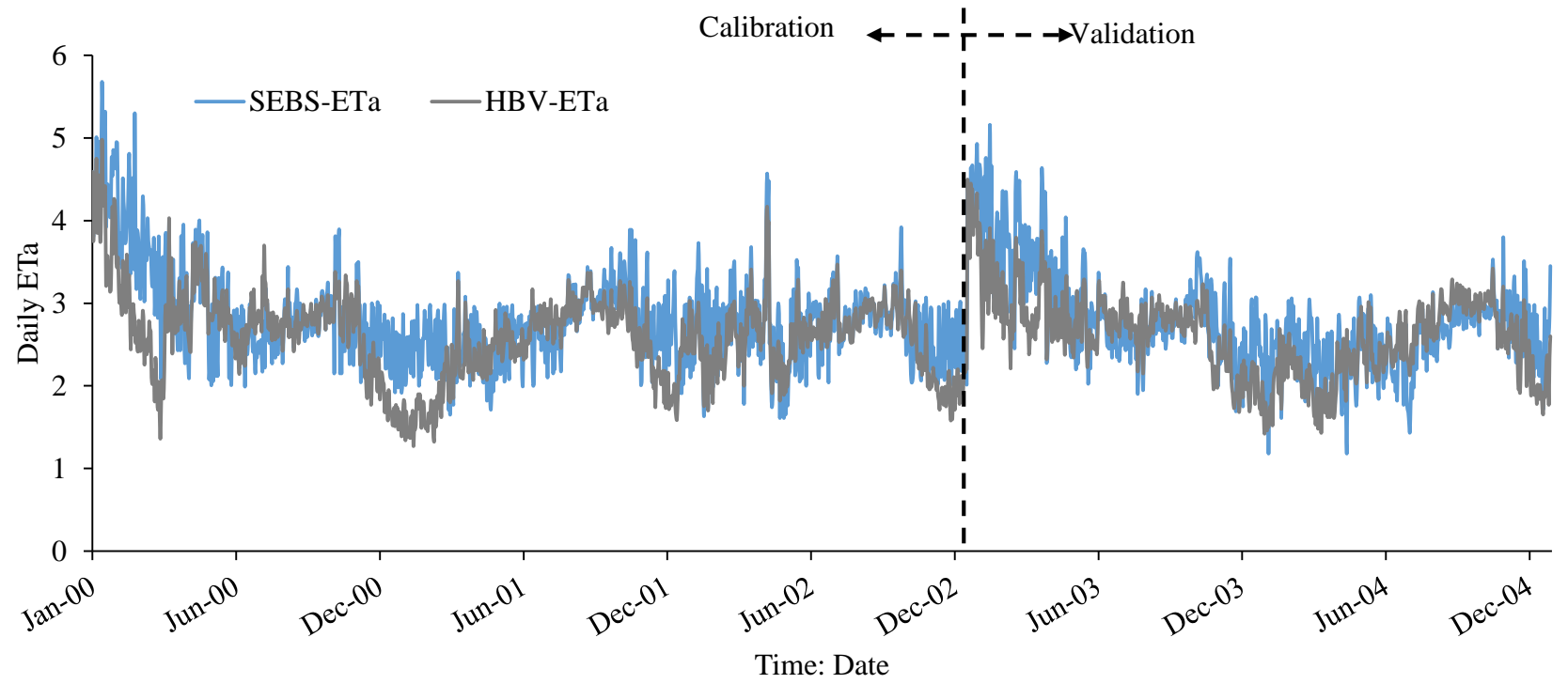


Figure 5-2 Time series of observed and simulated daily streamflow for calibration and validation period for 1<sup>st</sup> Jan 2000-31<sup>st</sup> Dec 2004 for (a) Abelti, (b) Gibe, (c) Gojeb, and (d) Wabe Sub-catchments for case 1.

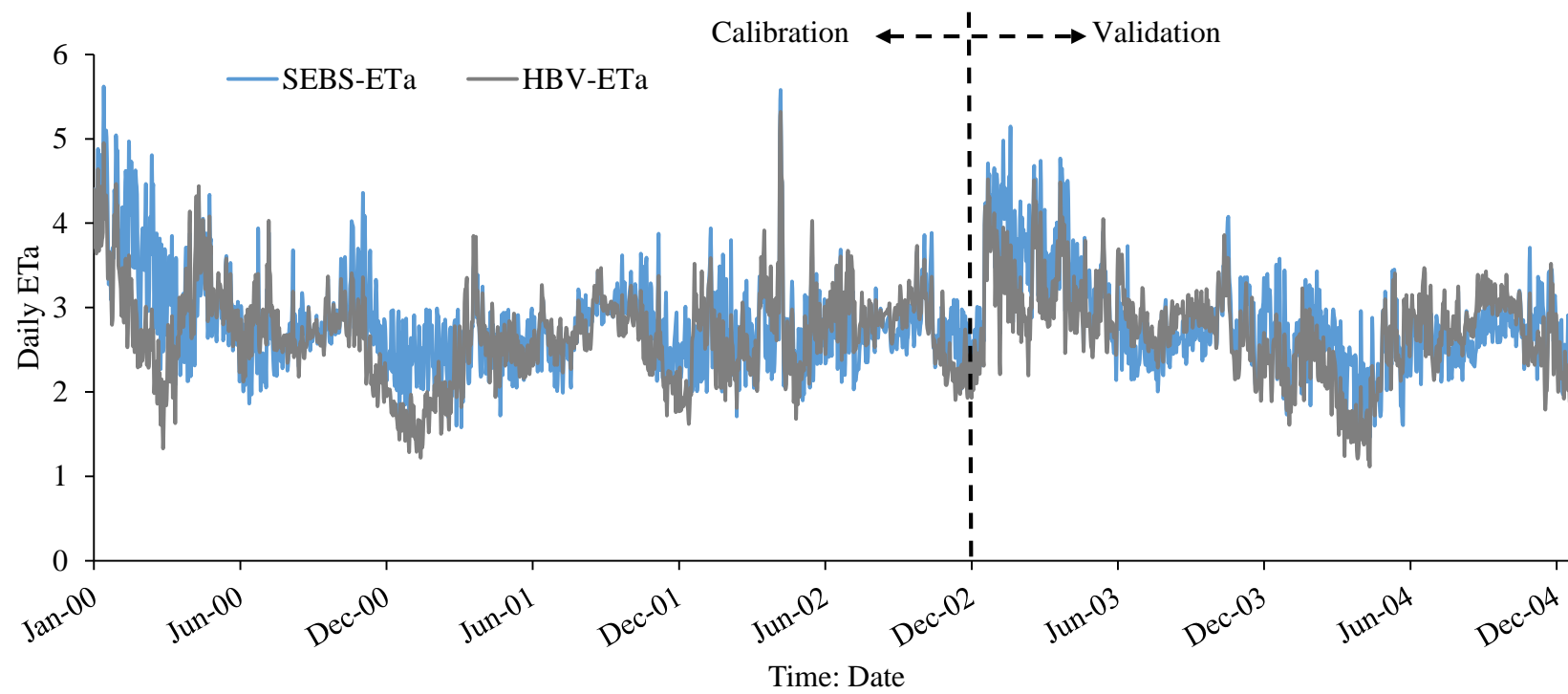
(a) Abelti sub-catchment



(b) Gibe Sub-catchment



(c) Gojeb sub-catchment



(d) Wabe sub-catchment

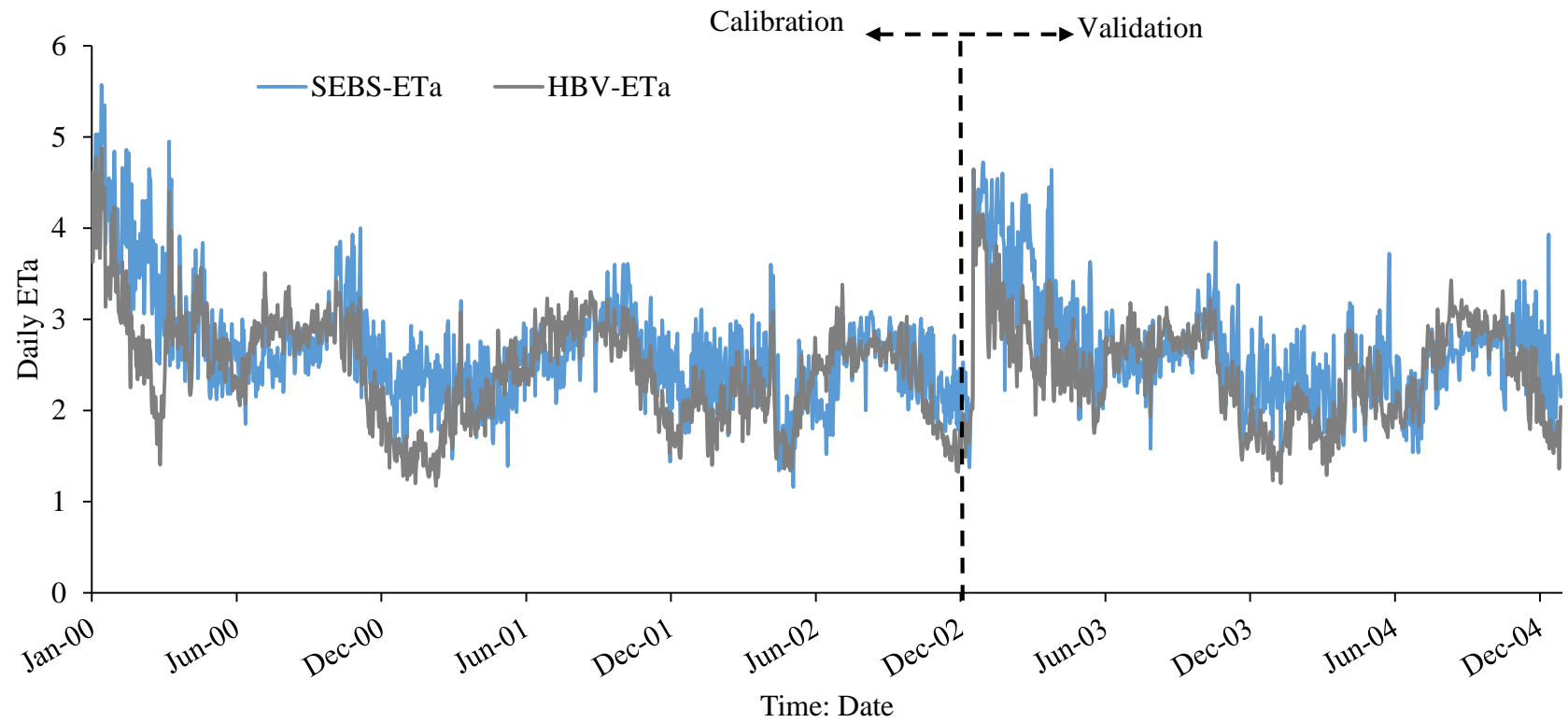
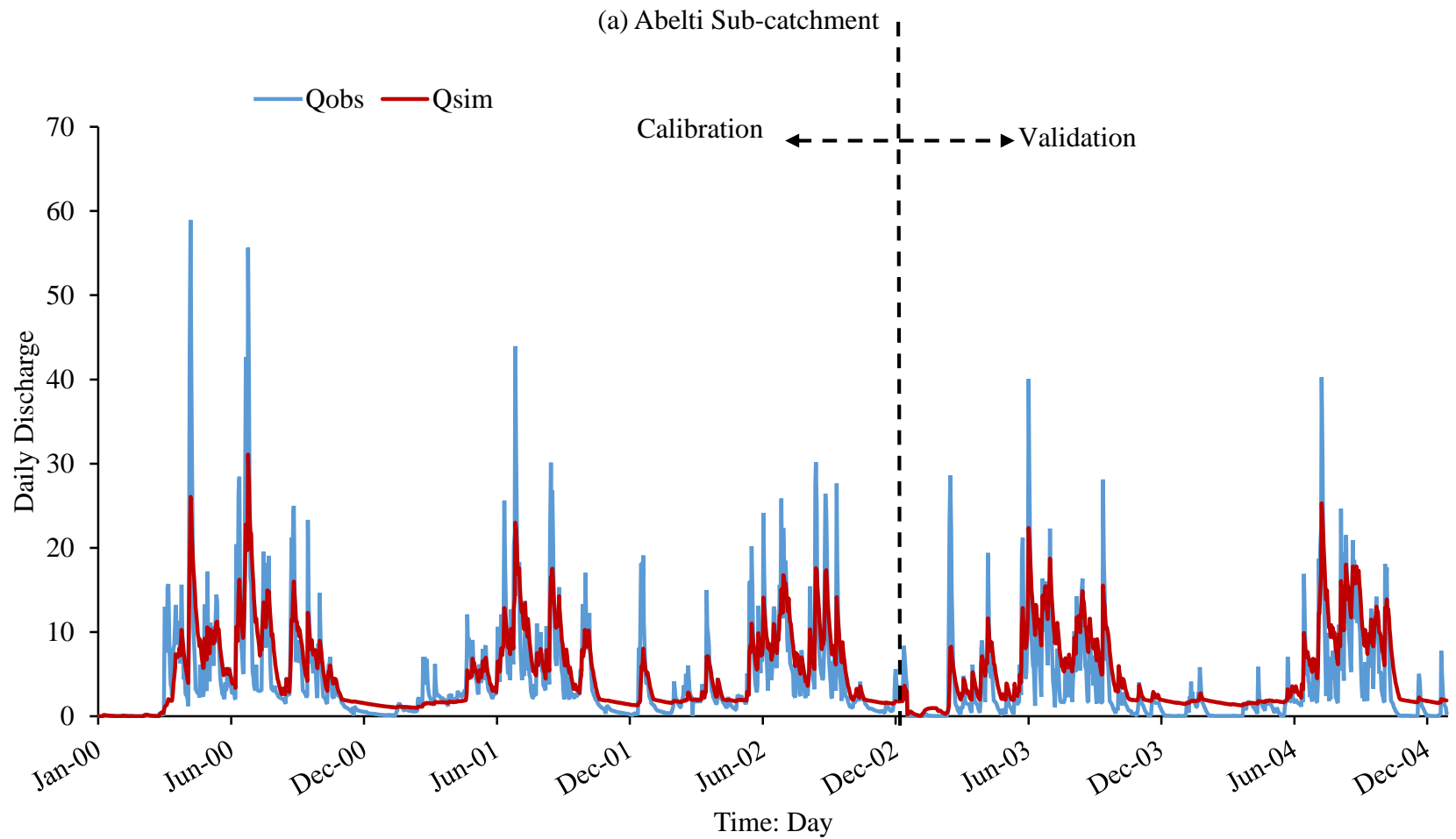
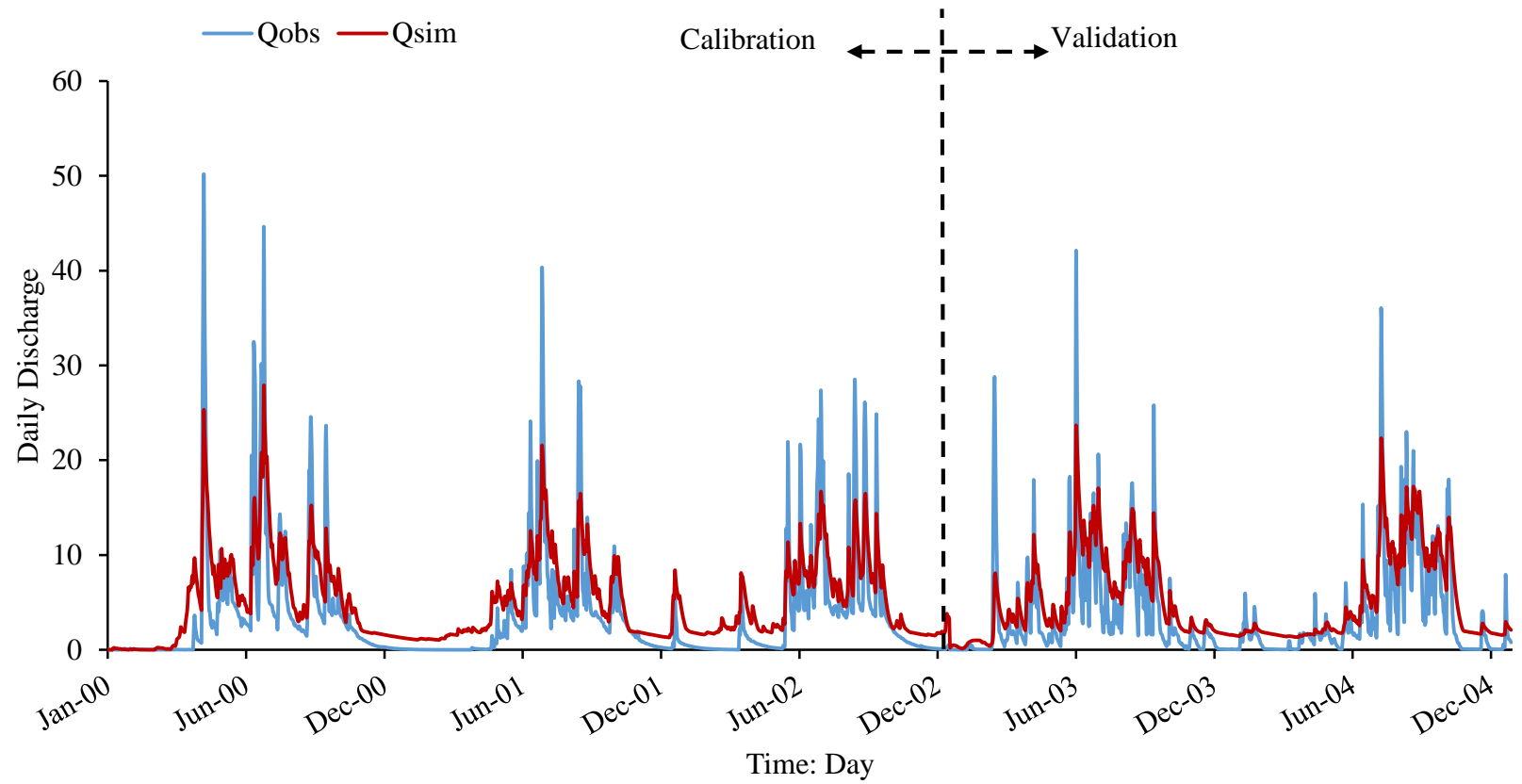


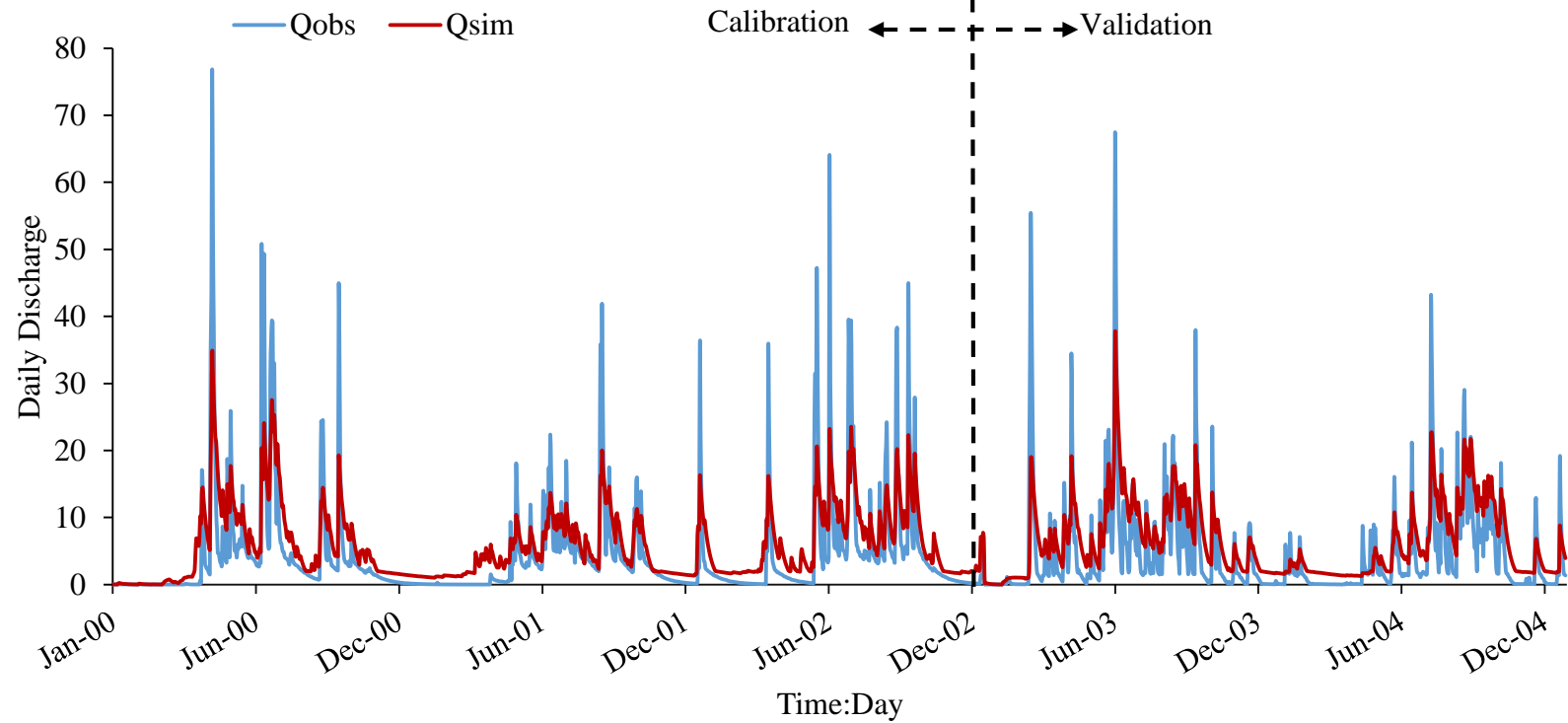
Figure 5-3 Time series of observed and simulated daily ETa for calibration and validation period for 1<sup>st</sup> Jan 2000-31<sup>st</sup> Dec 2004 for (a) Abelti, (b) Gibe, (c) Gojeb, and (d) Wabe Sub-catchments for case 1.



(b) Gibe Sub-catchment



(c) Gojeb Sub-catchment



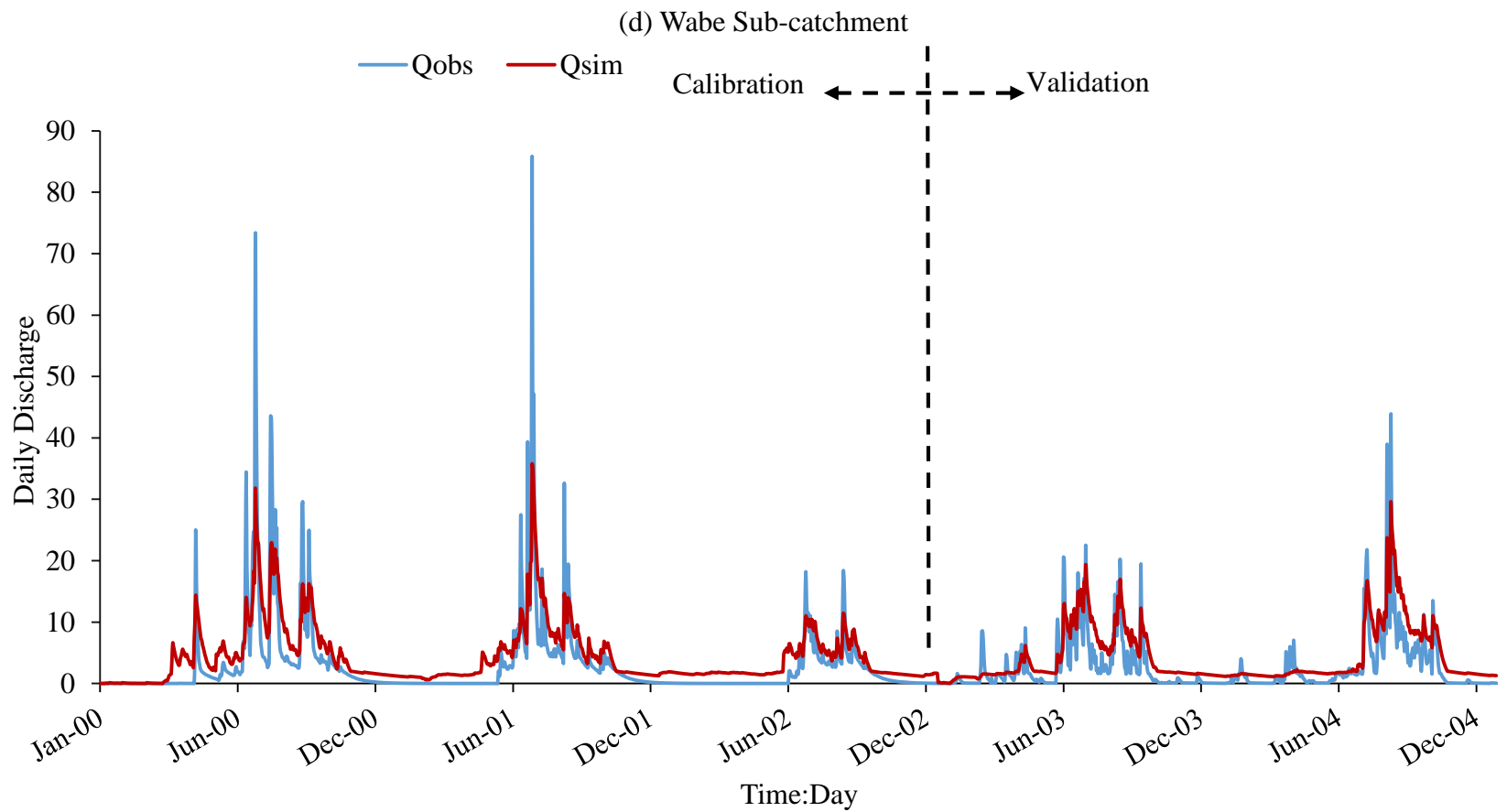
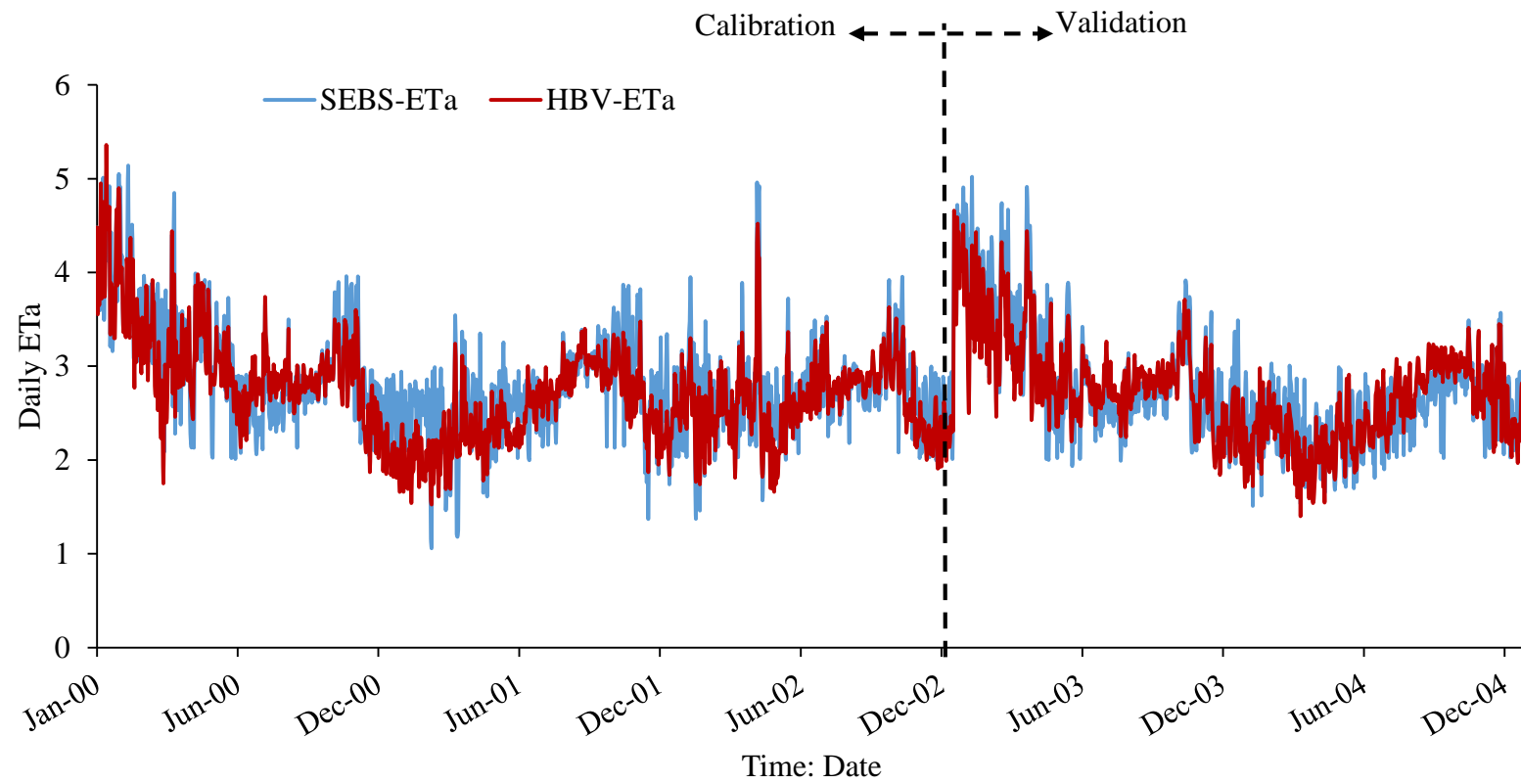
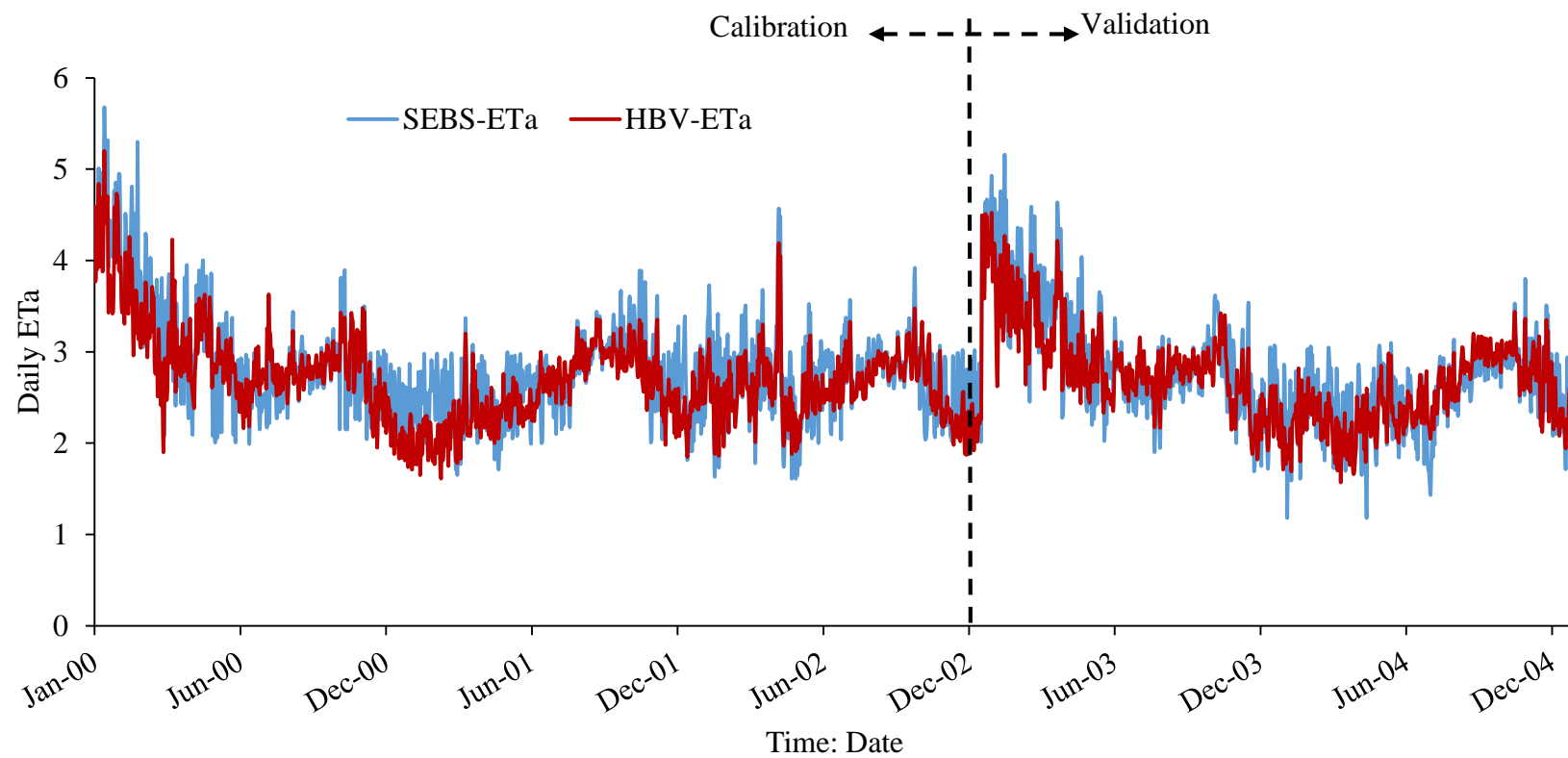


Figure 5-4 Time series of observed and simulated daily streamflow for calibration and validation period for 1st Jan 2000-31st Dec 2004 for (a) Abelti, (b) Gibe, (c) Gojeb, and (d) Wabe Sub-catchments for case 2.

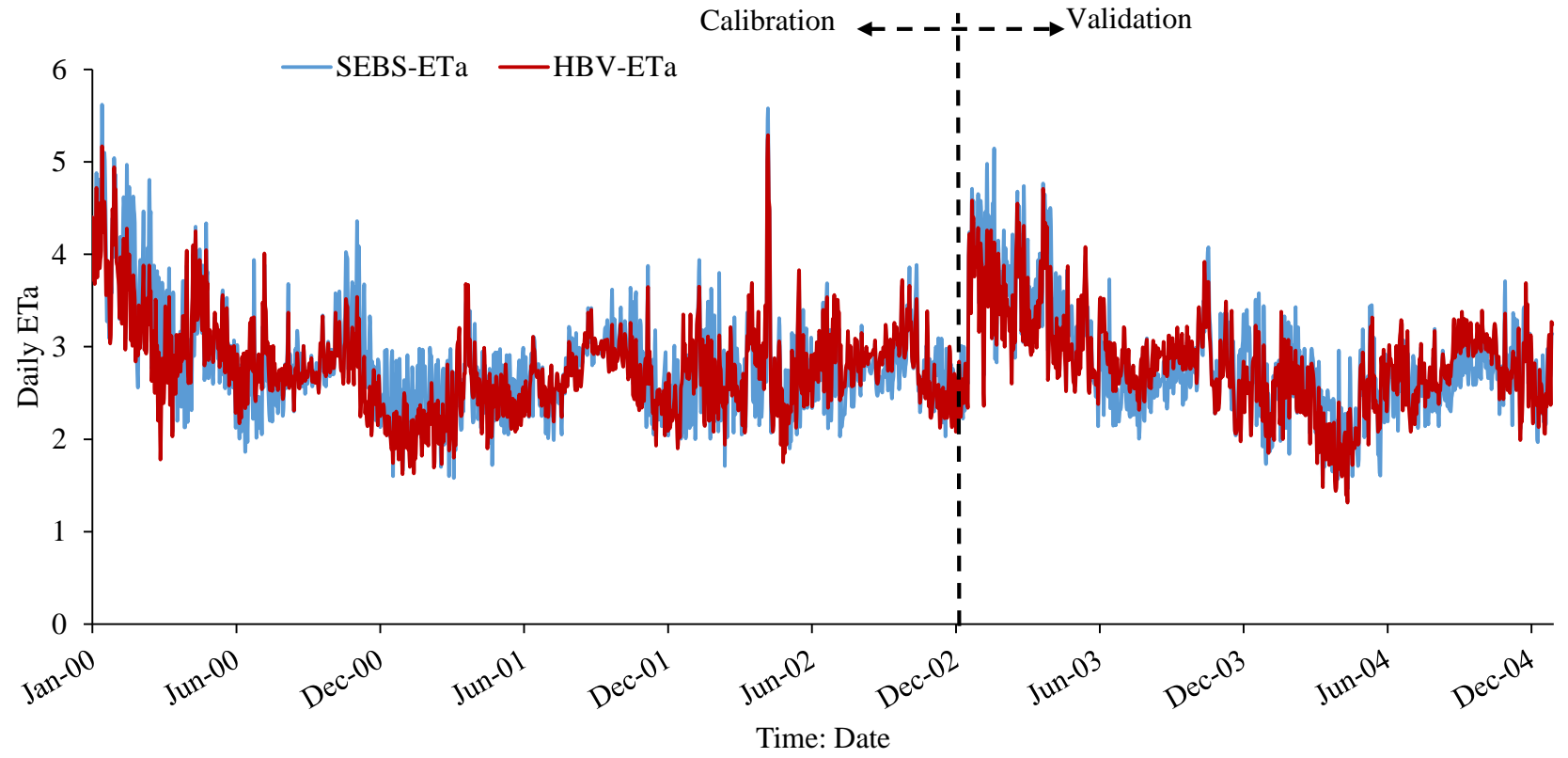
(a) Abelti Sub-catchment



(b) Gibe Sub-catchment



(c) Gojeb Sub-catchment



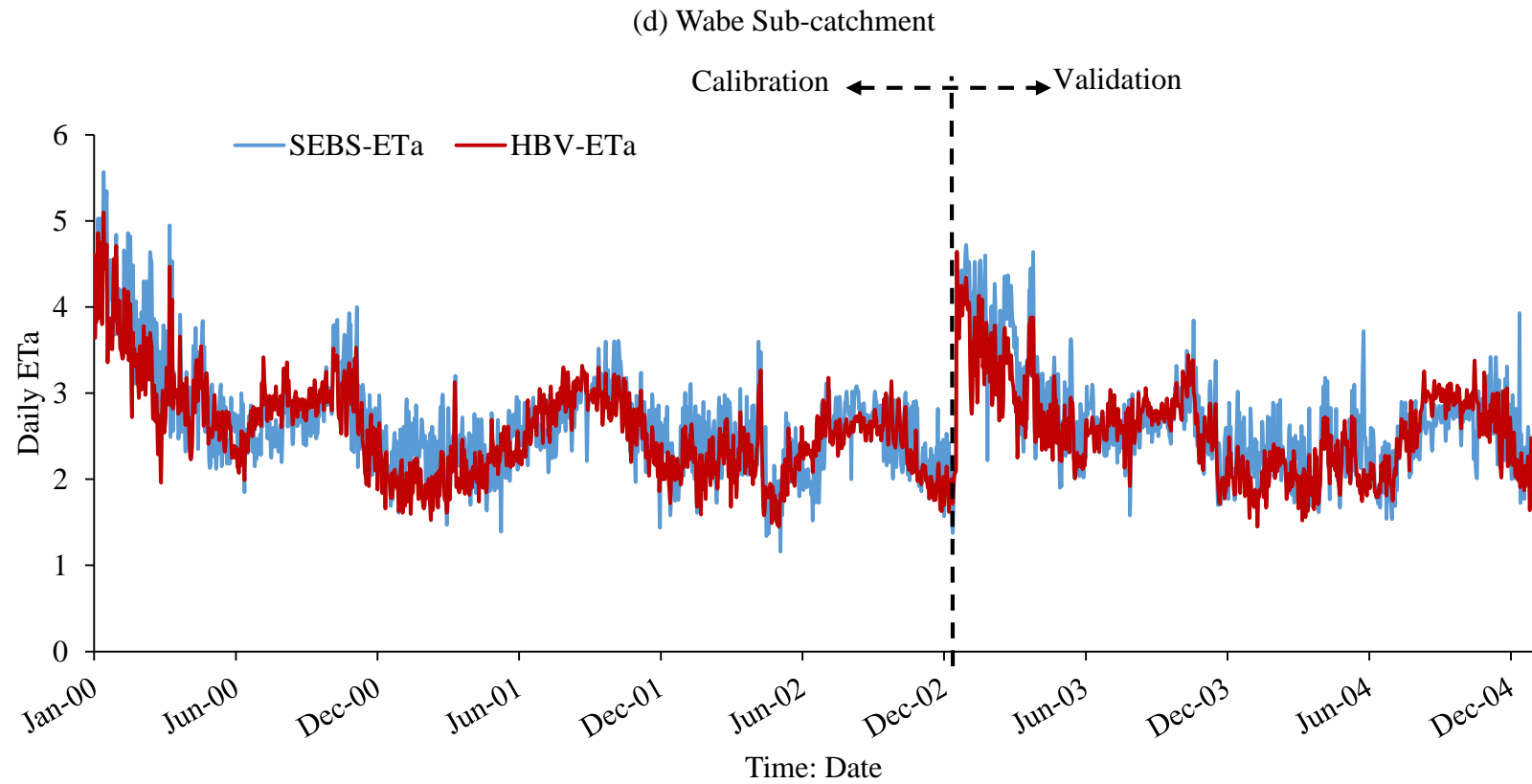


Figure 5-5 Time series of observed and simulated daily ETa for calibration and validation period for 1st Jan 2000-31st Dec 2004 for (a) Abelti, (b) Gibe, (c) Gojeb, and (d) Wabe Sub-catchments for case 2.

## **5.5. Conclusions and Recommendations**

In this study, the conceptual semi-distributed HBV light rainfall-runoff hydrological model was selected and used for calibration and verification based on multi-variable evaluation using streamflow and ETa to test the efficiency of SEBS-ETa in UOGB Ethiopia. Based on MCS, the model was calibrated and validated in two different cases using streamflow and ETa. The performance and applicability of HBV light were successfully evaluated through sensitivity analysis, model calibration, and verification, and reproducing simulated streamflow and ETa. Also, the efficiency of SEBS-ETa using the HBV hydrological model was assessed. The study showed that surface and subsurface water model parameters are sensitive and have physical meaning, especially the FC, LP, BETA, PERC, ALPHA, K1, and K2 were the most sensitive parameters with regard to streamflow and ETa prediction in the UOGB.

In the first scenario, the calibration and validation process is carried out for HBV hydrological model to verify whether or not the model is applicable in the study area. For calibration and validation of the model, the consideration was only in the streamflow, and the objective function NSE, RVE, and Y for daily ETa show low-performance values (less than satisfactory) for SEBS-ETa. Though the model performance of the HBV for simulating streamflow in the UOGB was very good, this shows the model has relatively high confidence and gives a very good result for the case of streamflow only. Moreover, the simulated streamflow peak was well represented in all of the days.

In the second scenario, the aim is to test the efficiency of SEBS-ETa in the study area and, with that in mind to test the performance of the HBV hydrological model. For calibration and validation purposes, the consideration was given to both in streamflow and satellite-based ETa. The result shows satisfactory to good performance for SEBS-ETa as well as streamflow. At the same time, the model was well simulated for both streamflow and ETa on the rising and falling limbs of the streamflow and ETa hydrograph during calibration and verification periods. Though, the streamflow and ETa peak were represented well and slightly underestimated the peaks for some days. Additionally, the objective function's

result shows satisfactory to good performance values contrary to a single variable calibration for both streamflow and ETa.

For model calibration and verification, the efficiency of the use of satellite-based ETa was confirmed. However, to reproduce the best outcomes from the model for water balance in the catchment during model calibration and verification, use of a combination of streamflow with estimated ETa should be necessary. Therefore, to provide reasonable solutions to reproduce and close the water balance in the catchment, it is required to use the preferred multi-variable calibration method. Moreover, the HBV hydrological model and SEBS approach can be used in other basins having similar characteristics.

The next chapters set out different production strategies to increase maize production in the water-scarce UOGB, Ethiopia,

## **CHAPTER 6: STRATEGIES TO INCREASE RAINFED MAIZE PRODUCTION IN THE UPPER OMO-GIBE BASIN, ETHIOPIA**

### **6.1. Introduction**

Water is fledgling as the most crucial and improperly used natural resource in the world. It is required for municipal, industrial and domestic activities and an important input for agricultural production. The demand for freshwater increases significantly on the basis of an increase in population and living standards. Owing to the depletion and contamination of freshwater, over-exploitation, and subsequent waste, the rise in population has been affected by severe food security. Seckler et al. (1998, 1999) stated that one-third of the population of developing countries is living in an entire region of water scarcity and does not have adequate water resources to meet their agricultural, environmental, industrial, and domestic requirements in 2025. An area is a water-scarce when a large number of experience water insecure (Rijsberman 2006). The per capita availability of water in Ethiopia is lower than 1000 m<sup>3</sup> per year (Asana Dowa et al. 2007). Increasing the productivity of existing water resources is often a feasible goal in semi-arid areas where prospects for exploiting new water resources are limited, and costs are increasing. Improving agricultural water productivity is vital for both social and economic development. In order to increase water productivity in agriculture, there is every reason to devote more effort to meet the potential food demand of the increasing population (Sarwar and Bastiaanssen 2001).

Ethiopia is part of sub-Saharan Africa and is situated within the tropics and therefore has no significant variation in its local temperature. On the basis of altitude and temperature, the climate of Ethiopia is divided into five thermal zones. Namely, (i) Bereha (a hot and hyper-arid type of climate, the elevation is less than 500 m, and the temperature is greater than 27.5°C), (ii) Kola (hot and dry climate, the elevation is between 500- 1500 m and the temperature is between 27.5°C-21.0°C), (iii) Woina-Dega (warm altitude climate, the elevation is between 1500 and 2500 m, and the temperature is between 21.0°C-16.0°C), (iv) Dega (temperate as highland climate, the elevation is between 2,500 and 3,000 m, and

the temperature is between 26.0°C-11.0/12.0°C), and (v) Wurch (cold climate, the elevation is more than 3000 m and temperature up to 7.5°C)(NMSA 2001). The altitude of the upper Omo-Gibe basin is between 718 and 3580 m above mean sea level (masl).

The rainfall in the basin can be divided into four zones, three of which have a unimodal and one bimodal rainfall. The northern part of the basin, including Waliso, Welkite, and south to just north of Jimma, has a rainfall of between 1,100 and 1,800 mm per year for about seven months from March to September. The little rain is from March to May and the largest one from June to September, with a noticeable increase in July and August. The southern area of the upper Omo-Gibe basin, including Jimma and Sodo, has a more even distribution of rainfall from March to September, with no peaks in July and August. The area typically receives more than 1,200 mm, rising to 2,000 mm on the western edges of the basin (Woodroffe and Associates 1995). During the rainy season (March–September), rainfed agriculture is used to produce the main cereal crop in the country. Generally, there is no single primary crop in Ethiopia; instead, five types of cereal productions are dominated: Teff, Barley, Wheat, Maize, and Sorghum, which account for about 75% of total cultivated area, and 29% of agricultural GDP (Aguilar et al. 2014).

Ethiopia is the second-most populous country in Africa with an estimated population of 100.6 million in 2015, with an average annual growth rate of 2.6 percent between 2010 and 2015 (FAO 2019), and expected to be 148.6 million in 2030, which is the end of sustainable development goal. Its economy is highly dependent on agriculture. The agriculture of Ethiopia is basically own-consumption, small-scale, and heavily dependent on rainfall. Approximately 90% of the country's agricultural production is produced by smallholder farmers using farming practices and traditional tools (Omiti et al. 2000). A low level of productivity characterizes Ethiopian agriculture. The average yield of grain for different crops in the country is less than one MT/ha. Over the last few decades, agriculture of the country has been incapable of producing adequate quantities to feed the rapidly growing population of the country (Belay and Manig 2004). Due to the lack of agricultural production, the country has been a significant recipient of food aid and commercial food grain importer. The population growth rate in the country's growing pressure on different

natural resources, land and average holding capacity of land per household is only around one ha (Belay and Manig 2004; Alemu 2005). In fact, more than 80% of the Ethiopian population lives in the highlands, where population pressure on farmland has always been immense.

The Ethiopian agriculture sector plays a central role in the lives and livelihoods of most Ethiopians, with some 12 million smallholder households accounting for an estimated 95% of agricultural production and 85% of jobs. Of the total number of farming households, 25% are women-headed. In addition, 87% of agricultural households work on less than 2 ha, 64% on less than 1 ha, and 40% on less than 0.5 ha. As with rain-fed agriculture, the average family of 6 people needs about 2.5 to 2.8 ha of land to fulfill the annual household food requirements (FAO 2014). Grain crops, including cereals, oilseeds, pulses, and other crops, are the main crops category to fulfill the annual household food requirements for the majority of the country's population, a source of household income and a foreign currency contributor. Cereal crops are the most important type of grain crop, both in terms of the planted area and the volume of production. Also, in terms of the diet, the majority of the population in the country use cereal crops. Cereals are grown in all regions with varying quantities and are produced in greater quantities than other crops since they are the main staple crops. The main staple crops in the country are teff, wheat, maize, barley, and sorghum.

Teff (*Eragrostis tef*) is the preferred staple food in much of the highlands. It is also an endemic cereal crop for the country, furnishes flour to make loaves of bread without yeast and Enjera, which are consumed in the highlands and the urban area of the country. Although commonly grown in the highlands, includes elevations from zero to 2800 meters above sea level (masl), Barely is the main livelihood crop in the country, which is mainly grown between 2000 and 3300 meters above sea level and is used for the production of food, beer and Tella (local beverage). Sorghum accounts for about 19.46% of all production and covers approximately 16.05% of the regional planted area with cereals(CSA 2018). Relative to other cereals, sorghum is usually tolerant of drought and embraces excess water conditions. Compared to other cereal crops, these characteristics

give sorghum a wide range of feasible climate regimes and grows best under semi-arid conditions. For instance, sorghum may produce cereal grain in areas that are too dry for maize (with an average annual rainfall of less than 250 mm). Maize (*Zea mays* L.) is one of the most important crops in the world, ranking third behind rice and wheat (WMO 2012). It's adaptability as a source of food, feed, and fuel to characterize it as a crop that can make an enormous contribution to food self-sufficiency and food security, considering its economic and social importance. Over the last few decades, maize production has increased enormously in the world and is now the most widely grown cereal crop with a total estimated production of  $1006.18 \times 10^6$  T (Greaves and Wang 2017). However, many developing countries face different challenges in the production of maize, such as dependence on rainfall, lack of financial resources, inadequate water for irrigation purposes, constraints in production, and limited infrastructure, which often leads to a decline in the level of maize crop production (WMO 2012). Maize is the second most widely grown cereal and is the most important cereal crop in the country and is sown as Meher and Belg for human consumption, animal feed, and industrial purposes. It is produced by more farms than any other crop. Besides being food grain, animal feed, and industrial purposes, parts of the maize plants are used as cooking fuel, fencing material, and fodder. On the basis of the volume of production, maize is the largest crop production in the country, producing more than 30% of the crop.

In the UOGB, cereals are grown in all regions with varying quantities. The UOGB accounts for about 8.67, 5.34, 5.97, 10.79, and 4.16 percent of the country's production for Teff, Barley, Wheat, Maize, and Sorghum, respectively (CSA 2018), and it is government policy to maintain and improve the amount of production until 2030 in order to stay self-sustaining. Approximately  $538.4 \times 10^6$  Kg of maize were produced in 2011, which means that production is expected to increase to about  $977.6 \times 10^6$  Kg by 2030. There are no clear strategies for increasing production by  $439.2 \times 10^6$  Kg. The key focus of this research work is to propose such a strategic plan.

In areas with limited water resources, among which is the UOGB, increased agricultural production contributes to land-use changes. For instance, deforestation and the

transformation of nature into agricultural land. In this case, the overall water consumption in the basin cannot be increased; instead, increasing grain production by using substituted vegetation on agricultural land because of the evapotranspired water. In addition to land-use changes, the management of fertilization, pesticide, quality seeds, seed rates, tillage and land preparation, protection work for soil erosion, and degradation will increase agricultural production. In case if water is not a limiting factor, the management of fertilization often has the greatest influence on crop yields as irrigation water is more efficient in a field that receives sufficient fertilizer (Wichelns 2003). Various studies have shown that fertilizer usage increases the production of grain crops (Kaliba et al. 2000; Rahman 2003; Asfaw et al. 2012; Nurudeen et al. 2015). Since 1960, fertilizer usage has increased the production rate almost five times in the world, which accounts for about 40% increase in per-capita production of food (FAO 2006) While there are regional and local differences and varying efficiencies. Applying fertilizers and water to optimum levels is the safest way to achieve maximum yields (Wichelns 2003).

An additional factor influencing crop production is the use of modern technology, such as improved seed rates (Yu et al. 2011; Nega et al. 2015; Sime and Aune 2018). Despite any additional demand for water resources, crop yields can be increased by managing non-water inputs, such as the supply of improved technologies. In terms of yield per cubic meter of water consumed, the productivity of water usage is enhanced due to an improved seed rate in the water-scarce area (Molden et al. 2009), such as the water-scarce upper Omo-Gibe basin. When water is scarce, understanding the magnitude of water consumption is important (Brauman et al. 2013). Irrespective of the opportunities to increase and the need for increasing water productivity (WP), the amount of water required for field crops and the relationship to yield dominate the need for additional water for food. In a situation where water is scarce relative to other sources involved in the production, it is appropriate to increase the productivity of water. Agricultural water production is increased due to (a) the contribution to economic development and poverty reduction, (b) ensuring that water is available for environmental use and alleviating pressure from re-allocation of water from agriculture to cities; and (c) meeting the demand for food from an increasingly urbanized

population, prosperous and growing of water scarcity (Molden et al. 2009). The objective of this study was, to investigate strategy to attain the 2030 target output of maize crops by increasing the production of maize through land alteration and yield enhancement in the current production area. Only currently available water resources can be used for these strategies, while not constraining all aspects and factors relating to agricultural practices and land suitability.

## 6.2. Land use, soil and water consumptions of the UOGB

### 6.2.1. Land use and soil

As illustrated in Figure 3.6 of chapter three, shows the major land-use types of UOGB; specifically, the area is mainly practiced rainfed agriculture, which encompasses a large area. Table 6.1 indicates agricultural area and pastoral lands and other land-use types, including urban areas, forests, and water bodies. Of which, the agricultural area covers 22,441.31 km<sup>2</sup>, pastoral land 6,670.3 km<sup>2</sup> and other land-use types 4,164.39 km<sup>2</sup>. Also, the major soil types of UOGB are described as detailed in section 3.4 of chapter three.

Table 6-1 the three major categories of land use type with their corresponding area in the UOGB

Sub-catchment	Area of land use types (ha)		
	Agricultural	Pastoral	Other
Abelti	1,213,381.57	199,324.61	160,293.82
Gibe	677,564.45	352,563.32	28,872.23
Gojeb	186,867.30	99,262.18	222,870.54
Wabe	166,220.68	15,876.60	4,402.72

### **6.2.2. Water consumption**

Water consumption in agricultural context refers to the immediate reduction of unusable water by means of evaporation from soils and open water bodies and by transpiration from crops and plants. The source of agricultural water consumption is estimated to be 22 percent of blue water, equal to 1570 km<sup>3</sup>, and 78 percent of green water. When considering the availability of water in relation to a broader range of agricultural practices and a variety of users, the concepts of green water and blue water are beneficial (CA 2007). The water found in reservoirs, rivers, aquifers, and lakes is considered to be blue water. It is also the main source of irrigated agriculture. In addition to agricultural use, blue water is a measured and managed freshwater resource intended to meet commercial, domestic, and hydroelectric power (UN 2006). At the same time, green water denotes the available soil moisture to plants produced by infiltrating rainfall and is the main source of rainfed agriculture. Irrigated agriculture uses blue water to supplement soil moisture for agricultural land, while rainfed agriculture uses only green water. During the dry season, farmers can retain their soil moisture by adding blue water to crops to reach their yield potential. Both blue and green water is “consumed” by plants and crops through the process of evapotranspiration and are not returned to the system.

However, as not all the water used for irrigation evaporates, the blue water consumption rate is lower than the withdrawal rate. As mentioned in the above paragraph, blue water consumed is 1570 km<sup>3</sup>. In contrast, agricultural irrigation consumed 60% of the water withdrawn for agriculture per year, and the remaining 40% goes back to groundwater and surface water. The ratio between consumption and withdrawal is a depleted fraction or consumptive fraction (Molden 1997). The consumptive fraction appears to be high in the area of water scares (where farmers reuse irrigation water and plants use shallow groundwater) while the consumption fraction is low in the area of water abundant.

The Surface Energy Balance System (SEBS) algorithm developed by Su (2002) has been used to estimate ET<sub>a</sub> for the UOGB. The procedure for estimating ET<sub>a</sub> for the whole cropping year (i.e., from November 2010 to October 2011) are described in chapters two

and four of this thesis. ETa for maize crops has been estimated for the entire crop year (i.e., from November 2010 to October 2011) and the crop growth season. The average annual precipitation of the UOGB is approximately 1121 mm, 1133 mm, 1223 mm, and 1223 mm in the south, east, north, and west of the basin, respectively. Seasonal ETa from rainfed maize is about 152.06 mm, which is equal to 1520.6m<sup>3</sup>/ha. Since UOGB is a water-scarce river basin, there are limited options for developing additional water resources to complement rainfed maize areas.

### **6.3. Crop water productivity and Relative evapotranspiration**

Two indicators evaluate the production of the agricultural system: crop water productivity (CWP) (Molden et al. 2003) and relative evapotranspiration (ETa/ETp) (Boss et al. 2005). Water productivity could have various definitions for different people and vary between and within groups of water users (Kijne et al. 2003; Tuong et al. 2004; Dugan et al. 2006; Playán and Mateos 2006; Wesseling and Feddes 2006; Zoebl 2006). Water productivity can be defined as the ratio of the net benefits from crop production, domestic use, forestry, fishery, livestock, industrial use, and mixed agricultural systems to the amount of water required to produce these benefits. For hydrologists, which is the ratio of the volume of water consumed efficiently (i.e., evaporation and transpiration) from the area to the volume of potentially available water for that purpose. For an economist, which may be defined as the value derived per unit of water used. In fisheries, it might mean the ratio of fish produced to the volume of water used. To an irrigation engineer, it might mean the ratio of the mass or the value of crops produced in a farm (or catchment) to the amount of water used. In livestock-related products, it may be defined as the ratio of livestock products to the volume of water consumed in production, including water, to feed those (Peden et al. 2007).

Moreover, for crop scientists, water productivity can have various definitions, e.g., water productivity for the whole plant is the ratio of above-ground dry matter per unit area to water usage, for the leaf is the ratio of photosynthetic leaf per transpiration, and for yield is the ratio of crop grain per unit area to water input (Hong-Xing et al. 2007). Additionally,

in the crop production system, CWP has been used to define the relationship between crops produced (Kg) and the amount of water consumed ( $m^3$ ) in crop production. In agriculture, more food production with less water is often encouraged as a strategy to increase CWP because water is a limiting factor in many parts of the world (Kijne et al. 2003; Boss et al. 2005; Sadras and Angus 2006; CA 2007; Amarasinghe et al. 2010), such as UOGB. Improving agricultural practice and water management is a useful task for increasing the impact of CWP (Breman et al. 2001; Liu et al. 2007; Nangia et al. 2008; Ahmad and Giordano 2010).

The relative evapotranspiration is the ratio of actual evapotranspiration to potential evapotranspiration. It is used to indicate that water is adequately available to sustain agricultural production during the growing season (Bos et al. 2007). When ET<sub>p</sub> is the same as ET<sub>a</sub> during the growing season, the crop is not affected by water scarcity, and the crop yield can be maximized in terms of weight per hectare (Bos et al. 2007). In terms of water consumption, while maintaining maximum crop production, the cumulative value of ET<sub>p</sub> is as high as 1.42 ET<sub>a</sub> (Bos et al. 2007). Appraisal of increased production on development strategies and crop water production requires information on land suitability for agricultural expansion, potential and current crop yields, the relationship between ET<sub>a</sub>/ET<sub>p</sub>, and yield and water consumption patterns via actual evapotranspiration. Due to relatively large size and remote areas, lack of field data is a major constraint for UOGB. Such field datasets are water used mostly by cropland and land use and land cover. Therefore, the use of satellite remote sensing data to observe land use/cover and associated properties in a spatially consistent manner is recommended in this study.

#### **6.4. Methodology**

The methodology adopted deems the assessment on the CWP and ET<sub>a</sub>/ET<sub>p</sub> of the current maize production area, land suitable for converting particular land cover to maize production areas, and strategies to increase maize production through land conversion and improved agricultural practice.

#### **6.4.1. Assessment of rainfed maize production**

Rainfed maize yields data (Kg/ha) were collected on a pilot scale at 3408 agricultural households for the 2003 and 2004 crop years. A household is considered an agricultural household when at least one household member is engaged in growing crops and raising and breeding livestock in private or collaborating with others. There are four major sub-catchments in the upper Omo-Gibe basin, which are Abelti, Gibe, Gojeb, and Wabe. 170 Enumeration Areas (EAs) were selected to represent the distribution of rainfed farming systems. The Enumeration Area in rural parts of the country is a locality that is less than or equal to a farmer's association area and usually consists of about 150 and 200 households. From these enumeration areas, 3408 agricultural households have been selected for the four sub-catchments of the upper Omo-Gibe basin. The selected households are 1611, 1085, 521, and 191, respectively, from Abelti, Gibe, Gojeb, and Wabe. Agricultural information on crop yield, seed rate, and fertilizer application was collected from the annual agricultural sample survey of the Central Statistical Agency of Ethiopia. Satellite-based ETa (which is already mentioned in Chapter 4 of this report) has been used for the water consumption of maize crops. Crop yields were related to ETa for the growing season. For all four sub-catchments, the relationship between yield and ETa/ETp, and yield and CWP were developed. The target value of ETa/ETp for rainfed maize is identified on the basis of the relationship. The target value is defined as the value above, in which the further increase in ETa/ETp does not have a significant effect on crop yield and maximized at a lower ETa value. An analysis of the crop production function was performed to quantify the effects of seed rate, nitrogen fertilizer, and water on yields in rainfed maize areas. By managing seed rates and fertilizers in existing maize crop areas, the probable increase in production was estimated based on the result of the analysis.

#### **6.4.2. Land suitability**

The topographic slope area for maize production has been used to identify land suitability analysis. Land suitability denotes the ability of a part of the land to endure crop production in a sustainable manner. Its assessment offers information on the opportunities and

hindrances for land use and thus informs decisions on the best use of resources, the knowledge of which is an important prerequisite for land use development and planning (Abdelrahman et al. 2016). Based on the characteristics of the terrain, the properties of the soil, and the current land use analysis, the land could be classified into spatially distributed agricultural potential zones (Bandyopadhyay et al. 2009). A land cover map based on the satellite image classification was used to classify the location with a particular land cover. A 30m\*30m resolution digital elevation model (DEM) obtained from Shuttle Radar Topography Mission (SRTM) has been used to classify the distribution of slopes across the UOGB. The slope percentage ranging from 0% to 3% is classified as fair, a slope ranging from 3 to 5% is classified as moderately suitable, and a slope ranging from 5% to 10% is, on average suitable for agricultural land (Bandyopadhyay et al. 2009), which is also suitable for the production of rainfed maize. The  $ET_a/ET_p$  assessment of rainfed maize water consumption compared to vegetation cover was higher or close to the average value. In areas where agriculture is not practiced, it is useful to locate areas where water is available to grow maize.

## **6.5. Result and Discussion**

### **6.5.1. Rainfed maize production**

$ET_a$  of maize areas in the pixels of the Abelti sub-catchment has been classified from low  $ET_a$  to a high  $ET_a$  in a variety of  $ET_a$  groups (Table 6.2). Seed rate, fertilizer indication, and highest and average yields were calculated to demonstrate various  $ET_a$  variation classes in yield across agricultural households in the Abelti sub-catchments based on the survey data collected by CSAE. All fertilizers used in Ethiopia are imported. Traditionally, ammonium sulfate and compound fertilizers have been the main fertilizers, and these fertilizers still account for a substantial proportion of imports. In addition to UREA and DAP fertilizers, most of the rural population in the country used the combustion of animal waste as local fertilizer. Moreover,  $ET_a$  classes for most optimally water uses are identified by calculating CWP and  $ET_a/ET_p$  for each class of  $ET_a$ . At the same time, the mid-value of respected  $ET_a$  classes divided from yield gives CWP. There is no household located in

areas where ETa is less than 170 mm/season from the sample data and land use map of the Abelti sub-catchment. The analysis is therefore carried out for the entire household maize area.

Table 6-2 Average and highest rainfed maize crop yield, ETa, seed rate, and fertilizer in the Abelti sub-catchment.

ETa (mm)	ETa/ETp	Average yield		Highest yield (Kg/ha)	Seed Rate (Kg/ha)	Fertilizer (Kg/ha)	NO. of Holders
		CWP (Kg/m <sup>3</sup> )	Yield (Kg/ha)				
<170	-	-	821	1409	-	98	-
170-310	0.29	0.4	1014	1807	66	127	14,698
310-450	0.46	0.5	2606	2926	65	84	38,209
450-590	0.63	0.4	2728	2926	63	76	17,485
590-730	0.80	0.3	2934	2876	100	98	2,677
730-870	0.97	0.3	2947	2992	87	105	834

In Table 6.2 the seasonal average CWP of maize of the Abelti sub-catchment is 0.3 Kg/m<sup>3</sup> with a minimum and a maximum values of 0.3 Kg/m<sup>3</sup> and 0.5 Kg/m<sup>3</sup>, respectively. Whereas the highest yield value of the Abelti sub-catchment ranges from 1409 Kg/ha to 2992 Kg/ha respectively in the respective ETa groups. When ETa/ETp is 0.97 (highest) the CWP is 0.3 Kg/m<sup>3</sup> (lower) and the average yield is 2947 Kg/ha. For ETa of 310-450 mm, the CWP is 0.5 Kg/m<sup>3</sup> (highest), the average yield is 2606 Kg/ha, and ETa/ETp is 0.46 (almost average). The average seed rate ranges between 63 Kg/ha to 100 Kg/ha, and the average fertilizer application rates are between 76 Kg/ha to 127 Kg/ha.

The average actual evapotranspiration of maize over the main maize growth span of six months (i.e., April 20011 to September 20011) is 520 mm (Table 6.2). The ETa of maize closely follows the same patterns of yield variability. The highest values were found in the “good aspects” of the high yield areas of maize. Other areas display relatively uniform and low values.

### 6.5.2. Crop production function

Crop production analysis and its planting can be studied from two different approaches. The first approach evaluates the crop yield as a function of the amount of seeds, fertilizers, pesticides utilized, weather factors, classic factors of production, and monthly temperature and rainfall (or other climate variables such as evaporation and soil moisture). The second approach depends on farmers’ decision making. In this approach, the primary concern of the farmers is to decide how much surface area is appropriate for seed plants, which is explained in terms of direct crop production costs ( i.e., pesticides, labor, fuels, fertilizers, etc.), Consumer Price Index (CPI), Agricultural Producers Price Index (APPI), and crop planting area (autoregressive model) (Suchánková and Bezděková 2011). Hussain et al. (2003) and Amarasinghe et al. (2010) point out that the function of crop production can estimate the impact of different factors on yields. In this study, to an estimation of the crop production function of the Abelti sub-catchment, a multiple regression analysis was performed, which explains the availability of water, seed rate, and fertilizer effect on maize yields (Equation 6.1). A set of linear and non-linear functional forms has been checked, from which the function most closely matches the set of data has been chosen on the basis of the coefficient of determinants ( $R^2$ ) (Table 6.3).

$$Yield = A_0 + A_1ET_a + A_2SR + A_3F \quad 6.1$$

Where, yield is maize yield (Kg/ha), ETa is actual seasonal evapotranspiration (mm), SR is the seed rate (Kg/ha), and F is the fertilizer application rate (Kg/ha).

Table 6-3 Correlation coefficients between crop yield (maize), ETa, seed rate, and fertilizer in the Abelti sub-catchment.

Sub-catchment	A <sub>0</sub>	A <sub>1</sub>	A <sub>2</sub>	A <sub>3</sub>	R <sup>2</sup>	No. of points
Rainfed maize of Abelti sub-catchment	3657.34	1.1515	2.3229	-	0.794	5
				17.6303		

From Table 6.3, the value of R<sup>2</sup> for the selected three variables for the production functions shows 0.794, which means that the selected variables represented approximately 80% of the variation in maize yields. In addition, each coefficient shows a change in maize yield per unit change in one variable, while the other variables remain unchanged. For example, the primary factor affecting yield in maize areas is fertilizer. In addition, the seed rate has a high yield impact, and an increase in the seed rate with one Kg/ha raises the yield by 2.32 Kg/ha.

### 6.5.3. Land suitability for rainfed maize

Based on the DEM-based slope map, areas with a slope between 0 to 3%, 3 to 5%, and 5 to 10% are categorized as suitable land for rainfed maize. Furthermore, ETa/ETp map, land cover map, and slope classification map are combined to classify further the appropriate land conversion area for rainfed maize yield. As stated in Table 6.2, ETa/ETp values range from 0.29 to 0.97 for rainfed maize in the Abelti sub-catchment area. And hence, pastoral land with ETa/ETp greater than 0.46 has been defined as suitable areas for the selected three slope classes for the expansion of rainfed maize (Table 6.4). ETa/ETp was chosen on the basis of the average rainfed maize yield value of Ethiopia, which is below 2000 Kg/ha (Wani et al. 2009) and for which the ETa/ETp values are between 0.29 and 0.46.

Table 6-4 Suitable pastoral land area for the three slope classes for the expansion of rainfed maize

Sub-catchments	Total Pastoral Land (ha)	Pastoral Land area (ha) for the three slope classes (%)		
		0%-3%	3%-5%	5%-10%
Abelti	199,324.61	3,995.89	6,311.99	5,343.51
Gibe	352,563.32	50,099.47	20,633.95	27,838.63
Gojeb	99,262.18	15,718.41	9,119.151	30,756.82
Wabe	15,876.60	8,276.853	2,204.275	2,044.055

From Table 6.4 on the expansion of rainfed maize in the upper Omo-Gibe basin, it is observed that the availability of land in the Wabe sub-catchment is comparatively low compared to the other three sub-catchments due to the small size of the sub-catchments. In addition to the Wabe sub-catchment, the availability of land for the Abelti sub-catchment is increasing due to the increasing size of the field. In contrast, the availability of suitable land for the Gojeb sub-catchment is comparatively medium. On the other hand, the availability of land for the Gibe sub-catchment is reasonably high due to the large size of the sub-catchment and its homogeneous terrain. Out of the total 667,026.71 ha of pastoral land, the total additional expansion area suitable for rainfed maize is about 30,287.17 ha, of which is Abelti, Gibe, Gojeb, and Wabe sub-catchments have contributed 2,599.70 ha, 16,372.82 ha, 9,234.23 ha, and 2,080.44 ha of suitable land in the same order. As new maize areas use the same amount of water from pastoral land prior to land conversion, the addition of rainfed maize to 30,287.17 ha of pastoral land in good to average land suitable areas does not affect the sub-catchments water balance.

#### **6.5.4. Rainfed maize production strategies**

##### ***Strategy I: Increase yield in the current maize production areas of rainfed maize production***

Before it settles around 11 to 12 billion by the end of the 21<sup>st</sup> century, the world population is predicted to hit 8 billion by 2025 (UN 2006). The majority of this population increase is expected to occur in low-income countries, where most poor people live, and rain-fed agriculture forms the dominant basis for subsistence survival. Both Asia and Africa are the leading countries to contribute to this increase in population. Ethiopia is one of the second most populous countries in Africa to contribute to this increase in population. More food will be required in the future, due to the projected rise in population in the country. Ethiopia would need to import more food to fulfill the food needs of the countries in the future. At least in the near future, plants, particularly cereals, will continue to supply much of the country's increased food demand, both for human consumption and for livestock feed, in order to meet the increasingly rising demand for eggs, milk, and meat in the newly developed industrialized countries. For example, for the UOGB, an additional  $37.1 \times 10^6$  Kg of grain crops is estimated to be needed yearly by 2030, of which  $37.1 \times 10^6$  Kg are contributed from maize crops. Most of this increase will be allocated from land already in use by improved yields (Borlaug and Dowsell 2003).

Source of growth in irrigated areas, such as increase in population and demand for land competing for other sectors of the economy, especially in the UOGB, most of the increase in food production would have to come from an increase in productivity per unit of land rather than an increase in an agricultural area. Rainfed agriculture must therefore increase in order to fill the gap. For example, in order to bridge this yield gap, it is assumed that the yield gap of all ETa classes in the upper Omo-Gibe basin can be minimized through seed rate and fertilizer management. The average and the maximum stated rainfed maize yield of ETa class between 310 and 450 mm per season is about 2606 Kg per hectare and 2926 Kg per hectare in the same order. Increased yield gaps of rainfed maize production by quarter (80 Kg per hectare), half (160 Kg per hectare), and three quarters (240 Kg per

hectare) are achieved by increasing fertilizer by about 4 Kg per hectare, increasing the seed rate by about 0.5 Kg per hectare and decreasing fertilizer by about 5 Kg per hectare, respectively. Table 6.5 shows an increase in rainfed maize production by means of improved agricultural practices, where average production rates have improved by quarter, half, and three-quarters of the yield gap.

Table 6-5 increase yield production in existing yield of a maize field

Sub-catchment	Average yield (Kg/ha)	Highest yield (Kg/ha)	Agricultural land (ha)	Increase in yield production (*10 <sup>6</sup> Kg)		
				0.25 yield gap	0.5 yield gap	0.75 yield gap
Abelti	2728	2926	201,542.68	10.0	20.0	30.0
Gibe	1520	2876	112,543.45	38.2	76.3	114.5
Gojeb	1723	2642	31,051.48	7.1	14.3	21.4
Wabe	2726	2876	27,609.25	1.0	2.1	3.1

Table 6.5 shows that the Wabe sub-catchment in the rainfed maize area produces a yield gap of 4.1\*10<sup>6</sup> Kg, which is lower than the other three sub-catchments. On the other hand, the yield gap for the Gibe sub-catchment (152.7\*10<sup>6</sup> Kg) is higher than the other three sub-catchments. As a result, for the entire UOGB, the increase in rainfed maize production results from observation point yields by one-fourth, two-fourth, and three-fourth of the yield gap, increasing the maize production by 56.3\*10<sup>6</sup> Kg, 112.7\*10<sup>6</sup> Kg, and 169.0\*10<sup>6</sup> Kg in the same order.

***Strategy II: The potentially suitable land area converted into rainfed maize from pastoral land to expand the area of rainfed maize***

The potential area suitable for the production of rainfed maize has been converted from pastoral land on the basis of the analysis mentioned in section 6.4 for the three slope classes, which is discussed in Table 6.4. Table 6.6 shows the outcomes of the increases in maize production for the three slope classes. The average and the maximum yields and the increase in yield gaps by one-fourth, two-fourth, and three-fourth were used to estimate the increases in maize production for each of the slope classes in the UOGB.

Based on the availability of pastoral lands suitable for expansion to a rainfed maize, the lowest ( $0.31 \times 10^6$  Kg) and the highest ( $22.2 \times 10^6$  Kg) production increase for the sum of the three slope classes were observed in Wabe and Gibe sub-catchments respectively. All in all, if the yield of the present average rainfed maize in the UOGB is retained as it is, the increase in production in the fair sloping class (0-3 %), the moderate sloping class (3-5 %), and the average sloping class (5-10 %) found to be  $14.02 \times 10^6$  Kg,  $6.30 \times 10^6$  Kg, and  $11.19 \times 10^6$  Kg, respectively. At the observation point of UOGB, the increment in yield production by one-fourth, two-fourth, and three-fourth of yield gap shows an increase of  $7.88 \times 10^6$  Kg,  $15.76 \times 10^6$  Kg, and  $23.64 \times 10^6$  Kg rainfed maize in the same order. These yield gaps indicate that the crop yields in these countries can be substantially increased if improved practices are adopted.

In the first strategy, in order to meet the expected 2030 rainfed maize production target for the UOGB, the increase in yield gaps by one-fourth, two-fourth and three-fourth contributes 23.12 %, 46.23 %, and 69.35 % of the overall targeted production in the existing rainfed maize area of the basin in the same order. Whereas, in the second strategy, the increase in production for an additional suitable land which are the fair sloping class (0-3 %), the moderate sloping class (3-5 %), and the average sloping class (5-10 %) contributed 0.80, 0.39, and 0.68, 1.61, 0.79 and 1.36 and 2.41, 1.18 and 2.04 % of the expected targeted production in the same order. Table 6.7 summarizes the two rainfed maize production strategies for the 2030 target.

Table 6-6 Maize production for the three slope classes

Sub-catchment	Slope classes (%)	Average yield (Kg/ha)	Highest yield (Kg/ha)	Additional pastoral land (ha)	Increase in yield production (*10 <sup>6</sup> Kg)					
					0.25 of the gap	0.50 of the gap	0.75 of the gap	0.25 of the yield gap	0.50 of the yield gap	0.75 of the yield gap
Abelti	0-3			663.72	0.03	0.07	0.10			
	3-5			1048.42	0.05	0.10	0.16			
	5-10	2728	2926	887.56	0.04	0.09	0.13			
Gibe	0-3			8,321.52	2.82	5.64	8.46			
	3-5			3,427.30	1.16	2.32	3.49			
	5-10	1520	2876	4,624.00	1.57	3.14	4.70			
Gojeb	0-3			2,610.83	0.60	1.20	1.80			
	3-5			1,514.69	0.35	0.70	1.04			
	5-10	1723	2642	5,108.71	1.17	2.35	3.52			
Wabe	0-3			1,374.78	0.05	0.10	0.15			
	3-5			366.13	0.01	0.03	0.04			
	5-10	2726	2876	339.51	0.01	0.03	0.04			

Table 6-7 Overview of the two strategies for producing rainfed maize in the UOGB for 2030.

	Expected rainfed maize production for the 2030 target (*10 <sup>6</sup> Kg)		
	0.25 of the yield gap	0.5 of the yield gap	0.75 of the yield gap
<b>Strategy I</b>			
Total production	101.55	203.11	304.66
%age cover of the 2030 target	23.12	46.23	69.35
<b>Strategy II</b>			
For a slope class of 0-3%			
Total production	3.53	7.07	10.60
%age cover of the 2030 target	0.80	1.61	2.41
For a slope class of 3-5%			
Total production	1.73	3.46	5.20
%age cover of the 2030 target	0.39	0.79	1.18
For a slope class of 5-10%			
Total production	2.99	5.97	8.96
%age cover of the 2030 target	0.68	1.36	2.04

## 6.6. Conclusions

This chapter aimed to identify different production strategies to increase maize production in the water-scarce UOGB, Ethiopia, by 2030. These strategies are the conversion of suitable pastoral land to agricultural land in order to increase the area of rainfed maize and increase the yield of existing agricultural land. The strategies identified are achieved by assessing rainfed maize production through analysis of crop production function, crop water productivity (CWP), and measurement of relative evaporation (ETa/ETp).

For each class of ETa in the four sub-catchments, ETa classes for most optimally water uses are identified by calculating CWP and ETa/ETp. Based on the analysis, the seasonal average CWP of maize of the Abelti sub-catchment is  $0.3 \text{ Kg/m}^3$  with a minimum and a maximum values of  $0.3 \text{ Kg/m}^3$  and  $0.5 \text{ Kg/m}^3$ , respectively. Additionally, it is found that the ETa of rainfed maize over the main maize growth span period is 520 mm.

Crop production function analysis and its planting can be studied as a function of the amount of seeds, fertilizers, and water utilized to evaluate the crop yield in the study area for rainfed maize area. The result indicates that the selected variables represented approximately 80% of the variation in the rainfed maize yields. Moreover, the seed rate has a high yield impact, and an increase in the seed rate with one Kg/ha raises the yield by 2.32 Kg/ha.

Based on the characteristics of the terrain, the properties of the soil, and the current land use analysis, the land could be classified into spatially distributed agricultural potential zones. A 30m\* 30m resolution DEM has been used to classify the distribution of slope across the UOGB. A total of 30,287.17 ha of suitable pastoral land has been converted/expanded to rainfed maize area in the three slope classes of the basin. The fairly suitable land sloping classes, the moderately suitable land sloping classes, and the average suitable sloping classes contributed 12,970.86 ha, 6,356.54 ha, and 10,959.79 ha of suitable land for rainfed maize area in the same order.

The defined two strategies to meet the expected 2030 rainfed maize production target for the UOGB are assessed based on the increase in yield gaps by one-fourth, two-fourth, and

three-fourth. In the first strategy, the increase in yield gaps by one-fourth, two-fourth, and three-fourth contributes 23.12%, 46.23%, and 69.35% of the overall targeted production in the existing rainfed maize area of the basin in the same order. Whereas, in the second strategy, the increase in production for an additional suitable land contributed to 0.80, 0.39 and 0.68, 1.61, 0.79, and 1.36 and 2.41, 1.18, and 2.04% of the expected target production in the same order.

The next chapter provides concluding remarks and recommendations and proposes the scope of future research work.

## **CHAPTER 7: SUMMARY AND CONCLUSIONS**

### **7.1. Summary**

Water resource scarcity is a hindrance to agricultural activities and sustainable development in various parts of the world. Water resource management is often hindered by a lack of information on the availability of streamflow data around the world because there are limitations on the available gauging stations or failure of the gauging stations. Lack of available data often leads to high uncertainty in the assessment of water resources management and low confidence in decision-making. The aim is to measure the spatiotemporal distribution of availability of water for agriculture, to test the effectiveness of ETa and streamflow and evaluate the possible increase in maize production to meet the demand by 2030 in the upper Omo-Gibe basin in Ethiopia. Integrating satellite remote sensing and hydrological modelling has been used in the basin. The results include the estimate of actual evapotranspiration, the statistics on the water balance, the calibration, validation, and performance assessment of the hydrological model, and the increase in maize production. This section comprises the important findings of this study to advance the field of physical hydrological modelling and water balance assessment for water resource management in the Upper Omo-Gibe Basin, Ethiopia. It also addresses some of the drawbacks of the HBV model and also provides important recommendations and scope for further study.

### **7.2. Conclusions**

#### **7.2.1. Actual evapotranspiration estimation and water balance analysis**

The Surface Energy Balance System (SEBS) algorithm was used for the period from November 2003 to October 2004 to estimate the ETa value in the upper Omo-Gibe basin using 16 cloud-free MODIS-TERRA satellite images and meteorological data for 23 rain gauge stations. In addition, the Thiessen polygon method was applied to the spatial interpolation of precipitation.

- The water balance determined using Thiessen polygon-based spatial interpolated precipitation and SEBS-based ETa indicates that the water balance of the basin is understood clearly. During the study period of the water balance analyses, the UOGB received 41,080Mm<sup>3</sup> of water in the form of precipitation and released 28,668Mm<sup>3</sup> of water in the form of evapotranspiration, while the uncountable volume of water remained 2,683Mm<sup>3</sup>, which means the difference between precipitation, evapotranspiration and surface outflow from the basin. In addition, the water closure term of the basin varies from 14.35% to 0.002%.
- From the analysis of the water balance studies, the highest monthly ETa values are observed during the months of April 2003 to October 2004, indicating the overall growing season of rainfed crops such as maize, wheat, barley, sorghum, teff, etc. The period between April and June is called the Belg period and the growing season for maize crops. The analysis also shows that ETa is high during the summer months, called Kiremt, which is primarily due to the rainy season and is also the main growing season for all types of crops.
- The standard FAO Penman-Monteith reference evapotranspiration method was used to compare SEBS-ETa. From the comparison, it has been observed that average of the SEBS-ETa values have the same result as the PM-ETa. Whereas, in the extreme case value there is some deviation between SEBS-ETa and PM-ETa. On the other hand, the temporal variation in the basin indicates that the inter-annual rainfall variability gradually decreases from east to west.
- From the water balance measurement analysis, the drainage ratio (which is about 0.1) in the basin indicates that the UOGB is a water-scarce area, and, on this basis, there are limited opportunities to develop additional water resources. As a result, the expected increase in agricultural production is achieved by expanding the rainfed agricultural area and by increasing the productivity of crop water in existing areas.

### **7.2.2. Calibration, validation, and performance evaluation of HBV hydrological model**

In this analysis, the HBV hydrological model was used to test multi-variable calibration using daily streamflow and ETa data. In addition, this hydrological model was calibrated on the basis of the Monte Carlo Simulation (MCS) procedure for two different scenarios. The performance and applicability of HBV light were successfully evaluated through sensitivity analysis, model calibration and validation, and simulated streamflow and ETa reproduction. Calibration and validation of the model were performed using five years of daily hydrological and meteorological data for each of the four major sub-catchments. In addition, the efficiency of SEBS-ETa using the HBV hydrological model has also been assessed.

- The study showed that some parameters of the hydrological model are sensitive and have physical meaning; in particular, the FC, LP, BETA, PERC, ALPHA, K1, and K2 were the most sensitive parameters for streamflow and ETa prediction in the UOGB.
- In the first scenario, a single variable calibration, such as streamflow, is being used for model calibration and validation, and the objective functions NSE, RVE, and Y for daily ETa are less than satisfactory for SEBS-ETa. While the model has relatively high confidence and provides a very good result for simulating streamflow. The simulated streamflow peak has also been well represented in all days.
- In the second scenario, the calibration and validation results of the HBV hydrological model indicate simulated daily flow and ETa were reasonably consistent with the measured daily flow value and the estimated SEBS-ETa value. Contrarily to a single variable calibration for both streamflow and ETa, the result of the objective function is satisfactory to good performance values. The aim of this scenario is, therefore, to test the efficiency of SEBS-ETa in the study area and, with that in mind, to test the performance of the HBV hydrological model.
- The model was found to have a good analytical capability for streamflow calibration and validation with NSE, RVE, and Y ranging from 0.66 to 0.69 and 0.62 to 0.68, 0.04 to 0.45 and 0.38 to 0.54, and 0.47 to 0.67 and 0.42 to 0.47 in the same order. Similarly,

from the model, the efficiency values for the calibration and validation periods for ETa for major sub-catchments indicate that NSE, RVE, and Y range from 0.56 to 0.66, and 0.64 to 0.73, 0.02 to 0.04, and 0.01 to 0.04, and 0.54 to 0.65, and 0.62 to 0.72 in the same order.

- The efficiency of the use of satellite-based ETa has been verified for model calibration and validation. However, it should be appropriate to reproduce the best results from the water balance model in the catchment during model calibration and to validate the use of a combination of streamflow and estimated ETa. Therefore, in order to have reasonable solutions for reproducing and closing the water balance in the catchment area, the preferred multi-variable calibration method would be used. This method reduces the uncertainty of the model parameters. In addition, the HBV hydrological model and the SEBS approach can be used in other basins with similar characteristics.

### **7.2.3. Increasing maize production**

Agricultural production, in especially maize crops in the water-scarce UOGB, can be increased by increasing crop water productivity and improving agricultural management.

- Based on the CWP and ETa / ETp analysis, the seasonal average Abelti maize CWP is 0.3 Kg/m<sup>3</sup>. In addition, ETa of rainfed maize over the main maize growth period has been found to be 520 mm per season.
- Crop production function analysis and its planting can be studied as a function of the amount of seeds, fertilizers, and water utilized to evaluate the crop yield in the study area for rainfed maize area. The result indicates that the selected variables represented approximately 80% of the variation in the rainfed maize yields. Moreover, the seed rate has a high yield impact, and an increase in the seed rate with one Kg/ha raises the yield by 2.32 Kg/ha.
- A total of 30,287.17 ha of suitable pastoral land has been converted/expanded to rainfed maize area in the three slope classes (namely fairly, suitable land sloping classes, the moderately suitable land sloping classes, and the average suitable sloping class) of the basin.

- The two strategies identified to meet the expected 2030 UOGB rainfed maize production target are assessed on the basis of a one-fourth, two-fourth, and three-fourth increase in yield gaps. In the first strategy, the increase in yield gaps by one-fourth, two-fourth, and three-fourth contributes 23.12%, 46.23%, and 69.35% of the total targeted production in the current rainfed maize area of the basin in the same order. Whereas, in the second strategy, the increase in production for additional suitable land contributed to 0.80, 0.39 and 0.68, 1.61, 0.79, and 1.36 and 2.41, 1.18, and 2.04% of the planned target production the same order.

### **7.3. Contribution from this research**

- In addition to spatial precipitation variation, the SEBS-based ETa estimation method for cloudy days to complete daily time series of cloud-free satellite images has been shown to be effective in the identification of water stress areas. Availability of water resources assessment through satellite-based ETa and spatial precipitation variation analysis provides a new perspective into the water balance studies in the study area.
- Without affecting the overall water balance in the basin on the basis of water use, the pastoral land classification showed suitable areas for the expansion of rainfed maize areas in the basin to meet the expected part of 2030 UOGB rainfed maize production target. However, this includes investment in enhanced water management and development technology and improvements in land use policy. However, the new strategy focuses on higher investment in irrigated agriculture. This study also indicates that there are major improvements to be made by enhancing land suitability and crop water productivity. It also supports decision-makers, land use and water resource planners, and a farmer's belief to increase maize crop yields in the basin to enhance managing fertilizers, seed rate, and water resources.

### **7.4. Recommendations and Perspectives for Future Studies**

- To model the upper Omo-Gibe basin missing streamflow records data and an inadequate number of gauging stations became the most thoughtful restrictions. If this condition continues, it will be more challenging for further studies; hence there need

for rapid quality control to predict long-term hydrological and climatic data records in government agencies and other stakeholders.

- Shortages of reliable and continuous hydro-meteorological data worried hydrological modelling efforts in the study area. The study suggests the requirement to increase the number of measurements and provide more streamflow measuring gauging stations in the outlets of each sub-basin. It is essential to search for more advanced automatic recording instruments at gauging stations to reduce unrealistic and unacceptable data.
- Since the UOGB's crop production areas depend on rain-fed subsistence agriculture and natural resources for their livelihoods. This study recommended increasing agricultural crop production across the UOGB in dry and wet seasons through the allocation of water resources by providing more small-scale irrigation projects as well as active management strategies.
- A number of river basins around the world are considered to be insufficient measurements of precipitation, especially in East Africa, including Ethiopia. For different hydrological variables, including streamflow, therefore, it is very important to predict reliable rainfall data for the river basin. Accordingly, this study suggests that the use of spatially distributed precipitation from other sources, such as satellites based meteorological data, could contribute to an improvement over data-scarce areas.
- The major role of each water balance is the long-term sustainable management of water resources for a given area; the water balance of the area cannot be taken as final due to changes in water needs, human influences, and climate variations and/or changes. The process must therefore be continuously controlled, monitored, and updated.
- In order to compare the impact assessment and catchment characteristics, it is vital to observe for the performance of other hydrological models.
- Water balance equations can be evaluated for any region and for any time period. The method of determining an overall water balance for a given area implies an assessment of all the inflow, outflow, and water storage components of the flow domain bounded by the impermeable base of the underlying groundwater, the land surface, and the imaginary vertical boundary of the area are required.

- It is understandable that hydrological impacts on changes in land use/land cover and climate variability and statistical and trend analysis of hydro-meteorological data could not be recognized in the current study.

## REFERENCES

- Abbott, M. B., Bathurst, J. C., Cunge, J. A., O'Connell, P. E., and Rasmussen, J. (1986). "An introduction to the European Hydrological System - Systeme Hydrologique Europeen, 'SHE', 1: History and philosophy of a physically-based, distributed modelling system." *J. Hydrol.*, 87(1-2), 45-59.
- Abdelrahman, M. A. E., Natarajan, A., and Hegde, R. (2016). "Assessment of land suitability and capability by integrating remote sensing and GIS for agriculture in Chamarajanagar district, Karnataka, India." *Egypt. J. Remote Sens. Sp. Sci.*, 19(1), 125-141.
- Abid, N., Mannaerts, C., and Bargaoui, Z. (2019). "Sensitivity of actual evapotranspiration estimation using the SEBS model to variation of input parameters (LST, DSSF, aerodynamics parameters, LAI, FVC)." *Int. Arch. Photogramm. Remote Sens. Spat. Inf. Sci.*, 42(2/W13), 1193-1200.
- Adeba, D., Kansal, M. L., and Sen, S. (2016). "Economic evaluation of the proposed alternatives of inter-basin water transfer from the Baro Akobo to Awash basin in Ethiopia." *Sustain. Water Resour. Manag.*, 2(3), 313-330.
- Aguilar, A., Carranza, E., Goldstein, M., Kilic, T., and Oseni, G. (2014). *Decomposition of gender differentials in agricultural productivity in Ethiopia. World Bank Africa Reg. Poverty Reduct. Econ.*
- Ahmad, M. ., Biggs, T., Turrall, H., and Scott, C. A. (2006). "Application of SEBAL approach and MODIS time-series to map vegetation water use patterns in the data scarce Krishna river basin of India." *Water Sci. Technol.*, 53, 83-90.
- Ahmad, M. D., Turrall, H., and Nazeer, A. (2009). "Diagnosing irrigation performance and water productivity through satellite remote sensing and secondary data in a large irrigation system of Pakistan." *Agric. Water Manag.*, 96, 551-564.

Ahmad, M. ud D., and Giordano, M. (2010). “The karkheh river basin: The food basket of iran under pressure.” *Water Int.*, 35(5), 522–544.

Akbari, M., Toomanian, N., Droogers, P., Bastiaanssen, W., and Gieske, A. (2007). “Monitoring irrigation performance in Esfahan, Iran, using NOAA satellite imagery.” *Agric. Water Manag.*, 88(1–3), 99–109.

Akhtar, M., Ahmad, N., and Booij, M. J. (2009). “Use of regional climate model simulations as input for hydrological models for the Hindukush-Karakorum-Himalaya region.” *Hydrol. Earth Syst. Sci.*, 13, 1075–1089.

Ako, A. A., Eyong, G. E. T., and Nkeng, G. E. (2010). “Water resources management and integrated water resources management (IWRM) in Cameroon.” *Water Resour. Manag.*, 24(5), 871–888.

Albek, M., Ögütveren, Ü. B., and Albek, E. (2004). “Hydrological modeling of Seydi Suyu watershed (Turkey) with HSPF.” *J. Hydrol.*, 285(1–4), 260–271.

Alemu, Z. G. (2005). *Causes of instability in cereal production in Ethiopia.*

Allen, R. G., Pereira, L. S., Raes, D., and Smith, M. (1998). *Crop evapo-transpiration Guidelines for computing crop water requirements. FAO Irrig. Drain. Pap. No. 56*, Food and Agriculture Organization of the United Nations, Rome, Italy.

Allen, R. G., Tasumi, M., Morse, A., and Trezza, R. (2005). “A Landsat-based energy balance and evapotranspiration model in Western US water rights regulation and planning.” *Irrig. Drain. Syst.*, 19, 251–268.

Allen, R. G., Tasumi, M., Morse, A., Trezza, R., Wright, J. L., Bastiaanssen, W., Kramber, W., Lorite, I., and Robison, C. W. (2007a). “Satellite-Based Energy Balance for Mapping Evapotranspiration with Internalized Calibration (METRIC) - Applications.” *J. Irrig. Drain. Eng.*, 133(4), 395–406.

Allen, R. G., Tasumi, M., and Trezza, R. (2007b). "Satellite-Based Energy Balance for Mapping Evapotranspiration with Internalized Calibration (METRIC) - Model." *J. Irrig. Drain. Eng.*, 133(4), 380–394.

Al Zayed, I. S., Elagib, N. A., Ribbe, L., and Heinrich, J. (2016). "Satellite-based evapotranspiration over Gezira Irrigation Scheme, Sudan: A comparative study." *Agric. Water Manag.*, 177, 66–76.

Amarasinghe, U. A., Malik, R. P. S., and Sharma, B. R. (2010). "Overcoming growing water scarcity: Exploring potential improvements in water productivity in India." *Nat. Resour. Forum*, 34(3), 188–199.

Anderson, M. C., Allen, R. G., Morse, A., and Kustas, W. P. (2012). "Use of Landsat thermal imagery in monitoring evapotranspiration and managing water resources." *Remote Sens. Environ.*, 122, 50–65.

Arnold, J. G., Srinivasan, R., Muttiah, R. S., and Williams, J. R. (1998). "Large Area Hydrologic Modeling and Assessment Part I: Model Development." *J. Am. Water Resour. Assoc.*, 34(1), 73–89.

Asana Dowa, A., Noel, S., Shone, G., Barron, J., and Soussan, J. (2007). *Water and Poverty Linkages in Africa: Ethiopia Case Study*. Stock. Environ. Inst.

Asfaw, S., Shiferaw, B., Simtowe, F., and Lipper, L. (2012). "Impact of modern agricultural technologies on smallholder welfare: Evidence from Tanzania and Ethiopia." *Food Policy*, 37(3), 283–295.

Awad, M., Khawlie, M., and Darwich, T. (2009). "Web based meta-database and its role in improving water resources management in the Mediterranean basin." *Water Resour. Manag.*, 23(13), 2669–2680.

Awulachew, S. B., Erkossa, T., and Namara, R. E. (2010). *Irrigation potential in Ethiopia: Constraints and opportunities for enhancing the system*. Int. Water Manag. Inst.

Awulachew, S. B., Yilma, A. D., Loulseged, M., Loiskandl, W., Ayana, M., and Alamirew, T. (2007). *Water Resources and Irrigation Development in Ethiopia*. International Water Management Institute, Colombo, Srilanka.

Ayyad, S., Zayed, I. S. Al, Ha, V. T. T., and Ribbe, L. (2019). “The performance of satellite-based actual evapotranspiration products and the assessment of irrigation efficiency in Egypt.” *Water*, 11(9), 19.

Bandara, K. M. P. S. (2003). “Monitoring irrigation performance in Sri Lanka with high-frequency satellite measurements during the dry season.” *Agric. Sci.*, 58, 159–170.

Bandyopadhyay, S., Jaiswal, R. K., Hegde, V. S., and Jayaraman, V. (2009). “Assessment of land suitability potentials for agriculture using a remote sensing and GIS based approach.” *Int. J. Remote Sens.*, 30(4), 879–895.

Bashir, M. A., Hata, T., Tanakamaru, H., Abdelhadi, A. W., and Tada, A. (2008). “Satellite-based energy balance model to estimate seasonal evapotranspiration for irrigated sorghum: A case study from the Gezira scheme, Sudan.” *Hydrol. Earth Syst. Sci.*, 12(4), 1129–1139.

Bastiaanssen, W. G. M., Ahmad, M.-D., and Chemin, Y. (2002). “Satellite surveillance of evaporative depletion across the Indus Basin.” *Water Resour. Res.*, 38(12), 9-1-9–9.

Bastiaanssen, W. G. M., and Bandara, K. M. P. S. (2001). “Evaporative depletion assessments for irrigated watersheds in Sri Lanka.” *Irrig. Sci.*, 21(1), 1–15.

Bastiaanssen, W. G. M., and Chandrapala, L. (2003). “Water balance variability across Sri Lanka for assessing agricultural and environmental water use.” *Agric. Water Manag.*, 58, 171–192.

Bastiaanssen, W. G. M., Noordman, E. J. M., Pelgrum, H., Davids, G., Thoreson, B. P., and Allen, R. G. (2005). “SEBAL Model with Remotely Sensed Data to Improve Water-Resources Management under Actual Field Conditions.” *J. Irrig. Drain. Eng.*, 131(1), 85–

93.

Bastiaanssen, W. G. M., Pelgrum, H., Wang, J., Ma, Y., Moreno, J. F., Roerink, G. J., and Wal, T. Van Der. (1998). "A remote sensing surface energy balance algorithm for land (SEBAL): 2. Validation." *J. Hydrol.*, 212–213(1–4), 213–229.

Bastiaanssen, W. G. M., Thiruvengadachari, S., Sakthivadivel, R., and Molden, D. J. (1999). "Satellite Remote Sensing for Estimating Productivities of Land and Water." *Int. J. Water Resour. Dev.*, 15(1–2), 181–194.

Bastiaanssen W.G.M., M. Meneti, R.A. Feddes, and Holtslag, aA A. M. (1998). "A remote sensing surface energy balance algorithm for land (SEBAL)1.Formulation." *J. Hydrol.*, 212–213(January), 198–212.

Baumgartner, M. F., and Apfl, G. M. (1997). "Remote sensing, geographic information systems and snowmelt runoff models - An integrated approach." *Remote Sens. Geogr. Inf. Syst. Des. Oper. Water Resour. Syst.*, 242, 73–82.

Belay, K., and Manig, W. (2004). "Access to rural land in Eastern Ethiopia: Mismatch between policy and reality." *J. Agric. Rural Dev. Trop. Subtrop.*, 105(2), 123–138.

Bergstroem, S. (1976). *Development and Application of a conceptual runoff model for Scandinavian catchment. Hydrol. OCH Oceanogr. Nr RHO 7*, Hydrologi OCH Oceanografi Nr RHO 7.

Bergström, S. (1990). *Parameter values for the HBV model in Sweden, in Swedish. SMHI Hydrol. Nr28*.

Bergström, S. (1992). *The HBV model - its Structure and application. SMHI RH 4, Norrköping*.

Bergström, S., and Forsman, A. (1973). *Development of a conceptual deterministic rainfall-runoff-model. Munksgaard, Copenhagen, Denmark*.

- Berhanu, B., Seleshi, Y., and Melesse, A. M. (2014). "Surface Water and Groundwater Resources of Ethiopia: Potentials and Challenges of Water Resources Development." *Nile River Basin*, 97–117.
- Beven, K. (1984). "Infiltration into a class of vertically non-uniform soils." *Hydrol. Sci. J.*, 29(4), 425–434.
- Beven, K., and Freer, J. (2001). "Equifinality, data assimilation, and uncertainty estimation in mechanistic modelling of complex environmental systems using the GLUE methodology." *J. Hydrol.*, 249(2), 11–29.
- Beven, K. J., and Kirkby, M. J. (1979). "A physically based, variable contributing area model of basin hydrology." *Hydrol. Sci. Bull.*, 24(1), 43–69.
- Bhattarai, N., Mallick, K., Stuart, J., Vishwakarma, B. D., Niraula, R., Sen, S., and Jain, M. (2019). "An automated multi-model evapotranspiration mapping framework using remotely sensed and reanalysis data." *Remote Sens. Environ.*, 229, 69–92.
- Bingner, R. L., and Theurer, F. D. (2005). *AnnAGNPS Technical processes*.
- Biradar, C. M., Thenkabail, P. S., Platonov, A., Xiao, X., Geerken, R., Noojipady, P., Turrall, H., and Vithanage, J. (2008). "Water productivity mapping methods using remote sensing." *J. Appl. Remote Sens.*, 2(1), 1–22.
- Booij, M. J. (2005). "Impact of climate change on river flooding assessed with different spatial model resolutions." *J. Hydrol.*, 303(1–4), 176–198.
- Booij, M. J., and Krol, M. S. (2010). "Balance between calibration objectives in a conceptual hydrological model." *Hydrol. Sci. J.*, 55(6), 1017–1032.
- Borah, D. K., Bera, M., and Shaw, S. (2003). "Water, sediment, nutrient, and pesticide measurements in an agricultural watershed in Illinois during storm events." *Trans. ASAE*, 46(3), 657–674.

Borlaug, N., and Dowsell, C. (2003). "Feeding a world of ten billion people: a 21st century challenge." *Proc. Int. Congr. wake double helix From green Revolut. to gene revolution. Ave. Media.*, 3–23.

Bos, M. G. (2004). "Using the depleted fraction to manage the groundwater table in irrigated areas." *Irrig. Drain. Syst.*, 18, 201–209.

Bos, M. G. (2005). "Is there enough fresh water?," International Institute for Geo-Information Science and Earth Observation, Enschede, Netherlands, 16 pp." 2005.

Bos, M. G., Bosch, H. van den, Diemont, H., Keulen, H., Lahr, J., Meijerink, G., and Verhagen, A. (2007). "Quantifying the sustainability of agriculture." *Irrig. Drain. Syst.*, 21(1), 1–15.

Boss, M., Burton, M., and Molden, D. (2005). *Irrigation and drainage performance assessment Practical Guidelines. CABI Publ.*

Boulet, G., Kerr, Y., Chehbouni, A., and Kalma, J. D. (2002). "Deriving catchment-scale water and energy balance parameters using data assimilation based on extended Kalman filtering." *Hydrol. Sci. J.*, 47(3), 449–467.

Brauman, K. A., Siebert, S., and Foley, J. A. (2013). "Improvements in crop water productivity increase water sustainability and food security - A global analysis." *Environ. Res. Lett.*, 8(2), 1–8.

Breman, H., Groot, J. J. R., and Keulen, H. Van. (2001). "Resource limitations in Sahelian agriculture." *Glob. Environ. Chang.*, 11(1), 59–68.

Brutsaert, W. (1982). *Evaporation to the atmosphere Theory, History, and Application.*

Brutsaert, W. (1999). "Aspects of bulk atmospheric boundary layer similarity under free-convective Conditions." *Rev. Geophys.*, 37(4), 439–451.

Butts, M. B., Payne, J. T., Kristensen, M., and Madsen, H. (2004). "An evaluation of the

impact of model structure on hydrological modelling uncertainty for streamflow simulation.” *J. Hydrol.*, 298(1–4), 242–266.

CA. (2007). *Water for food water for life: A Comprehensive assessment of water management in agriculture. Int. Water Manag. Inst.*

Cai, X., and Rosegrant, M. W. (2003). “World Water Productivity: Current Situation and Future Options.” *CAB Int. 2003. Water Product. Agric. Limits Oppor. Improv. (eds J.W. Kijne, R. Bark. D. Molden)*, R. B. and D. M. J.W. Kijne, ed., 163–178.

Camberlin, P., and Philippon, N. (2002). “The East African March-May rainy season: Associated atmospheric dynamics and predictability over the 1968-97 period.” *J. Clim.*, 15(9), 1002–1019.

Campo, L., Caparrini, F., and Castelli, F. (2006). “Use of multi-platform , multi-temporal remote-sensing data for calibration of a distributed hydrological model : an application in the Arno basin , Italy.” *Hydrol. Process.*, 20(13), 2693–2712.

Carrera, J., and Neuman, S. P. (1986). “Estimation of Aquifer Parameters Under Transient and Steady State Conditions.” *Water Resour. Res.*, 22(2), 199–210.

Cermak, J., and Nadezhdina, N. (1998). “Sapwood as the scaling parameter - defining according to xylem water content or radial pattern of sap flow?” *Ann Sci*, 55(5), 509–521.

Chanyalew, D., Berhanu, A., and John, M. (2010). *Ethiopia’s Agricultural Sector Policy and Investment Framework (PIF) 2010-2020. MoARD.*

Chartres, C., and Sood, A. (2013). “The Water for Food Paradox.” *Aquat. Procedia*, 1, 3–19.

Chen, J. M., Chen, X., Ju, W., and Geng, X. (2005). “Distributed hydrological model for mapping evapotranspiration using remote sensing inputs.” *J. Hydrol.*, 305(1–4), 15–39.

Chen, Q., Jia, L., Menenti, M., Hutjes, R., Hu, G., Zheng, C., and Wang, K. (2019). “A

numerical analysis of aggregation error in evapotranspiration estimates due to heterogeneity of soil moisture and leaf area index.” *Agric. For. Meteorol.*, 269–270, 335–350.

Chirouze, J., Boulet, G., Jarlan, L., Fieuzal, R., Rodriguez, J. C., Ezzahar, J., Er-Raki, S., Bigeard, G., Merlin, O., Garatuza-Payan, J., Watts, C., and Chehbouni, G. (2014). “Intercomparison of four remote-sensing-based energy balance methods to retrieve surface evapotranspiration and water stress of irrigated fields in semi-arid climate.” *Hydrol Earth Syst Sci*, 18(3), 1165–1188.

Choi, H. T., and Beven, K. (2007). “Multi-period and multi-criteria model conditioning to reduce prediction uncertainty in an application of TOPMODEL within the GLUE framework.” *J. Hydrol.*, 332(3–4), 316–336.

Choudhury, B. J., Ahmed, N. U., Idso, S. B., Reginato, R. J., and Daughtry, C. S. T. (1994). “Relations between Evaporation Coefficients and Vegetation Indices Studied by Model Simulations.” *Remote Sens. Environ.*, 50(1), 1–17.

Costanza, R., Voinov, A., Boumans, R., Maxwell, T., Villa, F., Wainger, L., and Voinov, H. (2002). “Integrated ecological economic modeling of the Patuxent River watershed, Maryland.” *Ecol. Monogr.*

Crow, W. T., Wood, E. F., and Pan, M. (2003). “Multiobjective calibration of land surface model evapotranspiration predictions using streamflow observations and spaceborne surface radiometric temperature retrievals.” *J. Geophys. Res.*, 108(23), 1–12.

CSA. (2018). *The Federal Democratic Republic of Ethiopia Central Statistical Agency Agricultural Sample Survey 2017/18 (2010 E.C.): Report on area and production for major crops (private peasant holdings, Meher season)*.

De Bruin, H. A. R., Hurk, B. J. J. M. Van den, and Kohsiek, W. (1995). “The scintillation method tested over a dry vineyard area.” *Boundary-Layer Meteorol.*, 76(1–2), 25–40.

D E Fraiture, C., Cai, X., Rosegrant, M., Molden, D., and Amarasinghe, U. (2003). “Addressing the unanswered questions in global water policy: a methodology framework.” *Irrig. Drain.*, 52(November 2002), 21–30.

Davie, T. (2004). *Review of different hydrological modelling frameworks for usage in the Motueka Integrated Catchment Management programme of research.*

Deckers, D. L. E. H., Booij, M. J., Rientjes, T. M., and Krol, M. S. (2010). “Catchment Variability and Parameter Estimation in Multi-Objective Regionalisation of a Rainfall – Runoff Model.” *Water Resour. Manag.*, 24(14), 3961–3985.

De Fraiture, C., and Wichelns, D. (2010). “Satisfying future water demands for agriculture.” *Agric. Water Manag.*, 97(4), 502–511.

De Smedt, F., Liu, Y., and Gebremeskel, S. (2000). “Hydrologic modeling on a catchment scale using GIS and remote sensed land use information.” *Risk Anal. II, WIT Press*, 295–304.

De Vos, N. J., Rientjes, T. H. M., and Gupta, H. V. (2010). “Diagnostic evaluation of conceptual rainfall–runoff models using temporal clustering.” *Hydrol. Process.*, 24(20), 2840–2850.

Devi, G. K., Ganasri, B. P., and Dwarakish, G. S. (2015). “A Review on Hydrological Models.” *Int. Conf. Water Resour. Coast. Ocean Eng.*, 4(Icwrcoe), 1001–1007.

Dhami, B. S., and Pandey, A. (2013). “Comparative Review of Recently Developed Hydrologic Models.” *J. Indian Water Resour. Soc.*, 33, 34–42.

DHI. (2007). “*MIKE SHE User Manual Voume 1: User Guide.*” *Danish Hydraul. Institute, Denmark.*

Dinpashoh, Y., Jahanbakhsh-Asl, S., Rasouli, A. A., Foroughi, M., and Singh, V. P. (2019). “Impact of climate change on potential evapotranspiration (case study: west and NW of

Iran)." *Theor. Appl. Climatol.*, 136(1–2), 185–201.

Domingo, F., Villagarcı, L., Boer, M. M., Alados-Arboledas, L., and Puigdefabregas, J. (2001). "Evaluating the long-term water balance of arid zone stream bed vegetation using evapotranspiration modelling and hillslope runoff measurements." *J. Hydrol.*, 243, 17–30.

Doorenbos, J., and Pruitt, W. O. (1977). "Guidelines for predicting crop water requirements." *FAO Irrig. Drain. Pap.*, 24, 144.

Downer, C. W., and Ogden, F. L. (2003). "Prediction of runoff and soil moistures at the watershed scale : Effects of model complexity and parameter assignment." *Water Resour. Res.*, 39(3), 1–13.

Downer, C. W., and Ogden, F. L. (2004). "GSSHA: Model To Simulate Diverse Stream Flow Producing Processes." *J. Hydrol. Eng.*, 9(3), 161–174.

Droogers, P., and Bastiaanssen, W. (2002). "Irrigation Performance using Hydrological and Remote Sensing Modeling." *J. Irrig. Drain. Eng.*, 128(1), 11–18.

Dugan, P., Dey, M. M., and Sugunan, V. V. (2006). "Fisheries and water productivity in tropical river basins: Enhancing food security and livelihoods by managing water for fish." *Agric. Water Manag.*, 80(1–3), 262–275.

Edwards, W. R. N. (1986). "Precision weighing lysimetry for trees, using a simplified tared-balance design." *Tree Physiol.*, 1(2), 127–144.

Elhaddad, A., and Garcia, L. (2008). "Surface Energy Balance-Based Model for Estimating Evapotranspiration Taking into Account Spatial Variability in Weather." *J. Irrig. Drain. Eng.*, 134(6), 681–689.

Elhaddad, A., and Garcia, L. A. (2011). "ReSET-Raster: Surface Energy Balance Model for Calculating Evapotranspiration Using a Raster Approach." *J. Irrig. Drain. Eng.*, 137(4), 203–210.

- Elhaddad, A., and Garcia, L. A. (2014). “Using a Surface Energy Balance Model ( ReSET-Raster ) to Estimate Seasonal Crop Water Use for Large Agricultural Areas : Case Study of the Palo Verde Irrigation District.” *J. Irrig. Drain. Eng.*, 2(10), 1–10.
- Erkossa, T. (2011). “Soil fertility effect on water productivity of maize in the upper blue Nile basin, Ethiopia.” *Agric. Sci.*, 02(03), 238–247.
- Ershadi, A., McCabe, M. F., Evans, J. P., and Walker, J. P. (2013). “Effects of spatial aggregation on the multi-scale estimation of evapotranspiration.” *Remote Sens. Environ.*, 131, 51–62.
- Esmailabadi, A. E. (2014). “Evapotranspiration: Application , Scaling and Uncertainty.” PhD. Thesis, University of New South Wales, Sydney, Australia.
- Ethiopia Central Statistical Agency (ECSA), and World Food Program (WFP). (2014). *Ethiopia Comprehensive Food Security and Vulnerability Analysis*.
- Etter, S., Strobl, B., Seibert, J., and Ilja Van Meerveld, H. J. (2018). “Value of uncertain streamflow observations for hydrological modelling.” *Hydrol. Earth Syst. Sci.*, 22(10), 5243–5257.
- Evans, R. G., and Sadler, E. J. (2008). “Methods and technologies to improve efficiency of water use.” *Water Resour. Res.*, 44(7), 1–15.
- Falkenmark, M. (1997). “Meeting water requirements of an expanding world population.” *Philos. Trans. R. Soc. Biol. Sci.*, 352, 929–936.
- Fallis, A. . (2013). “FAO: Crops & Drops.” *J. Chem. Inf. Model.*, 53(9), 1689–1699.
- FAO. (2003). *Review of world water resources by country, Water Report 23. Food Agric. Organ. United Nations, Rome*.
- FAO. (2006). *Fertilizer use by crops. Viale delle Terme di Caracalla, Rome, Italy*.

FAO. (2011). *The State of the World's Land and Water Resources for Food and Agriculture Managing System at risk*. Food Agric. Organ. United Nations, Rome.

FAO. (2014). *Ethiopian country programming framework Revised Document*.

FAO. (2016). *AQUASTAT Country profile – Ethiopia*. Food and Agriculture Organization of the United Nations (FAO). Rome, Italy.

FAO. (2019). *Country Gender Assessment Series National Gender Profile of Agriculture and Rural Livelihoods Ethiopia*.

Farah, H. O., Bastiaanssen, W. G. M., and Feddes, R. A. (2004). “Evaluation of the temporal variability of the evaporative fraction in a tropical watershed.” *Int. J. Appl. Earth Obs. Geoinf.*, 5(2), 129–140.

Farnsworth, R., Barrett, E., and Dhanji, M. (1984). *Application of Remote Sensing to Hydrology Including Groundwater*. *Int. Hydrol. Program. United Nations Educ. Sci. Cult. Organ. Unesco Paris*.

Fazzini, M., Bisci, C., and Billi, P. (2015). “The Climate of Ethiopia.” *Landscapes Landforms Ethiop.*, 65–87.

Fenicia, F., Zhang, G. P., Rientjes, T., Hoffman, L., Pfiste, L., and Savenije, H. H. G. (2005). “Numerical simulations of runoff generation with surface water – groundwater interactions in the Alzette river alluvial plain ( Luxembourg ).” *Phys. Chem. Earth*, 30(4–5), 277–284.

Franks, S. W., and Beven, K. J. (1997). “Bayesian estimation of uncertainty in land surface-atmosphere flux Predictions.” *J. Geophys. Res.*, 102(D20), 23,991-23,999.

Göttinger, J., and B'ardossy, A. (2005). “Advances in Geosciences Integration and calibration of a conceptual rainfall-runoff model in the framework of a decision support system for river basin management.” *Adv. Geosci.*, 5, 31–35.

Garg, S. K. (2005). *Irrigation Engineering and Hydraulic Structures*. Hindustan Offset Press, Naraina, Delhi.

Gassman, P., and Williams, J. (2009). *The Agricultural Policy Environmental Extender (APEX) model: An emerging tool for landscape and watershed environmental analyses. Cent. Agric. Rural Dev.*

Ghandhari, A., and Alavi Moghaddam, S. M. R. (2011). “Water balance principles: A review of studies on five watersheds in Iran.” *J. Environ. Sci. Technol.*, 4(5), 465–479.

Gibson, L. A., Munch, Z., and Engelbrecht, J. (2011). “Particular uncertainties encountered in using a pre-packaged SEBS model to derive evapotranspiration in a heterogeneous study area in South Africa.” *Hydrol Earth Syst Sci*, 15(1), 295–310.

Gleick, P. H. (2003). “Global freshwater resources: soft-path solutions for the 21st century.” *Am. Assoc. Adv. Sci. 1200 New York Ave. NW, Washington, DC 20005*, 302(5650), 1524–1528.

Gokmen, M., Vekerdy, Z., Verhoef, A., Verhoef, W., Batelaan, O., and Tol, C. van der. (2012). “Integration of soil moisture in SEBS for improving evapotranspiration estimation under water stress conditions.” *Remote Sens. Environ.*, 121, 261–274.

Golmohammadi, G., Prasher, S., Madani, A., and Rudra, R. (2014). “Evaluating Three Hydrological Distributed Watershed Models: MIKE-SHE, APEX, SWAT.” *Hydrology*, 1(1), 20–39.

Gomis-Cebolla, J., Jimenez, J. C., Sobrino, J. A., Corbari, C., and Mancini, M. (2019). “Intercomparison of remote-sensing based evapotranspiration algorithms over amazonian forests.” *Int. J. Appl. Earth Obs. Geoinf.*, 80, 280–294.

Greaves, G. E., and Wang, Y.-M. (2017). “Yield response, water productivity, and seasonal water production functions for maize under deficit irrigation water management in southern Taiwan.” *Plant Prod. Sci.*, 20(4), 353–365.

Gupta, H. V, Bastida, L. A., Sorooshian, S., Shuttleworth, W. J., and Yang, Z. L. (1999). "Parameter estimation of a land surface scheme using multicriteria methods." *J. Geophys. Res.*, 104(16), 19,491-19,503.

Gupta, H. V, Sorooshian, S., and Yapo, P. O. (1998). "Toward improved calibration of hydrologic models : Multiple and noncommensurable measures of information." *Water Resour. Res.*, 34(4), 751–763.

Gupta, H. V, Wagener, T., and Liu, Y. (2008). "Reconciling theory with observations : elements of a diagnostic approach to model evaluation." *Hydrol. Process.*, 22(18), 3802–3813.

Ha, L. T., Bastiaanssen, W. G. M., Griensven, A. van, Dijk, A. I. J. M. van, and Senay, G. B. (2018). "Calibration of spatially distributed hydrological processes and model parameters in SWAT using remote sensing data and an auto-calibration procedure: A case study in a Vietnamese river basin." *Water (Switzerland)*, 10(212), 1–21.

Haile, A. T., Habib, E., and Rientjes, T. (2013). "Evaluation of the climate prediction center (CPC) morphing technique (CMORPH) rainfall product on hourly time scales over the source of the Blue Nile River." *Hydrol. Process.*, 27(12), 1829–1839.

Harlin, J., and Kung, C. (1992). "Parameter uncertainty and simulation of design floods in Sweden." *J. Hydrol.*, 137(1–4), 209–230.

Hartanto, I. M., Kwast, J. van der, Alexandridis, T. K., Almeida, W., Song, Y., Andel, S. J. van, and Solomatine, D. P. (2017). "Data assimilation of satellite-based actual evapotranspiration in a distributed hydrological model of a controlled water system." *Int. J. Appl. Earth Obs. Geoinf.*, 57, 123–135.

Hatfield, J. L. (1983). *Evapotranspiration Obtained from Remote Sensing Methods*. *Adv. Irrig.*, Academic Press, Inc.

Hemakumara, H. M., Chandrapala, L., and Moene, A. F. (2003). "Evapotranspiration

fluxes over mixed vegetation areas measured from large aperture scintillometer.” *Agric. Water Manag.*, 58, 109–122.

Herman, M. R., Nejadhashemi, A. P., Abouali, M., Hernandez-Suarez, J. S., Daneshvar, F., Zhang, Z., Anderson, M. C., Sadeghi, A. M., Hain, C. R., and Sharifi, A. (2018). “Evaluating the role of evapotranspiration remote sensing data in improving hydrological modeling predictability.” *J. Hydrol.*, 556, 39–49.

Hollenbeck, K. J., Schmutge, T. J., Hornberger, G. M., and Wang, J. R. (1996). “Identifying soil hydraulic heterogeneity by detection of relative change in passive microwave remote sensing observations.” *Water Resour. Res.*, 32(1), 139–148.

Hong-Xing, C., Zheng-Bin, Z., Ping, X., Li-Ye, C., Hong-Bo, S., Zhao-Hua, L., and Jun-Hong, L. (2007). “Mutual physiological genetic mechanism of plant high water use efficiency and nutrition use efficiency.” *Colloids Surfaces B Biointerfaces*, 57(1), 1–7.

Hua, L., He, X., Yuan, Y., and Nan, H. (2012). “Assessment of runoff and sediment yields using the AnnAGNPS model in a three-gorge watershed of China.” *Int. J. Environ. Res. Public Health*, 9(5), 1887–1907.

Hussain, I., Sakthivadivel, R., Amarasinghe, U., Mudasser, M., and Molden, D. (2003). *Land and Water Productivity of Wheat in the Western Indo-Gangetic Plains of India and Pakistan: A Comparative Analysis*. Int. Water Manag. Institute, Colombo, Sri Lanka.

Ibrahim, Y., and Atta, M. (2014). “Improving Growth , Yield and Water Productivity of Some Maize Cultivars by New Planting Method.” *Innov. Water Manag. Award Win. Pap. 2014*, 1–12.

Immerzeel, W. W., and Droogers, P. (2008). “Calibration of a distributed hydrological model based on satellite evapotranspiration.” *J. Hydrol.*, 349(3–4), 411–424.

Immerzeel, W. W., Droogers, P., and Gieske, A. (2006). “Remote Sensing and Evapotranspiration Mapping : State of the Art.” *FutureWater.*, 39.

Immerzeel, W. W., Gaur, A., and Zwart, S. J. (2008). “Integrating remote sensing and a process-based hydrological model to evaluate water use and productivity in a south Indian catchment.” *Agric. Water Manag.*, 95, 11–24.

Islam, M. M., and Sado, K. (2002). “Development priority map for flood countermeasures by remote sensing data with geographic information system.” *J. Hydrol. Eng.*, 7(5), 346–355.

Islam, Z. (2011). *A Review on Physically Based Hydrologic Modeling*.

Jamshidi, S., Zand-Parsa, S., Pakparvar, M., and Niyogi, D. (2019). “Evaluation of Evapotranspiration over a Semi-Arid Region using Multi-Resolution Data Sources.” *J. Hydrometeorol.*, 20(5), 947–964.

Jarvis, P. G. (1976). “The interpretation of the variations in leaf water potential and stomatal conductance found in canopies in the field.” *Philos. Trans. R. Soc. London. B, Biol. Sci.*, 273(927), 593–610.

Jia, L., Su, Z., Hurk, B. Van Den, Menenti, M., Moene, A., Bruin, H. A. R. De, Baselga, J. J., Ibanez, M., and Cuesta, A. (2003a). “Estimation of sensible heat flux using the Surface Energy Balance System ( SEBS ) and ATSR measurements.” *Phys. Chem. Earth*, 28, 75–88.

Jia, L., Su, Z., Hurk, B. van den, Menenti, M., Moene, A., Bruin, H. A. R. De, Yrisarry, J. J. B., Ibanez, M., and Cuesta, A. (2003b). “Estimation of sensible heat flux using the Surface Energy Balance System (SEBS) and ATSR measurements.” *Phys. Chem. Earth*, 28(1–3), 75–88.

Jia, L., Xi, G., Liu, S., Huang, C., Yan, Y., and Liu, G. (2009). “Regional estimation of daily to annual regional evapotranspiration with MODIS data in the Yellow River Delta wetland.” *Hydrol Earth Syst Sci*, 13(10), 1775–1787.

Jia, L., Zheng, C., Hu, G. C., and Menenti, M. (2017). “Evapotranspiration.” *Compr.*

*Remote Sens.*, 1–9(April 2018), 25–50.

Jin X., L. Wan, and Su, Z. (2005). “Research on evaporation of Taiyuan basin area by using remote sensing.” *Hydrol. Earth Syst. Sci. Discuss.*, 2, 209–227.

Jin, X., Zhu, X., and Xue, Y. (2019). “Satellite-based analysis of regional evapotranspiration trends in a semi-arid area.” *Int. J. Remote Sens.*, 40(9), 3267–3288.

Kaliba, A. R. M., Verkuyl, H., and Mwangi, W. (2000). “Factors Affecting Adoption of Improved Maize Seeds and Use of Inorganic Fertilizer for Maize Production in the Intermediate and Lowland Zones of Tanzania.” *J. Agric. Appl. Econ.*, 32(1), 35–47.

Kayastha, N. (2014). “Refining the Committee Approach and Uncertainty Prediction in Hydrological Modelling.” *IHE Delft Inst. Water Educ.*

Kherde, R. V. K., and Sawant, P. H. (2013). “Integrating geographical information systems (GIS) with hydrological modelling -applicability and limitations.” *Int. J. Eng. Technol.*, 5(4), 3374–3381.

Khu, S., Madsen, H., and Pierro, F. di. (2008). “Incorporating multiple observations for distributed hydrologic model calibration: An approach using a multi-objective evolutionary algorithm and clustering.” *Adv. Water Resour.*, 31(10), 1387–1398.

Kijne, J. W., Tuong, T. P., Bennett, J., Bouman, B., and Oweis, T. (2003). *Ensuring food security via improvement in crop water productivity. CABI Publ./IWMI, Cambridge, MA/Colombo, Sri Lanka.*

Kim, G., and Barros, A. P. (2002). “Space-time characterization of soil moisture from passive microwave remotely sensed imagery and ancillary data.” *Remote Sens. Environ.*, 81(2–3), 393–403.

Kim, K. B., Kwon, H. H., and Han, D. (2018). “Exploration of warm-up period in conceptual hydrological modelling.” *J. Hydrol.*, 556, 194–210.

- Kite, G. W., and Kouwen, N. (1992). "Watershed modeling using land classifications." *Water Resour. Res.*, 28(12), 3193–3200.
- Kite, G. W., and Pietroniro, A. (1996). "Remote sensing applications in hydrological modelling." *Hydrol. Sci. J.*, 41(4), 563–591.
- Koloskov, G., Mukhamejanov, K., and Tanton, T. . (2007). "Monin – Obukhov length as a cornerstone of the SEBAL calculations of evapotranspiration." *J. Hydrol.*, 335, 170–179.
- Korecha, D., and Barnston, A. G. (2007). "Predictability of June-September rainfall in Ethiopia." *Mon. Weather Rev.*, 135(2), 628–650.
- Kurkura, M. (2011). "Water balance of upper awash basin based on satellite -derived data (remote sensing)." MSc. Thesis, Addis Ababa University.
- Kustas, W. P., and Daughtry, C. S. T. (1990). "Estimation of the soil heat flux/net radiation ratio from spectral data." *Agric. For. Meteorol.*, 49(3), 205–223.
- Kustas, W. P., and Norman, J. M. (2009). "Use of remote sensing for evapotranspiration monitoring over land surfaces." *Hydrol. Sci. J.*, 41(4), 495–516.
- Kustas, W. P., Perry, E. M., Doraiswamy, P. C., and Moran, M. S. (1994). "Using satellite remote sensing to extrapolate evapotranspiration estimates in time and space over a semiarid Rangeland basin." *Remote Sens. Environ.*, 49(3), 275–286.
- Kwast, J. Van Der. (2009). "Quantification of top soil moisture patterns." *Ultratec Univ. , Netherl.*
- Legates, D. R., and McCabe Jr, G. J. (1999). "Evaluating the use of 'goodness-of-fit' measures in hydrologic and hydroclimatic model validation." *Water Resour. Res.*, 35(1), 233–241.
- Legesse, D., Vallet-Coulomb, C., and Gasse, F. (2003). "Hydrological response of a catchment to climate and land use changes in Tropical Africa: Case study south central

Ethiopia.” *J. Hydrol.*, 275(1–2), 67–85.

Li, Z. L., Tang, R., Wan, Z., Bi, Y., Zhou, C., Tang, B., Yan, G., and Zhang, X. (2009). “A review of current methodologies for regional Evapotranspiration estimation from remotely sensed data.” *Sensors*, 9(5), 3801–3853.

Lindström, G., Johansson, B., Persson, M., Gardelin, M., and Bergström, S. (1997). “Development and test of the distributed HBV-96 hydrological model.” *J. Hydrol.*, 201(1–4), 272–288.

Lindström, G., Pers, C., Rosberg, J., Stromqvist, J., and Arheimer, B. (2010). “Development and testing of the HYPE (Hydrological Predictions for the Environment) water quality model for different spatial scales.” *Hydrol. Res.*, 41(3–4), 295–319.

Liou, Y. A., and Kar, S. K. (2014). “Evapotranspiration estimation with remote sensing and various surface energy balance algorithms-a review.” *Energies*, 7(5), 2821–2849.

Liu, J., Wiberg, D., Zehnder, A. J. B., and Yang, H. (2007). “Modeling the role of irrigation in winter wheat yield, crop water productivity, and production in China.” *Irrig. Sci.*, 26(1), 21–33.

Liu, Y. B., and Smedt, F. De. (2009). “WetSpa Extension , A GIS-based Hydrologic Model for Flood Prediction and Watershed Management Documentation and User Manual.” *Management*, (March), 1–126.

Loheide, S. P., and Gorelick, S. M. (2005). “A local-scale, high-resolution evapotranspiration mapping algorithm (ETMA) with hydroecological applications at riparian meadow restoration sites.” *Remote Sens. Environ.*, 98(2–3), 182–200.

Losgedaragh, S. Z., and Rahimzadegan, M. (2018). “Evaluation of SEBS, SEBAL, and METRIC models in estimation of the evaporation from the freshwater lakes (Case study: Amirkabir dam, Iran).” *J. Hydrol.*, 561, 523–531.

Loukas, A., Vasiliades, L., Domenikiotis, C., and Dalezios, N. R. (2005). “Basin-wide actual evapotranspiration estimation using NOAA / AVHRR satellite data.” *Phys. Chem. Earth*, 30, 69–79.

Luo, C., Li, Z., Li, H., and Chen, X. (2015). “Evaluation of the annAGNPS model for predicting runoff and nutrient export in a typical small watershed in the hilly region of taihu lake.” *Int. J. Environ. Res. Public Health*, 12(9), 10955–10973.

Ma, W., Hafeez, M., Ishikawa, H., and Ma, Y. (2013). “Evaluation of SEBS for estimation of actual evapotranspiration using ASTER satellite data for irrigation areas of Australia.” *Theor. Appl. Climatol.*, 112(3–4), 609–616.

Ma, W., Ma, Y., Li, M., Hu, Z., Zhong, L., Su, Z., Ishikawa, H., and Wang, J. (2009). “Estimating surface fluxes over the north Tibetan Plateau area with ASTER imagery.” *Hydrol Earth Syst Sci*, 13(1), 57–67.

Madsen, H. (2000). “Automatic calibration of a conceptual rainfall – runoff model using multiple objectives.” *J. Hydrol.*, 235(3–4), 276–288.

Madsen, H. (2003). “Parameter estimation in distributed hydrological catchment modelling using automatic calibration with multiple objectives.” *Adv. Water Resour.*, 26(2), 205–216.

Markstrom, S. L., Niswonger, R. G., Regan, R. S., Prudic, D. E., and Barlow, P. M. (2008). “GSFLOW—Coupled Ground-Water and Surface-Water Flow Model Based on the Integration of the Precipitation-Runoff Modeling System (PRMS) and the Modular Ground-Water Flow Model (MODFLOW-2005).” *U.S. Geol. Surv.*, (Techniques and Methods 6-D1), 240.

Matinfar, H. R., and Soorghali, M. (2014). “Estimate evapotranspiration (ET) using SEBS model based on Landsat 5 (TM) thermal data and GIS.” *Indian J. Fundam. Appl. Life Sci.*, 4(3), 30–34.

Mausser, W., and Schädlich, S. (1998). “Modelling the spatial distribution of

evapotranspiration on different scales using remote sensing data.” *J. Hydrol.*, 212–213(1–4), 250–267.

Mccabe, M. F., Franks, S. W., and Kalma, J. D. (2005). “Calibration of a land surface model using multiple data sets.” *J. Hydrol.*, 302(1–4), 209–222.

McCabe, M. F., and Wood, E. F. (2006). “Scale influences on the remote estimation of evapotranspiration using multiple satellite sensors.” *Remote Sens Env.*, 105(4), 271–285.

Meiresonne, L., Nadezhdin, N., Cermak, J., Slycken, J. Van, and Ceulemans, R. (1999). “Measured sap flow and simulated transpiration from a poplar stand in Flanders (Belgium).” *Agric. For. Meteorol.*, 96(4), 165–179.

Meixner, T., Bastidas, L. A., Gupta, H. V., and Bales, R. C. (2002). “Multicriteria parameter estimation for models of stream chemical composition.” *Water Resour. Res.*, 38(3), 1–9.

Melrose, J., Perroy, R., and Careas, S. (2015). *World population prospects: The 2015 Revision, Key Findings and Advance Table*. United Nations New York.

Menenti, M., and Choudhury, B. J. (1993). “Parameterization of land surface evaporation by means of location dependent potential evaporation and surface temperature range.” *Proc. IAHS Conf. L. Surf. Process.*, 0(212), 561–568.

Mensah, F. A. (2010). “Integrated Water Resources Management in Ghana: Past, Present, and the Future.” *World Environ. Water Resour. Congr. 2010 Challenges Chang.*, (January 2010), 2026–2037.

Merz, R., and Bloßschl, G. (2004). “Regionalisation of catchment model parameters.” *J. Hydrol.*, 287, 95–123.

Migliaccio, K. W., and Srivastava, P. (2007). “Hydrologic components of watershed-scale models.” *Am. Soc. Agric. Biol. Eng.*, 50(5), 1695–1703.

Mohaideen, M. M. D., and Varija, K. (2018). “Improved vegetation parameterization for

hydrological model and assessment of land cover change impacts on flow regime of the Upper Bhima basin, India.” *Acta Geophys.*, 66, 697–715.

Molden, D. (1997). “Accounting for Water Use and Productivity.” *Int. Irrig. Manag. Institute, Colombo, Sri Lanka*, (February 2014), 26.

Molden, D., Murray-Rust, H., Sakthivadivel, R., and Makin, I. (2003). “A water-productivity framework for understanding and action.” *Water Product. Agric. limits Oppor. Improv.*, 1–18.

Molden, D., Oweis, T., Steduto, P., Bindraban, P., Hanjra, M. A., and Kijne, J. (2009). “Improving agricultural water productivity: Between optimism and caution.” *Agric. Water Manag.*, 97(4), 528–535.

Monteith, J. L. (1973). *Principles of Environmental Physics*. Edward Arnold Press, London.

Monteith, J. L. (1981). “Evaporation and surface temperature.” *Quartely J. R. Meteorol. Soc.*, 107, 1–27.

Montzka, C., Canty, M., Kunkel, R., Menz, G., Vereecken, H., and Wendland, F. (2008). “Modelling the water balance of a mesoscale catchment basin using remotely sensed land cover data.” *J. Hydrol.*, 353(3–4), 322–334.

MoWR. (2001). *Initial National Communication of Ethiopia to the United Nations Framework Convention on Climate Change*. Addis Ababa.

MoWR. (2002a). *Water Sector Development Program Volume II*. Addis Ababa.

MoWR. (2002b). *Water sector development program 2002-2016. Fed. Democr. Repub. Ethiop.*

Muhammed, A. H. (2012). “Satellite Based Evapotranspiration Estimation and Runoff Simulation : a Topmodel Application To the Gilgel Abay Catchment , Ethiopia.” *Thesis*.

- Muthuwatta, L. P., Ahmad, M. ud D., Bos, M. G., and Rientjes, T. H. M. (2010). “Assessment of water availability and consumption in the Karkheh river basin, Iran-using remote sensing and geo-statistics.” *Water Resour. Manag.*, 24(3), 459–484.
- Muthuwatta, L. P., Rientjes, T. H. M., and Bos, M. G. (2013). “Strategies to increase wheat production in the water scarce Karkheh River Basin , Iran.” *Agric. Water Manag.*, 124, 1–10.
- Nagler, P. L., Scott, R. L., Westenburg, C., Cleverly, J. R., Glenn, E. P., and Huete, A. R. (2005). “Evapotranspiration on western U.S. rivers estimated using the Enhanced Vegetation Index from MODIS and data from eddy covariance and Bowen ratio flux towers.” *Remote Sens. Environ.*, 97(3), 337–351.
- Nangia, V., Turrall, H., and Molden, D. (2008). “Increasing water productivity with improved N fertilizer management.” *Irrig. Drain. Syst.*, 22(3–4), 193–207.
- Nash, J., and Sutcliffe, J. (1970). “River flow forecasting through conceptual models part I - a discussion of principles.” *J. Hydrol.*, 10, 282–290.
- National Planing Commision [NPC]. (2016). *Federal Democratic Republic of Ethiopia Growth and Transformation Plan II (GTP II)*. Addis Ababa.
- Ncube, N., Zhakata, D., and Muchandiona, A. (2016). “Application Of A Remote Sensing Technique In Estimating Evapotranspiration For Nyazvidzi Sub- Catchment., Zimbabwe.” *Eur. Sci. J.*, 12(21), 101–115.
- Nega, Y., Abraha, A., and Samuel, G. (2015). “Interaction Effects of In-Organic N-Fertilizer and Seed Rates on Yield and Quality Traits of Malt Barley Varieties in the Highland of Tigray, North Ethiopia.” *Int. J. Agric. Sci. Res.*, 4(8), 158–167.
- Nichols, W. E., and Cuenca, R. H. (1993). “Evaluation of the evaporative fraction for parameterization of the surface energy balance.” *Water Resour. Res.*, 29(11), 3681–3690.

Nishida, K., Nemani, R. R., Glassy, J. M., and Running, S. W. (2003). “Development of an evapotranspiration index from Aqua/MODIS for monitoring surface moisture status.” *IEEE Trans. Geosci. Remote Sens.*, 41(2 PART 1), 493–500.

NMSA. (2001). *Initial National Communication of Ethiopia to the United Nations Framework Convention on Climate Change (UNFCCC)*.

Norman, J. M., Kustas, W. P., and Humes, K. S. (1995). “Source approach for estimating soil and vegetation energy fluxes in observations of directional radiometric surface temperature.” *Agric. For. Meteorol.*, 77(3–4), 263–293.

Nurudeen, A. R., Tetteh, F. M., Fosu, M., Quansah, G. W., and Osuman, A. S. (2015). “Improving Maize Yield on Ferric Lixisol by NPK Fertilizer Use.” *J. Agric. Sci.*, 7(12), 233–237.

Omiti, J. M., Parton, K. A., Ehui, S. K., and Sinden, J. A. (2000). “Some policy implications of the resurfacing of rural factor markets following Agrarian de-collectivization in Ethiopia.” *Hum. Ecol.*, 28(4), 585–603.

Ouillon, S., Forget, P., Froidfond, J.-M., and Naudin, J.-J. (1997). “Estimating Suspended Matter Concentrations from SPOT Data and from Field Measurements in the Rhone River Plume.” *MTS J.*, 31(2), 15–20.

Parajka, J., Blöschl, G., and Merz, R. (2007a). “Regional calibration of catchment models : Potential for ungauged catchments.” *Water Resour. Res.*, 43(6), 1–16.

Parajka, J., Merz, R., and Blöschl, G. (2007b). “Uncertainty and multiple objective calibration in regional water balance modelling : case study in 320 Austrian catchments.” *Hydrol. Process.*, 21(4), 435–446.

Parajuli, K., Jones, S. B., Tarboton, D. G., Flerchinger, G. N., Hipps, L. E., Allen, L. N., and Seyfried, M. S. (2019). “Estimating actual evapotranspiration from stony-soils in montane ecosystems.” *Agric. For. Meteorol.*, 265, 183–194.

Parajuli, P. B., Nelson, N. O., Frees, L. D., and Mankin, K. R. (2010). "Comparison of AnnAGNPS and SWAT model simulation results in USDA-CEAP agricultural watersheds in south-central Kansas." *Wiley Interisci.*, 2274(15), 2267–2274.

Paulos, D. (2002). "Present and future trends in natural resources management in agriculture: An overview." *Proc. a MoWR/EARO/IWMI/ILRI Int. Work. held ILRI, Addis Ababa, Ethiop. 2–4 December 2002*, 29–37.

Peden, D., Tadesse, G., Misra, A. K., Ahmed, F. A., Astatke, A., Ayalneh, W., Herrero, M., Kiuwua, G., Kumsa, T., Mati, B., Mpairwe, D., Wassenaar, T., and Yimegnuhal, A. (2007). "Water and livestock for human development Coordinating." *Water Livest. Hum. Dev. (No. H040205). Int. Water Manag. Institute.*, 30.

Peng, L., Zeng, Z., Wei, Z., Chen, A., Wood, E. F., and Sheffield, J. (2019). "Determinants of the ratio of actual to potential evapotranspiration." *Glob. Chang. Biol.*, 25(4), 1326–1343.

Playán, E., and Mateos, L. (2006). "Modernization and optimization of irrigation systems to increase water productivity." *Agric. Water Manag.*, 80(1–3), 100–116.

Poméon, T., Diekkrüger, B., and Kumar, R. (2018). "Computationally efficient multivariate calibration and validation of a grid-based hydrologic model in sparsely gauged West African river basins." *Water*, 10(10), 1–26.

Qin, C., Jia, Y., Su, Z., Zhou, Z., Qiu, Y., and Suhui, S. (2008). "Integrating Remote Sensing Information Into A Distributed Hydrological Model for Improving Water Budget Predictions in Large-scale Basins through Data Assimilation." *Sensors*, 8(7), 4441–4465.

Raes, D., Willems, P., and Gbaguidi, F. (2006). "RAINBOW—A software package for hydrometeorological frequency analysis and testing the homogeneity of historical data sets." *Proc. 4th Int. Work. 'Sustainable Manag. Marg. drylands. Islamabad, Pakistan*, 27–31.

Rahman, S. (2003). "Environmental impacts of modern agricultural technology diffusion in Bangladesh: An analysis of farmers' perceptions and their determinants." *J. Environ. Manage.*, 68(2), 183–191.

Raju, P. L. N. (2006). "Fundamentals of geographical information system." *Satell. Remote Sens. GIS Appl. Agric. Meteorol.*, 103–120.

Refsgaard, J. C. (1997). "Parameterisation, calibration and validation of distributed hydrological models." *J. Hydrol.*, 198(1–4), 69–97.

Reggiani, P., and Rientjes, T. H. M. (2005). "Flux parameterization in the representative elementary watershed approach: Application to a natural basin." *Water Resour. Res.*, 41(4), 1–18.

Rientjes, T. H. M., Muthuwatta, L. P., Bos, M. G., Booij, M. J., and Bhatti, H. A. (2013a). "Multi-variable calibration of a semi-distributed hydrological model using streamflow data and satellite-based evapotranspiration." *J. Hydrol.*, 505, 276–290.

Rientjes, T., Tamiru, A., and Almaw, A. (2013b). "Diurnal rainfall variability over the Upper Blue Nile Basin: A remote sensing based approach." *Int. J. Appl. Earth Obs. Geoinf.*, 21, 311–325.

Rijsberman, F. R. (2006). "Water scarcity: Fact or fiction?" *Agric. Water Manag.*, 80, 5–22.

Rockström, J., Axberg, G. N., Falkenmark, M., Lannerstad, M., Rosemarin, A., Caldwell, I., Arvidson, A., and Nordström, M. (2005). *Sustainable Pathways to Attain the Millennium Development Goals: Assessing the Key Role of Water, Energy and Sanitation. Stock. Environ. Inst.*

Roerink, G. J., Su, Z., and Menenti, M. (2000). "S-SEBI: A simple remote sensing algorithm to estimate the surface energy balance." *Phys. Chem. Earth, Part B*, 25(2), 147–157.

- Romanowicz, R. J., Osuch, M., and Grabowiecka, M. (2013). "On the choice of calibration periods and objective functions: A practical guide to model parameter identification." *Acta Geophys.*, 61(6), 1477–1503.
- Rungee, J., Bales, R., and Goulden, M. (2019). *Evapotranspiration response to multiyear dry periods in the semiarid western United States. Hydrol. Process.*
- Rwasoka, D. T., Gumindoga, W., and Gwenzi, J. (2011). "Estimation of actual evapotranspiration using the Surface Energy Balance System (SEBS) algorithm in the Upper Manyame catchment in Zimbabwe." *Phys. Chem. Earth*, 36(14–15), 736–746.
- Rwetabula, J., Smedt, F. De, and Rebhun, M. (2007). "Prediction of runoff and discharge in the Simiyu River ( tributary of Lake Victoria , Tanzania ) using the WetSpa model." *Hydrol. Earth Syst. Sci. Discuss.*, (4), 881–908.
- Sadras, V. O., and Angus, J. F. (2006). "Benchmarking water-use efficiency of rainfed wheat in dry environments." *Aust. J. Agric. Res.*, 57(8), 847–856.
- Sadras, V. O., Grassini, P., and Steduto, P. (2012). "Status of water use efficiency of main crops ." *SOLAW Backgr. Themat. Rep. - TR07*, 2013(October).
- Salama, M. A., Yousef, K. M., and Mostafa, A. Z. (2015). "Simple equation for estimating actual evapotranspiration using heat units for wheat in arid regions." *J. Radiat. Res. Appl. Sci.*, 8(3), 418–427.
- Samboko, H. (2016). "A remote sensing based approach to determine evapotranspiration in the Mbire District of Zimbabwe." MSc. Thesis, University of Zimbabwe.
- Sarwar, A., and Bastiaanssen, W. G. M. (2001). "Long-term effects of irrigation water conservation on crop production and environment in semiarid areas." *J. Irrig. Drain. Eng.*, 127(6), 331–338.
- Schmugge, T., Gurney, R. J., and Gurney, R. J. (1988). "Applications of Remote Sensing

in Hydrology.” *Dev. water Sci.*, 35, 383–388.

Schmugge, T. J., Kustas, W. P., Ritchie, J. C., Jackson, T. J., and Rango, A. (2002). “Remote sensing in hydrology.” *Adv. Water Resour.*, 25, 1367–1385.

SDSN. (2013). *Solutions for Sustainable Agriculture and Food Systems - Technical Report for the Post-2015 Development Agenda*.

Seckler, D., Amarasinghe, U., Molden, D., Silva, R. de, and Barker, R. (1998). *World Water Demand and Supply, 1990 to 2025: Scenarios and Issues David. Int. Water Manag. Inst. (IIMI), Colombo, Sri Lanka*.

Seckler, D., Molden, D., and Barker, R. (1999). “Water Scarcity in the Twenty-first Century.” *Int. J. Water Resour. Dev.*, 15(1–2), 29–42.

Seibert, J. (1996). *HBV light Version 2 User ’ s Manual. Stock. Univ. Dep. Phys. Geogr. Quat. Geol.*

Seibert, J. (1997). “Estimation of Parameter Uncertainty in the HBV Model.” *Nord. Hydrol.*, 28(4/5), 247–262.

Seibert, J. (1999). “Regionalisation of parameters for a conceptual rainfall-runoff model.” *Agric. For. Meteorol.*, 98, 279–293.

Seibert, J., and Vis, M. J. P. (2012). “Teaching hydrological modeling with a user-friendly catchment-runoff-model software package.” *Hydrol. Earth Syst. Sci.*, 16(9), 3315–3325.

Senay, G. B., Budde, M., Verdin, J. P., and Melesse, A. M. (2007). “A coupled Remote Sensing and Simplified Surface Energy Balance Approach to Estimate Actual Evapotranspiration from Irrigated Fields.” *Sensors*, 7(6), 979–1000.

Shafii, M., Tolson, B., and Matott, L. S. (2014). “Uncertainty-based multi-criteria calibration of rainfall-runoff models: A comparative study.” *Stoch. Environ. Res. Risk Assess.*, 28(6), 1493–1510.

Shiklomanov, I. A. (1998). *World Water Resources- A new Appraisal and Assessment for the 21st century. United Nations Educ. Sci. Cult. Organ. Paris.*

Shiklomanov, I. A. (2000). "Appraisal and Assessment of World Water Resources." *Int. Water Resour. Assoc. Water Int.*, 25(1), 11–32.

Shoko, C., Dube, T., Sibanda, M., and Adelabu, S. (2015). "Applying the Surface Energy Balance System ( SEBS ) remote sensing model to estimate spatial variations in evapotranspiration in Southern Zimbabwe." *Trans. R. Soc. South Africa*, 70(1), 47–55.

Shrestha, J. P., Alfredsen, K., and Timalsina, N. (2014). "Regional Modeling for Estimation of Runoff from Ungauged Catchments: Case Study of the Saptakoshi Basin, Nepal." *Hydro Nepal*, (14), 65–72.

Shuttleworth, W., Gurney, R., Hsu, A., and Ormsby, J. (1989). "FIFE: the variation in energy partition at surface flux sites." *Remote Sens. Large-Scale Glob. Porc. (Proceedings IAHS Third Int. Assem. Balt. MD, May 1989).*, 67–74.

Sime, G., and Aune, J. B. (2018). "Sustainability of improved crop varieties and agricultural practices: A case study in the central rift valley of Ethiopia." *Agric.*, 8(177), 1–16.

Singh, V. P., and Woolhiser, D. A. (2002). "Mathematical Modeling of Watershed Hydrology." *J. Hydrol. Eng.*, 7(4), 270–292.

Snyder, R. L. (1992). "Equation for evaporation pan to evapotranspiration conversions." *J. Irrig. Drain Eng.*, 118(6), 977–980.

Stisen, S., Jensen, K. H., Sandholt, I., and Grimes, D. I. F. (2008). "A remote sensing driven distributed hydrological model of the Senegal River basin." *J. Hydrol.*, 354(1–4), 131–148.

Su, H., McCabe, M. F., Wood, E. F., Su, Z., and Prueger, J. H. (2005). "Modeling evapotranspiration during SMACEX: Comparing two approaches for local- and regional-

scale prediction.” *J. Hydrometeorol.*, 6(6), 910–922.

Su, Z. (2002a). “The Surface Energy Balance System (SEBS) for estimation of turbulent heat fluxes.” *Hydrol. Earth Syst. Sci.*, 6(1), 85–99.

Su, Z. (2002b). “The Surface Energy Balance System (SEBS) for estimation of turbulent heat fluxes.” *Hydrol. Earth Syst. Sci.*, 6(1), 85–99.

Su, Z., Li, X., Zhou, Y., Wan, L., Wen, J., and Sintonen, K. (2003a). “Estimating areal evaporation from remote sensing.” *Geosci. Remote Sens. Symp. Proceedings. IEEE Int.*, 1166–1168.

Su, Z., Schmugge, T., Kustas, W. P., and Massman, W. J. (2001). “An Evaluation of Two Models for Estimation of the Roughness Height for Heat Transfer between the Land Surface and the Atmosphere.” *J. Appl. Meteorol.*, 40(11), 1933–1951.

Su, Z., Yacob, A., Wen, J., Roerink, G., He, Y., Gao, B., Boogaard, H., and Diepen, C. van. (2003b). “Assessing relative soil moisture with remote sensing data: theory , experimental validation , and application to drought monitoring over the North China Plain.” *Phys. Chem. Earth*, 28, 89–101.

Suchánková, T., and Bezděkovská, R. (2011). “Crop production function - study.” *Proc. 30th Int. Conf. Math. Methods Econ. Crop*, 842–847.

Sundin, C. (2017). “Exploring the water-energy nexus in the Omo river basin A first step toward the development of an integrated hydrological-OSeMOSYS energy model.” Royal Institute of Technology, Stockholm (KTH).

Swinbank, W. C. (1951). “The measurement of vertical transfer of heat and water vapor by eddies in the lower atmosphere.” *J. Meteorol.*

Tait, A. B., Hall, D. K., Foster, J. L., and Armstrong, R. L. (2000). “Utilizing multiple datasets for snow-cover mapping.” *Remote Sens. Environ.*, 72(1), 111–126.

- The United Nations. (2016). "The United Nations World Water Development Report." 164.
- Timmermans, W. J., Gieske, A. S., Kustas, W. P., Wolski, P., Arneeth, A., and Parodi, G. N. (2004). "Determination of water and heat fluxes with MODIS imagery - Maun, Botswana." *Remote Sens. Agric. Ecosyst. Hydrol.* V, 5232(0), 444–455.
- Trajkovic, S., Gocic, M., Pongracz, R., and Bartholy, J. (2019). "Adjustment of Thornthwaite equation for estimating evapotranspiration in Vojvodina." *Theor. Appl. Climatol.*, 138(3–4), 1231–1240.
- Tuong, T., Bouman, B. A. M., and Mortimer, M. (2004). "More rice, less water-Integrated approaches for increasing water productivity in irrigated rice based systems in Asia." "New Dir. a Divers. planet". *Proc. 4th Int. Crop Sci. Congr. 26 Sep – 1 Oct 2004, Brisbane, Aust. Publ. CDROM.*, 1–13.
- Uliana, E. M., Silva, D. D. da, Moreira, M. C., and Pereira, D. dos R. (2019). "Global sensitivity analysis methods applied to hydrologic modeling with the SAC-SMA model." *Eng. Agrícola*, 39(1), 65–74.
- UN. (2006). *Water, a shared responsibility*.
- UNESCO. (2009). *The United Nations World Water Development Report: Water in a Changing World. United Nations Educ. Sci. Cult. Organ.*
- USACE-HEC. (2010). "Hydrologic Modeling System HEC-HMS v3.5. User's Manual, US Army Corps of Engineers." *Hydrol. Eng. Cent.*, (August), 318.
- USDA. (2017). "Water management." *Nat. Resour. Conserv. Serv.*, <<https://www.nrcs.usda.gov/wps/portal/nrcs/main/national/water/manage/>> (Apr. 27, 2017).
- Verma, S. B. (1990). "Micrometeorological methods for measuring surface fluxes of mass and energy." *Remote Sens. Rev.*, 5(1), 99–115.

Wagener, T., Boyle, D. P., Lees, M. J., Wheeler, H. S., Gupta, H. V., and Sorooshian, S. (2001). “A framework for development and application of hydrological models.” *Hydrol. Earth Syst. Sci.*, 5(1), 13–26.

Wagener, T., McIntyre, N., Lees, M. J., Wheeler, H. S., and Gupta, H. V. (2003). “Towards reduced uncertainty in conceptual rainfall-runoff modelling: Dynamic identifiability analysis.” *Hydrol. Process.*, 17(2), 455–476.

Wale, A., Rientjes, T. H. M., Gieske, A. S. M., and Getachew, H. A. (2009). “Ungauged catchment contributions to Lake Tana ’ s water balance.” *Hydrol. Process.*, 23(26), 3682–3693.

Walker, E., García, G. A., and Venturini, V. (2019). “Evapotranspiration estimation using SMAP soil moisture products and bouchet complementary evapotranspiration over Southern Great Plains.” *J. Arid Environ.*, 163, 34–40.

Wallace, J. (2000). “Increasing agricultural water use efficiency to meet future food production.” *Agric. Ecosyst. Environ.*, 82, 105–119.

Wallace, J. S., and Gregory, P. J. (2002). “Water resources and their use in food production systems.” *Aquat. Sci.*, 64(4), 363–375.

Wang, H., Chen, Y., and Chen, Z. (2013). “Spatial distribution and temporal trends of mean rainfall and extremes in the arid region, northwest of China, during 1960- 2010.” *Hydrol. Process.*, 27(12), 1807–1818.

Wang, J., Price, K. P., and Rich, P. M. (2001). “Spatial patterns of NDVI in response to precipitation and temperature in the central Great Plains.” *Int. J. Remote Sens.*, 22(18), 3827–3844.

Wang, Y., and Li, X. (2011). “Sensible heat flux estimation using Surface Energy Balance System (SEBS), modis products, and NCEP reanalysis data.” *Int. Geosci. Remote Sens. Symp.*, (1), 4269–4272.

- Wang, Z. M., Batelaan, O., and Smedt, F. De. (1997). "A distributed model for water and energy transfer between soils, plants and atmosphere (WetSpa)." *Phys. Chem. Earth.*, 21(3)(3), 189–193.
- Wani, S. P., Sreedevi, T. K., Rockström, J., and Ramakrishna, Y. S. (2009). "Rainfed agriculture - past trends and future prospects." *Rainfed Agric. Unlocking Potential*, 1–35.
- Wesseling, J. G., and Feddes, R. A. (2006). "Assessing crop water productivity from field to regional scale." *Agric. Water Manag.*, 86(1–2), 30–39.
- Wichelns, D. (2003). "Enhancing water policy discussions by including analysis of non-water inputs and farm-level constraints." *Agric. Water Manag.*, 62(2), 93–103.
- Wigmosta, M., Nijssen, B., and Storck, P. (2002). "The distributed hydrology soil vegetation model." *Math. Model. Small Watershed Hydrol. Appl.*, 7–42.
- Winsemius, H. C., Savenije, H. H. G., and Bastiaanssen, W. G. M. (2008). "Constraining model parameters on remotely sensed evaporation: justification for distribution in ungauged basins?" *Hydrol. Earth Syst. Sci.*, 12, 1403–1413.
- WMO. (2012). *Guide to Agricultural Meteorological Practices. World Meteorol. Organ.*
- Wood, E. F., Su, H., McCabe, M., and Su, B. (2003). "Estimating Evaporation from Satellite Remote Sensing." *IEEE*, 00, 1163–1165.
- Woodroffe, R., and Associates. (1995). *Omo-Gibe river basin development master plan study survey and analysis report Volume IV land resource survey.*
- Woodroffe, R., and Associates. (1996). *Omo-Gibe river basin development master plan study survey and analysis report. Volume IV.*
- World Bank. (2006). *Ethiopia Managing Water Resources to Maximize Sustainable Growth.*

World Meteorological Organization. (1975). “‘*Intercomparison of conceptual models used in operational hydrological forecasting.*’” *Oper. Hydrol. Rep. No. 7, Geneva, Switzerland, 172 pp.*

World Meteorological Organization. (1992). “‘*Simulated Real-Time Intercomparison of Hydrological Models.*’” *Oper. Hydrol. Rep. No. 38, Geneva, Switzerland.*

Wu, X., Zhou, J., Wang, H., Li, Y., and Zhong, B. (2015). “Evaluation of irrigation water use efficiency using remote sensing in the middle reach of the Heihe river, in the semi-arid Northwestern China.” *Hydrol. Process.*, 29(9), 2243–2257.

Xu, M., Han, H., and Kang, S. (2016). “Modeling Glacier Mass Balance and Runoff in the Koxkar River Basin on the South Slope of the Tianshan Mts . during 1959 to 2009 , China.” (October), 1–22.

Yapo, P. O., Gupta, H. V., and Sorooshian, S. (1998). “Multi-objective global optimization for hydrologic models.” *J. Hydrol.*, 204(1–4), 83–97.

Young, A. R. (2006). “Stream flow simulation within UK ungauged catchments using a daily rainfall-runoff model.” *J. Hydrol.*, 320(1–2), 155–172.

Yu, B., Nin-Pratt, A., Funes, J., and Gemessa, S. A. (2011). *Cereal Production and Technology Adoption in Ethiopia. Int. food policy Res. Inst.*

Zhang, K., Kimball, J. S., and Running, S. W. (2016a). “A review of remote sensing based actual evapotranspiration estimation.” *Wiley Interdiscip. Rev. Water*, 3(6), 834–853.

Zhang, Y., Peña-Arancibia, J. L., McVicar, T. R., Chiew, F. H. S., Vaze, J., Liu, C., Lu, X., Zheng, H., Wang, Y., Liu, Y. Y., Miralles, D. G., and Pan, M. (2016b). “Multi-decadal trends in global terrestrial evapotranspiration and its components.” *Sci. Rep.*, 6(December 2015), 1–12.

Zhao, J., Chen, X., Zhang, J., Zhao, H., and Song, Y. (2019). “Higher temporal

evapotranspiration estimation with improved SEBS model from geostationary meteorological satellite data.” *Sci. Rep.*, 9(1), 1–15.

Zhao, L., Xia, J., Xu, C. yu, Wang, Z., Sobkowiak, L., and Long, C. (2013). “Evapotranspiration estimation methods in hydrological models.” *J. Geogr. Sci.*, 23(2), 359–369.

Zheng, C., Jia, L., Hu, G., and Lu, J. (2019). “Earth observations-based evapotranspiration in Northeastern Thailand.” *Remote Sens.*, 11(2), 17.

Zhong, L., Xu, K., Ma, Y., Ziyu, H., Wang, X., and Ge, N. (2019). “Evapotranspiration estimation using surface energy balance system model: A case study in the Nagqu River Basin.” *Atmosphere (Basel)*, 10(268), 1–13.

Zhou, Y., Li, X., Yang, K., and Zhou, J. (2018). “Assessing the impacts of an ecological water diversion project on water consumption through high-resolution estimations of actual evapotranspiration in the downstream regions of the Heihe River Basin, China.” *Agric. For. Meteorol.*, 249, 210–227.

Zoebl, D. (2006). “Is water productivity a useful concept in agricultural water management?” *Agric. Water Manag.*, 84(3), 265–273.

Zwart, S. J., and Bastiaanssen, W. G. M. (2004). “Review of measured crop water productivity values for irrigated wheat, rice, cotton and maize.” *Agric. Water Manag.*, 69(2), 115–133.

## APPENDIX 1

Table 1 Details of the selected meteorological station for upper Omo-Gibe basin

S No	Name of Station	Longitude	Latitude	Altitude (m)	Annual Average rainfall (mm)
1	Areka	7.07	37.70	1765	1190.60
2	Assendabo	7.77	37.23	1760	1403.62
3	Bele	7.08	37.58	1712	1190.60
4	Bonga	7.22	36.23	1712	1583.15
5	Butajira	8.12	38.37	2099	1207.92
6	Chekorsa	7.62	36.73	1816	1586.21
7	Cumbi	8.12	37.47	1933	1271.51
8	Dedo	7.52	36.87	2111	1496.60
9	Durame	7.24	37.89	2000	1128.76
10	Gedo	9.05	37.43	2431	1492.74
11	Gesuba	6.72	37.56	1522	1171.20
12	Gibe Farm	8.23	37.58	1092	1182.80
13	Hosana	7.57	38.85	2307	1185.03
14	Indibir	8.12	37.94	2082	1162.48
15	Jimma	7.67	36.83	1718	1496.60
16	Limu Genet	8.10	36.95	1731	1385.18
17	Meto'so	7.43	36.88	2066	1459.92
18	Shebe	7.52	36.52	1720	1586.21
19	Waliso	9.00	37.00	2043	1330.10
20	Welkite	8.27	37.75	2000	1218.20
21	Wolaita Sodo	6.83	37.75	1815	1172.18
22	Wushwush	7.30	36.12	1970	1583.15
23	Yaya	8.37	37.53	1538	1218.20

## **PUBLICATIONS**

### **International Journal Papers**

1. Nesru, M., Nagaraj, M.K. & Shetty, A. Assessment of consumption and availability of water in the upper Omo-Gibe basin, Ethiopia. *Arab J Geosci* 13, 13 (2020). <https://doi.org/10.1007/s12517-019-4897-8>.
2. Nesru, M., Shetty, A. & Nagaraj, M.K. Multi-variable calibration of hydrological model in the upper Omo-Gibe basin, Ethiopia. *Acta Geophys.* 68, 537–551 (2020). <https://doi.org/10.1007/s11600-020-00417-0>.

### **International conference paper**

1. Nesru, M., Nagaraj, M.K. (2018). “Comparative review on model selection for hydrological studies.” In Book of abstracts Hydro-2018 international Conference (Hydraulics, Water Resources, and Coastal Engineering) NITP, December 19-21, 2018, NIT Patna, India.